EFFECT OF LOAD SPECTRUM VARIABLES ON FATIGUE CRACK INITIATION AND PROPAGATION

Bryan/Potter, *editors*

ASTM STP 714

AMERICAN SOCIETY FOR TESTING AND MATERIALS

EFFECT OF LOAD SPECTRUM VARIABLES ON FATIGUE CRACK INITIATION AND PROPAGATION

A symposium
sponsored by ASTM
Committee E-9 on Fatigue
AMERICAN SOCIETY FOR
TESTING AND MATERIALS
San Francisco, Calif., 21 May 1979

ASTM SPECIAL TECHNICAL PUBLICATION 714
D. F. Bryan, The Boeing Wichita Co., and
J. M. Potter, Air Force Flight Dynamics
Laboratory, editors

04-714000-30

AMERICAN SOCIETY FOR TESTING AND MATERIALS
1916 Race Street, Philadelphia, Pa. 19103

Library of Congress Catalog Card Number: 80-66078

NOTE

The Society is not responsible, as a body,
for the statements and opinions
advanced in this publication.

Printed in Baltimore, Md.
October 1980

Foreword

The symposium on Effect of Load Spectrum Variables on Fatigue Crack Initiation and Propagation was presented at San Francisco, Calif., 21 May 1979. The symposium was sponsored by the American Society for Testing and Materials through its Committee E-9 on Fatigue. D. F. Bryan, The Boeing Wichita Co., and J. M. Potter, Air Force Flight Dynamics Laboratory, presided as symposium chairmen and editors of this publication.

Related ASTM Publications

Part-Through Crack Fatigue Life Predictions, STP 687 (1979), $26.65, 04-687000-30

Service Fatigue Loads Monitoring, Simulation, and Analysis, STP 671 (1979), $29.50, 04-671000-30

Fatigue Crack Growth under Spectrum Loads, STP 595 (1976), $34.50, 04-595000-30

Manual on Statistical Planning and Analysis for Fatigue Experiments, STP 588 (1975), $15.00, 04-588000-30

Handbook of Fatigue Testing, STP 566 (1974), $17.25, 04-566000-30

Damage Tolerance in Aircraft Structures, STP 486 (1971), $19.50, 04-486000-30

A Note of Appreciation to Reviewers

This publication is made possible by the authors and, also, the unheralded efforts of the reviewers. This body of technical experts whose dedication, sacrifice of time and effort, and collective wisdom in reviewing the papers must be acknowledged. The quality level of ASTM publications is a direct function of their respected opinions. On behalf of ASTM we acknowledge with appreciation their contribution.

ASTM Committee on Publications

Editorial Staff

Contents

Introduction

The effects of variations in the parameters that characterize in-service loading on the life of engineering structures has received ever-increasing attention in recent years. Many investigators have shown fatigue crack initiation and growth to be sensitive to loading variables such as load sequence, frequency and magnitude of peak overloads and underloads, load spectrum truncation, compression hold times, and others. The ability of the stress analyst to predict the useful life of a particular structure depends not only on having a truly representative loading spectrum, but also on knowing the effects of variations in the load history parameters.

This symposium is a timely and logical follow-on to the American Society for Testing and Materials (ASTM) sponsored symposium on Service Fatigue Loads Monitoring, Simulation, and Analysis presented in Atlanta, Ga., 14–15 Nov. 1977. The objective of the present symposium was to bring together engineers, scientists, and academicians to exchange ideas and present state-of-the-art papers on the analytical and experimental evaluation of various load spectrum effects on crack initiation and propagation.

The papers in this publication cover a wide range of subjects from various engineering fields. Load spectra representative of aircraft structures, gas turbines, and windmill structures are presented along with analytical and experimental fatigue and fracture results. The effects of spectrum editing, time dependent changes in material characteristics, compression loads, and gust alleviation are discussed. A crack growth model incorporating both retardation and acceleration effects and a unique approach to ranking 7000 series aluminum alloys are included. The state-of-the-art information in this publication should be helpful to those engineers responsible for life predictions of structures subjected to repetitive loads. Scientists and educators in the field of engineering structures should likewise find this publication of great interest.

The symposium organizing committee wishes to express sincere appreciation to the authors, reviewers, and ASTM staff for their efforts in making this publication possible.

D. F. Bryan

The Boeing Wichita Company, Wichita, Kans. 67210; symposium cochairman and coeditor.

J. M. Potter

AFFDL/FBE. Wright-Patterson Air Force Base, Ohio 45433; symposium cochairman and coeditor.

D. F. Socie[1] *and P. J. Artwohl*[1]

Effect of Spectrum Editing on Fatigue Crack Initiation and Propagation in a Notched Member

REFERENCE: Socie, D. F. and Artwohl, P. J., "**Effect of Spectrum Editing on Fatigue Crack Initiation and Propagation in a Notched Member,**" *Effect of Load Spectrum Variables on Fatigue Crack Initiation and Propagation, ASTM STP 714,* D. F. Bryan and J. M. Potter, Eds., American Society for Testing and Materials, 1980, pp. 3-23.

ABSTRACT: A method for eliminating small, nondamaging cycles from irregular loading histories is described. Analytic estimates of crack initiation, crack propagation, and total fatigue lives are compared to experimental data for full and edited load histories from the Society of Automotive Engineers Cumulative Fatigue Damage Test Program. Load histories edited to have equal crack initiation lives do not have equal crack propagation lives.

KEY WORDS: fatigue (materials), crack initiation, crack propagation, life prediction, spectrum editing

For many years, the problem of fatigue has plagued all designers who work on structures and components subjected to cyclic loads. The main problem in dealing with fatigue in design is that the mechanisms of fatigue are very complex and, even though much research is being done in this area, a complete understanding of the subject is still a long way off. For this reason many varied groups have been responsible for establishing programs to investigate various aspects of fatigue. One typical group dealing primarily in the ground vehicle industry established a round robin test program through the Society of Automotive Engineers (SAE). This work has produced a great deal of test data and a considerable number of theoretical concepts for fatigue damage analysis [*1*].[2] Fuchs et al [*2*] showed

[1] Assistant professor and research assistant, respectively, Mechanical Engineering, University of Illinois, Urbana, Ill. 61801.

[2] The italic numbers in brackets refer to the list of references appended to this paper.

that 90 percent of the cycles do only 10 percent of the calculated fatigue damage.

The purpose of this investigation was to verify experimentally analytic procedures for editing small nondamaging events from a variable amplitude load history without significantly changing the fatigue damage done by the original history. This will allow accelerated component fatigue tests to be performed and will result in substantial reductions in testing time.

Data from the SAE Cumulative Fatigue Damage Test Program were analyzed in order to estimate crack initiation and propagation lives. A strain cycle fatigue analysis was employed to determine the relative fatigue damage of each cycle. Small amplitude cycles were eliminated until the remaining cycles had at least 80 percent of the calculated fatigue damage of the original history. Tests, employing the edited load histories, were then conducted under the same conditions as the original test program. Analytic methods for estimating crack initiation and propagation lives are compared to experimental data for full and edited histories. The test program as well as the analytical models will be reviewed, briefly, for those unfamiliar with them. The overall life estimation procedure for estimating total fatigue lives is shown in Fig. 1.

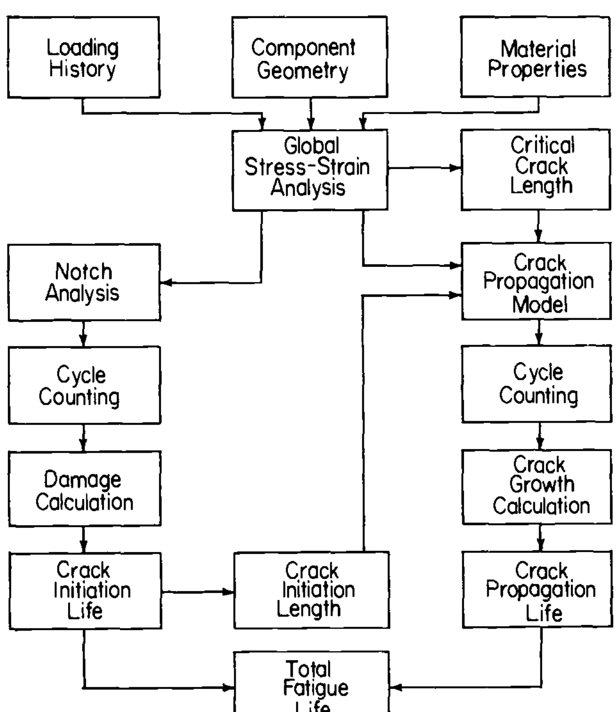

FIG. 1—*Overall analysis procedure.*

Analytical Techniques

Strain Cycle Fatigue Concepts

The basic hypothesis of cumulative fatigue damage analysis, employing materials data obtained from laboratory specimens, is that if the local stresses and strains at the critical location of the component are known, the crack initiation life of the structure can be related to the life of the specimen. Cumulative damage analysis reduces the complex problem of fatigue into one of determining the local stresses and strains from nominal stresses or loads, and the proper relationship between stresses, strains, and fatigue life.

Fatigue resistance of metals can be characterized by strain-life curves that are determined from smooth laboratory specimens that are tested in completely reversed strain control. The relationship between strain amplitude, $\Delta\epsilon/2$, and reversals to failure, $2N_f$, may be expressed in the following form

$$\frac{\Delta\epsilon}{2} = \epsilon_f{}' \, (2N_f)^c + \frac{\sigma_f{}'}{E} \, (2N_f)^b \quad (1)$$

where

$\sigma_f{}'$ = fatigue strength coefficient,
b = fatigue strength exponent,
$\epsilon_f{}'$ = fatigue ductility coefficient,
c = fatigue ductility exponent, and
E = elastic modulus.

Morrow [3], Tucker et al [4], provide definitions of these fatigue properties and tabulate values for a number of metals. Morrow suggested that the strain-life equation could be modified to account for mean stress, σ_0, by reducing the fatigue strength coefficient by an amount equal to the mean stress.

$$\frac{\Delta\epsilon}{2} = \epsilon_f{}' \, (2N_f)^c + \frac{\sigma_f - \sigma_0}{E}(2N_f)^b \quad (2)$$

When the fatigue properties are known and the service environment defined, the problem of fatigue life prediction becomes one of determining the local strain amplitude and mean stress for each load range identified by cycle counting, so that Eq 2 can be solved for life.

Since the introduction of Neuber's rule [5] which equates the theoretical stress concentration factor to the geometric mean of the stress and strain concentration factors, several investigators [6–8] have shown how this simple concept can be extended to relate the stress-strain behavior of the metal at a notch root to the nominal load history on a notched specimen subjected to variable amplitude loading.

$$K_T(\Delta S\ \Delta e)^{1/2} = (\Delta\sigma\ \Delta\epsilon)^{1/2} \tag{3}$$

where

ΔS, Δe = nominal stress and strain range,
$\Delta\sigma$, $\Delta\epsilon$ = notch stress and strain range, and
K_T = theoretical stress concentration factor.

This equation adequately represents the fatigue behavior of notched specimens when the theoretical stress concentration factor is replaced by a fatigue concentration factor, K_f, which accounts for notch acuity and material effects. Current practice accepts a notch size effect wherein K_f can be estimated in terms of K_T by an empirical theory utilizing experimentally determined material constants. The most common one in use was proposed by Peterson [*9*].

$$K_f = 1 + \frac{K_T - 1}{1 + a/r} \tag{4}$$

where

a = material constant and
r = notch radius.

For blunt notches ($K_T < 4$), the Peterson equation makes a small but appropriate correction for weakest link type size and stress gradient effects. However, for sharp notches, it reflects an inappropriate comparison between initiation controlled smooth specimen endurance limits and sharp notch endurance limits involving nonpropagating cracks and threshold stress intensity behavior, where the failure stress is independent of K_T [*10*].

Notch root stresses and strains are determined on a cycle-by-cycle basis using Eq 3 and the cyclic stress-strain properties of the material. An alternate method to Neuber's rule involves the direct determination of the relationship between applied load and notch root strain. These relationships may be obtained by experimental stress analysis method or analytically by finite element or difference techniques. Although this method provides a better estimate of the strains for a complex geometry, it does not significantly improve life estimates for the notched plates employed in this investigation [*6*]. Once the notch root strains are determined, notch root stresses are calculated from a material response model [*11*] that describes the history dependence of cyclic deformation. The strain history is then rainflow counted [12] to determine the strain ranges and mean stresses required to solve Eq 2 for life.

Figure 2 shows a typical strain time history along with its corresponding stress time history. Events C-D and E-D have identical mean strains and strain ranges but have quite different mean stresses and stress ranges. Following the elastic unloading (B-C), the material exhibits a discontinuous accumulation of plastic strain upon deforming from C to D. When Point B is reached, the material "remembers" its prior deformation (that is, A-B), and deforms along path A-D as if event B-C never occurred.

In this simple sequence, four events that resemble constant amplitude cycling are easily recognized: A-D-A, B-C, D-E, and F-G. These events are closed hysteresis loops, each event is associated with a strain range and mean stress. The apparent reason for the superiority of rainflow counting is that it combines load reversals in a manner that defines cycles by closed hysteresis loops. Each closed hysteresis loop has a strain range and mean stress associated with it that can be compared with the constant amplitude fatigue data in order to calculate fatigue damage. Miner's linear damage rule is employed to sum the fatigue damage from individual cycles.

The definition of an initiated crack has been the subject of much controversy. No satisfactory solution to this problem exists. Fatigue cracks start with dislocation movement on the first load cycle and end with fracture

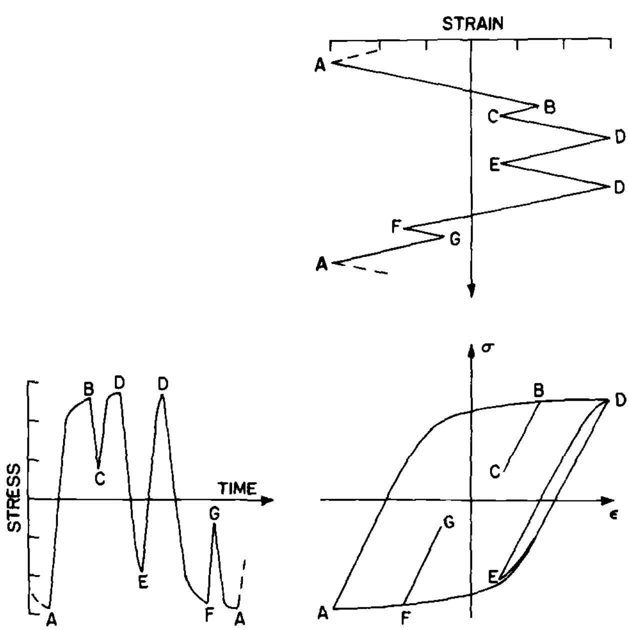

FIG. 2—Rainflow counting example.

on the last. Crack initiation lies somewhere between the two. For purposes of strain cycle fatigue analysis, crack initiation is defined as a crack in the structure or component that is the same size as the cracks observed in the strain cycle fatigue specimen. Frequently, this is the specimen radius that is on the order of 2.5 mm. Dowling [*13*] proposed reporting strain cycle fatigue data in terms of the number of cycles required to form a crack of fixed length. He found that for steels with fatigue lives below the transition fatigue life, cracks 0.25 mm long were formed at approximately one half of the life required for specimen separation. For smooth specimens at longer lives where the bulk behavior of the material is primarily elastic, the first crack is observed prior to specimen fracture.

The definition of crack initiation applied to strain cycle fatigue analysis always includes a portion of life where the crack is indeed propagating. It should be noted, however, that the behavior of small cracks (less than 0.25 mm) is different than long cracks cycled under equal stress intensities [*14-16*]. As a result, the analysis described in the next section does not apply to them. For design purposes, crack initiation is defined as the formation of a crack between 0.25 mm and 2.5 mm long.

Crack Propagation Concepts

Perhaps the most widely accepted correlation between constant amplitude fatigue crack growth and applied loads has been proposed by Paris [*17*]. The rate of crack propagation per cycle, da/dN, is directly related to cyclic stress intensity, ΔK, in the following form

$$\frac{da}{dN} = C(\Delta K)^m \tag{5}$$

where

C = crack growth coefficient and
m = crack growth exponent.

In the simplest form, crack propagation lives are obtained by substituting an effective stress intensity and integrating Eq 5 with the following result

$$N_p = \int_{a_0}^{a_f} \frac{da}{C(\Delta K_{\text{eff}})^m} \tag{6}$$

where

a_0 = initial crack size,
a_f = final crack size,

N_p = crack propagation life, and
ΔK_{eff} = effective stress intensity range.

Several models have been proposed for determining effective stress intensities that account for load ratio, sequence, and crack closure effects.

Simple models for determining effective stress intensities for variable amplitude loading are based on the interaction of the plastic zone of the current load cycle with the plastic zone of previous cycles [*18*]. These models do not account for compressive loads and notch root plasticity. Nelson and Fuchs [*19*] showed that models that did not include notch plasticity effects were inadequate for notched members that involved compressive yielding at the notch root. Crack closure models, although more difficult to implement, have successfully been employed for these problems [*20*]. Closure models are based on the hypothesis that cracks can only grow when the crack surfaces at the crack tip are open. Crack surfaces open when the external load overcomes the compressive residual stresses near the crack tip. In the present investigation, crack opening loads were determined with finite element techniques. For short spectra such as those employed in this investigation, the crack opening and closing loads remain constant and are determined by the largest load cycle in the history. Tests suggest that an appropriate cycle counting technique for crack propagation is to rainflow count that portion of the load history that lies above the crack closure load. This produces effective load ranges that are converted into effective stress intensity ranges so that Eq 6 can be solved through numerical integration procedures.

SAE Test Program

Three load histories designated suspension, bracket, and transmission were used in the research program. The original load histories shown in Fig. 3 are strain measurements from ground vehicles under actual service conditions. They were scaled to various maximum load levels and applied to the specimens, shown in Fig. 4, made from both Man-Ten and RQC-100 steels. This design provides both axial and bending stresses and strains at the notch root. Specimens were cut from a hot-rolled plate by production machining techniques. The hole was drilled and reamed with no edge preparation and was then saw cut from one side to provide the notch. Specimens for this investigation were obtained from the same plate as the original test program. Mechanical properties of these materials are shown in Table 1. A considerable quantity of experimental data was generated during the round-robin test program described in Ref *1*. Crack initiation for this test program was defined as a crack 2.5 mm long, because it has approximately the same crack area as a smooth specimen.

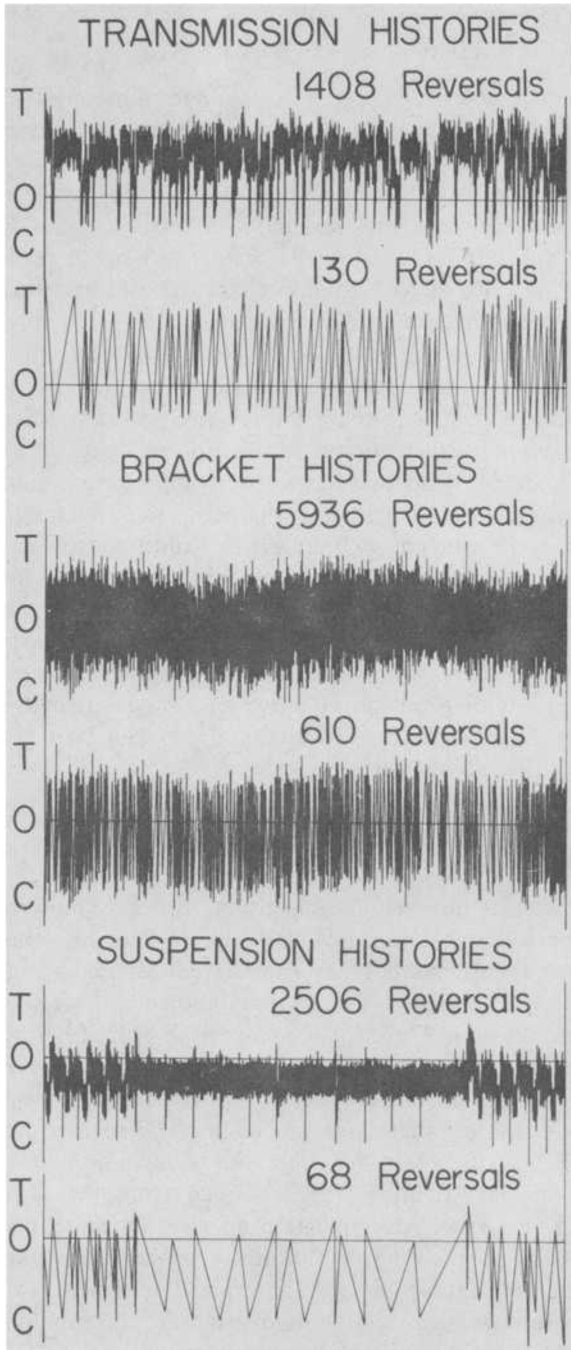

FIG. 3—*SAE load histories.*

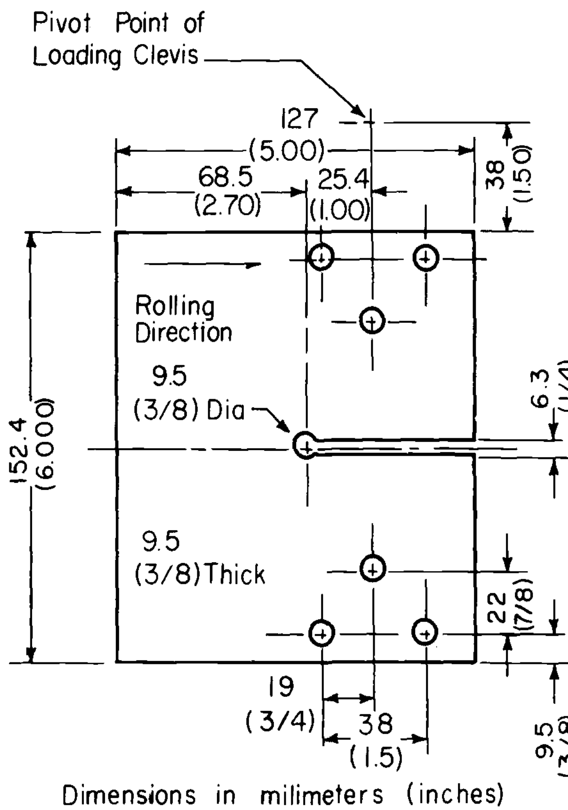

FIG. 4—*SAE keyhole specimen.*

Editing Technique

Procedure

Strain cycle fatigue analysis procedures, previously described, were employed to edit the load histories. Peak points were omitted using a computer algorithm that would omit any points that would add a hysteresis loop and its corresponding fatigue damage less than a specified value. The limiting value, designated as a threshold value, could be changed to make the final edited history as large as the original history or as small as two points. The algorithm compared each successive range to the previous range that had fit the specified conditions. If the new range had a change larger than the threshold, the new range would be kept and then become the comparison range. On the other hand, if the new range did not produce a change greater than the specified threshold value, the range would be merely omitted. In this manner, a history could be edited and still keep the original sequence of events.

TABLE 1—*Mechanical properties of Man-Ten and RQC-100.*

Monotonic Properties	Man-Ten		RQC-100	
Elastic modulus, E	206 GPa	(30×10^3 ksi)	206 GPa	(30×10^3 ksi)
Yield strength, S_y	324 MPa	(47 ksi)	827 MPa	(120 ksi)
Tensile strength, UTS	565 MPa	(82 ksi)	863 MPa	(125 ksi)
Reduction in area, %	...	65%	...	55%
True fracture strength, σ_f	1000 MPa	(145 ksi)	1190 MPa	(173 ksi)
True fracture ductility, ϵ_f	...	1.19	...	0.78
Strength coefficient, K	965 MPa	(140 ksi)	1200 MPa	(174 ksi)
Strain hardening exponent, n	...	0.21	...	0.08
Cyclic Properties				
Fatigue ductility coefficient, ϵ_f'	...	0.26	...	1.06
Fatigue ductility exponent, c	...	−0.47	...	−0.75
Fatigue strength coefficient, σ_f'	917 MPa	(133 ksi)	1160 MPa	(168 ksi)
Fatigue strength exponent, b	...	−0.095	...	−0.075
Cyclic strength coefficient, K'	1200 MPa	(174 ksi)	1150 MPa	(167 ksi)
Cyclic strain hardening exponent, n'	...	0.20	...	0.10
Cyclic yield strength, S_y'	331 MPa	(48 ksi)	586 MPa	(85 ksi)
Fracture Properties				
Crack growth coefficient, c	3.0×10^{-9} mm/cycle MPa^{-m}	(8.6×10^{-11}) in./cycle ksi^{-m}	5.2×10^{-9}	(1.5×10^{-10})
			...	...
Crack growth exponent, m	...	3.43	...	3.25
Fracture toughness, K_c (10 mm thickness)	121 MPa $\sqrt{m}$	(110 ksi$\sqrt{in.}$)	154 MPa$\sqrt{m}$	(140 ksi$\sqrt{in.}$)

Figure 5 shows the effect of the editing level calculated initiation life. The solid curve is the cumulative damage distribution for all rainflow counted strain ranges up to a given strain range. The dashed line represents the cumulative distribution of cycles up to a given strain range. The steps in the curves are due to the algorithm, which breaks strains down into 50 finite categories. Increasing the number of strain ranges would tend to smooth out the curve.

The two examples in the figure show how to read the curves. Points A and A′ show that 92 percent of the cycles account for 3 percent of the calculated strain cycle fatigue damage of a block. One repetition of the load history represents one block of loading. Points B and B′ show the edited version of the transmission history.

Full and edited transmission, bracket, and suspension histories are shown in Fig. 3. The size of the transmission history was reduced 92 percent, the bracket history 90 percent, and the suspension history 97 percent.

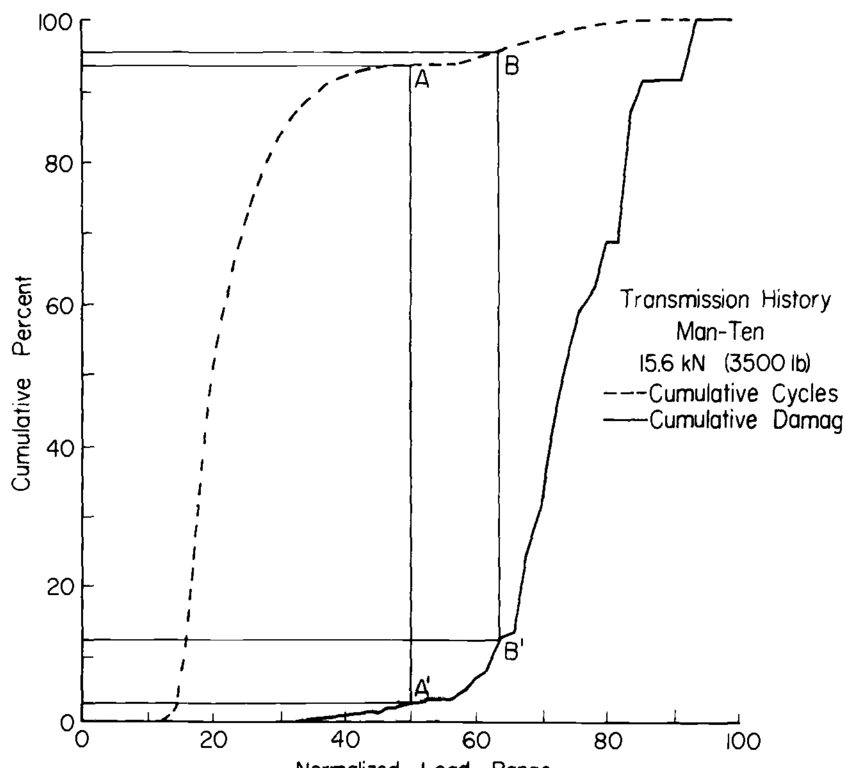

FIG. 5—*Cumulative distribution of fatigue damage and cycles.*

Effect of Material Properties

To establish a basis for comparison of different materials, the cumulative damage and total cumulative cycles were compared for Man-Ten and RQC-100 specimens. Material properties have an effect on the editing level; however, the general shape of the curves remained unchanged as shown in Fig. 6. Changing properties from Man-Ten to RQC-100 moved the percent damage curves to the right for every test condition indicating that the smaller cycles are less damaging in the stronger material. The actual amount of shift in the curve depended on the history and load level employed for the analysis. Results shown in Fig. 6 were typical for all test conditions. Editing was done in the region where the difference in material properties had little or no effect. Man-Ten material properties were used to edit the histories for both Man-Ten and RQC-100 tests. The results show that the single edited history is sufficient for both material tests.

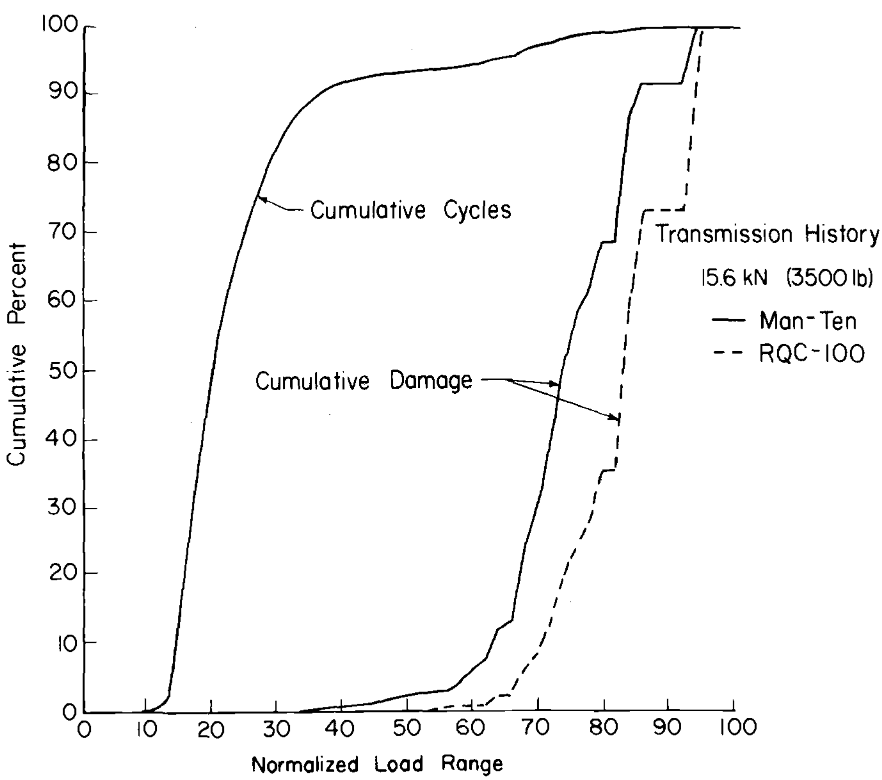

FIG. 6—*Effect of material properties on the cumulative distribution of fatigue damage.*

Effect of Load Level

To compare the effect of load level on the editing process, a similar procedure was followed. Results were very similar to those dealing with a change in material. The cumulative damage curve kept its general shape with increasing load levels, but was shifted slightly to the left indicating that the smaller cycles do more damage at higher loads. This would be expected since the strain life curve has a smaller slope at lower lives. All test conditions were evaluated with varying load levels. A typical curve is shown in Fig. 7. The top solid line represents the cumulative percent cycles for both loads. The lower solid line is the cumulative percent damage with a maximum load of 15.6 kN (3500 lb). The slightly shifted dashed line represents the corresponding cumulative percent damage with a 35.5 kN (8000 lb) maximum load.

Man-Ten material properties at a low-load level were used for editing all of the load histories. The load level was 15.6 kN (3500 lb) for the bracket and transmission histories, and 26.7 kN (6000 lb) for the suspension history.

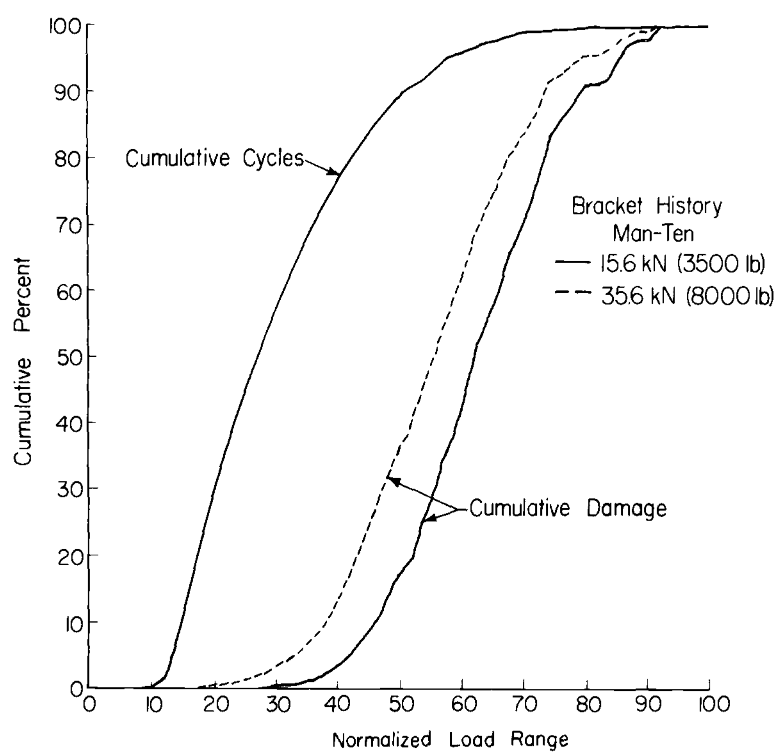

FIG. 7—*Effect of load level on the cumulative distribution of fatigue damage.*

Effect of Overstrain Material Properties

Recent studies employed material properties obtained from overstrain tests to account for errors associated with Miner's linear damage rule [*21*]. Overstrain data makes lower loads more significant with respect to fatigue damage. A strain cycle fatigue analysis was performed for all test conditions using both regular and overstrain material properties. Results shown in Fig. 8 were typical for every test condition. In each case, the cumulative damage with an overstrain curve was to the left of the other cumulative damage curve; however, the shift was more pronounced in the lower part of the curve. This shift reduced to zero at the top of the curve.

Since the effect of material properties and load level had relatively small effect on the editing level, only one load level and material was employed to edit the histories. This results in a single edited history for all tests.

Load level and material may have a significant effect on the editing level for other histories and geometries. For these three histories and two materials, the effect was very small for the load levels tested.

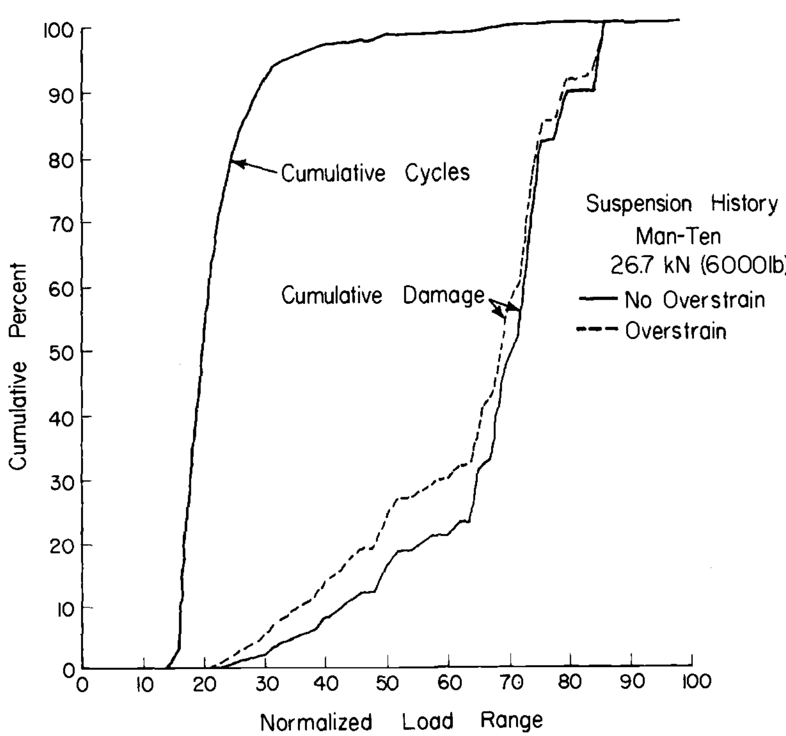

FIG. 8—*Effect of overstrained material properties on the cumulative distribution of fatigue damage.*

Results and Discussion

Crack Initiation

Tabulated results of the edited history test program are shown in Table 2. Crack initiation was defined as a crack 2.5 mm long to be consistent with the original test program. Experimental and predicted results from a strain cycle fatigue analysis are shown in Fig. 9. The solid lines are the predicted results for full history tests, and the dashed lines are the predicted results for edited history tests. Full history test data are represented by solid symbols and edited history test data by open symbols. When making comparisons of the test data, it should be noted that the original tests employing full histories were performed by seven different laboratories, while the edited tests were performed by only one laboratory that was not part of the original test program.

As a result, the comments that follow represent general trends rather than a statistical analysis of the data. Only a limited number of duplicate tests were performed because specimens from the original test program were not available.

Good agreement was found between the predicted and test results with one exception. The analysis for both full and edited histories predicts fatigue lives approximately 20 times longer for RQC-100 specimens sub-

TABLE 2—*Edited history test results.*

	Maximum Load				
Man-Ten	kN	lb	Initiation Blocks	Propagation Blocks	Total Blocks
Transmission	35.6	8 000	282	119	401
	15.6	3 500	18 356	1 914	20 270
	15.6	3 500	11 226	1 570	12 796
Bracket	35.6	8 000	43	53	96
	15.6	3 500	3 556	1 811	5 367
	15.6	3 500	1 645	1 241	2 866
	15.6	3 500	2 647	1 621	4 268
Suspension	40.0	9 000	566	3 007	3 573
	26.7	6 000	3 734	41 488	45 222
RQC-100					
Transmission	35.6	8 000	503	351	854
Bracket	35.6	8 000	76	287	354
	15.6	3 500	2 027	1 957	3 984
	15.6	3 500	2 722	1 607	4 329
	15.6	3 500	2 799	2 615	5 414
Suspension	40.0	9 000	1 698	24 371	26 069
	31.1	7 000	9 328	50 812	60 140

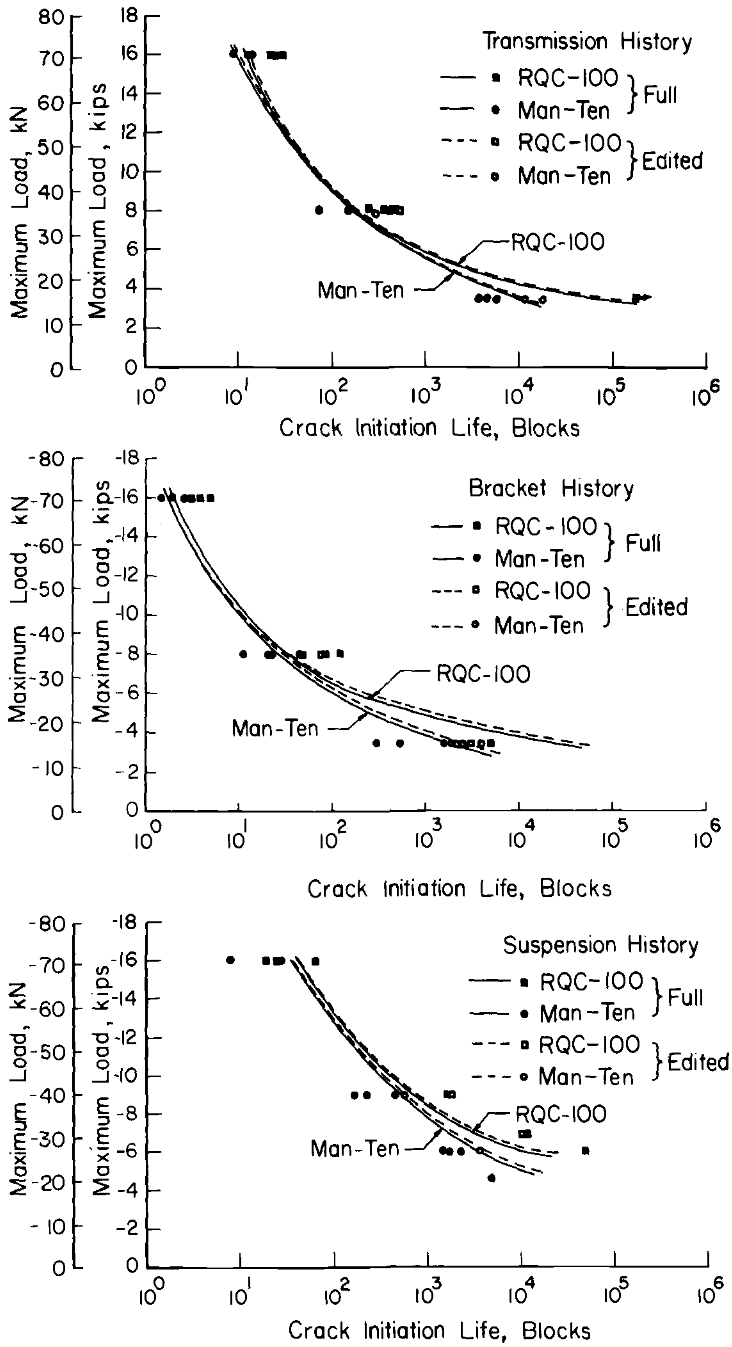

FIG. 9—*Experimental and predicted crack initiation lives for full and edited histories.*

jected to the bracket history at 15.6 kN (3500 lb). Experimentally, the edited history tests had shorter crack initiation lives than the full history tests. Of the remaining eleven test conditions, only one of the edited tests had a shorter crack initiation life.

For the worst case (Man-Ten specimens subjected to the transmission history at 15.6 kN (3500 lb)), the edited history tests had a life three times longer than the full history tests. Analytically, the small omitted cycles accounted for only 20 percent of the fatigue damage but, experimentally, they accounted for 65 percent of the fatigue damage. That is, most of the fatigue damage was done by the small cycles for this test condition. As a result, one might speculate that a strain cycle fatigue analysis employing Miner's linear damage rule would grossly overestimate fatigue lives for spectra that have thousands of small cycles and only a few larger cycles.

Crack Propagation

Propagation results shown in Fig. 10 also had good correlation with the predicted results for full and edited histories. For example, the analysis predicts that the crack propagation lives for bracket history tests for full and edited histories in both materials should be about the same at lower load levels. Predicted lives for edited suspension history tests were approximately three times longer than corresponding full history tests. Experimentally, the average difference between full and edited suspension history test was 2.1. In the worst case, the experimental edited history propagation life was seven times the average full history test life, while the predicted difference was 2.8.

Total Fatigue Life

Experimental and predicted total fatigue lives are shown in Fig. 11. Again, good correlation is found between the analysis and experimental data for total fatigue life despite the arbitrary assumption of crack initiation as a crack 2.5 mm long. If crack initiation is assumed to be 0.25 mm, the estimated total fatigue life does not increase by more than 30 percent. The total fatigue lives of suspension history tests that are primarily compressive are dominated by crack propagation. Total fatigue lives of transmission history tests that are primarily tensile are controlled by crack initiation.

Summary

A method for eliminating small nondamaging events from variable amplitude loading histories has been presented. Correlation between pre-

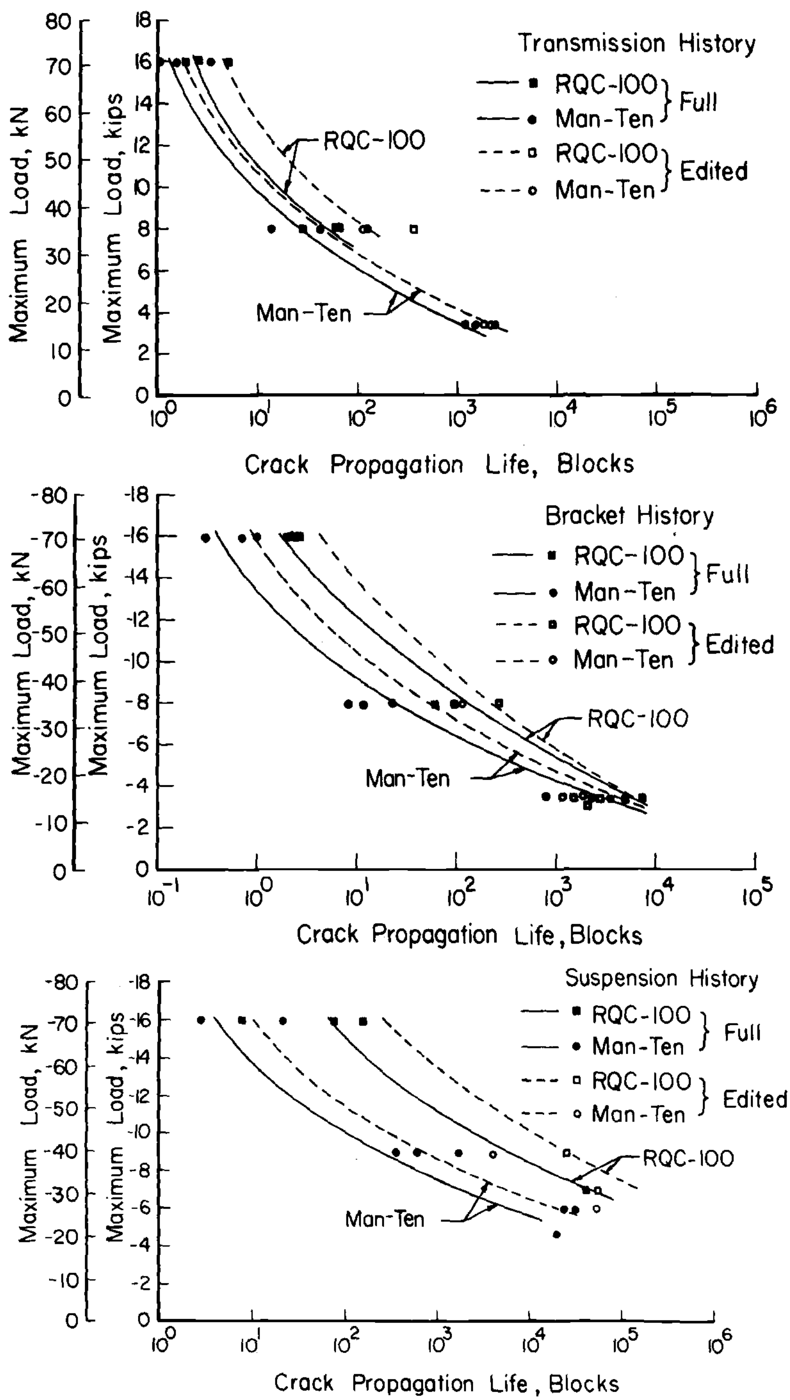

FIG. 10—*Experimental and predicted crack propagation lives for full and edited histories.*

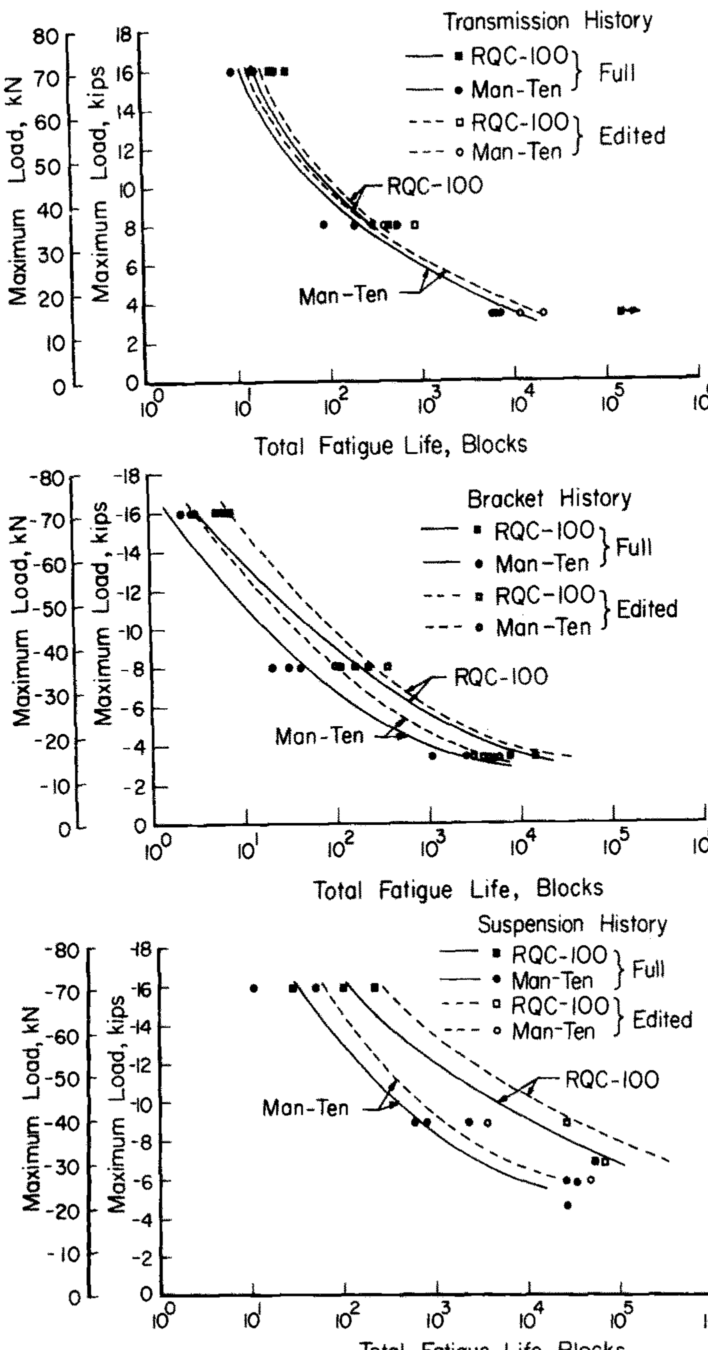

FIG. 11—*Experimental and predicted total fatigue lives for full and edited histories.*

dicted and experimental test lives was considered good for the three load histories, two materials, and three load levels employed in this investigation. Spectra edited to have equal crack initiation lives do not have equal crack propagation lives. Therefore, it is essential to determine the dominant failure mode before editing histories.

Acknowledgment

The authors wish to thank Dr. Ron Landgraf of Ford Motor Company for providing test specimens. This investigation was performed in the Materials Engineering Research Laboratory at the University of Illinois. Financial support was provided by the Fracture Control Program of the College of Engineering. The text is a shortened version of Fracture Control Report No. 31, December 1978.

References

[*1*] "Fatigue Under Complex Loading: Analysis and Experiments," *Advances in Engineering*, Society of Automotive Engineers, Vol. 6, 1977.
[*2*] Fuchs, H. O., Nelson, D. V., and Burke, M. A., "Shortcuts in Cumulative Damage Analysis," Paper 730565, presented at Society of Automotive Engineers National Automobile Engineering meeting, Detroit, Mich., 1973; see also Ref *1*, p. 145.
[*3*] Raske, D. and Morrow, J. in *Manual on Low Cycle Fatigue Testing, ASTM STP 465*, American Society for Testing and Materials, 1969, pp. 1-32.
[*4*] Tucker, L., Landgraf, R., and Brose, W., "Proposed Technical Report on Fatigue Properties for the SAE Handbook," Paper 740279, presented at SAE Automotive Engineering Congress, Detroit, Mich., Feb. 1974; see also *SAE Handbook*, Society of Automotive Engineers, 1976.
[*5*] Neuber, H., *Journal of Applied Mechanics*, Dec. 1961, pp. 544-550.
[*6*] Landgraf, R. W., Richards, F. D., and LaPointe, N. R., "Fatigue Life Predictions for a Notched Member Under Complex Load Histories," Paper 750040, presented at Society of Automotive Engineers Automotive Engineering Congress, Detroit, Mich., Feb. 1975.
[*7*] Topper, T. H., Wetzel, R. M., and Morrow, J., *Journal of Materials*, Vol. 4, No. 1, March 1969, pp. 200-209.
[*8*] Socie, D. F., "Fatigue Life Prediction Using Local Stress-Strain Concepts," *Experimental Mechanics*, Vol. 17, No. 2, Feb. 1977, pp. 50-56.
[*9*] Peterson, R. E. in *Metal Fatigue*, Sines and Waisman, Eds., McGraw-Hill, New York, 1959, pp. 293-306.
[*10*] Dowling, N. E. in *Fracture Mechanics, ASTM STP 677*, American Society for Testing and Materials, 1979, pp. 247-273.
[*11*] Martin, J. F., Topper, T. H., and Sinclair, G. M., *Materials Research and Standards*, Vol. 11, No. 2, Feb. 1971, pp. 23-29.
[*12*] Dowling, N. E., *Journal of Materials*, Vol. 7, No. 1, March 1972, pp. 71-87.
[*13*] Dowling, N. E. in *Cyclic Stress-Strain and Plastic Deformation Aspects of Fatigue Crack Growth, ASTM STP 637*, American Society for Testing and Materials, 1977, pp. 97-121.
[*14*] Hammouda, M. N. and Miller K. J. in *Elastic-Plastic Fracture, ASTM STP 668*, American Society for Testing and Materials, 1979, pp. 703-719.
[*15*] El Haddad, M. H., Smith, K. N., and Topper, T. H., *Journal of Engineering Materials and Technology*, Vol. 101, No. 1, 1979, pp. 42-46.

[16] El Haddad, M. H., Smith, K. N., and Topper, T. H. in *Fracture Mechanics, ASTM STP 677*, American Society for Testing and Materials, 1979, pp. 274-289.
[17] Paris, P. C., "The Fracture Mechanics Approach to Fatigue," Proceedings of the Tenth Sagamore Conference, Syracuse University Press, Syracuse, N.Y., 1963.
[18] Gallagher, J. P., "A Generalized Development of Yield Zone Models," AFFDL-TM-74-28-FBR, Air Force Flight Dynamics Laboratory, Dayton, Ohio, 1974.
[19] Nelson, D. V. and Fuchs, H. O. in *Fatigue Crack Growth Under Spectrum Loads, ASTM STP 595*, American Society for Testing and Materials, 1976, pp. 267-291.
[20] Socie, D. F., *Journal of Engineering Fracture Mechanics*, Vol. 9, No. 4, pp. 849-865.
[21] Dowling, N. E., Brose, W. R., and Wilson, W. K., "A Discussion of the Local Strain Approach to Notched Member Fatigue Life Prediction," Scientific Paper 76-1E7-PALFA-P1, Westinghouse Research Laboratory, Pittsburgh, Pa., 1976; see also Ref *1*, p. 72.

DISCUSSION

H. O. Fuchs (written discussion)—The authors' experiments are a welcome verification of the analytic predictions we made in 1973. A cost effective application of this work consists of applying the analytical techniques to decide how much a particular test program can be speeded up by editing. The nature of the load spectra, of the materials, and of the geometry all have an influence on the suitable amount of condensation (or truncating, or editing).

We do not yet have general rules that tell us how much condensation is appropriate for a particular case. An analysis that includes ranges of stresses, or of strains, and of effective stress intensity factors where appropriate, can be made at an expense much smaller than the amount that will be saved by shortening test times. However, if fretting fatigue or corrosion fatigue are involved, it seems unlikely that we can shorten test time before we know more about those subjects.

[1] Mechanical Engineering Department, Stanford University, Stanford, Calif. 94305.

J. R. Carroll, Jr. [1]

Time Dependent Changes in Notch Stress/Notch Strain and Their Effects on Crack Initiation

REFERENCE: Carroll, J. R., Jr., "**Time Dependent Changes in Notch Stress/Notch Strain and Their Effects on Crack Initiation,**" *Effect of Load Spectrum Variables on Fatigue Crack Initiation and Propagation, ASTM STP 714,* D. F. Bryan and J. M. Potter, Eds., American Society for Testing and Materials, 1980, pp. 24-40.

ABSTRACT: An analytical and experimental program was conducted to evaluate the time-dependent changes in the stress-strain state at stress concentrations. Load-time interaction effects on creep and stress relaxation were evaluated utilizing simple coupon, super-scale, and simplified stress concentration test specimens. Periods of sustained compression loads included in a load sequence or spectrum were shown to affect a reduction in specimen fatigue life due to creep and stress relaxation occurring during the hold period. Experiments were designed such that a quantitative assessment of time-dependent changes in both notch stress and notch strain was possible. Resulting data were used to formulate a creep and stress relaxation module for inclusion in an automated hysteresis fatigue analysis program. Agreement between experimental and predicted lives using the hysteresis analysis is significantly better than predictions using a linear analysis method.

KEY WORDS: fatigue (materials), cumulative damage, stress concentration, residual stress, stress relaxation, creep properties, crack propagation

Structural cracking continues to be a major factor in aircraft design and in assessing the useful structural life in an operational environment. The structures analyst must be able to identify potential crack initiation sites and accurately describe the structural loading conditions and stress-strain state in order to establish a time to crack initiation. In general, the cracking will initiate at or near stress concentrations such as fastener holes. Numerous analysis methods are available to predict crack initiation; however, few of these consider the complete stress-strain history, the load and mechanically induced plasticity that may exist at the stress concentration, and the time dependent changes in notch stress and notch strain. It has

[1] Aircraft development engineer, specialist, Advanced Structures Department, Lockheed-Georgia Company, Marietta, Ga. 30063.

been demonstrated by various investigators *[1-3]*[2] that overloads and underloads can induce residual stresses that may drastically affect the fatigue life of metal structures. Hysteresis fatigue analysis methods have been formulated from studies of this type that allow the analyst to include the effects of overloads and underloads and the resulting residual stress history in fatigue life predictions.

The evolution of this hysteresis analysis methodology has also included studies of cycle-dependent changes of residual stress *[3-5]*. These studies indicate that residual stresses that can be introduced by overloads and underloads or both, may tend to relax during subsequent cyclic loadings. Also, Neulieb et al *[6]* and Carroll *[7]* have shown that there are time dependent changes in residual stress and strain that also affect the fatigue life of notched structures. Their results indicate a definite influence of sustained load hold periods on the time to crack initiation for simple notched coupons and low load transfer joint specimens. A summary of the data from these two programs *[6-7]* is included in Table 1.

In Table 1, Sequence 1 is the baseline constant amplitude data. Sequences 2 and 3 illustrate the effects of overloads and underloads and the influence of load induced residual stresses on the specimen fatigue life as reported

TABLE 1—*Initial notched coupon and low load transfer joint test data.*

	Loading Sequence	Open Hole Test Data, Neulieb	Low Load Transfer Test Data, Carroll
1		50 500	146 000
2	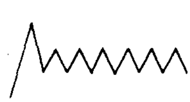	910 000	510 000
3		214 400	323 000
4	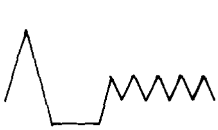 24 HRS.	126 000	51 500

[2] The italic numbers in brackets refer to the list of references appended to this paper.

by various investigators. Sequence 4 includes a sustained compression load hold period immediately following the overload/underload combination. When the sustained load hold periods are included in the test sequences, the specimen fatigue life is significantly less than that obtained with only the overloads/underloads included; namely, the comparison between Sequences 3 and 4.

The implications from these limited tests are that there are time dependent changes in the stress-strain field around stress risers. It was hypothesized that the beneficial load induced residual stresses were relaxing with time under the sustained load conditions and, in addition, that creep was occurring simultaneously with the stress relaxation. This would, of course, have far reaching significance to the fatigue analyst in the establishment of fatigue test programs (from coupon to full scale), in the fatigue life prediction, and assessment of in-service cracking events. These events (overloads and periods of sustained loading) do occur in service and during fatigue testing and must be considered in any realistic assessment of structural fatigue life.

The research reported here is a summary of a multiphase, in-depth study of these time dependent changes in notch stress and notch strain and their influence on fatigue life predictions. The life shortening effects of the hold periods, illustrated in Table 1, were considered significant enough to warrant the further experimental study and analytical modeling for inclusion in the hysteresis fatigue analysis methodology. Also, no known prior research had been conducted in this specific area except that reported in Refs *6* and *7*. Initially, the program included fatigue tests and strain measurements on a super-scale test specimen at a central circular hole. Although this phase of the program provided comparative fatigue data for different load-time test sequences, it did not provide sufficient constitutive data to model the creep and stress relaxation. Additional tests were then conducted utilizing simple coupons and a unique simplified stress concentration specimen (SSC) to collect first creep and then stress relaxation and creep data. Finally, the constitutive data were used to formulate a creep and stress relaxation model that was incorporated into an existing hysteresis analysis model for fatigue life prediction.

Subsequent paragraphs discuss each phase of the experimental program and include a discussion of the fatigue analysis predictions using the hysteresis analysis model. Additional data and a detailed discussion of the research are included in Refs *8* and *9*.

Experimental Procedures

General Test Methods

Three different types of tests were performed during the experimental evaluations; namely, super-scale, single-bar coupon, and three-bar simplified stress concentration tests. All testing was performed in modern electrohydraulic servo-controlled test systems manufactured by MTS Systems Corporation. Each test system was interfaced to a digital computer that was used to command the different profiles, monitor loads and strains, and perform fail-safe functions. Additionally, the computer was used to store, reduce, tabulate, and plot data in a reportable format. The data collection, reduction, and display functions operated in near real time as the test progressed. The heart of each system was a PDP-11 computer and a modified BASIC programming language that was interactive. Inputs and outputs were managed through a teletype terminal and CRT supported by a hard-copy unit.

A user program was written in BASIC for each different test type, and each program contained options to accomodate the different profiles required. The super-scale tests were performed under load control, and outputs from the load and strain transducers were recorded at programmed time intervals throughout the tests. The time intervals were controlled by a programmable clock that resulted in precise load-strain-time history data.

The coupon and three-bar SSC tests were also performed under load control; however, the test system computer program was written so that loading was reversed once a desired value of strain was reached during the initial tensile loading. For the SSC tests, the load reversal was based on strain in the center bar. All subsequent events in the profiles were applied under unconditional load control. Coupon strains were measured using an extensometer. Strains for the three bar SSC tests were measured using an extensometer on the center bar and one outer bar, and strain gages on the other outer bar. (As was done for the super-scale tests, load and strain data were recorded at programmed time intervals throughout the tests.)

Evidence for Cyclic Dependent Behavior

A multiphase analytical and experimental program was initiated to determine if meaningful data could be measured to quantify the stress-strain time history and to develop an analytical model to predict time to crack initiation. In the first phase of the experimental program, attempts were made to measure strain inside a 50.8 mm (2.0 in.) diameter hole in a "super-scale" test specimen utilizing a mechanical transducer. The test specimen and strain transducer are illustrated in Fig. 1. The transducer is a Lockheed modification to that described in Ref *10* and is designed such that only extensional strain in the direction of loading is recorded. The gage length is approximately 1.78 mm (0.07 in.). All specimens were fabricated from 7075-T6511 aluminum plate.

Thirty-two different test sequences were evaluated during this phase of the study. The sequences, as illustrated in Table 2 include overloads,

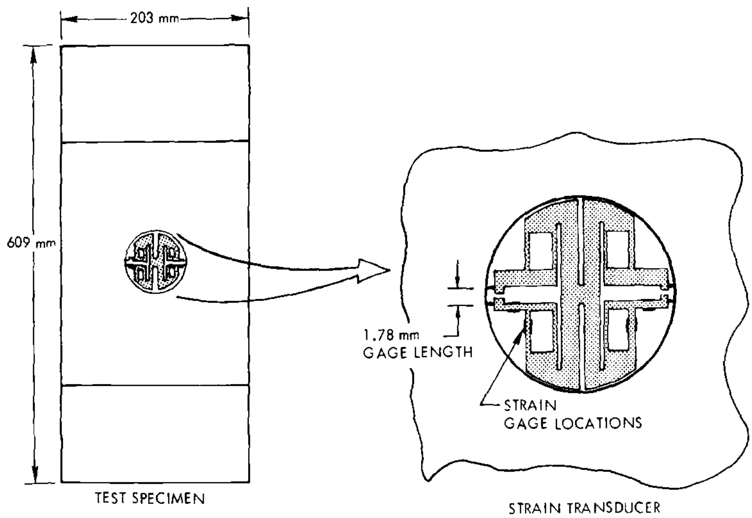

FIG. 1—*Super-scale test specimen and strain transducer.*

TABLE 2—*Super-scale test sequence definition and fatigue life data.*

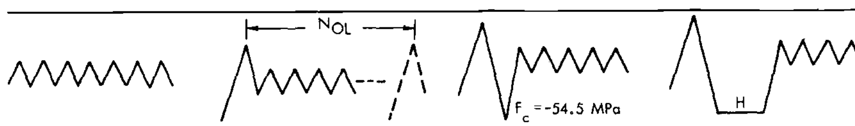

A Sequence Type	B Cycles to Overload, N_{OL} ~ Cycles × 10^{-3}	C Hold Period, H ~ hours	D Crack Initiation, Cycles × 10^{-3}
1A	...	...	48
1B	15	...	2000 NF[a]
2B	1	...	1000
1C	15	...	712
2C	1	...	309
3C	1	...	286
1D	15	24	141
2D	15	1	337
3D	1	24	101
4D	30	24	215
5D	...	24	80

[a] NF = no failure.

underloads, and sustained load hold periods combined with constant amplitude load cycles. The overload in each case is 326.2 MPa (47.3 ksi), net section stress. This tensile stress was selected to assure plasticity at the stress concentration and a residual stress (compression in most cases) upon unloading. Various compression stresses were evaluated, ranging from zero to −224 MPa (−32.5 ksi); however, the data illustrated in

Table 2 are all for −54.5 MPa (−7.9 ksi). Data for other compression stress levels are similar and are reported in Refs *8* and *9*. The test sequences included initial overloads only as well as periodic overloads and overload/underload combinations. The cyclic periods between overloads (N_{OL}) included 1-, 15-, and 30-thousand cycles of constant amplitude cycling. In all cases, the constant amplitude cycling was done at a mean stress of 103.4 MPa (15 ksi) and a 68.95 MPa (10 ksi) alternating stress. Compression load hold periods (H) in Sequence D were 1 and 24 h.

A comparison of the cycles to crack initiation illustrates vividly the effects of overload/underload combinations and the life-shortening effects of compression load hold periods. For example, comparing Sequence 1 for each of the four Sequence Types (A-D), the baseline specimen life is increased from 48 000 cycles to greater than 2 000 000 cycles with the application of the overload every 15 000 cycles. With the underload applied immediately following the overloads, this life is reduced to 712 000 cycles; but, when 24-h sustained load hold periods are included, the life is reduced to only 141 000 cycles. This is only slightly greater than the constant amplitude baseline specimen life.

The most significant result from this data sample is the life shortening effects of the sustained load hold periods. The hold period in any combination with an overload or underload will affect the residual stress at the stress concentration and negate the beneficial life-lengthening plasticity effects.

Notch Strain Behavior

In addition to the comparative fatigue life data just discussed, a primary objective of the super-scale specimen tests was to determine if meaningful strain changes could be measured at the stress concentration during the sustained load hold periods. To accomplish this objective, the strain transducer and strain gages were used to measure strain and strain changes during the various test sequences in Table 2. A typical example of this data is illustrated in Fig. 2. These data definitely confirm that creep is taking place immediately adjacent to the stress concentration during the hold period and, for this illustrative example, the strain change inside the hole (transducer) and immediately adjacent to the hole (Strain Gage 1) are of the opposite sense.

The super-scale test specimen and strain transducer were adequate for initial studies to measure strain changes (creep) in the load induced plastic zone during these hold periods. These changes, although not large, are apparently sufficient to affect the changes seen in specimen life. The effect of the measured strain changes can be illustrated by the data shown in Fig. 3*a*. These data are from Sequence C tests for different values of under-

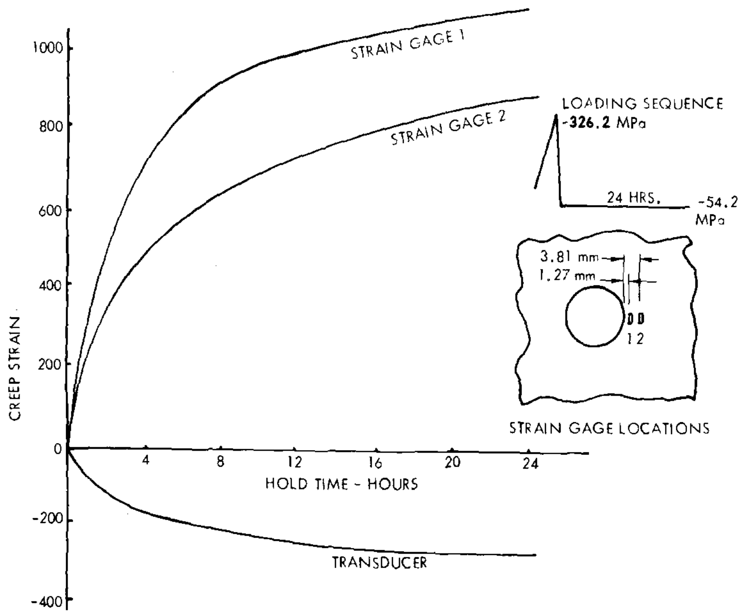

FIG. 2—*Super-scale specimen creep data.*

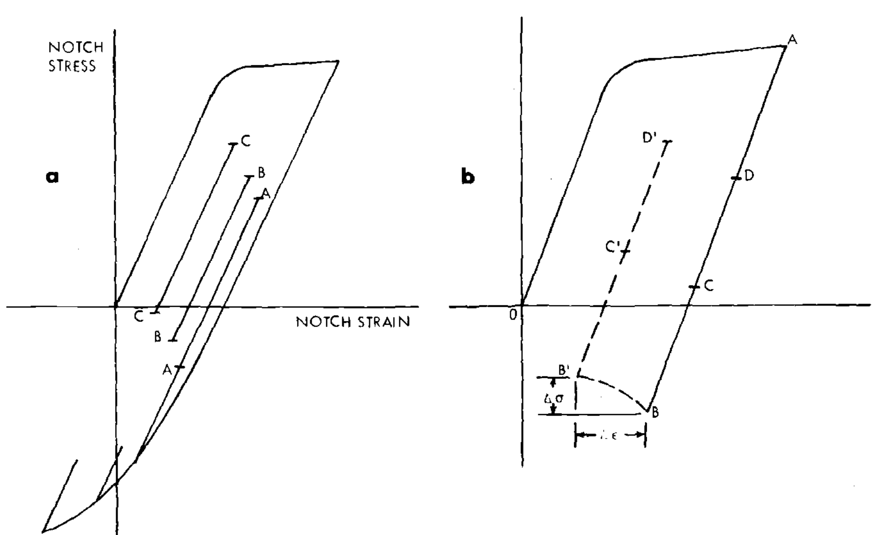

FIG. 3—*Hypothesis of time dependent stress-strain changes.* (a) *underload magnitude effects and* (b) *creep and stress relaxation.*

load but do not include hold periods; however, the cyclic limits and times to failure tend to illustrate the time-dependent changes in the plastic zone. For example, cycling between Limits A-A, as shown, is similar to a sequence with no underload. Cycling between B-B is typical of Sequence B, and Limits C-C tend to show the effect of the hold time or Sequence D. Note that as the cyclic limits change from A to C there is both a change in stress and strain. From this observation of fatigue life test data, it was hypothesized that there is a complex, time dependent relationship between stress and strain that tends to significantly affect time to crack initiation or fatigue life in this case. This hypothesis is illustrated in Fig. *3b*. In this figure, both a time dependent creep, $\Delta\epsilon$, and a time dependent stress relaxation, $\Delta\sigma$, are shown.

So far, the experiments discussed have only shown the comparative fatigue results, the life-shortening effects of the hold periods, and have given a qualitative assessment of the existence of the strain changes at the stress concentration. The impact of the hold period may be very significant to the analyst in fatigue life predictions; however, additional data are necessary to model the stress-strain hypothesis shown in Fig. *3b*.

Coupon Creep Tests

The super-scale tests did provide comparative fatigue data but were not sufficient to completely quantify the stress relaxation and creep data necessary to formulate the hysteresis analysis model. Additional tests were then conducted utilizing coupon specimens to collect constitutive data necessary for the analysis model formulation and to verify the hypothesis in Fig. 3.

Simple unnotched coupon specimens were tested under both strain and load control to develop constitutive data for creep and stress relaxation under sustained load conditions. Twelve coupon specimens were tested and the loading conditions, along with the data recorded during the hold periods, are identified in Table 3. A schematic of the loading conditions is illustrated in the sketch in the table. Tests 1 through 4 were run under automatic load control with the strain data recorded from extensometers attached to the specimen. Tests 5 and 6 were run in a strain control mode using feedback from the extensometer to automatically control the tests. All tests were run at laboratory ambient conditions. The data shown in the table are the average of two tests.

Each specimen was initially loaded to a positive strain of 0.016 (sufficient to produce plastic deformation) and then unloaded, and reloaded into compression for three periods of sustained loading. The first sustained load hold was 24 h. This was followed by two, 1-h periods; the first at a different stress/strain and the second at the initial stress/strain loading.

TABLE 3—*Simple bar creep/stress relaxation data.*

Sequence Number	Hold Period Definition: Applied Stress or Strain		Hold Period Definition: Time, h	Measured Creep Strain or Stress Relaxation	
1	−344.7 MPa	(−50 ksi)	24	1070	
	−455.1	(−66 ksi)	1	700	
	−344.7		1	0	
2	−455.1 MPa		24	2200	
	−344.7		1	0	
	−455.1		1	0	
3	−275.8 MPa	(−40 ksi)	24	625	
	−455.1		1	1450	
	−275.8		1	0	
4	−241.3 MPa	(−35 ksi)	24	340	
	−344.7		1	95	
	−241.3		1	0	
5	0.0025	μ strain	24	38.96 MPa	(5.65 ksi)
	−0.0030		1	47.57	(6.90 ksi)
	0.0025		1	6.89	(1.0 ksi)
6	−0.0040	μ strain	24	73.08 MPa	(10.6 ksi)
	−0.0010		1	3.45	(0.5 ksi)
	−0.0040		1	1.73	(0.25 ksi)

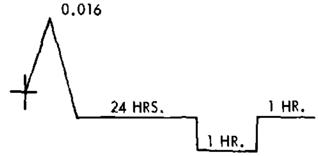

LOADING SEQUENCE

The variation in load in each sequence was to evaluate the "memory" of prior loadings and any subsequent effects. The data shown in the table are the total strain or stress measured for each condition. A typical stress-strain curve (for Sequence 3) is illustrated in Fig. 4. During the initial hold period at −275.8 MPa (−40 ksi), a total strain change of 650 μ strain was recorded. Approximately 1600 μ strain occurred at the −455.1 MPa (−66 ksi) level during the second hold period, but then no change was recorded during the third hold period. Figure 5 illustrates the strain time history for this sequence. In each sequence, the "primary" creep/relaxation accounts for the largest percentage of the total measured. The stress relaxation time histories (Sequences 5 and 6) are similar to the data in Fig. 5. Approximately 80 percent of the total strain or stress change occurs during the first hour of the sustained load hold period.

There appears to be a limiting value of creep that occurs, at least at stress levels above −275.8 MPa (−40 ksi). For example, in Sequences 1 through 3, the maximum strain change averages 2000 μ strain. There is some variation from test to test that may be attributed to basic differences

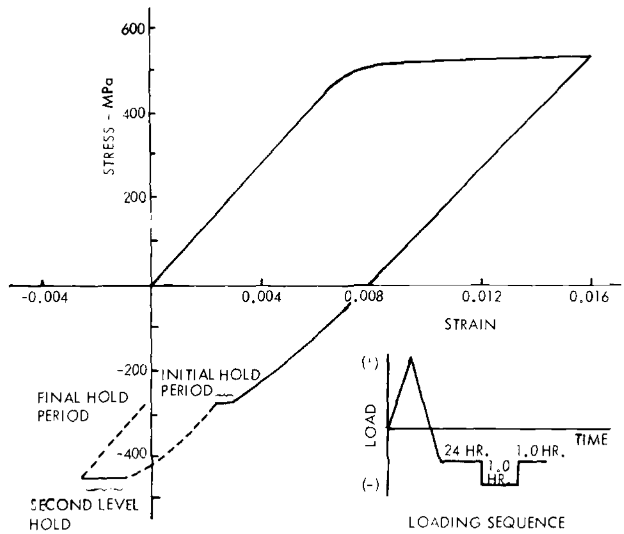

FIG. 4—*Stress-strain curve for a coupon specimen.*

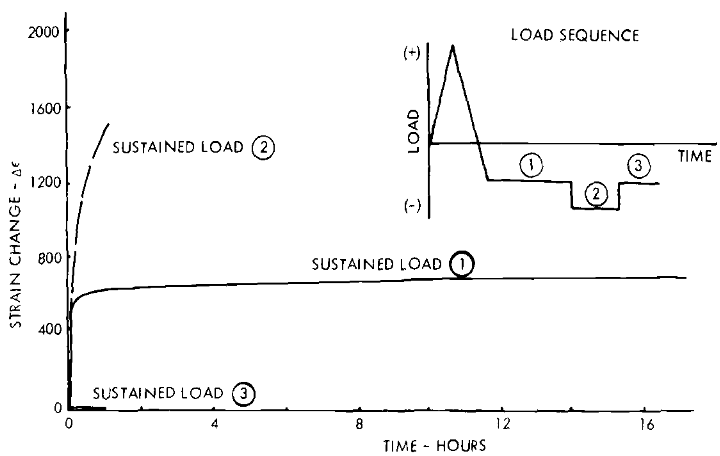

FIG. 5—*Coupon specimen creep data.*

in specimen and material. The sequence of applied stress does not affect the total strain change measured. In Sequence 2, for example, slightly over 2000 μ strain was measured at the initial 445.1 MPa (-66 ksi) hold period, while approximately the same total was measured in Sequence 3 at two stress levels. A similar trend is shown in Sequence 1, although the totals are somewhat less. The creep and stress relaxation seen in these tests does not appear to be sequence dependent. That is, by increasing load, strain, and stress, changes continue to increase in the classical "primary-secondary" sense. On returning to a lower loading, there is little or no change in the measured data.

It should be emphasized here that the stress and strain changes were measured from these specimens at room temperature. It is significant in that creep in metal alloys is generally associated with higher temperature regions and is not generally considered in the fatigue analysis of aircraft structures where high temperature is not present. In many instances, this creep and stress relaxation, if it occurs, may be a contributing factor to the so-called "early" fatigue failures and should possibly be included in the initial fatigue life assessment.

Notch Stress Determination Using Simplified Stress Concentration Specimens

In all coupon and super-scale testing conducted here, strain data were collected with reasonable ease. However, stress can not be measured directly, specifically the change in stress of interest in these experiments. Since it has been hypothesized that the time-dependent effects on life would be a complex function of both stress and strain, it was of prime importance to devise an experiment to measure stress and stress change. Burski [*11*] had previously used a unique three-member specimen to evaluate residual stress relaxation as a function of cyclic loading. This specimen was used here to evaluate the time-dependent changes in stress during the periods of sustained loading.

This simplified stress concentration (SSC) specimen is illustrated in Fig. 6. The specimen behaves like a notched coupon in that it will have plastic and elastic regions existing simultaneously when loaded axially. It is designed so that the center bar can yield while the two outer bars remain elastic. For this experiment, the specimen geometry is such that the elastic stress concentration is the same as the center notched super-scale specimens tested previously; that is, approximately 2.43.

In the analysis of this specimen, it is assumed that the elongation is the same in all three bars when an external load is applied. This allows for the calculation of the inelastic stresses in the center bar when only the elastic stresses in the two outer bars and the applied load are known. A schematic representation of the specimen, including a definition of terms used here, is illustrated in Fig. 6.

Stresses σ_1 and σ_2 were calculated directly from the measured elastic strain data in the two outer bars. Where multiple measurements were made on any single bar, the average values were used. These outer bar stresses were then converted to loads (P_1 and P_2) and the center bar load calculated from

$$P_3 = P_T - (P_1 + P_2).$$

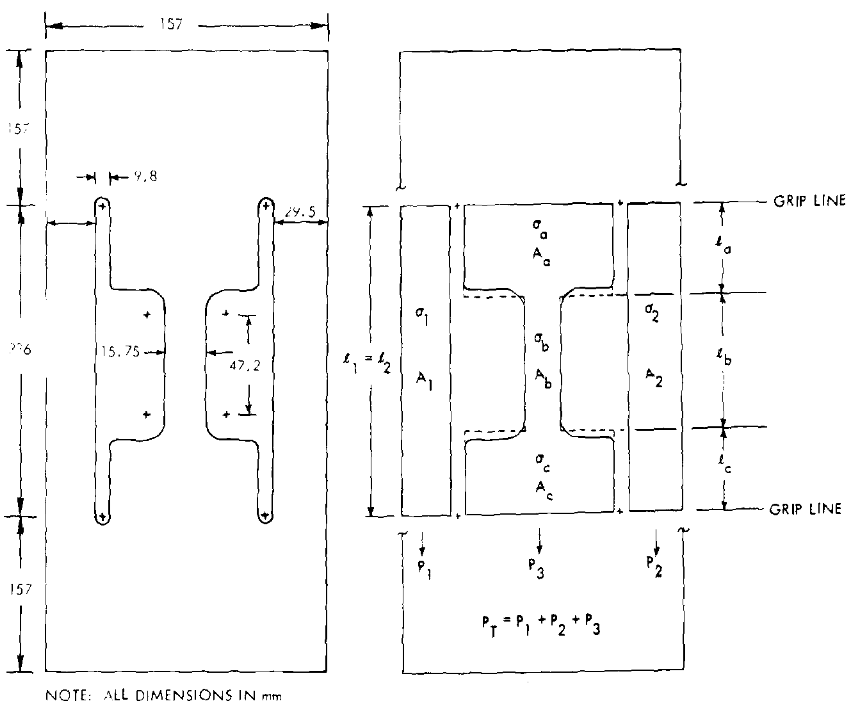

FIG. 6—*Simplified stress concentration specimen.*

This load was then converted to stress in the center bar by dividing by the center bar area, A_3. The calculated center bar stress and changes in this stress during hold periods are then plotted versus strain and strain changes measured during the loading sequences.

A stress-strain curve for the center bar of the SSC specimen is illustrated in Fig. 7. The test sequence included two loading-unloading cycles, each followed by a 24-h sustained load hold period. Both stress relaxation and creep were evident during the hold periods, as illustrated. These data support the hypothesis discussed earlier and illustrated in Fig. 3. Stress relaxation, $\Delta\sigma$, and creep, $\Delta\epsilon$, for both hold periods are shown in Fig. 8. Additional test sequences with multiple hold periods (a maximum of ten 1-h periods were included) indicate that both the stress relaxation and creep may tend to reach a stable condition beyond which changes are minimal.

The SSC specimen has provided a unique experimental tool for quantifying inelastic stress and in mapping both the residual stress changes and strain changes during sustained load hold periods and during cyclic loadings. The tests conducted here were considered highly successful as far as providing insight into the relationship between creep and stress relaxation.

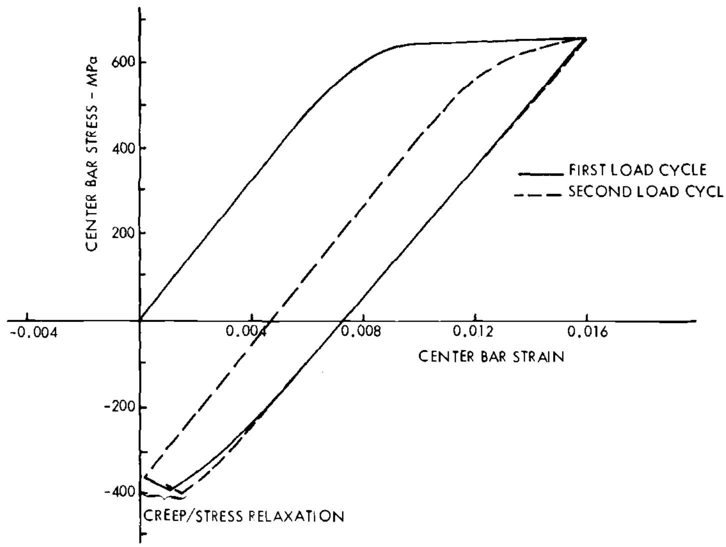

FIG. 7—*Simplified stress concentration specimen—center bar stress-strain data.*

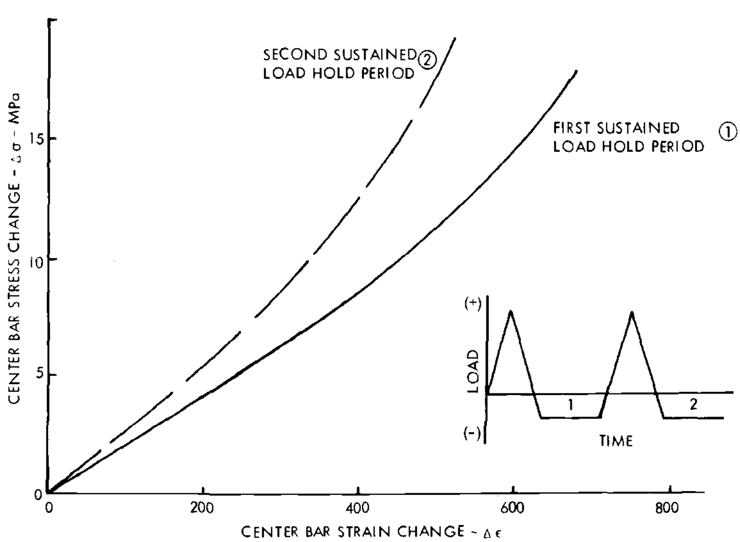

FIG. 8—*Simplified stress concentration specimen creep and stress relaxation.*

These tests provided, for the first time, constitutive data that could be used to empirically model creep and stress relaxation for inclusion in a hysteresis fatigue analysis program.

The coupon, super-scale, and simplified stress concentration test programs are discussed in more detail in Refs *8* and *9*.

Incorporation of Data into Fatigue Analysis

The final section of this paper discusses the use of the experimental data in a hysteresis analysis computer program and correlation studies, using this program, for several coupon, component, and full scale fatigue tests. The data from the coupon and simplified stress concentration specimen tests have been used to formulate a creep/stress relaxation module for inclusion in a hysteresis fatigue analysis. This analysis program contains the following elements: (1) Notch stress-notch strain algorithm: Locus curves, branch curves, and Neuber analysis (modified); (2) material hardening or softening; (3) creep/stress relaxation, and (4) fatigue damage computation.

A sample output from the computer program is included in Fig. 9 and illustrates an example of the creep/stress relaxation prediction capabilities. This analysis program has been used to correlate various coupon, component, and full-scale test results, including the super-scale specimen tests discussed earlier, to compare actual and predicted fatigue life. Table 4 illustrates the comparison between the test life and analytical predictions

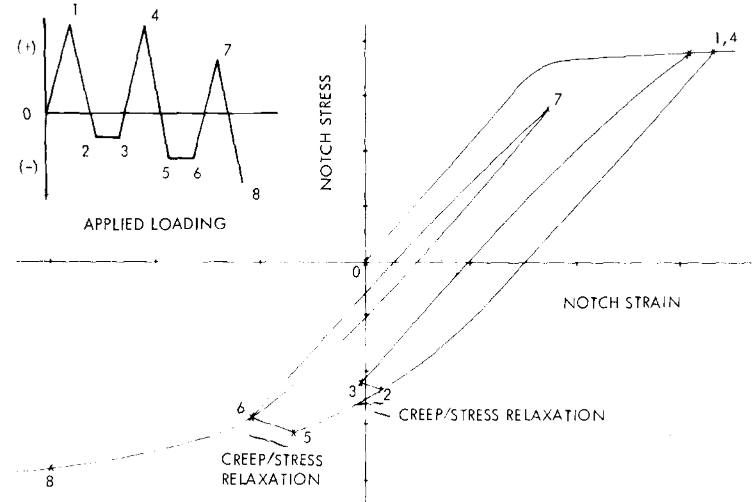

FIG. 9—*Example of creep and stress relaxation from hysteresis analysis computer program.*

TABLE 4—*Analysis and experimental results for super-scale specimen test sequences.*

	Test Sequence Definition	Test Life, cycles	Analytical life, $\Sigma\, n/N$	Analytical Life Hysteresis
1	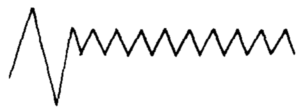	286 800	97 955	526 900
2	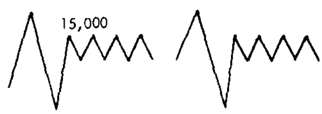	715 000	97 804	615 800
3		308 000	96 500	364 400
4	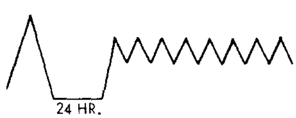	80 018	97 955	450 500
5	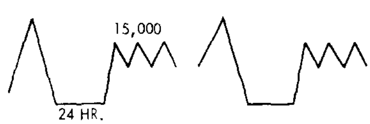	141 000	97 804	431 100
6	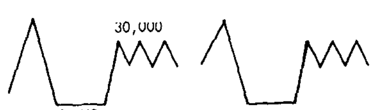	214 546	97 765	440 500

using both a linear analysis and the hysteresis analysis for six super-scale specimen test sequences. Test life in this table is defined as total specimen rupture since measured crack growth in these tests comprised only 5 percent of the total life.

The hysteresis analysis predictions, in most cases, reflect the residual stress accountability associated with the applied loading sequence, whereas the linear analysis (Miner) does not. Also, these predictions reflect the life-shortening effects associated with the sustained load hold periods; that is, compare Sequences 2 and 4. The linear analysis cannot discriminate among the different loading conditions and predicts approximately the same life regardless of the applied loading.

Table 5 presents the results of additional correlation studies for more complex fatigue loading spectra than were used in the super-scale testing in Table 4. Coupon, component, and full-scale test results were evaluated using both the linear damage model and the sequence accountable hysteresis fatigue analysis program. The test life for the four individual tests shown was normalized for comparison with individual predictions only. A very simple three-flight spectrum with overloads and sustained load hold periods was used for the coupon test. Both the linear and hysteresis analysis methods predict a life reasonably close to the test data. A much more complex spectrum was used in the component testing. This spectrum included 23 different flight definitions randomly applied in this flight-by-flight spectrum. There was no spectrum truncation and 4.6×10^6 cycles were included in each lifetime. Correlation here was excellent.

Two studies were done on a wing cracking area of a full-scale transport aircraft test article. In one test, limit loads were applied periodically during fatigue loading, which introduced residual stresses in the structure. The linear analysis does not account for these residual stresses and predicts a life five-times as long as that demonstrated. The hysteresis analysis predictions are much closer to the test demonstrated life. A final correlation study considered load dumps that unfortunately occur during fatigue testing. Test 4 in Table 5 is identical to Test 3 except that the history of loading dumps was reconstructed and sequenced with the load spectrum. As can be seen from the analysis, the correlation between actual and predicted life is excellent.

This kind of a sequence accountable, hysteresis analysis with capability to assess creep and stress relaxation could be an invaluable tool in evaluating fatigue test results and in-service cracking events.

Conclusions

1. Overloads and underloads induce a plastic zone around a stress concentration. The plasticity induced by overloads results in a life lengthening effect in structures. Underloads can reduce life lengthening effects produced by overloads.

TABLE 5—*Evaluation of hysteresis analysis.*

	Test Life	Linear Analysis	Hysteresis Analysis
1 Coupon simple $F \times F$	1.0	0.51	1.43
2 Component complex $F \times F$	1.0	8.0	0.81
3 Full-scale block spectrum with limit loads	1.0	5.0	2.0
4 Full-scale block spectrum with no load dumps	1.0	5.0	2.0
with load dumps	1.0	5.0	0.77

2. Creep and stress relaxation occur in this plastic zone at the stress concentration during sustained load hold periods. This creep and relaxation is a complex function of both notch stress and notch strain.

3. The cyclic period between overload-underload combinations has a significant impact on specimen life. Multiple overload-underload combinations result in a longer life than a single application of an overload-underload.

4. There is evidence of a cyclic dependent change in mean stress that may affect specimen life.

5. The loading events included in the test sequences do occur in service and may affect component and full-scale tests, test spectra development, and interpretation of data. These effects may be reflected in both crack initiation and crack growth data.

Acknowledgments

This work was sponsored in part by the Independent Research and Development program of the Lockheed-Georgia Company and under contract from the Air Force Flight Dynamics Laboratory, Wright-Patterson Air Force Base, Ohio, under Contract F33615-75-C-3078.

References

[*1*] Topper, T. H. et al, "Cumulative Fatigue Damage Under Cyclic Strain Control," *Journal of Materials*, Vol. 4, No. 1, March 1969, pp. 189–199.

[*2*] Kirkby, W. T., "*Some Effects of Change in Spectrum Severity and Shape or Fatigue Behavior Under Random Loading,*" Advisory Group for Aerospace Research and Development, Symposium on Random Load Fatigue, AGARD CP 118, Lyngby, Denmark, 1972.

[*3*] Impellizzeri, L. F. in *Effects of Environment and Complex Load History or Fatigue Life, ASTM STP 462,* American Society for Testing and Materials, 1970, pp. 40–68.

[*4*] Potter, J. M. in *Cyclic Stress-Strain Behavior—Analysis, Experimentation and Failure Prediction, ASTM STP 519,* American Society for Testing and Materials, 1973, pp. 109–132.

[*5*] Rotvel, F., "*On Residual Stresses During Random Load Fatigue,*" Advisory Group for Aerospace Research and Development, Symposium on Random Load Fatigue, AGARD CP 118, Lyngby, Denmark, 1972.

[*6*] Neulieb, R. L. et al, "Load-Time Dependent Relaxation of Residual Stresses," *Journal of Aircraft,* Vol. 9, No. 12, Dec. 1972.

[*7*] Carroll, J. R., "Time Dependent Residual Stress Relaxation in Low Load Transfer Joints," Lockheed Report SMN 388, 1975.

[*8*] Carroll, J. R. et al, "Investigation of Stress-Strain History Modeling at Stress Risers, Phase I," AFFDL-TR-76-150, Air Force Flight Dynamics Laboratory, June 1977.

[*9*] Carroll, J. R. et al, "Investigation of Stress-Strain History Modeling at Stress Risers, II," AFFDL-TR-78-167, Air Force Flight Dynamics Laboratory, Dec. 1978.

[*10*] Awards Abstract, "Self Supporting Strain Transducer," Case LAR 11263-1, National Aeronautics and Space Administration, Washington, D.C., filing date 23 May 1974.

[*11*] Burski, M. L., "The Influence of Cyclic Loading on Residual Stress Relaxation," thesis presented to the School of Engineering of the Air Force Institute of Technology, Dec. 1975.

R. J. Bucci,[1] A. B. Thakker,[2] T. H. Sanders,[3] R. R. Sawtell,[4] and J. T. Staley[5]

Ranking 7XXX Aluminum Alloy Fatigue Crack Growth Resistance Under Constant Amplitude and Spectrum Loading

REFERENCE: Bucci, R. J., Thakker, A. B., Sanders, T. H., Sawtell, R. R., and Staley, J. T., **"Ranking 7XXX Aluminum Alloy Fatigue Crack Growth Resistance Under Constant Amplitude and Spectrum Loading,"** *Effect of Load Spectrum Variables on Fatigue Crack Initiation and Propagation, ASTM STP 714,* D. F. Bryan and J. M. Potter, Eds., American Society for Testing and Materials, 1980, pp. 41–78.

ABSTRACT: Fatigue crack growth (FCG) experiments were conducted on controlled variations of Type 7075 and 7050 aluminum alloys. Alloy FCG resistance was ranked under constant amplitude and simple variable amplitude load spectra. Fracture mechanics and fractographic approaches were used to interpret causes for variation in ranking of 7XXX aluminum alloy FCG resistance with loading conditions. The interpretation is built around clarification of a controlling FCG mechanism that is dependent upon interaction of microstructure and load history. This clarification represents a necessary first step toward knowing which microstructure or which design (test) procedure is optimum for a particular class of application, for example, fighter as opposed to bomber or transport aircraft.

KEY WORDS: aluminum alloys, fatigue (materials), crack growth, aircraft, material selection, test methods, spectrum loading, fracture mechanics, fractography, microstructures, crack propagation

This investigation deals with the ranking of fatigue crack growth (FCG) resistance of high-strength aluminum-zinc-magnesium-copper aircraft alloys

[1]Staff engineer, Engineering Properties and Design Division, Alcoa Laboratories, Alcoa Center, Pa. 15069

[2]Pratt and Whitney, Aircraft Division, West Palm Beach, Fla. 33402; formerly, Alcoa Laboratories.

[3]Fatigue and Fracture Research Laboratory, Georgia Institute of Technology, Atlanta, Ga.; formerly, Alcoa Laboratories.

[4]Alcoa Davenport Works, Davenport, Iowa.

[5]Alloy Technology Division, Alcoa Laboratories, Alcoa Center, Pa. 15069.

(7075, 7475, 7050, and 7010) in peak strength (T6) and overaged (T7) tempers. Rating constant amplitude FCG resistance of materials of this type has been addressed in several recent investigations [*1–5*].[6] Principal conclusions drawn from these results are:

1. At intermediate FCG rates (generally characterized by linear log *da/dN* versus log ΔK relationship), propagation resistance of 7050, 7075, and 7475 in comparable tempers is similar in dry environment. In ambient or moist atmospheres, or in aqueous or salt environments, intermediate FCG rates of 7050 are generally slower (by about 50 percent) than those of 7X75 alloys in comparable tempers.
2. Overaging from peak strength (T6) tempers to T7-type tempers and increasing copper from about 1 to 2.3 percent increases FCG resistance by reducing degradation by environment.
3. Improving fracture toughness by increasing alloy purity increases FCG resistance at high ΔK. Marginal improvements are also apparent at intermediate ΔK.

Constant amplitude loading conditions are used to describe steady-state characteristics of FCG behavior. Most metallurgical studies on FCG processes have been confined to this loading condition. The typical load history encountered in service, however, is variable amplitude or spectrum loading rather than constant amplitude loading. Variable amplitude loading produces a transient material response that is not measured in the constant amplitude test. Several investigations, for example, have demonstrated that high tensile overloads produce significant FCG delay during low magnitude stress cycles following the overload [*6, 7*]. The characteristics of FCG retardation are highly dependent on load history. The magnitude, number, and frequency of occurrence of the overload with respect to more numerous cycles at lower stress amplitude are, perhaps, the most important loading parameters affecting FCG retardation [*6–8*].

Independent investigations, for example Figs. 1 and 2 and data summarized in Ref *8*, indicate that under simulated flight loading conditions, FCG performance of 7050 is most often better than that of 7075 and 7475 alloys tested under similar conditions. However, the superior performance of 7050 under simulated flight spectra cannot be generalized as indicated by results shown in Fig. 3 [*5*]. In the latter investigation, FCG resistance of 7075 was notably better than that of 7050 at comparable temper when both alloys were subjected to a severe flight-by-flight fighter spectrum. The identical alloys, however, when subjected to constant-amplitude loading, indicated that 7050 FCG resistance was superior to that of 7075.

From the foregoing example, it is evident that ranking of alloy FCG resistance based on constant amplitude results may not always be reliable. Available data also indicate that even when qualitative ranking of spectrum

[6]The italic numbers in brackets refer to the list of references appended to this paper.

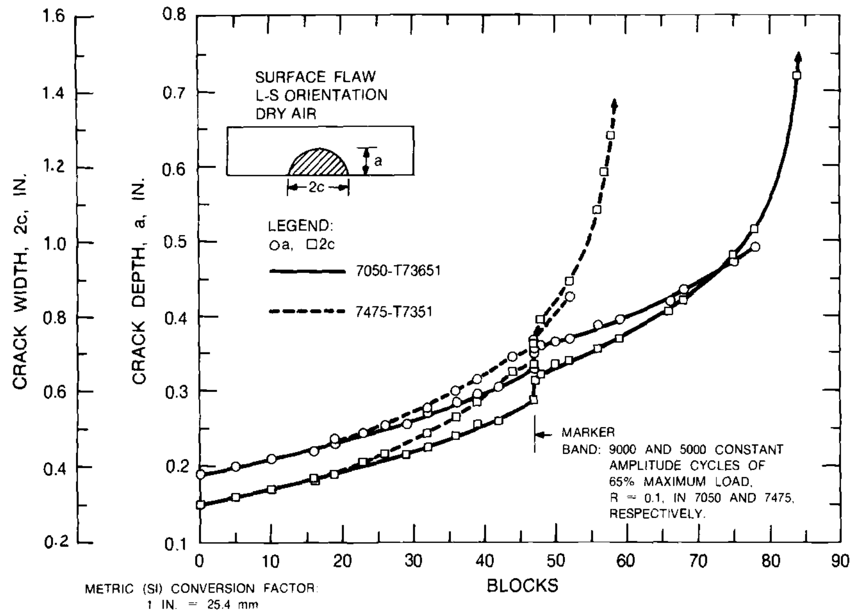

FIG. 1—*Crack size versus blocks to failure for part-through crack specimens of aluminum alloys 7050-T73651 and 7475-T7351 subjected to eight load-level test spectrum* [4].

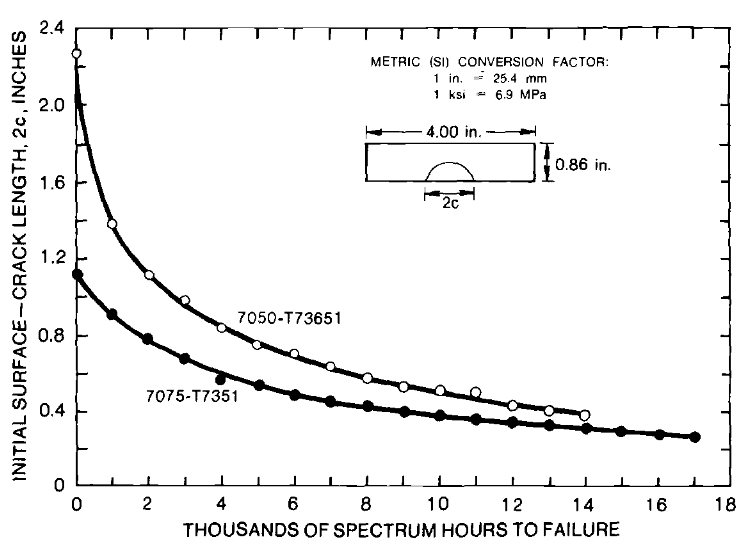

FIG. 2—*Flight spectrum hours required for failure of 7050 and 7075 aluminum alloy part-through crack specimens tested in laboratory air at 326.4 MPa (36 ksi) design level stress.* (Courtesy McDonnell Aircraft Co.)

MECHANICAL PROPERTIES

ALLOY & TEMPER	σ_{ys}(KSI)	σ_{UTS}(KSI)	K_{IC}(KSI$\sqrt{\text{IN.}}$)
7049-T73	71	78	28
7050-T736	67	75	40
7075-T736	63	76	42

METRIC (SI) CONVERSION FACTORS: 1 KSI = 6.9 MPa
1 KSI $\sqrt{\text{IN.}}$ = 1.1 MPa$\sqrt{\text{m}}$
1 IN. = 25.4 mm

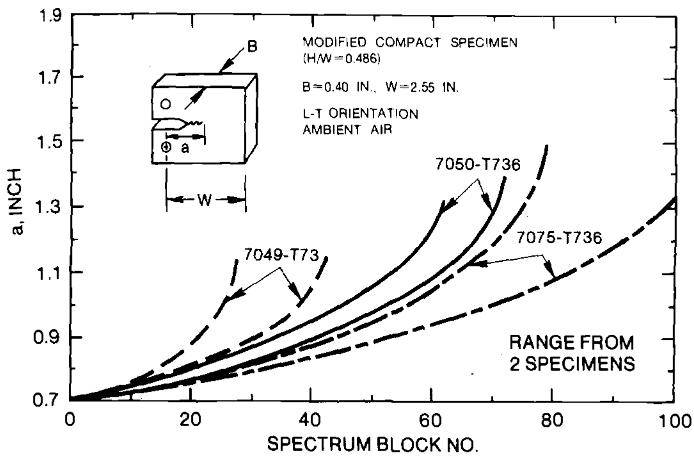

FIG. 3—*Comparison of spectrum (typical of military fighter wing attach area) fatigue crack growth resistance of aluminum forging alloys* [5].

and constant amplitude alloy behavior agree, quantitative differences in spectrum performance cannot always be accurately predicted from constant amplitude results, for example, Ref *8*.

The objective of this paper is to: (*a*) explain how alloy strength, microstructure, and stress history interact to affect ranking of alloy FCG resistance; (*b*) characterize FCG retardation behavior of 7075, 7050, 7475, and 7010 aluminum alloys; and (*c*) assess implication of the foregoing on experimental and analytical procedures for evaluating FCG resistance of materials.

The understanding developed is largely based on work performed under ALCOA contract to the U.S. Naval Air Systems Command [*9*].

Materials

Alloys 7075 and 7050 are high-strength, precipitation-hardening aluminum alloys containing three types of second-phase particles namely, secondary intermetallics, dispersoids, and metastable precipitates) that influence mechanical properties, such as toughness and strength [*10–12*].

Secondary Intermetallics

Secondary Intermetallics (~ 1 to 30 μm) are the largest of these particles. They form during solidification by the combination of impurity elements iron and silicone with aluminum and solute atoms. These coarse intermetallic particles do not contribute to strength, but, because they are brittle, they fracture or separate from the matrix at high local strains [*10*]. Decreasing volume fraction of these particles increases fracture toughness and resistance to constant amplitude FCG at high stress intensity factor range, ΔK, [*1,2,10–12*]. The newer alloys, that is, 7475 and 7050, fabricated with increased purity (lower iron and silicone) offer significant improvement in fracture toughness over their older counterpart, 7075, at equivalent strength [*10,13*]. In particular, 7475 offers the highest toughness-strength combination attainable in a commercial 7XXX alloy.

Dispersoid

Dispersoid particles (0.02 to 0.3 μm) form by solid-state precipitation of chromium and zirconium at temperatures above about 425°C. Under monotonic tension loading, dispersoids decrease energy to propagate cracks by initiating microvoids that coalesce to link incipient cracks initiated at larger constituent particles [*10*]. Energy required to propagate a crack under monotonic tension loading increases as volume fraction decreases and as dispersoid spacing decreases. Dispersoid particles may influence strength, and hence toughness, indirectly because of their ability to suppress recrystallization in identically fabricated products. Constant amplitude FCG resistance shows no effect of dispersoids at intermediate ΔK. At high ΔK, observed variation in FCG resistance is attributed to the dispersoid's effect on toughness [*1,2,11,12*].

Metastable Precipitates

Metastable Precipitates (0.002 to 0.01 μm) are the smallest type second-phase particle, and they contain the major solute elements zinc, magnesium, and copper. Precipitates develop in uncontrolled manner during quenching or in a controlled manner during aging. The structure and composition of precipitates have a direct effect on strength and resistance to environment. Maximum strength occurs in the peak-aged T6 temper when the alloy has the greatest volume fraction of closely-spaced particles. In this case, dislocations caused by stressing tend to shear the particles. Overaging increases the size of the precipitates, and, at high stress, the larger particles tend to be looped by dislocations rather than sheared. Overaging to T7 type tempers increases toughness and resistances to exfoliation and stress corrosion with an accompanying reduction in strength [*10,13*]. Overaging also improves FCG resistance by increasing resistance to degradation by environment [*1,2,11–13*].

To evaluate the role of microstructure on spectrum FCG, eight variants of 7XXX type alloy compositions were selected, Table 1. These alloys provided a full factorial experiment of composition variables affecting make-up of second-phase particles known to influence mechanical properties and corro-

TABLE 1—*Remelt chemical analyses.*

	Composition, percent by weight							
Alloy Type[a]	Si	Fe	Cu	Zr	Cr	Mg[b]	Zn[c]	Ti
High-purity 7010	0.06	0.10	1.56	0.12	0.00	2.19	6.20	0.02
7010[d]	0.19	0.27	1.55	0.12	0.00	2.22	5.96	0.03
7475	0.06	0.11	1.46	0.00	0.21	2.09	5.90	0.02
7075	0.23	0.28	1.51	0.00	0.23	2.26	6.34	0.02
7050	0.07	0.11	2.10	0.13	0.00	2.16	6.16	0.02
Low-purity 7050	0.19	0.28	2.16	0.11	0.01	2.18	5.83	0.02
High-copper 7475	0.06	0.11	2.27	0.00	0.21	2.08	5.90	0.02
High-copper 7075	0.23	0.28	2.29	0.00	0.20	2.23	6.13	0.02

[a]For descriptive purposes alloys coded as shown.
[b]Magnesium content within allowable range for commercial 7075 and 7050.
[c]Zinc content near maximum for commercial 7075 and near nominal for commercial 7050.
[d]Falls within composition limits of European Alloy 7010.

sion resistance. These variables include high and low levels of iron and silicone bearing intermetallics, chromium versus zirconium dispersoids, and high and low copper variants of precipitate structure. Alloys were fabricated from laboratory-cast ingot to 6.5 mm (0.25 in.) plate in a T7 type temper. Heat treatment practices are given in Table 2. The target yield strength was 450 MPa (66 ksi), which is near nominal for commercial 7050-T73651 plate. Portions of 7075 and 7050 plate were also aged to T6, T76, and T73 type tempers. Longitudinal tensile properties and relative toughness for each alloy and temper combination investigated are given in Table 3. A listing of the alloy phases identified and their relative amounts is given in Table 4. Additional detail on alloy microstructure is given in Ref. *9*.

TABLE 2—*Heat treatments.*

Alloy Type[a]	Temper Type	Aging Practice
High-purity 7010	T7	24 h 121°C + 37 h 163°C
7010	T7	24 h 121°C + 24 h 163°C
7475	T7	24 h 121°C + 21 h 163°C
7075	T7	24 h 121°C + 12 h 163°C
7050	T7	24 h 121°C + 40 h 163°C
Low-purity 7050	T7	24 h 121°C + 32 h 163°C
High-copper 7475	T7	24 h 121°C + 18 h 163°C
High-copper 7075	T7	24 h 121°C + 24 h 163°C
7075	T6	24 h 121°C
7075	T76	24 h 121°C + 6 h 163°C
7075	T73	24 h 121°C + 24 h 163°C
7050	T6	100 h 121°C

[a]Solution heat-treatment—2 h 488°C, quench in water at room temperature, stretch 1½%.

TABLE 3—*Longitudinal mechanical properties of 6.4 mm (0.25 in.) 7XXX plate.*

Alloy Type and Temper	Tensile Strength		Yield Strength		Elongation in 51 mm (2 in.)		Unit Propagation Energy[b]	
	MPa	ksi	MPa	ksi	%	TrS/YS[a]	kJ/m^2	in. lb/in.^{2}
High-purity 7010-T7	517	75.0	454	65.9	13	1.45	105	595
7010-T7	490	71.1	435	63.1	11.5	1.28	66.5	380
7475-T7	505	73.2	441	64.0	13	1.38	89.5	510
7075-T7	505	73.2	454	65.8	11	1.16	49.0	280
7050-T7	511	74.1	440	63.8	14	1.46	115	645
Low-purity 7050-T7	496	71.9	435	63.1	12	1.29	67.5	385
High-copper 7475-T7	532	77.1	470	68.1	12	1.32	79.0	450
High-copper 7075-T7	505	73.3	446	64.7	11.5	1.19	47.5	270
7075-T6	558	81.0	530	76.9	9.5	1.02	35.0	200
7075-T76	546	79.2	507	73.6	11	1.16	49.0	280
7075-T73	484	70.2	417	60.5	12	1.24	46.0	260
7050-T6	612	88.7	570	82.7	12	1.19	95.5	545

[a]Tear strength/yield strength ratio correlates ability of material to resist fracture by development of plastic deformation at severe stress concentration. Increase in TrS/YS implies increase in notch toughness [*13*].

[b]Unit propagation energy (UPE) correlates with resistance to stable crack growth in thin sections, K_c. UPE increase implies increase in toughness [*13*].

Fatigue Crack Growth Tests

The test configuration employed for FCG work was the center crack tension (CCT) specimen shown in Fig. 4. Test environment was maintained at high relative humidity (RH >90 percent). Crack growth was monitored electronically by crack propagation gages with intermittent visual measurements to verify the data. Crack length versus cycles and FCG rates, *da/dN*, were determined from numerical analysis of the data. To ensure valid comparison

TABLE 4—*Secondary metallic and dispersoid phases identified by guinier-de Wolff X-ray diffraction.*

		Al_7Cu_2Fe	$Al_{12}Mg_2Cr$	Al_2CuMg	$(Fe,Cu)Al_6$
Alloy Type	Mg_2Si	β(Al-Cu-Fe)	*E*	*S*	α(Al-Cu-Fe)
High-purity 7010	small	small	...	...	...
7010	medium	medium	...	...	...
7475	small	small	medium	possible trace	possible trace
7075	medium	medium	medium	possible trace	trace
7050	small	small	...	...	...
Low-purity 7050	medium	medium	...	possible trace	...
High-copper 7475	small	small	medium	...	...
High-copper 7075	medium	medium	medium	possible trace	...

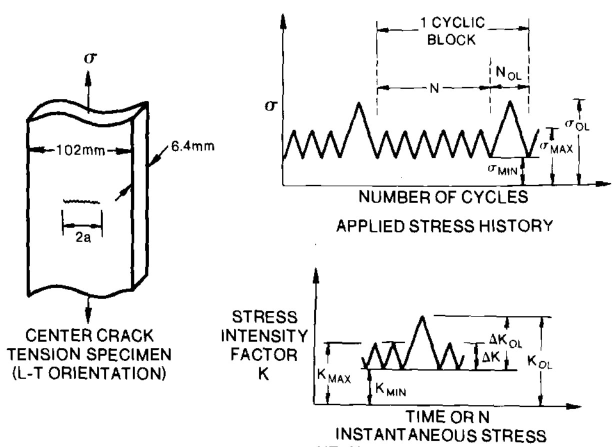

σ_{MAX} = 55.2 MPa, σ_{MIN} = 18.3 MPa

R = CONSTANT AMPLITUDE STRESS RATIO = $\sigma_{MIN}/\sigma_{MAX}$ = K_{MIN}/K_{MAX} = 1/3

OLR = OVERLOAD RATIO = σ_{OL}/σ_{MAX} = K_{OL}/K_{MAX}

N = NUMBER OF CONSTANT AMPLITUDE CYCLES

N_{OL} = NUMBER OF OVERLOAD CYCLES (=1)

OCR = OCCURRENCE RATIO = N_{OL}/N

NOTE: APPLIED STRESS HISTORY CONSTANT FOR DURATION OF TEST. NOMINAL K VALUES, THEREFORE, INCREASE WITH CRACK EXTENSION

FIG. 4—*Description of periodic single spike overload tests. (Note: applied stress history constant for duration of test. Nominal* K*-values, therefore, increase with crack extension.)*

between alloys, precrack and test procedures were controlled to be as identical as possible for a prescribed load history. Test results obtained from replicate tests of selected microstructures and loading conditions showed good reproducibility [*9*].

Each alloy composition was tested under constant amplitude and spectrum loading conditions. The basic load spectrum employed to evaluate sensitivity of microstructure-load interaction on FCG retardation was the periodic tensile spike overload spectrum shown in Fig. 4. Definition of terms and stress levels describing this spectrum are also given in Fig. 4. The applied loads of intermittent cycles between periodic overloads was equivalent to that employed in constant amplitude tests. The constant amplitude load cycles corresponded to a ΔK increase of about 6 to 16 MPa $\sqrt{m}$ over the usable crack length portion of the CCT specimen.

For initial screening tests, two tempers (T7 and T6) of 7075 and 7050 were selected. This selection allowed comparisons to be made at distinct levels of yield strength. Constant amplitude FCG rates were first obtained. An overload ratio (OLR) of 1.8 and occurrence ratio (OCR) of 1/4000 was the first combination of spectrum load parameters tested. Over the midrange of specimen crack length, this sequence was estimated to provide high interaction between successive overloads according to arguments of Mills and Hertzberg [*14*]. For direct comparison, additional tests were performed with OLR = 1.4, OCR = 1/4000, with OLR = 2.2, OCR = 1/4000, and with OLR = 1.8, OCR = 1/8000. Increasing magnitude of the overload was expected to increase FCG retardation and extend life. Either decreasing OLR or decreasing OCR was expected to reduce interaction between successive overloads for a major portion of the test. After initial materials were evaluated using simple overload spectra, results were compared to data from tests using the eight-level block spectrum shown in Fig. 5.

From related experience to this point, results from the OLR = 1.8, OCR = 1/8000 tests were judged to be the most sensitive to microstructure. On that basis, this spectrum was selected to evaluate retardation characteristics of the six remaining alloy composition variants in the T7 temper. Remaining tempers of 7075 were tested using selected spectra.

Selected test specimen fracture surfaces were subjected to fractographic and metallographic examinations. Some overload tests were also interrupted and specimens sectioned to further reveal details of FCG mechanisms.

Test Results

Constant Amplitude

Constant amplitude results for the four base line alloys, namely, 7075-T6, 7075-T7, 7050-T6, and 7050-T7, are given in Table 5 and Fig. 6.[7] Over the

[7]Raw test data, from which these and other test results reported here were established, is given in Ref. *9*.

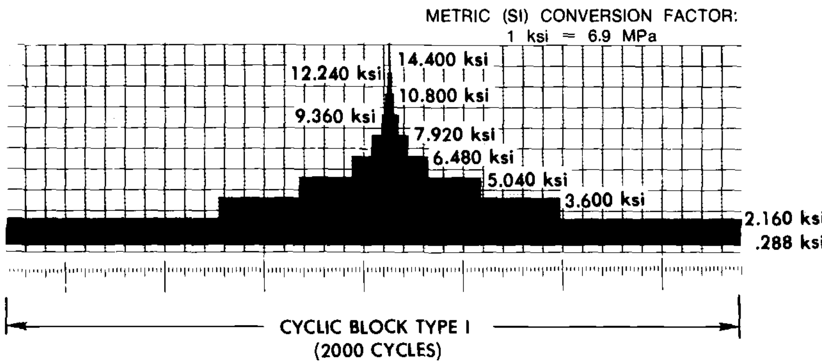

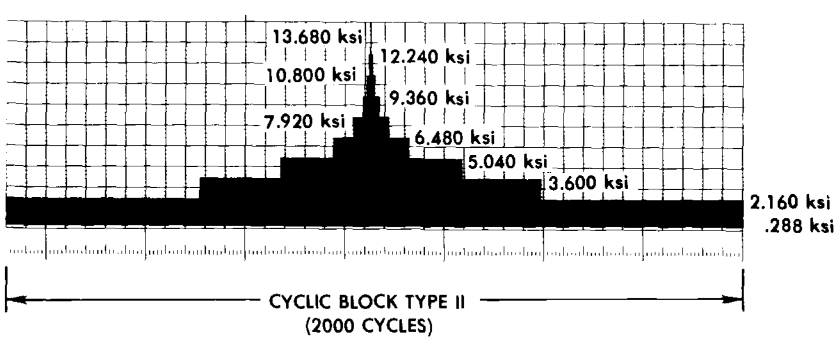

FIG. 5—*Eight-level block loading spectrum. Cyclic block Type I repeated twice and Type II repeated three times in that order continuously. (Note: spectrum composition based on J. C. Ekvall correspondence, 18 Aug. 1976, to ASTM E9.05 Task Group on Development of Reference Test Spectra.*

TABLE 5—*Results of constant-amplitude-loading fatigue crack growth tests*[a] *of 7050 and 7075 in T6 and T7 type tempers.*

Alloy Type and Temper	Life,[b] cycles	Crack Growth Rate, da/dN (cm/cycle), at half-crack length, a		
		1.5 cm[c]	2.2 cm[c]	3.0 cm[c]
7050-T6	56 000	2.45×10^{-5}	4.75×10^{-5}	1.05×10^{-4}
7050-T7	136 000	1.12×10^{-5}	2.00×10^{-5}	4.70×10^{-5}
7075-T6	36 000	4.00×10^{-5}	8.20×10^{-5}	1.90×10^{-4}
7075-T7	92 000	1.53×10^{-5}	3.30×10^{-5}	6.70×10^{-5}

[a]Relative humidity >90% for all tests.
[b]Crack propagation life from half-crack length, a, of 1.02 to 3.3 cm.
[c]Crack lengths of 1.5, 2.2, and 3.0 cm correspond to ΔK values of 8.4, 11.0, and 14.6 MPa $\sqrt{m}$, respectively, for the applied loading conditions.

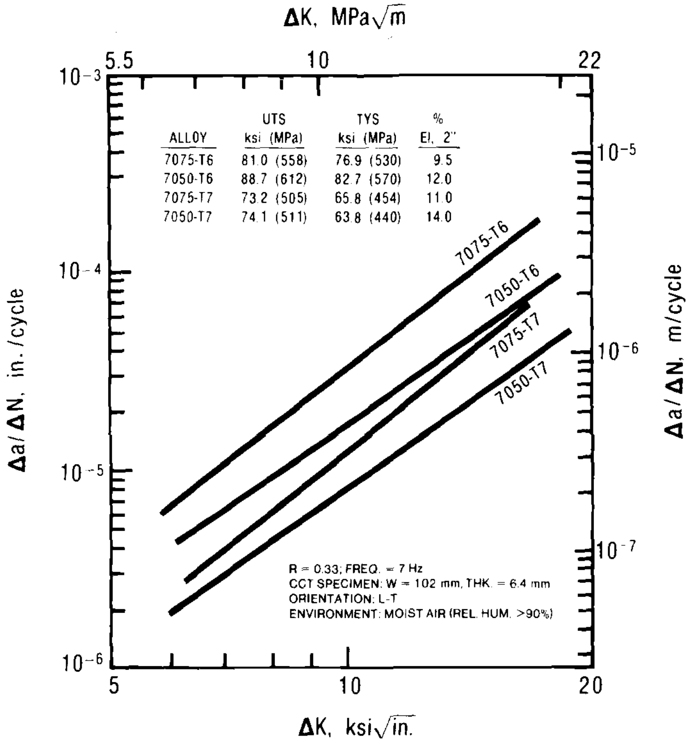

FIG. 6—*Stress intensity factor range, ΔK, versus fatigue crack growth rate, Δa/ΔN, of 7075 and 7050 aluminum alloys.*

range of ΔK traversed, FCG resistance of 7050 was superior to that of 7075, and performance of the T7 temper superior to the peak strength T6 temper. Results for the eight alloy compositions in the T7-type temper are given in Table 6. Constant amplitude FCG resistance for the T7 type alloys are ranked according to microstructural features in Fig. 7. Factors that increase resistance to stress corrosion cracking, that is, overaging and increasing copper content, increased resistance to FCG at both intermediate and high ΔK. Increasing toughness by increasing purity (lowering iron and silicone) reduced FCG rate at the high ΔK but had little effect at intermediate ΔK. These findings are consistent with those noted previously.

Periodic Single Spike Overloads

Results of single spike overload tests on the four baseline alloys are given in Table 7. The effect of overload magnitude and its frequency of application on alloy ranking is shown in Figs. 8 and 9. The trend in FCG rate behavior noted in Fig. 9 for 7075 was comparable to that observed for 7050.

TABLE 6—*Results of constant-amplitude-loading fatigue crack growth tests*[a] *of eight variants of 7050 and 7075 in T-7 type tempers.*

Alloy Type	Life,[b] Cycles	Crack Growth Rate, da/dN (cm/cycle), at half-crack length, a		
		1.5 cm[c]	2.2 cm[c]	3.0 cm[c]
High-purity 7010	96 000	1.52×10^{-5}	3.10×10^{-5}	7.40×10^{-5}
7010	84 000	1.92×10^{-5}	3.48×10^{-5}	7.50×10^{-5}
7475	104 000	1.58×10^{-5}	2.60×10^{-5}	6.00×10^{-5}
7075	92 000	1.53×10^{-5}	3.30×10^{-5}	6.70×10^{-5}
7050	136 000	1.12×10^{-5}	2.00×10^{-5}	4.70×10^{-5}
Low-purity 7050	124 000	1.27×10^{-5}	2.40×10^{-5}	6.15×10^{-5}
High-copper 7475	108 000	1.15×10^{-5}	2.45×10^{-5}	5.00×10^{-5}
High-copper 7075	108 000	1.38×10^{-5}	2.60×10^{-5}	6.35×10^{-5}

[a]Relative humidity >90% for all tests.
[b]Crack propagation life from half-crack length, a, of 1.02 to 3.3 cm.
[c]Crack lengths of 1.5, 2.2, and 3.0 cm correspond to ΔK values of 8.4, 11.0, and 14.6 MPa $\sqrt{m}$, respectively, for the applied loading conditions.

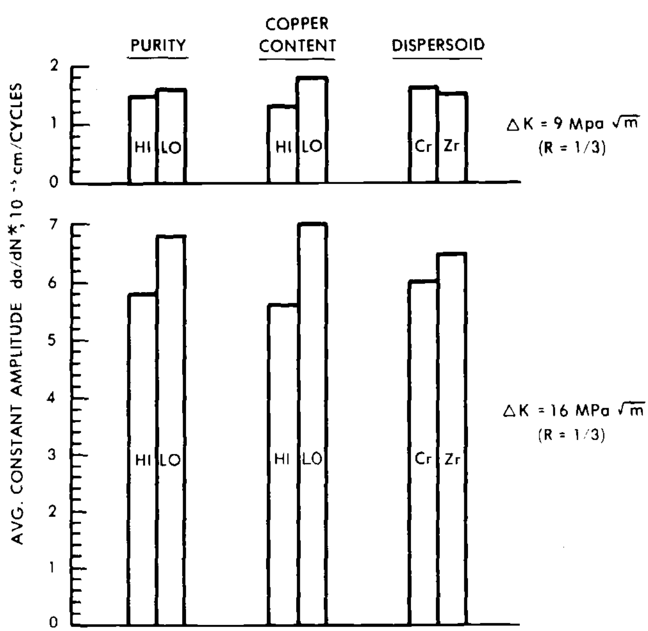

FIG. 7—*Effect of purity, copper content, and dispersoid on constant amplitude crack growth resistance of 7XXX-T7 alloys in high-humidity air. (Computed as average of four microstructures containing same controlled variable).*

TABLE 7—*Results of periodic-spike-overload fatigue crack growth tests*[a] *of 7050 and 7075 in T6 and T7 type tempers.*

Alloy Type and Temper	Spectrum[b]		Life[c]		Crack Growth Rate, da/dN (cm/cycle), at half-crack length, a		
	OLR	OCR	Blocks	Cycles	1.5 cm	2.2 cm	3.0 cm
7050-T6	1.4	1/4000	19	76 000	2.00×10^{-5}	4.60×10^{-5}	7.89×10^{-5}
7050-T7			38	152 000	1.15×10^{-5}	2.05×10^{-5}	5.00×10^{-5}
7075-T6			9	36 000	4.50×10^{-5}	7.20×10^{-5}	1.45×10^{-4}
7075-T7			23	92 000	1.65×10^{-5}	3.50×10^{-5}	6.90×10^{-5}
7050-T6	1.8	1/4000	484	1 936 500	7.00×10^{-7}	1.70×10^{-6}	2.90×10^{-6}
7050-T7			210	840 200	2.17×10^{-6}	2.28×10^{-6}	4.30×10^{-6}
7075-T6			485	1 940 500	8.10×10^{-7}	1.00×10^{-6}	3.44×10^{-6}
7075-T7			279	1 116 300	1.50×10^{-6}	2.25×10^{-6}	4.00×10^{-6}
7050-T6	2.2	1/4000	1621	6 484 000	2.62×10^{-7}	3.91×10^{-7}	5.66×10^{-7}
7050-T7[d]			...	...	...	...	...
7075-T6			1800	7 200 000	1.85×10^{-7}	4.54×10^{-7}	1.41×10^{-6}
7075-T7			1167	4 668 000	3.21×10^{-7}	6.10×10^{-7}	1.11×10^{-6}
7050-T6	1.8	1/8000	14	112 000	1.40×10^{-5}	3.20×10^{-5}	6.20×10^{-5}
7050-T7			62	496 100	1.95×10^{-6}	1.05×10^{-5}	2.20×10^{-5}
7075-T6			100	800 100	5.00×10^{-6}	2.50×10^{-6}	2.00×10^{-6}
7075-T7			128	1 024 000	2.12×10^{-6}	2.40×10^{-6}	3.00×10^{-6}

[a] Relative humidity >90% for all tests.
[b] Refer to Fig. 4.
[c] Crack propagation life from half-crack length of 1.02 to 3.3 cm.
[d] This temper not tested.

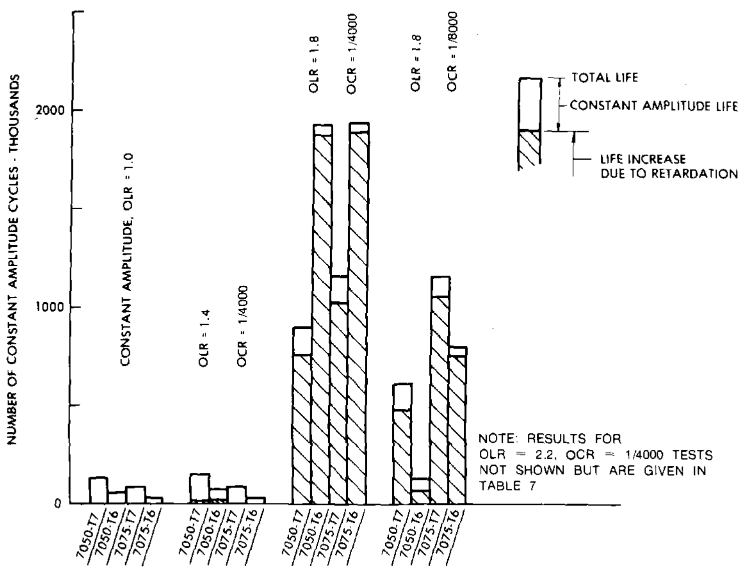

FIG. 8—*Relative ranking of fatigue crack growth resistance of 7075 and 7050 alloys under constant amplitude and periodic spike overload conditions.*

For the spectrum having a low-level overload (OLR = 1.4 and OCR = 1/4000), the relative performance rating of all materials was comparable to constant amplitude results. For this loading sequence, lives of 7050 increased by about 25 percent over constant amplitude lives, while no improvement in total life was noted for 7075 in either temper, Fig. 8.

A progressive increase in overload magnitude, OLR = 1.8 and 2.2, respectively, at the same occurrence ratio (OCR = 1/4000) produced large increases in life (60 to 200 times greater than constant amplitude lives) for all alloys. Ranking of alloy performance at the high overloads did not conform to the constant amplitude rating. In addition, ranking also depended upon the frequency of overload application, Fig. 8, and crack length, Fig. 9. With OCR = 1/4000 lives of specimens in T6 tempers were significantly longer than those in T7 tempers, while alloy type had little effect. When frequency of overload occurrence was decreased to OCR = 1/8000 while maintaining OLR at 1.8, the T7 tempers outperformed T6 tempers, and lives of 7075 alloys were significantly longer than lives of 7050 alloys.

Multi-Level Spectrum

Results for the eight-level block spectrum for the four baseline alloys are given in Table 8. Observed lives under this spectrum were between one and two orders of magnitude greater than lives estimated using a linear cumulative FCG model (that is, assuming no load interaction) with constant

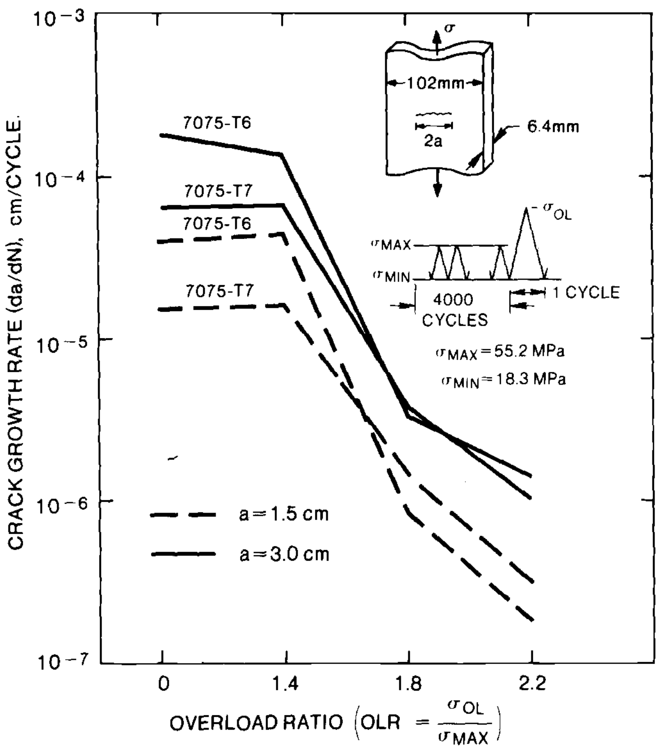

FIG. 9—*Interaction of overload ratio, crack length, and temper on fatigue crack growth rates of 7075 subject to periodic single spike overloading.*

TABLE 8—*Results of eight-level-block-spectrum*[a] *fatigue crack growth tests*[b] *of 7050 and 7075 in T6 and T7 type tempers.*

Alloy Type and Temper	Life[c,d]		Crack Growth Rate, da/dN (cm/cycle), at half-crack length, a[d]		
	Blocks	Cycles	1.5 cm	2.2 cm	3.0 cm
7050-T6	1458	2 916 000	5.50×10^{-7}	9.00×10^{-7}	1.45×10^{-6}
7050-T7	1802	3 604 000	4.40×10^{-7}	7.20×10^{-7}	1.40×10^{-6}
7075-T6	1143	2 286 000	6.20×10^{-7}	1.45×10^{-6}	3.50×10^{-6}
7075-T7	1789	3 578 000	2.30×10^{-7}	7.40×10^{-7}	1.70×10^{-6}

[a] Refer to Fig. 5.
[b] Relative humidity >90% for all tests.
[c] Crack propagation life from half-crack length of 1.02 to 3.3 cm.
[d] FCG rate, da/dN, determined from slope of crack length versus cycle curve. There are 2000 cycles in each block Types 1 and 2, and 10 000 cycles in one repetition of the load sequence (Refer to Fig. 5).

amplitude data. Thus, significant retardation was present in these tests. Relative effect of alloy and temper on lives in the eight-level spectrum test was less significant than observed in constant amplitude and single spike periodic overload tests.

The remaining discussion will center on constant amplitude and periodic spike overload test results since these tests proved more revealing from the standpoint of clarifying controlling FCG mechanisms. Utility of these simple tests for the correlation of alloy FCG performance under more complex loading conditions will become more evident in ensuing discussions.

Effect of Eight Composition Variants on Spectrum Behavior

The periodic spike overload spectrum with OLR = 1.8, OCR = 1/8000 was selected to evaluate FCG retardation characteristics of the eight alloy composition variants in the T7 type temper. Observed lives and FCG rates are recorded in Table 9. The relative retardation ratio (either in terms of increased life or reduced FCG rate) is given for each alloy in Table 10.

At short crack length, the degree of retardation between alloys varied by about 2.5. At longer crack lengths, this factor increased to about 20. For high-purity low-copper alloys (namely, high-purity 7010 and 7475), the relative retardation remained about constant over the entire range of crack extension, though the level of retardation was appreciably better in the alloy containing chromium (7475). For high-purity, high-copper alloys (namely, 7050 and high-copper 7475), the ability to retard crack growth decreased with increasing crack length. Significant increase in FCG retardation was observed at long crack lengths in low-purity alloys namely, 7010, low-purity 7050, 7075, and high-copper 7075). At intermediate crack lengths low-purity alloys containing chromium (namely 7075, high-copper 7075) showed better retardation than low-purity alloys containing zirconium (namely, 7010, low-purity 7050). Under the applied spectrum, greatest increases in total life were noted in low-purity alloys.

Effect of Aging (Temper) on Spectrum Results

Some effects of degree of overaging were obtained from tests of 7075 and 7050 in T6 and T7 type tempers, Tables 5, 7, and 8. Supplementary information was obtained from two additional overaged tempers of 7075 tested with OLR = 1.4 and 1.8 and OCR = 1/4000, Table 11.

Regardless of crack length, FCG performance of 7075 in the 1.4 OLR tests increased progressively with increasing degree of overaging. Likewise, performance of 7050-T7 was superior to that of 7050-T6 for the same spectrum, Table 7. These ratings were consistent with conclusions developled from constant amplitude conditions.

In the 1.8 OLR, 1/4000 OCR tests, ranking of 7075 tempers depended on

TABLE 9—*Results of periodic-spike-overload fatigue crack growth tests*[a] *of eight variants of 7050 and 7075 in T7 type tempers.*

Alloy Type	Spectrum[b]		Life[c]		Crack Growth Rate, da/dN (cm/cycle), at half-crack length, a		
	OLR	OCR	Blocks	Cycles	1.5 cm	2.2 cm	3.0 cm
High-purity 7010	1.8	1/8000	22	176 000	8.00×10^{-6}	2.15×10^{-5}	4.00×10^{-5}
7010			63	504 100	3.60×10^{-6}	5.81×10^{-6}	5.20×10^{-6}
7475	1.8	1/8000	83	664 100	2.75×10^{-6}	4.60×10^{-6}	9.00×10^{-6}
7075			128	1 024 100	2.12×10^{-6}	2.40×10^{-6}	3.00×10^{-6}
7050	1.8	1/8000	62	496 100	1.95×10^{-6}	1.05×10^{-5}	2.20×10^{-5}
Low-purity 7050			79	632 100	2.60×10^{-6}	5.80×10^{-6}	4.50×10^{-6}
High-copper 7475	1.8	1/8000	38	304 000	4.30×10^{-6}	1.40×10^{-5}	3.60×10^{-5}
High-copper 7075			95	760 100	2.95×10^{-6}	3.40×10^{-6}	4.10×10^{-6}

[a] Relative humidity >90% for all tests.
[b] Refer to Fig. 4.
[c] Crack propagation life from half-crack length of 1.02 to 3.3 cm.

TABLE 10—*Relative retardation for periodic-spike-overload (OLR = 1.8, OCR = 1/4000) fatigue crack growth tests of eight variants of 7050 and 7075 in T7 type tempers.*

Alloy Type	N_{OL}/N_{CA} [a]	$(da/dN)_{OL}/(da/dN)_{CA}$ [a] Specimen Half-Crack length, a 1.5 cm [b]	2.2 cm [b]	3.0 cm [b]
High-purity 7010	1.8	0.53	0.69	0.54
7010	6.0	0.19	0.17	0.069
7475	6.4	0.17	0.18	0.15
7075	11.1	0.14	0.073	0.045
7050	3.6	0.17	0.53	0.47
Low-purity 7050	5.1	0.20	0.24	0.073
High-copper 7475	2.8	0.37	0.57	0.72
High-copper 7075	7.0	0.21	0.13	0.065

[a] Respective ratios of spectrum life or FCG rate to constant-amplitude life of FCG rate. Lives established from specimen half-crack length of 1.02 to 3.3 cm.
[b] Crack lengths of 1.5, 2.2, and 3.0 cm correspond to ΔK values of 8.4, 11.0, and 14.6 MPa $\sqrt{m}$, respectively, for constant-amplitude loading conditions.

crack length, and performance did not change monotonically with degree of overaging at any crack length. At short and intermediate crack lengths, the peak aged T6 temper generally outperformed overaged tempers. Similarly, performance of 7050-T6 was superior to that of 7050-T7 for this spectrum, Table 7. At short crack length, 7075-T6 outperformed 7075-T7 when the OLR was increased to 2.2, but at long crack length, the ranking reversed, Fig. 9. Chanani [*15*] reported a similar result when comparing 7075-T6 versus 7075-T73 FCG performance under simple overload conditions. His results indicated a slower rate of FCG after overloading in 7075-T73 when the ratio of overload peak stress to maximum baseline stress was less than about two. When this ratio was greater than two, the T6 temper showed greater ability to retard FCG following the overload.

Fractographic and Metallographic Examinations

Locations of periodic spike overloads on the fractured surface were clearly visible under low-power optical magnification. Spacings between overload marks were longer when FCG rate was high, for example, Fig. 10*a*, and shorter when FCG rate was low, for example, Fig. 10*b*. Dark bands marking the overloads tended to become more prominent with increasing stress intensity factor (crack length), and were decidedly wider in the low-purity (low-toughness) materials.

Periodic markings were not as visible on specimens tested using the eight-level spectrum. Greater amounts of fretting, disclosed by black spots of aluminum oxide, were noted on these fracture surfaces than were noted on fracture surfaces from spike overload and constant amplitude tests. This dif-

TABLE 11—*Results of periodic-spike-overload fatigue crack growth tests*[a] *on peak strength and overaged tempers of 7075.*

Temper[b]	Spectrum[c]		Life[d]		Crack Growth Rate, da/dN (cm/cycle), at half-crack length, a		
Type	OLR	OCR	Blocks	Cycles	1.5 cm	2.2 cm	3.0 cm
T6	1.4	1/4000	9	36 000	4.50×10^{-5}	7.20×10^{-5}	1.50×10^{-4}
T76			16	84 000	2.00×10^{-5}	5.30×10^{-5}	8.80×10^{-5}
T7			23	92 000	1.65×10^{-5}	3.50×10^{-5}	6.90×10^{-5}
T73			28	112 000	1.35×10^{-5}	2.54×10^{-5}	5.80×10^{-5}
T6	1.8	1/4000	485	1 940 500	8.10×10^{-7}	9.00×10^{-7}	3.44×10^{-6}
T76			451	1 804 500	9.00×10^{-7}	1.40×10^{-6}	3.30×10^{-6}
T7			279	1 116 300	1.50×10^{-6}	2.25×10^{-6}	4.00×10^{-6}
T73			348	1 392 300	1.15×10^{-6}	1.90×10^{-6}	3.00×10^{-6}

[a] Relative humidity >90% for all tests.
[b] Degree of overaging increases with temper in the order listed.
[c] Refer to Fig. 4.
[d] Crack propagation life from half-crack length of 1.02 to 3.3 cm.

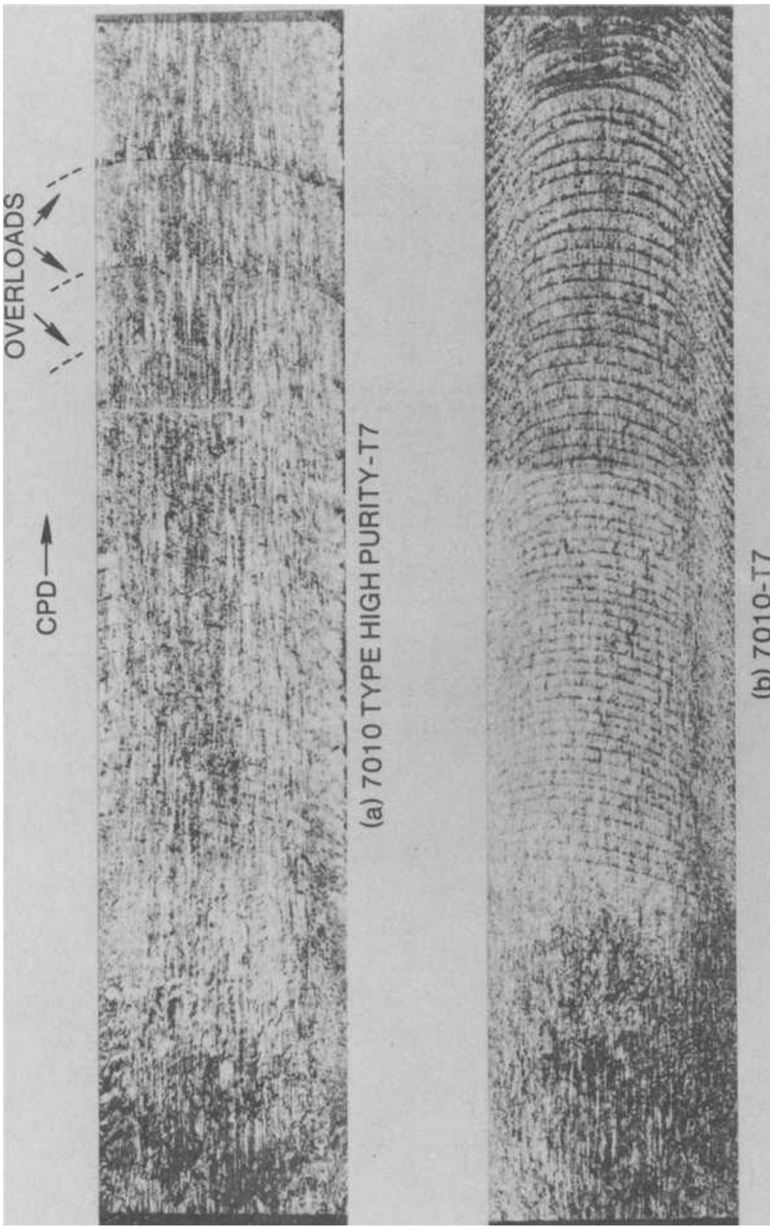

FIG. 10—*Macro fractographs of various alloys, 1.8 overload ratio, 1/8000 occurrence ratio.*

ference is attributed to the reduced minimum stress of the eight-level test (2 MPa as opposed to 18.3 MPa for other tests) that resulted in a greater degree of contact between mating fracture surfaces.

Constant amplitude specimen surfaces viewed by scanning electron microscope (SEM) revealed typical intermediate FCG rate fracture topography for this loading condition, for example, Fig. 11*a*. Appearance of low overload (OLR = 1.4, OCR = 1/4000) fractures were very similar to constant amplitude samples, Fig. 11*b*. A small amount of tearing during overloading was noted only for 7075 at long crack length (high K).

SEM fracture appearances for high overload tests were drastically different from low overload and constant amplitude samples. In low-purity materials, fissures, and numerous secondary cracks were typical at overload sites, particularly at long crack lengths. Fracture topography between overload sites was reminiscent of constant amplitude behavior at reduced ΔK. Typical examples of secondary cracking at high overload locations in 7075 are shown in Fig. 12.

High-purity materials typically did not exhibit large fissures and numerous secondary cracks. Rather, high overloads in these materials produced stretch zones followed by transition toward normal topography until the application of the next overload. The rate of return to normal topography with crack extension after the overload varied with alloy. The greatest transition in fracture appearance occurred in 7475-T7 and the slightest transition in high-copper 7475-T7, Figs. 13*a* and *b*, respectively.

Special interrupted tests were conducted on 7075-T6 and 7050-T7 using the overload sequence OLR = 1.8 and OCR = 1/4000. These alloys respectively gave maximum and minimum life (retardation) under this spectrum. Two specimens were tested for each alloy. The first test was interrupted immediately after the overload, and the second 2000 cycles after the overload. Half crack length at point of interruption was 2.5 cm. The crack path was examined metallographically on parallel planes near and beneath the specimen rolled surface. Periodic crack branching was noted along the propagation path, with one of the branches eventually dominating. The branching was typically associated with large intermetallic particles, Fig. 14. Magnitude of the branching was much greater in 7075-T6 than in 7050-T7. Specimens examined directly after the application of the 1.8 overload exhibited localized deformation directed toward intermetallic particles. This localized deformation was absent in samples tested for the additional 2000 cycles following the overload.

High- and low-purity variants of high-copper alloys containing chromium were selected for additional overload tests. Tests were interrupted at long and short crack lengths. Specimens were then sectioned and polished to permit observation of the crack front into the direction of growth.

Representative photomicrographs that illustrate direct contrast of crack front geometry with purity level are shown in Fig. 15. The presence of in-

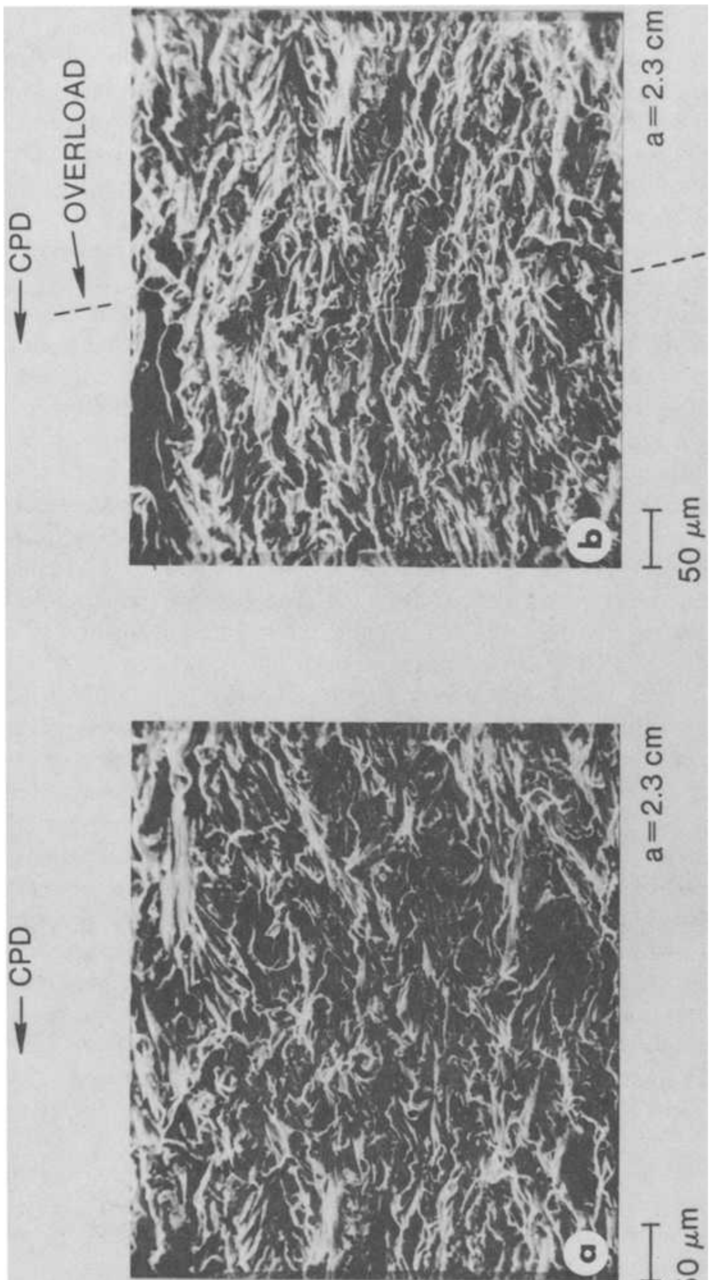

FIG. 11—*SEM fractographs of 7050-T7: (a) constant amplitude, (b) 1.4 overload ratio, 1/4000 occurrence ratio.*

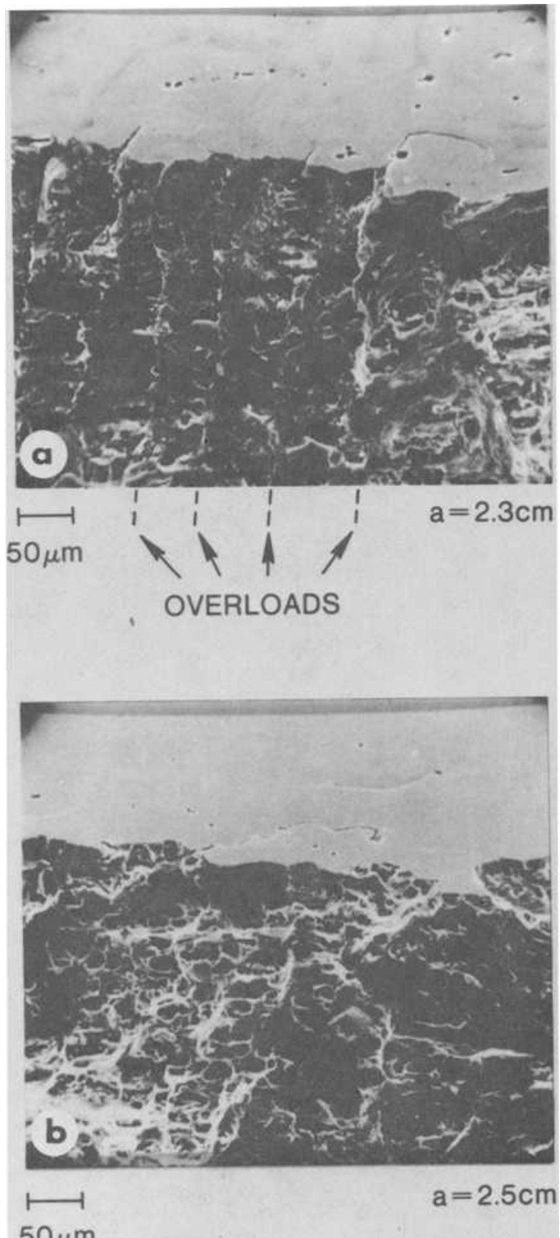

FIG. 12—*Typical SEM fractographs showing secondary cracks at overload sites in 7075.* (a) *7075-T6 (OLR = 1.8, OCR = 1/4000),* (b) *7075-T7 (ORL = 1.8, OCR = 1/8000).* (*Note: fractured specimens sectioned at plane 45 deg to fracture surface and metallographically polished to reveal subsurface features.*)

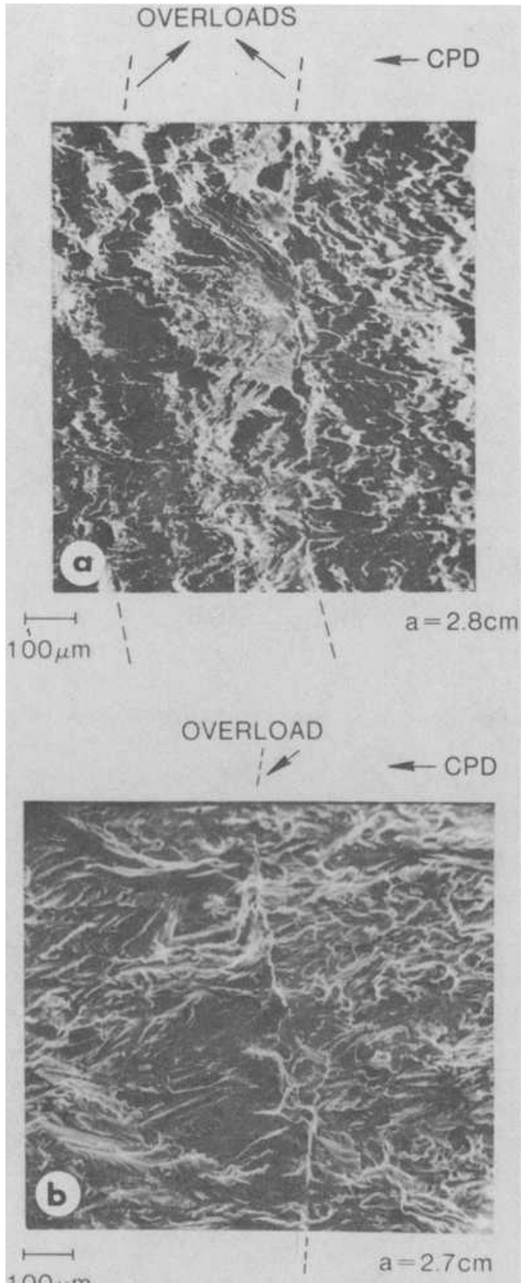

FIG. 13—*Typical SEM fractograph of high-purity 7XXX subject to 1.8 OLR, 1/8000 OCR:* (a) *7475-T7,* (b) *high-copper 7475-T7.*

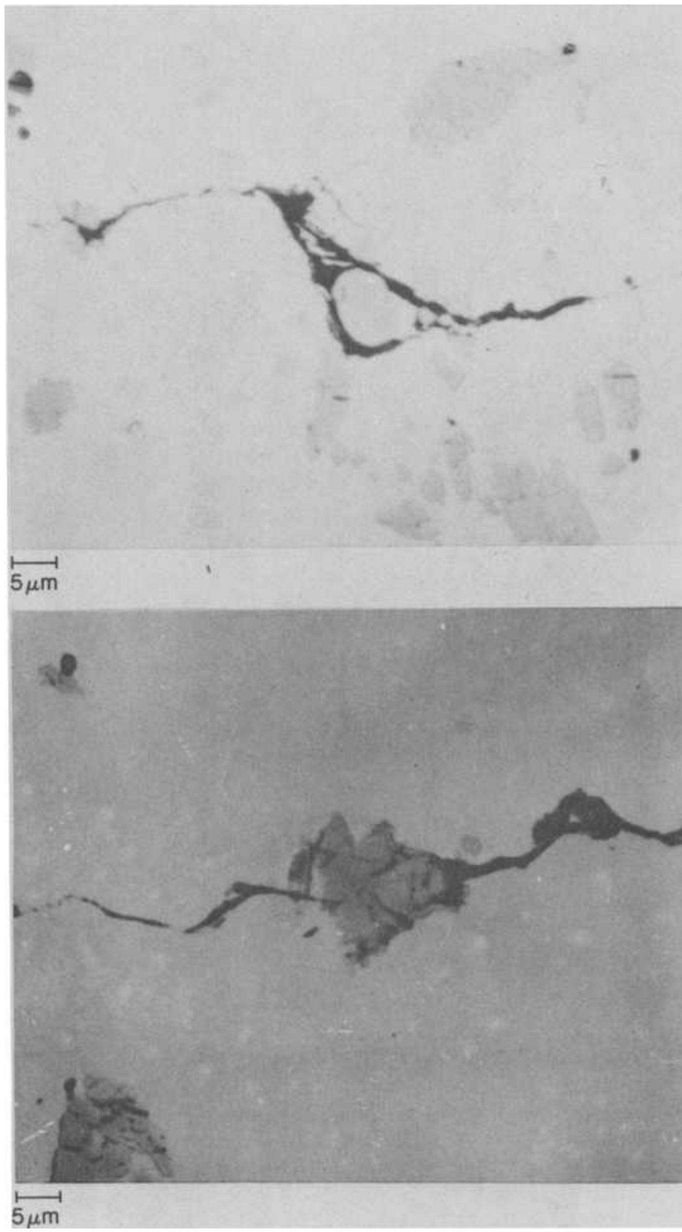

FIG. 14—*Periodic crack branching along crack in 7075-T6 subject to OLR = 1.8, OCR = 1/4000. Branching appeared to be associated with large intermetallic phases.*

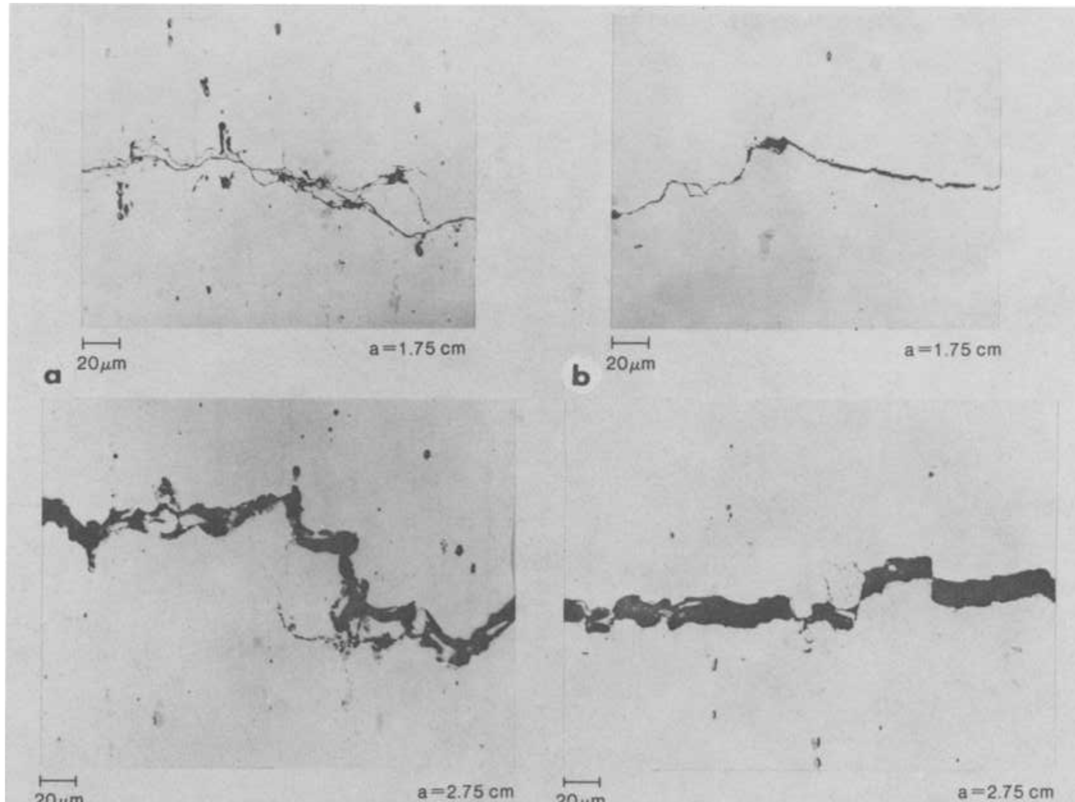

FIG. 15—*Optical micrographs along crack front of periodic spike overload (OLR = 1.8, OCR = 1/8000) tests of high- and low-purity 7XXX alloys:* (a) *high-copper 7075-T7 (low-purity),* (b) *high-copper 7475-T7 (high-purity). (Note: crack propagation direction perpendicular to plane of view.)*

termetallic particles significantly altered crack front profile in both alloys. The low-purity alloy, with higher volume fraction of secondary intermetallics exhibited the greatest degree of secondary cracking. Separation of the matrix-particle interface was generally observed, suggesting a cause and effect relationship between secondary intermetallics and crack tip geometry.

Discussion

Fatigue crack growth is comprised of several simultaneously operating (and sometimes competing) mechanisms. Performance under a particular set of testing conditions is controlled by the FCG mechanism that dominates over the greatest portion of the test life. Moreover, separate FCG mechanisms may dominate various stages of the FCG life (for example, low ΔK versus high ΔK). The reversals of alloy performance ratings observed in this and other investigations suggest that controlling mechanisms are sensitive to the interaction of alloy metallurgy and loading (stress) history. Understanding how the material interacts with test conditions is, therefore, a necessary step for accurate transfer of laboratory test results to predict performance in the field.

Plastic Zone Concepts Related to Overload Interaction

Overload induced FCG retardation has been correlated, with moderate success, to dimensions of the crack tip plastic zone produced by the overload, for example, Ref *16*. A basic assumption of this correlation is that retardation exists when the following relationship holds

$$(a_{\mathrm{OL}} + r_{Y\mathrm{OL}}) - (a + r_y) > O$$

where $r_{Y\mathrm{OL}}$ corresponds to the monotonic plastic zone developed by a preceding tensile overload at crack length, a_{OL}, and r_Y corresponds to the monotonic plastic zone associated with the current loading at crack length a. Retardation is attributed to crack tip compression that results from residual deformation left by the overload. The compressive crack tip residual stress reduces the "effective" ΔK, thereby decreasing the rate of FCG.

If a second load is introduced while the crack is still under the influence of a previous overload, the amount of FCG retardation may be greater than if the second overload were introduced after the crack had grown out the influence of the preceding overload [*17*]. For aluminum alloy 2024-T3, maximum overload retardation resulted when periodic spike overloads were spaced by an increment of crack extension at base line stresses equal to about one-fourth the overload monotonic plastic zone size [*14*]. Within the monotonic plastic zone at the crack tip there exists a smaller region of intensive tension-to-compression deformation that occurs during each load-unload excursion

[18]. The distance from the crack tip to the boundary of this intense region of deformation is also about one fourth the distance from the crack tip to the boundary monotonic plastic zone [19].

Plastic zone concepts were used to assess how alloy ranking in spike overload tests was affected by degree of overload interaction. Figures 16 and 17 plot crack length versus the ratio of crack extension per block to monotonic or reversed plastic zone size of the overload. The monotonic and reversed plastic zone sizes were estimated, respectively, by relationships of Irwin [20] and Rice [19].

Overload interaction was low for materials subjected to the OLR = 1.4, OCR = 1/4000 sequence. For this spectrum, crack extension during intermittent cycles grew out of the monotonic plastic zone of the preceding overload before application of the next overload, Fig. 16. Increasing OLR to 1.8 while retaining OCR constant at 1/4000 resulted in high interaction between successive overloads. For alloys subjected to the latter spectrum, the crack

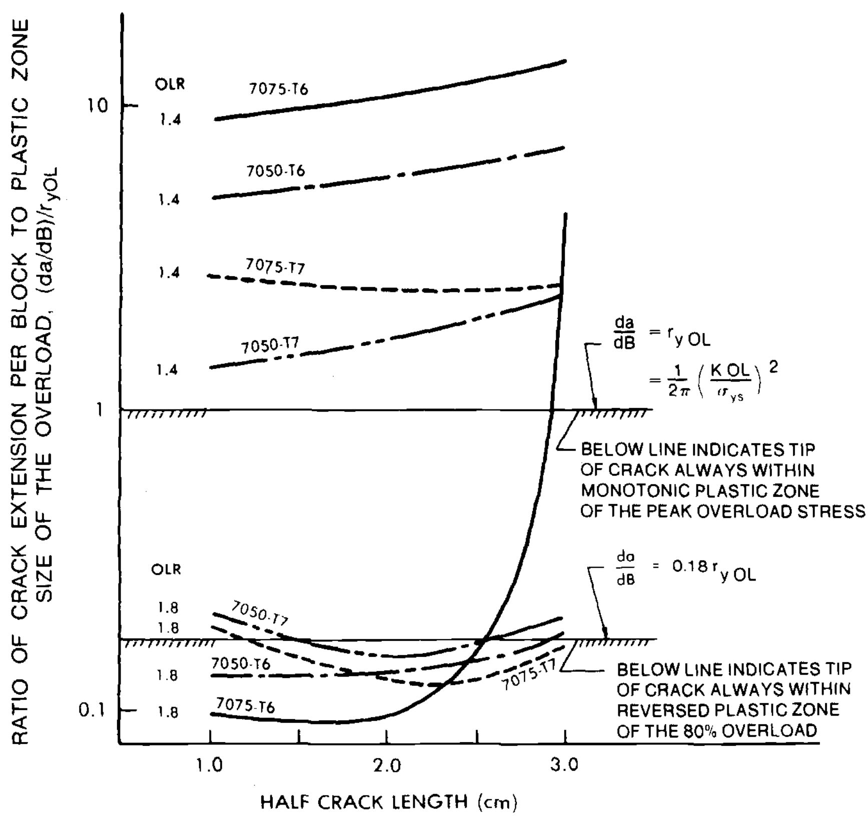

FIG. 16—*Crack growth per block relative to plastic zone size for periodic spike overloads with 1.4 and 1.8 overload ratio and with 1/4000 occurrence ratio.*

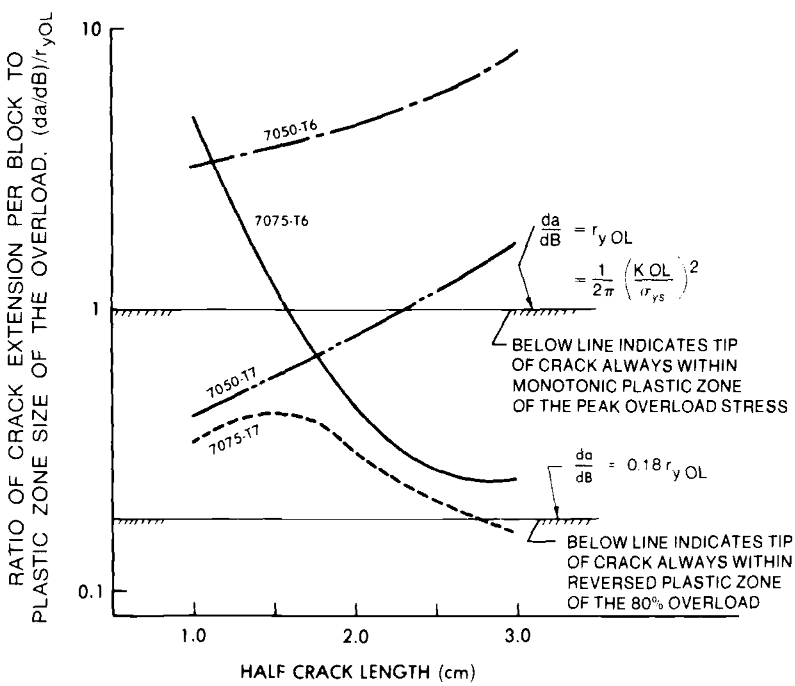

FIG. 17—*Crack growth per block relative to plastic zone size for periodic spike overloads with 1.8 overload ratio and with 1/8000 occurrence ratio.*

tip remained embedded within the reversed plastic zone of the preceding overload for the majority of the test. Alloy performance ranked differently in spectra having high and low degrees of interaction between overloads. Degree of overload interaction and alloy performance ranking changed again by decreasing the overload frequency to 1/8000 while maintaining OLR at 1.8, Fig. 17.

Plastic zone computations for the eight-level spectrum indicated high interaction between maximum peak overloads that occurred once every 2000 cycles. Crack extension during intermittent cycles between these overloads never grew out of the reversed plastic zone of the preceding overload for the majority of the test.

Results of Fig. 17 illustrate how various factors compete for control of alloy performance. For the applied spectrum (OLR = 1.8, OCR = 1/8000), T7 alloys outperformed T6 alloys at shortest crack lengths, where ΔK is lowest for the test. At the short crack length (lower ΔK), FCG resistance is more sensitive to environment, and magnitude of the overload monotonic plastic zone has major influence on the amount of FCG retardation. Both resistance to environment and monotonic plastic zone size are greater in the T7 temper than in the T6. At longer crack length (high ΔK), 7075 outperforms 7050.

This is attributed to the more dominant role of secondary cracks as a major retardation mechanism in 7075 that contains a greater number of intermetallic particles. Secondary cracks formed at 7075 particle sites during overloading tended to divide (reduce) ΔK to the extent that the main crack front never grew out of the influence of secondary cracks before the next overload was applied.

In general, when overload magnitude is relatively low, or when significant overloads tend to act as independent events, performance of alloys having comparable yield strength would be expected to rank similar to constant amplitude performance. Reduction of alloy yield strength would increase magnitude of crack-tip plasticity, and thus, favor the plastic zone retardation mechanism. As overload interaction increases, alloy performance rankings may change. This is typical of the example where overload magnitude is high, and secondary crack formation is the underlying cause of FCG retardation.

Microstructure Effect on Spectrum Results

Secondary Intermetallics—High volume fraction of coarse intermetallic particles increased FCG resistance in high overload tests. The observed effect is explained by the illustration of Fig. 18. At short crack length, the overload stress intensity factor is insufficient to affect constituent particles, so no effect is detected. As crack length and K increase, incipient cracks nucleate at

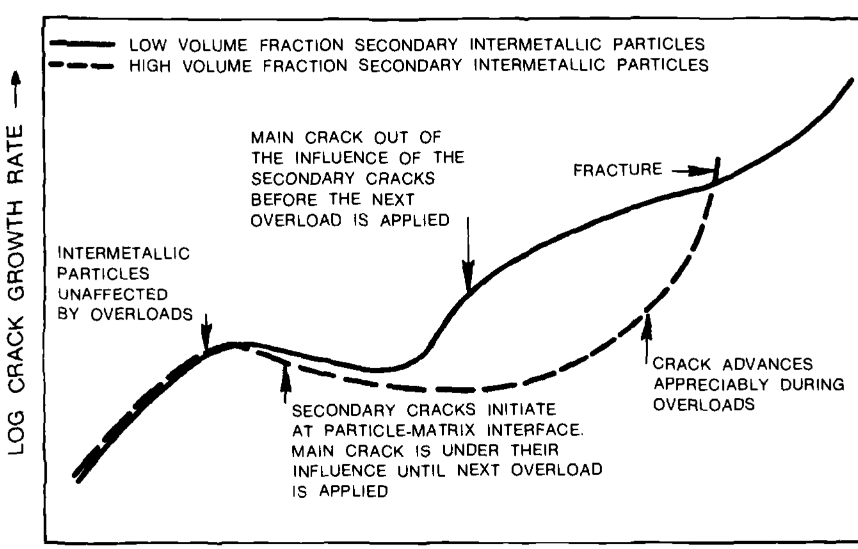

FIG. 18—*Effect of volume fraction of coarse intermetallic particles on fatigue crack growth rate under loading conditions where high tensile overloads are applied frequently.*

particle sites during overloading. The secondary cracks divide "effective" ΔK, thereby retarding FCG. With a lower intermetallic particle volume fraction, fewer secondary cracks are produced, so magnitude of the retardation is lower. At a particular crack length, however, stress intensity factor becomes large enough to cause significant crack extension during overloading. Acceleration of FCG rate now occurs more rapidly in material with high constituent volume fraction. Then, as K approaches the material fracture toughness, fracture instability occurs. Whether total life of a part will be longer in material with lower or higher volume fraction of intermetallic particles depends on details of the loading (or K) history.

Dispersoids—The smaller dispersoid particles contribute to the propagation of secondary cracks formed at intermetallic particle sites upon overloading. Their effect on FCG would be similar, though on a smaller scale, than that shown in Fig. 18 for the larger intermetallic particles. The energy required to propagate secondary cracks in material containing chromium dispersoids is less than that required to propagate these cracks in material containing zirconium dispersoids. Periodic spike overload tests of alloys containing zirconium and chromium dispersoids behaved similarly at short and intermediate crack length. At long crack length, the effect of dispersoid type was greatest in alloys containing high volume fraction of secondary intermetallics. In alloys containing chromium, the crack advanced appreciably more during the overload, and FCG rates accelerated at shorter crack lengths during final stages of the test.

Precipitates (Degree of Overaging)—Fine precipitate particles influence FCG resistance by their effects on resistance to environment and on strength-toughness combinations. Resistance to FCG increases with increase in degree of overaging under variable amplitude loading where either overload stress level is low or the overloads are applied infrequently. This improvement is attributed to an environmental effect, because analogous improvement in intermediate constant amplitude FCG rates has been shown to be independent of strength [*1,2*].

Monotonic improvement in FCG performance with increasing degree of overaging was not generally observed in high overload tests. An explanation for this observation is postulated in Fig. 19. At short crack length where ΔK of intermittent baseline cycles is lowest for the test (Region A), compressive residual stresses developed by overload plastic deformation retard FCG. Amount of retardation increases with increase in overload plastic zone size, which varies inversely to the square of the yield stength. Overaging to lower strength, therefore, enhances FCG resistance in region A by increasing the amount of plasticity-induced FCG retardation, in addition to increasing resistance to environment. As K level increases with crack extension (Region B), intermetallic constituent particles begin to separate from the matrix upon overloading. These incipient cracks reduce "effective" ΔK and retard FCG. The severity of cracks induced at particle locations decreases with increasing

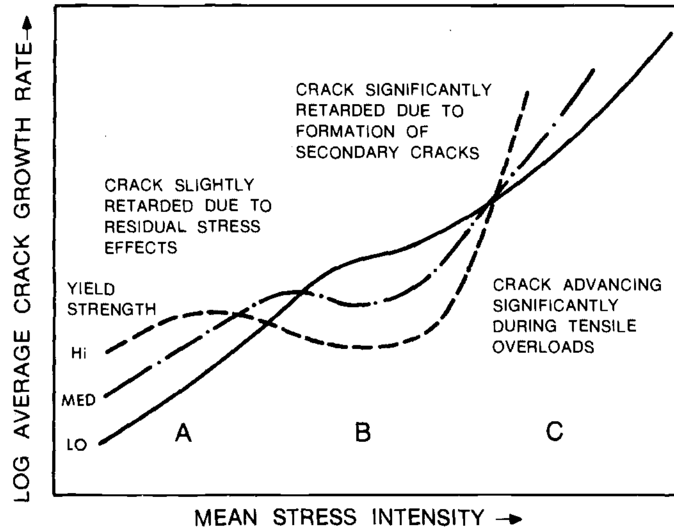

FIG. 19—*Schematic effect of yield strength (peak and overaged tempers) on fatigue crack growth rate under spectrum loading.*

toughness (decreasing yield stength). Consequently, in Region B, FCG is slower in material aged to higher strength when overloads are sufficient to cause particle matrix decohesion. Eventually, as crack length and K increase, appreciable crack advance occurs at peak loads, particularly in material having lower toughness (higher strength, Region C).

Additional Remarks on Yield Strength Effects

Inspection of Fig. 19 suggests that total lives of precracked specimens subjected to spectrum loading may not change monotonically with decreasing strength, since curves cross. An example of such behavior is shown by the data of Fig. 20 plotted as FCG life versus yield strength of 7050 forging subjected to flight simulation loading [*21*]. In the referenced investigation, strength was modified by decreasing quench rate and by overaging. The experimental results suggested a trend where life initially shortened with increasing yield stength, then lengthened with further strength increase before life decreased again. This observation suggests competition between FCG mechanisms, with a different mechanism being dominant in each of three yield strength ranges.

The proposed trend is supported by more limited results of this investigation on 7075 peak strength and overaged tempers subjected to periodic spike overloads, Fig. 21. These results also suggest that effect of yield strength on FCG resistance is sensitive to the K level or crack increment or both over which measurements are taken.

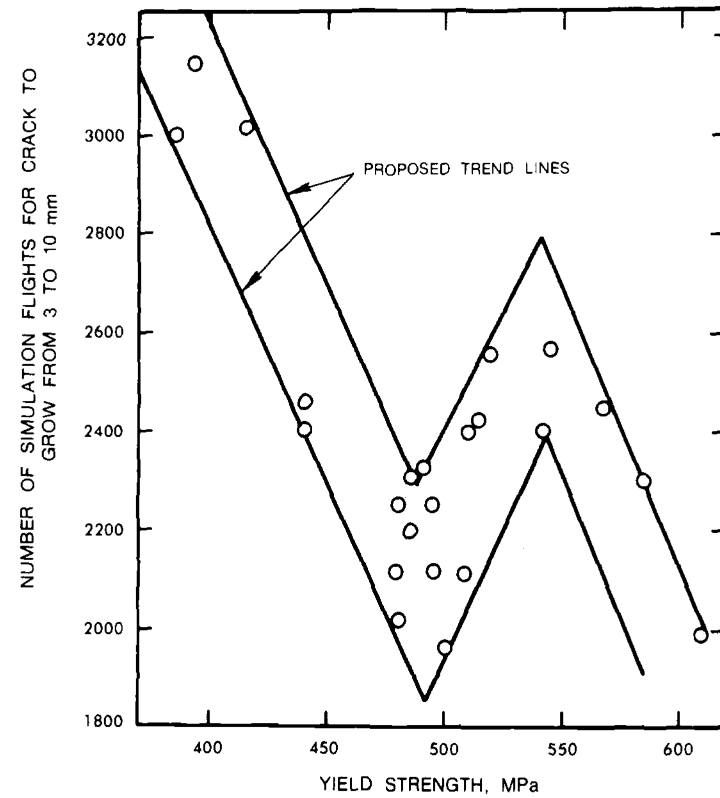

FIG. 20—*Effect of yield strength on fatigue crack propagation life of 7050 forging under flight simulation loading. (Experimental data replotted from data in Ref* 21.)

Remarks on FCG Life Prediction Models

Several fracture-mechanics-based life prediction models that have been proposed and shown to predict FCG behavior under variable amplitude loading with moderate success [*16, 22-26*]. These models do not incorporate load-microstructure interaction mechanisms directly into their computational strategy. Material input is generally in the form of constant amplitude FCG rates, tensile, and fracture toughness properties.

Treatment of overload-retardation phenomenon in the preceding models is based primarily on plastic zone size concepts. Thus, each model would predict the degree of retardation to increase with reduction in yield strength. A plastic zone interaction FCG model cannot completely explain our results. To demonstrate this, the FCG prediction computer program, EFFGRO, based on the Vroman retardation model [*23*],[8] was used to predict experi-

[8]The Vroman retardation model is similar in construction and gives life predictions comparable to those of the Willenborg model [*22*] developed by the U.S. Air Force.

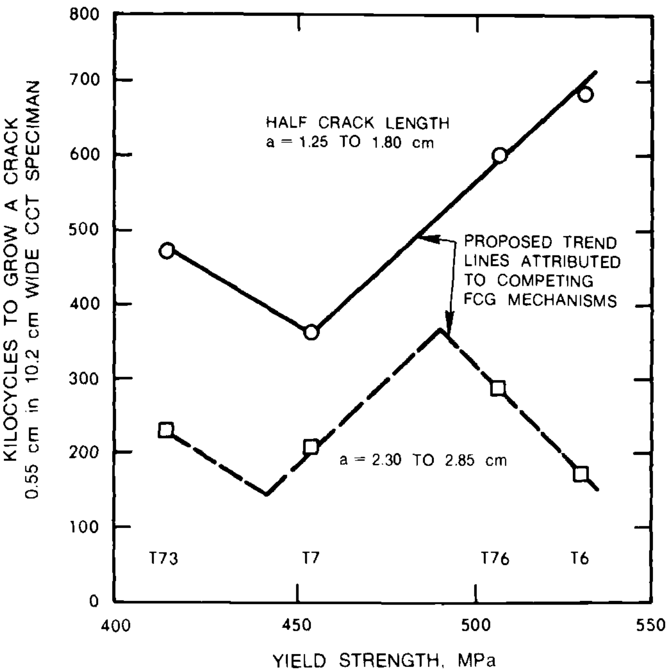

FIG. 21—*Effect of degree of overaging on fatigue crack propagation life of 7075 subjected to periodic spike overloads (1.8 overload ratio, 1/4000 occurrence ratio).*

TABLE 12—*Comparison of experimental and predicted cyclic crack growth lives by flaw growth prediction model (EFFGRO).*

Alloy Type and Temper	OLR	OCR	*Ne*, Experimental Cyclic Life (blocks) a = 10.2 to 33 mm	*Np*, Predicted Cyclic Life (blocks), a = 10.2 to 33 mm	*Ne/Np*, Ratio of Experimental to Predicted Life	*Ne/Np* Mean	*Ne/Np* Standard Deviation
7050-T6	1.4	1/4000	19	16	1.2	8.5	13.3
	1.8	1/4000	484	17	28.5	...	...
	1.8	1/8000	16	9	1.8	...	...
	8-level		1516	660	2.3	...	...
7050-T7	1.4	1/4000	38	35	1.1	2.8	2.0
	1.8	1/4000	225	46	4.9	...	...
	1.8	1/8000	77	19	4.1	...	...
	8-level		1725	1585	1.1	...	...
7075-T6	1.4	1/4000	9	9	1.0	18.4	21.7
	1.8	1/4000	485	10	48.5	...	...
	1.8	1/8000	100	5	20.0	...	...
	8-level		1143	275	4.2	...	...
7075-T7	1.4	1/4000	28	23	1.2	6.0	5.0
	1.8	1/4000	279	30	9.3	...	...
	1.8	1/8000	145	13	11.2	...	...
	8-level		1833	880	2.1	...	...

mental lives for 7075 and 7050 subjected to spectrum loading conditions of this investigation. Constant amplitude FCG rate data established for the same materials served as input to the model.

Comparison of experimental to predicted lives is made in Table 12. Predicted lives varied from 1 to about 50 times shorter than observed lives. Though estimated life was generally conservative, relative performance ranking between materials was not predicted correctly. The discrepancy in predicted degree of retardation is related to omission of the secondary cracking mechanism in the model. For example, Table 12 indicates greatest variability in accuracy of life prediction occurred for lower purity 7075 in the peak strength (T6) temper, while best predictions were those for higher purity 7050 in the overaged T7 temper. In the former alloy, combinations of purity and strength enhanced the role of constituent-overload interaction that is not considered by EFFGRO.

Summary and Conclusions

Rankings of FCG resistance under variable amplitude loading are not always consistent with rankings observed under constant amplitude loading conditions. Even when ranking is the same, quantitative variations between alloy performance may not be reliably predicted with present fracture-mechanics-based life prediction technology. Alloy ranking is sensitive to interaction of alloy metallurgy with loading parameters, such as overload magnitudes, spacings, and nominal stress intensity factor.

Crack growth mechanisms attributed to overload-induced retardation phenomena compete, and observed behavior is controlled by the particular mechanisms that dominate. In some cases, a different controlling mechanism may exist at different stages of a test (for example, short versus long crack length). Resistance to FCG under spectrum loading cannot be consistently correlated with strength or toughness because behavior depends on the load-microstructure interaction that dominates.

Alloy fatigue response is application dependent. This circumstance, coupled with the limited knowledge of how alloy microstructure relates to design of a fatigue resistant part, restricts the present ability to optimize alloy design or alloy selection or both for high FCG resistance. However, based on improved phenomenological understanding of how alloy microstructure influences FCG processes and mechanical property tradeoffs, one can *begin* to make some crude generalizations. Thus, if the overriding fatigue failure mechanism is known for a particular class of application (for example, fighter versus transport aircraft), an optimum alloy microstructure or design approach or both might be recommended. The dominant failure mechanism might be established by experience or failure analysis or both.

For 7X75 and 7050 type aluminum alloys, some generalities on how microstructure influences FCG performance under various simple loading conditions are summarized in Table 13 and may be stated as follows:

1. Overaging to T7 tempers and higher copper content increase FCG resistance, in part, by reducing degradation by the environment. This attribute is beneficial for constant amplitude loading, and for spectrum loading with either low level overloads, high level overloads infrequently spaced, or low nominal stress intensities. Under these conditions, performance of 7050 is superior to performance of 7075, 7475, and 7010, while T7 tempers outperform T6 tempers.

2. When the structural member is highly stressed, coarse intermetallic constituent particles in the alloy initiate incipient cracks. These secondary cracks reduce toughness and constant amplitude FCG resistance at high ΔK. However, for certain spectra (for example, simple spectra with high overloads frequently superimposed upon the base at moderate ΔK), increasing volume fraction of intermetallic particles is beneficial. In those cases, incipient cracks at particle locations introduced by overloads retard FCG at lower stresses by dividing the "effective" ΔK at the crack tip. Alloy 7075 with higher intermetallic constituent volume fraction (iron, silicone) than 7050 or 7475 favors the secondary crack mechanism of overload induced retardation.

3. Overaging progressively decreases strength and increases toughness as well as increasing resistance to the environment. Increased toughness has

TABLE 13—*Generalities for simplified load histories*[a].

Typical Load History Characteristic	Dominant FCG Characteristic	Remarks
Constant amplitude Low level overloads High overloads infrequently spaced Spectra with low nominal ΔK	FCG rate controlled by resistance to environment Degree of FCG retardation controlled by plastic zone interaction	Favors high-copper and overaged tempers Favors 7050 over 7075 and 7475 Favors T7 over T6 type tempers
High overloads superimposed frequently upon base at moderate ΔK	Degree of FCG retardation controlled by secondary cracks initiated during tensile overloads	Favors alloys with lower purity Favors 7075 over 7050 and 7475 Favors T6 over T7 type tempers
High overloads at high ΔK Large number of base line cycles at moderate or high ΔK	FCG rate controlled by crack advance during high tensile loads	Favors high-purity alloys Favors 7475 and 7050 over 7075 Favors T7 over T6 type tempers

[a]In simple spectra at low nominal stress intensity or in more complex spectra, effect of different microstructural features may compete. Consequently, relative ranking may change with alloy, temper, and spectrum.

both positive and negative effects in spectrum loading. It reduces growth of the main crack during high overloads that is positive, but decreases severity of secondary cracks and thus has a negative effect on retardation during subsequent low stress cycles. The controlling mechanism depends on the alloy and load history. As a generality, peak strength (T6) aging should provide better performance in simple spectrum where the ratio of the tensile overload to the base is high and stress intensity is moderate. Overaged T7 tempers should provide superior performance where base stress intensity is high and tensile overloads frequent.

Recommendations

To (*a*) increase probability of success for "fatigue improvement" and (*b*) to expedite implementation of advanced alloys into service, suitable generalizations are needed to relate results of laboratory tests to performance in the field. Greater use of standardized reference load spectra to compare alloy performance for a specific class of applications, for example see Refs *27–29*, is expected to address this need. Further clarification of controlling FCG mechanisms is required. Simplified spectra like those employed in this study are useful for the latter purpose. Life prediction methodology must include metallurgical parameters to assure that the analysis can accommodate material variations. Finally, we should improve the rather limited knowledge of metallurgical factors that influence FCG behavior in the near threshold (low ΔK) regime where the greatest portion of component FCG life is often spent. This characterization is also important to consideration of overload induced FCG retardation attributed to reduction in "effective" ΔK at the crack tip.

References

[*1*] Truckner, W. G., Staley, J. T., Bucci, R. J., and Thakker, A. B., "Effects of Microstructure on Fatigue Crack Growth of High-Strength Aluminum Alloys," USAF Technical Report AFML-76-169, Oct. 1976.

[*2*] Staley, J. T., Truckner, W. G., Bucci, R. J., and Thakker, A. B., "Improving Fatigue Resistance on Aluminum Aircraft Alloys," WESTEC 77 Paper No. 3, American Society of Metals, Metals Park, Ohio, 1977.

[*3*] Brownhill, D. J., Davies, R. E., Nordmark, G. E., and Ponchel, B. M., "Exploratory Development for Design Data on Structural Aluminum Alloys in Representative Aircraft Environments," USAF Technical Report AFML-TR-77-102, 1977.

[*4*] Jones, R. L., and Coyle, T. E., "The Mechanical, Stress-Corrosion, Fracture Mechanics, and Fatigue Properties of 7050, 7475, and Ti-8 Mo-8 V-2 Fe-3 Al Plate and Sheet Alloys," General Dynamics Fort Worth Division Report FGT-5791, 1976.

[*5*] Lauchner, E. A., "Alloy Selection for a Military Fighter Aircraft," Northrop Corporation Aircraft Division, Report NOR-75-147, Oct. 1975.

[*6*] *Fatigue Crack Growth Under Spectrum Loads, ASTM STP 595*, American Society for Testing and Materials, 1976.

[*7*] Wood, H. A., "The Use of Fracture Mechanics Principles in the Design and Analysis of Damage Tolerant Aircraft Structures," *AGARDograph* No. 176, Advisory Group for Aerospace Research & Development, Nov. 1973.

[8] Bucci, R. J. in *Flow Growth and Fracture, ASTM STP 631,* American Society for Testing and Materials, 1977, pp. 388-401.
[9] Sanders, T. H., Jr., Sawtell, R. R., Staley, J. T., Bucci, R. J., and Thakker, A. B., "Effect of Microstructure on Fatigue Crack Growth of 7XXX Aluminum Alloys Under Constant Amplitude and Spectrum Loading," Final Report, Naval Air Development Center Contract No. N0019-76-C-0482, 14 April 1978.
[10] Staley, J. T. in *Properties Related to Fracture Toughness, ASTM STP 605,* American Society for Testing and Materials, 1976, pp. 71-103.
[11] Staley, J. T., "How Microstructure Affects Fatigue and Fracture of Aluminum Alloys," *Fracture Mechanics,* N. Perrone et al, Eds., University Press of Virginia, 1978, p. 671.
[12] Sanders, T. H., Jr. and Staley, J. T., "Review of Fatigue and Fracture Research on High Strength Aluminum Alloys," presented at the 1978 ASM Materials Science Seminar, St. Louis, Mo., 14-15 Oct. 1978.
[13] Bucci, R. J., "Selecting Aluminum Alloys to Resist Failure by Fracture Mechanisms," *Engineering Fracture Mechanics,* Vol. 12, 1979, pp. 407-441.
[14] Mills, W. J. and Hertzberg, R. W., "Load Interaction Effects on Fatigue Crack Propagation in 2024-T3 Aluminum Alloy," *Engineering Fracture Mechanics,* Vol. 8, No. 4, 1976, p. 657.
[15] Chanani, G. R., "Fundamental Investigation of Fatigue Crack Growth Retardation in Aluminum Alloys," USAF Technical Report AFML-TR-76-156, Sept. 1976.
[16] Wheeler, O. E., "Crack Growth Under Spectrum Loading," *Journal of Basic Engineering Transactions,* March 1972, pp. 181-186.
[17] Trebules, V. W., Roberts, R., and Hertzberg, R. W., in *Progress in Flaw Growth and Fracture Toughness Testing, ASTM STP 536,* American Society for Testing and Materials, 1973, pp. 115-146.
[18] Paris, P. C., "The Fracture Mechanics Approach to Fatigue," *Fatigue—An Interdisciplinary Approach,* Syracuse University Press, 1964.
[19] Rice, J. R., *Fatigue Crack Propagation, ASTM STP 415,* American Society for Testing and Materials, 1967, pp. 247-311.
[20] Irwin, G. R., "Plastic Zone Near a Crack and Fracture Toughness," *Proceedings,* Seventh Sagamore Ordnance Materials Research Conference, Syracuse University Research Institute, Aug. 1960.
[21] Schra, L. and VanLeeuwen, H. P., "Heat Treatment Studies of Aluminum Alloy Type 7050 Forgings," Interim Report No. 2, NLR-TR-76008C, National Aerospace Lab, NLR the Netherlands, 1976.
[22] Willenborg, J., Engle, R. M., and Wood, H. A., "A Crack Growth Retardation Model Using an Effective Stress Concept," USAF Technical Report TM-71-1-FBR, Jan. 1971.
[23] Vroman, G., "Analytical Prediction of Crack Growth Retardation Using a Critical Stress Intensity Concept," North American Rockwell, Los Angeles Division, Technical Report TFR 71-701, 1971.
[24] Bell, P. D. and Wolfman, A. in *Fatigue Crack Growth Under Spectrum Loads, ASTM STP 595,* American Society for Testing and Materials, 1976, pp. 306-317.
[25] Dill, H. D. and Saff, C. R. in *Fatigue Crack Growth Under Spectrum Loads, ASTM STP 595,* American Society for Testing and Materials, 1976, pp. 306-317.
[26] Wood, H. A., Gallagher, J. P., Engle, R. M., and Potter, J. M., "Current Practice on Estimating Crack Growth Damage Accumulation with Specific Application to Structural Safety, Durability and Reliability," USAF Technical Report, AFFDL-TR-75-32, Jan. 1976.
[27] "Description of a *F*ighter *A*ircraft *L*oading *STA*ndard *F*or *F*atigue evaluation, FALSTAFF," combined report of following laboratories: F+W, Switzerland; LBF, Darmstadt, Germany; NLR Amsterdam, Netherland; IABG, Ottobrunn, Germany; presented at AGARD meeting Ottawa, Advisory Group for Aerospace Research and Development, March 1976.
[28] Schutz, D., "A Standardized Flight-by-Flight Test Program for the Fatigue Life Evaluation of Wing Components of Transport Aircraft," *Fail Safe Aircraft Structures,* A. M. Stagg, Ed., Royal Aircraft Establishment, Farnsborough, 1973 (RAE TR 73183), S. 3.4/1-34.
[29] Tucker, L. and Bussa, S. in *Fatigue Under Complex Loading,* R. M. Wetzel, Ed., Society of Automotive Engineers, Inc., Warrendale, Pa., 1977, pp. 1-53.

T. M. Hsu[1] *and W. M. McGee*[1]

Effects of Compressive Loads on Spectrum Fatigue Crack Growth Rate

REFERENCE: Hsu, T. M. and McGee, W. M., "**Effects of Compressive Loads on Spectrum Fatigue Crack Growth Rate,**" *Effect of Load Spectrum Variables on Fatigue Crack Initiation and Propagation, ASTM STP 714,* D. F. Bryan and J. M. Potter, Eds., American Society for Testing and Materials, 1980, pp. 79-90.

ABSTRACT: A procedure, which allows flight-simulation profiles to be applied under stress intensity factor control, was used to study effects of compressive-compressive load cycles on spectrum fatigue crack growth rate. This approach eliminates the maximum stress-intensity factor, K_{max}, and its associated plastic-zone size as a variable within a given test, and allows a small amount of crack growth representing instantaneous conditions in conventional load control tests. Tests were performed on center-cracked 7075-T651 aluminum alloy specimens subjected to typical flight-spectra, simulating both transport and bomber airplanes. The results indicated that the number of compressive-compressive cycles has little effect on spectrum-crack-growth rate and that essentially the same results were produced by a single compressive load. It was also found that the crack growth rate was relatively insensitive to the magnitude of the compressive load. A saturated condition was reached at a fairly low load level. The sequence of overload-comprensive load was also evaluated. For low stress intensity factor, the crack growth rate obtained was slightly higher when the application of compressive loads preceded an overload. However, the opposite occurred when the stress intensity factor was larger.

KEY WORDS: crack-growth rate, spectrum load, retarding, aluminum alloy, fatigue (materials), crack propagation

Analytical methodology to predict slow crack growth in aerospace structures subjected to simulated-flight loading is an essential element in the overall fracture-control program currently being applied on fracture-critical structures. Current predictive methodologies for such complex loading are not precise; however, considerable effort has been, and is being, directed toward a better understanding of the crack-growth process. From

[1]Aircraft Development Engineers-Specialists, Lockheed-Georgia Company Marietta, Ga. 30063.

such efforts will evolve improved modeling of fatigue crack growth. Within the current state of technology, it is possible to obtain an unconservative or conservative crack-growth life prediction, depending upon the analysis methodology and baseline data used. Consequently, current predictive methods must be judiciously applied and substantiated by adequate testing. Eventually, unconservative methods must be eliminated for reasons of safety and structural life, and overly conservative methods must be eliminated since their impact diffuses throughout the entire design process to adversely affect total performance and cost.

It is generally agreed that linear cumulative techniques, by integrating basic constant-amplitude growth-rate data obtained from laboratory tests on simple coupons, produce good crack-growth predictions for constant-amplitude loading. But, when the load is of arbitrarily varying amplitude, the linear analysis that computes an accumulation of growth under individual loads without regard for load history is often found to be overly conservative. This is because, under variable-amplitude cyclic loading, the crack-growth rate is affected by load-interaction effects not present in constant-amplitude load tests. As examples, a tensile overload causes extensive plastic deformation of the crack tip which, in turn, impedes the crack growth during subsequent lower load cycles [*1,2*],[2,3] while a compressive load and sometimes even a tensile underload may either accelerate the crack growth of subsequent tensile load cycles or reduce the beneficial retardation effect created by an overload [*3-6*].

The importance of the retardation produced by tensile overloads on the accurate prediction of structural life has been recognized, and quite a few investigations [*7-14*] have been stimulated in this area. A number of theories [*2,15,16*] have been proposed to explain the retardation phenomenon, and several models [*17-23*] have been suggested to account for its effect in the prediction of fatigue crack growth. Although attempts [*21-23*] have been made to account for the effect of compressive loads on crack growth under a simple spectrum, there is practically no model that can adequately address the effect of compressive loads on crack growth under simulated flight spectrum loadings. When compressive load cycles are neglected, crack growth life predictions could be seriously unconservative. The purpose of this research is to develop the needed understanding of the effect of cyclic compressive-compressive loads on crack growth under simulated flight loading and to provide guidance for the

[2] The italic numbers in brackets refer to the list of references appended to this paper.

[3] Both accelerated crack growth and reduction of retardation imply an increase in the crack growth rate. However, acceleration is used when the associate crack growth rate is higher than the one obtained under the constant amplitude load condition, while the reduction of retardation is used when the associate crack growth rate, though increased, is still under retarded condition, that is, less than the coresponding constant-amplitude crack growth rate.

development of a better analytical model to more accurately predict crack growth under such complex loading.

Experimental Procedures

To date, all of the experimental studies conducted on the effect of compressive loads on crack growth have been limited to cases where there is only a single application of compressive load immediately preceded or followed by the overload. In order to study effects of multiple cycles of compressive loads on spectrum fatigue crack growth, a test system computer program was developed that allows flight simulation profiles to be applied under stress-intensity factor control on center-cracked specimens. In operation, a specified maximum stress intensity factor, K_{max}, is assigned to the maximum stress contained in the given simulated flight spectrum. The corresponding maximum test load, P_{max}, is then computed using specimen dimensions (including the current crack length) and the stress intensity factor equation with a finite-width correction, that is

$$P_{max} = \frac{K_{max} WB}{\sqrt{\pi a \sec\left(\frac{\pi a}{W}\right)}} \tag{1}$$

where W and B are the width and the thickness of the specimen, and a is one-half of total crack length. This maximum test load is then used to proportionally scale down the entire spectrum profile and provide corresponding loads for the entire flight. The analog voltages representing these test loads are then programmed to command the electrohydraulic servo-controlled MTS test system. The test system contained the necessary electronic elements, properly integrated to provide control of the servo loop, monitor loads, and perform the fail-safe function. During test, the specimens were fitted with Teflon-lined support bars to prevent buckling, and crack-length measurements were made on one surface of the specimen using an optical technique. Measurements were made to within ± 0.025 mm (0.001 in.) by microscopically observing the crack tip against a reference grill lightly engraved on the specimen surface. As the crack grew, the computer program was periodically provided with the current crack length, which was used to reduce the loads in accordance with Eq 1, and thereby maintain all K-values quasi-constant. Crack length data were updated at intervals such that the K-values were maintained constant to within one percent. In this manner, K-values for each condition in the flight remained essentially constant as the crack grew. This approach eliminates the maximum stress-intensity factor and its associated plastic-zone size as a variable within a given test, and permits a small amount of crack growth representing instantaneous conditions in conventional load-control tests. Conditions for different crack lengths can be simulated by assigning different maximum stress-intensity factor values to the maximum stress in the far-field stress spectrum. This approach was used on 6.35 mm (0.25 in.) thick center-cracked specimens of 7075-T651 aluminum plate alloy to evaluate effects of compressive-compressive load cycles on spectrum fatigue-crack growth rate. The width and length of the test section were 101.6 and 203.2 mm (4 and 8 in.), respectively. The most frequent flight from a multi-mission C-141 transport aircraft and a typical flight of a bomber aircraft were selected for use in the tests. The flight profiles of the transport and the bomber aircrafts are shown in Figs. 1 and 2, respectively. The baseline transport spectrum consists of six load layers or 337 load cycles, while the baseline bomber spectrum contains 40 load layers or 109 load cycles. For each spectrum, two levels of the K_{max} representing the stress-intensity factors corresponding to a wide range of crack lengths of practical interest were used in the tests. The K_{max} values used in the tests were 10.99 and 27.45 MN/m$^{3/2}$ (10 and 25 ksi$\sqrt{\text{in.}}$) for the transport spectrum and 10.99 and 21.98 MN/m$^{3/2}$ (10 and 20 ksi$\sqrt{\text{in.}}$) for the bomber spectrum.

Three different numbers of compressive-compressive load cycles were used with each value of K_{max}. They represent the baseline condition (N = 4), single-underload (N = 0.5), and a large number of compressive-compressive load cycles (N = 300). Three levels of the minimum stress intensity factor (K_{min} = 0, −0.5 and −1.0 K_{max}), were tested under the single-underload condition to evaluate the effect of the magnitude of compressive load on spectrum fatigue crack-growth rate. Tests were also conducted to determine how the sequence of overload-underload affects such growth rate.

During the tests, ten measurements of spectrum fatigue crack growth rate, da/dF, were made for each load variation to provide statistical significance to the data. For the transport spectrum, each measurement is the average of 25 flights for the higher K-value and 200 flights for the lower K-value; while for the bomber spectrum, each measurement is the average of 17 flights for the higher K-value and 125 flights for the lower K-value.

Results and Discussion

The results of the tests are presented in Figs. 3 through 8. In the figures, each vertical bar represents the range of scatter of ten data measurements and the symbols (circle and triangle) represent the average of ten data point. Figures 3 and 4 show the spectrum fatigue crack growth rate, da/dF, as a function of number of compressive-compressive load cycles for the transport and bomber spectra, respectively. The data indicate that the number of compressive-compressive load cycles has little effect on spectrum

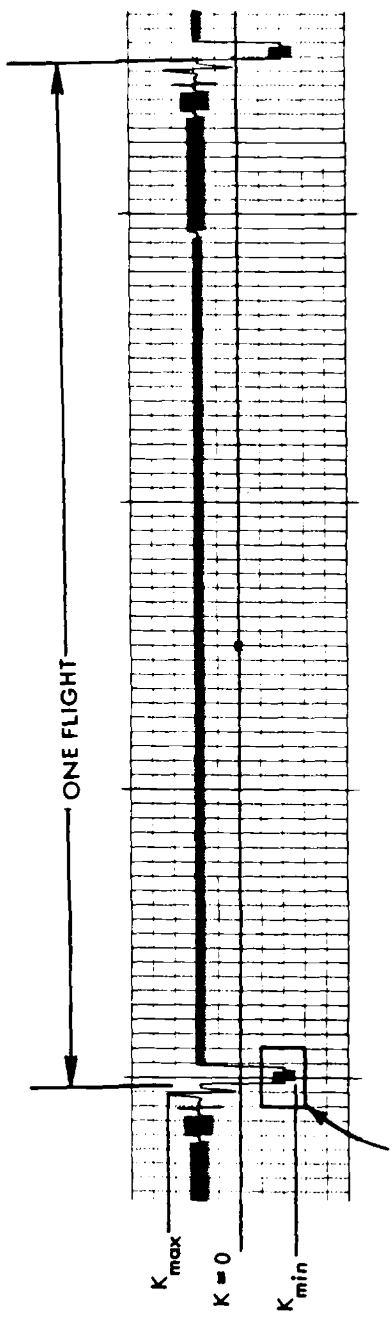

FIG. 1—K profile for the transport flight and compressive load variables evaluated.

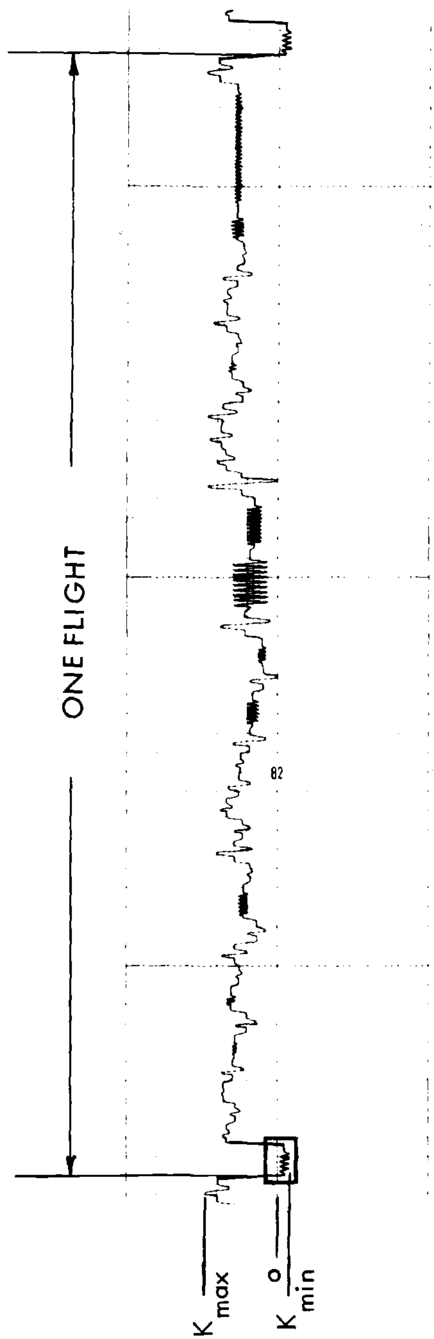

FIG. 2—K profiles for the bomber flight and compressive load variables evaluated.

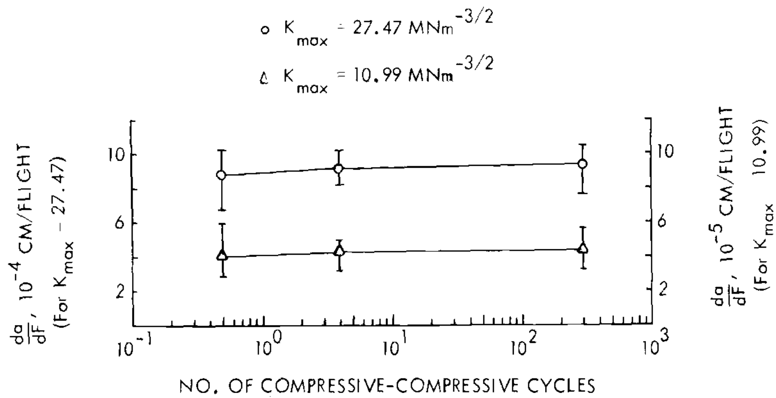

FIG. 3—*Effect of number of compressive-compressive loads on the transport spectrum fatigue crack-growth rate.*

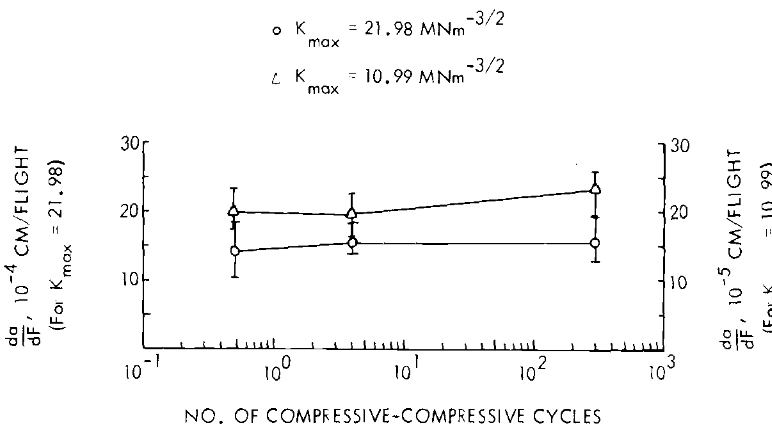

FIG. 4—*Effect of number of compressive-compressive loads on the bomber spectrum fatigue crack-growth rate.*

crack growth rate and that essentially the same results were produced by a single compressive load. The cracks grew an average of about 12 percent faster for $N = 400$ than for $N = 0.5$. Figures 5 and 6 show the effect of the magnitude of the single compressive load on spectrum crack growth rate for the transport and bomber spectra, respectively. As seen from these two figures, the trend indicated that the spectrum crack growth rate was relatively insensitive to the magnitude of the compressive load, and a saturated condition was reached at a fairly low load level as was previously obtained under constant-amplitude load conditions [*6*]. For example, da/dF for the bomber spectrum (Fig. 6) increased by less than 7 percent

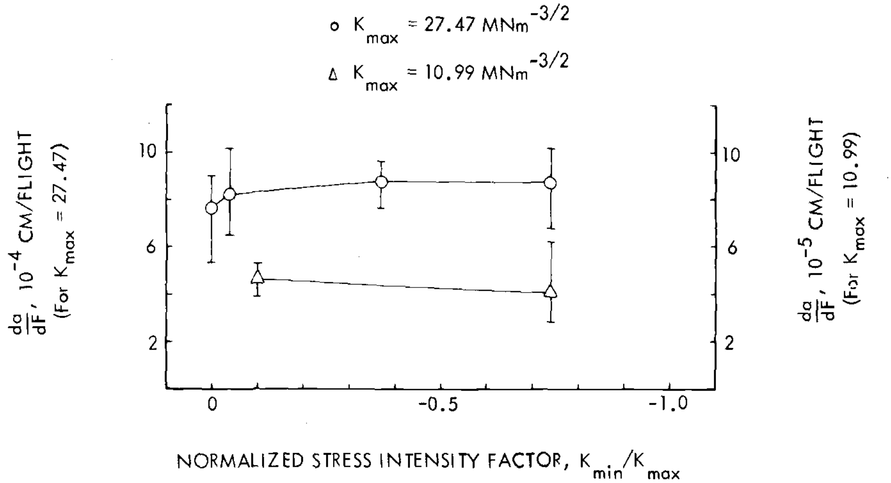

FIG. 5—*Effect of the magnitude of single compressive load on the transport spectrum fatigue crack-growth rate.*

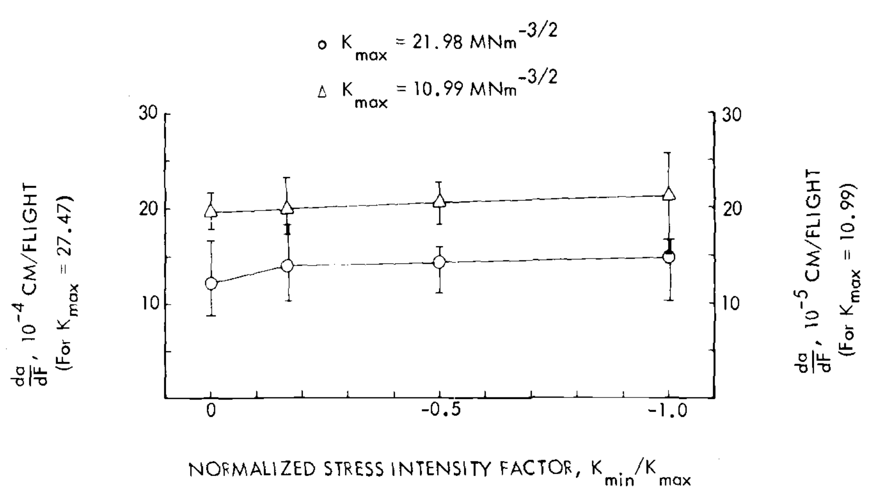

FIG. 6—*Effect of the magnitude of single compressive load on the bomber spectrum fatigue crack-growth rate.*

when K_{min}/K_{max} was changed from -0.2 to -1.0. The results obtained here suggested that a large number of compressive-compressive loads may be represented by a single compressive load in the crack growth prediction.

The effect of the sequence of overload-underload on the transport-spectrum crack-growth rate is presented in Fig. 7, and limited data generated using the bomber spectrum are presented in Fig. 8. The solid lines in Figs. 7 and 8 describe the spectrum crack-growth rate as a function of the number of

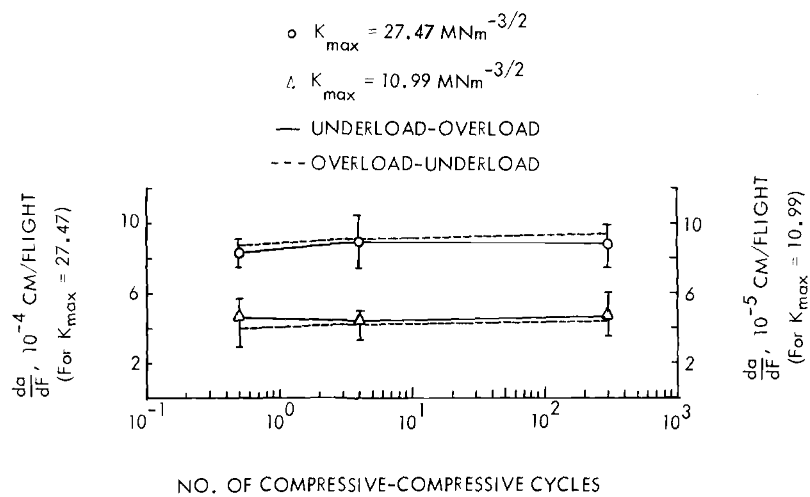

FIG. 7—*Effect of number of compressive-compressive loads and the sequence of overload-underload on the transport spectrum fatigue crack-growth rate.*

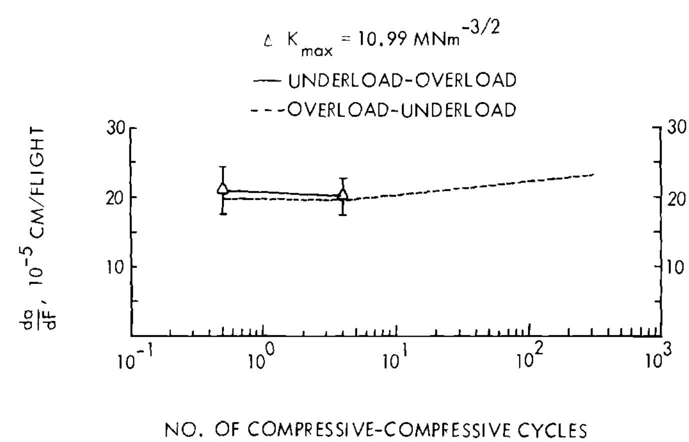

FIG. 8—*Effect of the sequence of overload-underload on the bomber spectrum fatigue crack-growth rate.*

compressive-compressive load cycles when the application of such compressives loads precede an overload. Similar results, for the case where the compressive-compressive cycles were applied immediately after an overload, were replotted from Figs. 3 and 4 as dashed lines. It is shown that the number of compressive-compressive cycles has little effect on growth rate, and that practically the same results were produced by a single compressive load. The other important observation from these two figures is that, for the lower level of stress-intensity factor, when the application of compressive-compressive loads preceded an overload, the corresponding spectrum crack-growth rate was higher than the one obtained when such compressive loads were applied after the overload by an average of about 6 percent. An equal but opposite trend was obtained for a higher level of stress-intensity factor. Physically, this means that, for a given flight spectrum, when the crack is small (the corresponding stress-intensity factor is low), the acceleration of crack growth following the compressive-compressive loads is more significant than the reduction of retardation effect due to the compressive-compressive loads. However, when the crack becomes long (resulting in a larger stress-intensity factor), then the reduction of retardation effect becomes more important than the acceleration of crack growth due to the occurrence of compressive-compressive load cycles. Mechanically, this may be because that, when the stress-intensity factor is low, a relatively smaller plastic zone at the crack tip results in conditions favorable for more brittle extension, and the sharpness of the crack is of primary importance. The application of compressive-compressive loads tends to sharpen the crack tip and accelerate the crack growth of subsequent tensile load cycles. When the stress-intensity factor becomes large, the state of stress near the crack tip is dominated by an extensive plastic zone and the sharpness of the crack tip is no longer primarily important in propagating the crack. In this case, the reduction of retardation effect due to prior overload plays a more significant role.

Conclusions

An experimental study on the effect of compressive loads on flight-simulation spectrum crack-growth rate was conducted. The study provides a better understanding of spectrum crack growth as it is affected by the inclusions of additional compressive loads. Based on the data obtained under this study, the conclusions reached may be summarized as follows:

1. The number of compressive-compressive cycles had little effect on spectrum crack-growth rate, and essentially the same results were produced by a single compressive load. Therefore, a large number of compressive-compressive load cycles may be represented by a single compressive load in the crack growth prediction.
2. The crack-growth rate was relatively insensitive to the magnitude of the compressive load. A saturated condition was reached at a fairly low load level. Further increase in the magnitude of compressive load did not show a significant change in the crack-growth rate.
3. For low stress-intensity factor, when the application of compressive-compressive loads preceded an overload, the corresponding spectrum crack-growth rate was slightly higher than the one obtained when such compressive loads were applied immediately after the overload. However, the opposite occurred when the stress-intensity factor became larger.

Acknowledgments

This work was sponsored by the Independent Research and Devlopment program of Lockheed-Georgia Company.

Reference

[1] Schijve, J., "Fatigue Crack Propagation in Light Alloy Sheet Material and Structures," NLR MP 195, Amsterdam, The Netherlands, Aug. 1960.
[2] Hudson, C. M. and Hardrath, H. F., "Effects of Changing Stress Amplitude on the Rate of Fatigue Crack Propagation of Two Aluminum Alloys," TN D-960, National Aeronautics and Space Administration, Washington, D.C., Sept. 1961.
[3] Crooker, T. W., "Effect of Tension-Compression Cycling on Fatigue Crack Growth in High Strength Alloys," Report 7220, U.S. Naval Research Laboratory, Washington, D.C., Jan. 1971.
[4] Rice, R. C. and Stephens, R. I. in *Progress in Flaw Growth and Fracture Toughness Testing, ASTM STP 536,* July 1973, American Society for Testing and Materials, pp. 95-113.
[5] Hsu, T. M. and Lassiter, L. W., *Journal of Aircraft,* Feb. 1975, pp. 100-104.
[6] McGee, W. M. and Hsu, T. M., "Effects of Underloads on Fatigue Crack Growth," AFFDL-TR-77-2, Air Force Flight Dynamics Laboratory, Wright Patterson Air Force Base, Ohio, March 1977.
[7] McMillan, J. D. and Pelloux, R. M. N. in *Fatigue Crack Propagation, ASTM STP 415,* American Society for Testing and Materials, June, 1967, pp. 505-533.
[8] Hudson, C. M. and Raju, K. W., "Investigation of Fatigue Crack Growth Under Simple Variable-Amplitude Loading," TN D-5702, National Aeronautics and Space Administration, Washington, D.C., March 1970.
[9] Von Euw, E. F. J., "Effect of Overload Cycle on Subsequent Fatigue Crack Propagation in 2024-T3 Aluminum Alloy," Ph.D. thesis, Department of Mechanical Engineering, Lehigh University, Bethlehem, Pa., March 1971.
[10] Von Euw, E. F. J., Hertzberg, R. W., and Roberts, R. in *Stress Analysis and Growth of Cracks, ASTM STP 513,* American Society for Testing and Materials, Sept. 1972, pp. 230-259.
[11] Hsu, T. M., "Investigation of Fatigue Crack Growth Under Simple Variable-Amplitude Loading," Report SMN 372, Lockheed-Georgia Company, Marietta, Ga., Feb. 1973.
[12] Corbly, D. M. and Packman, P. F., *Engineering Fracture Mechanics,* Vol. 5, June 1973, pp. 479-497.
[13] Trebules, V. M., Jr., Roberts, R., and Hertzberg, R. W. in *Progress in Flaw Growth and Fracture Toughness Testing, ASTM STP 536,* American Society for Testing and Materials, July 1973, pp. 115-139.
[14] Wei, R. P., Shih, T. T., and Fitzgerald, J. H., "Load Interaction Effects on Fatigue Crack Growth in Ti-6AI-4V Alloy," CR-2239, National Aeronautics and Space Administration, Washington, D.C., April 1973.
[15] Hudson, C. M. and Hardrath, H. F., "Investigation of Variable Loadings of Fatigue Crack Propagation Patterns," TN D-1803, National Aeronautics and Space Administration, Washington, D.C., Aug. 1963.
[16] Elber, W. in *Damage Tolerance in Aircraft Structures, ASTM STP 486,* American Society for Testing and Materials, pp. 230-242.
[17] Wheeler, O. E., *Journal of Basic Engineering,* March 1972, pp. 181-186.
[18] Willenborg, J., Engle, R. M., and Wood, H. A., "A Crack Growth Retardation Model Using an Effective Stress Concepts," TM 71-1-FER, Air Force Flight Dynamics Lab, Wright Patterson Air Force Base, Ohio, Jan. 1971.
[19] Gallagher, J. P., and Hughes, T. F., "Influence of Yield Strength on Overload Fatigue Crack Growth Behavior in 4340 Steel," AFFDL-TR-74-27, Air Force Flight Dynamics Laboratory, Wright-Patterson Air Force Base, Ohio, July 1974.
[20] Gray, T. D. and Gallagher, J. P., "Predicting Fatigue Crack Retardation Following a

Single Overload Using a Modified Wheeler Model," presented at the 8th National Symposium on Fracture Mechanics, Brown University, Providence, R.I., 26-28 Aug. 1974.

[*21*] Bell, P. D. and Creager, M., "Crack Growth Analysis for Arbitrary Spectrum Loading," AFFDL-TR-74-129, Air Force Flight Dynamics Laboratory, Wright-Patterson Air Force Base, Ohio, October 1974.

[*22*] Hsu, T. M., "Development of Load-Interaction Model," Report SMN 390, Lockheed-Georgia Company, Marietta, Ga., Feb. 1976.

[*23*] Dill H. D. and Saff, C. R. in *Cyclic Stress-Strain and Plastic Deformation Aspects of Fatigue Crack Growth, ASTM STP 637*, American Society of Testing and Materials, pp. 141-152.

J. M. Larsen[1] *and C. G. Annis, Jr.*[2]

Observation of Crack Retardation Resulting from Load Sequencing Characteristic of Military Gas Turbine Operation

REFERENCE: Larsen, J. M. and Annis, C. G., Jr., **"Observation of Crack Retardation Resulting from Load Sequencing Characteristic of Military Gas Turbine Operation,"** *Effect of Load Spectrum Variables on Fatigue Crack Initiation and Propagation, ASTM STP 714,* D. F. Bryan and J. M. Potter, Eds., American Society for Testing and Materials, 1980, pp. 91-107.

ABSTRACT: The nature of crack propagation resulting from flight loading representative of military gas turbine operation is investigated. Mission stress profiles for turbine disks fabricated from the superalloys GATORIZED IN 100 and Waspaloy contain load sequences that produce synergistic effects on crack propagation. Major load throttle excursions, overloads, occur routinely during flight, and a retardation in subsequent crack propagation generally results. Such mission load interaction effects have been addressed in crack propagation testing employing repetitive overload-fatigue sequences. The influences of overload ratio ($P_{overload}/P_{max}$) and the number of fatigue cycles between overloads have been investigated for crack propagation at 649°C (1200°F), and an interpolative model of these effects is presented. A determination of the instantaneous crack retardation following a mission major load excursion is accomplished with an unconventional method. The existence of a deceleration in crack growth rate, delayed retardation, following a mission overload is verified. Typically, this period is greater than the total number of baseline fatigue cycles applied between engine mission overloads, and delayed retardation is largely, if not entirely, responsible for the beneficial effects of the overloading.

KEY WORDS: crack propagation, fatigue (materials), retarding agents, superalloys

Nomenclature

a Crack length

C_1 SINH material coefficient = 0.5

[1]Materials engineer, Air Force Wright Aeronautical Laboratories, Wright-Patterson Air Force Base, Ohio 45433.

[2]Assistant project engineer, Pratt and Whitney Aircraft Group, West Palm Beach, Fla. 33402.

C_2	SINH horizontal scaling coefficient
C_3	SINH horizontal inflection coefficient
C_4	SINH vertical inflection coefficient
da/dN	Cyclic rate of crack growth
ΔK	Applied stress intensity factor range
ΔN_{OL}	Number of fatigue cycles applied between periodic overloads
K	Stress intensity factor
K_{max}	Maximum stress intensity factor
K_{min}	Minimum stress intensity factor
K_{OL}	Overload stress intensity factor
N	Number of cycles
N^*	Number of cycles during which crack growth rate is retarded following an overload
N_{DR}	Period of delayed retardation
P	Applied load
P_{max}	Maximum applied load
P_{min}	Minimum applied load
P_{OL}	Magnitude of applied overload
R	Load ratio (P_{min}/P_{max})

Operational loading spectra imposed on rotating disks in a military gas turbine engine contain load sequences that differ significantly from the high cycle loading encountered in flight of an airframe. Fatigue of a superalloy engine disk is a low cycle phenomenon resulting from throttle excursions and associated thermal stresses. Major and minor throttle excursions compose a load sequence from which synergistic crack propagation results, and this load interaction is complicated by elevated temperature operation and concomitant time dependent behavior.

Typical loading spectra are derived from service missions that include ferry, training, and terrain following radar (TFR) activity. A mission composite is presented in Fig. 1 [*1*].[3] The loading spectra may contain frequent single or multiple major load excursions (overloads) with a small number (usually no more than 50) of less severe throttle excursions between overloads. As a result of this frequent overloading, crack growth immediately following an overload is of increased significance, while the crack retardation commonly observed many cycles after an overload application is of reduced importance since this retarded growth is soon interrupted by another overload excursion.

This paper reports the findings of an investigation into the effects of frequent overloading on elevated temperature fatigue crack propagation of the superalloys GATORIZED IN 100 and Waspaloy. An empirical model

[3]The italic numbers in brackets refer to the list of references appended to this paper.

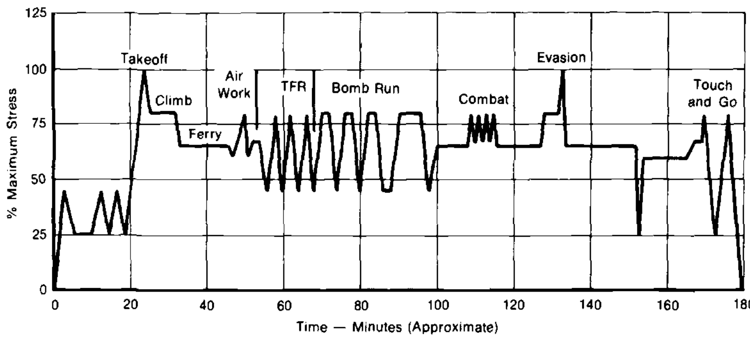

FIG. 1—*Composite mission stress profile.*

of these overload effects is described, and the characteristic retardation of crack growth that follows the frequent overloads is determined.

Crack Retardation

The crack propagation resulting under the complex conditions of loading and environment encountered in a military gas turbine engine is not predicted satisfactorily by residual stress [*2,3*] or closure [*4*] models, and a need for further study of this isolated problem exists. The current work has employed an empirical model [*5-7*] of elevated temperature fatigue crack propagation under spectrum loading. The philosophy of this approach is that any complex mission spectrum can be segregated into elemental damage events that can be quantitatively described. The crack propagation life expected under such a spectrum can then be computed as a linear addition of the damage associated with properly segregated events. Mission segregation is based on the definition of an "elemental damage event" as the smallest repeating load-time sequence that results in fatigue crack propagation not predictable by linear damage accumulation alone. A simplified mission, consisting of a single overload followed by a block of constant load amplitude fatigue cycles, is such an elemental damage event.

Figure 2 (*top*) presents a schematic of a crack growth curve, crack length (a) versus number of applied fatigue cycles (N), illustrating the common effects of a single overload on previously unretarded crack growth. When the crack growth produced by constant load amplitude fatigue is interrupted by an overload, crack growth accelerates corresponding to the overload [*8*]. Thereafter, the rate of crack propagation quickly decelerates, and after a small number of subsequent fatigue cycles the rate of crack growth achieves a minimum. This deceleration to a minimum rate of crack propagation is known as delayed retardation, and the period of delayed retardation is defined as the number (N_{DR}) of post-overload fatigue cycles required to achieve the minimum crack growth rate. Following delayed retardation,

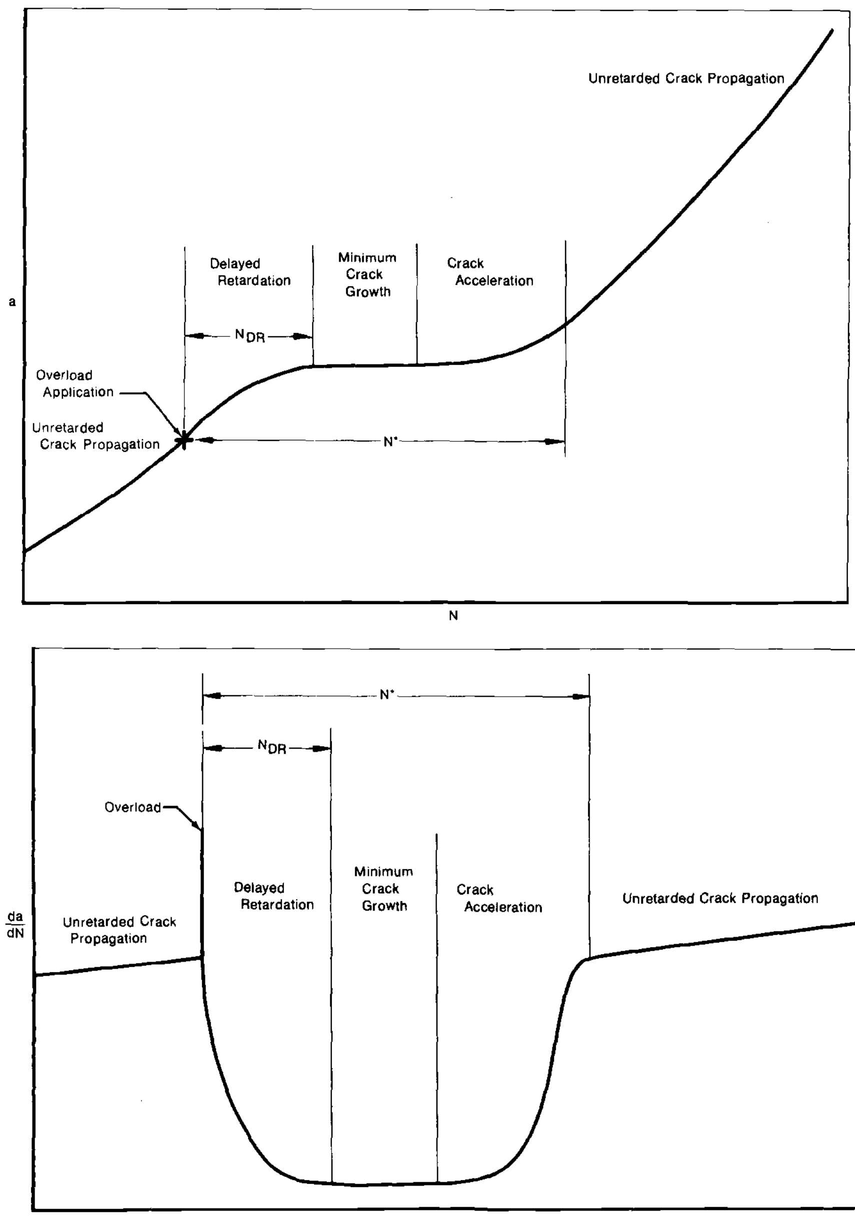

FIG. 2—*Fatigue crack retardation resulting from the application of a single overload.*

crack growth continues at a near minimum rate for an extended period, and the exhaustion of the retardation process is marked by an acceleration of crack growth to regain the unretarded rate. The total period of crack retardation, N^*, is defined as the number of cycles during which crack growth rate is retarded following an overload application. The nature of the transient crack propagation behavior that results following an overload is further revealed by differentiating the crack growth curve, Fig. 2 (*top*), to give crack propagation rate, da/dN, as a function of N, Fig. 2 (*bottom*).

Overloads that occur at cyclic intervals less than N^* interrupt and restart the crack retardation process. The beneficial effect offered by intermittent overloads has been observed to be reduced as the number of cycles between overloads, ΔN_{OL}, is reduced to fewer than N^* cycles [9,10]. As ΔN_{OL} becomes small, the relative importance of delayed retardation is increased, and the average crack growth rate associated with the overload-fatigue sequence increases.

Procedure

Fatigue crack propagation tests of the nickel-base superalloys GATORIZED IN 100 and Waspaloy were conducted on electrohydraulic testing machines operated under load control. All tests were performed in air at 649°C (1200°F), and the loading waveform was that of an isosceles triangle applied at a frequency of 0.167 Hz (10 cpm). Compact specimens (Fig. 3) of circumferential-radial (C-R) orientation, as defined in accordance with the ASTM Test for Plane-Strain Fracture Toughness of Metallic Materials (E 399-72), were machined from disk forgings representative of engine disk material. The test specimens were pre-cracked at room temperature using

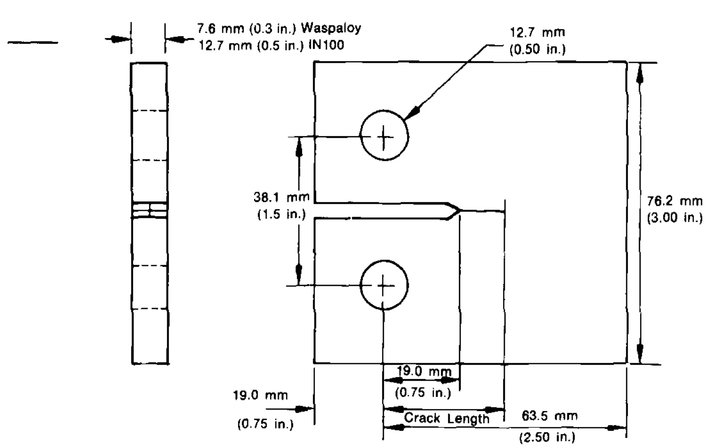

FIG. 3—*Compact specimens.*

standard procedures of ASTM Test for Constant-Load-Amplitude Fatigue Crack Growth Rates Above 10^{-8} m/Cycle (E 647-78T).

Testing was designed to evaluate the influence of frequently applied periodic overloads on otherwise constant load amplitude (ΔP) fatigue crack growth. A schematic of the basic loading sequence is presented in Fig. 4. The baseline load ratio (R = minimum load/maximum load = P_{min}/P_{max}) was 0.5 for all tests. The variables of test were the overload ratio (OLR = P_{OL}/P_{max} = 1.25, 1.50) and the number of baseline fatigue cycles between overloads (ΔN_{OL} = 5, 20, and 40).

During propagation testing, crack lengths were measured on both surfaces of the specimen with a traveling microscope. To facilitate this procedure, the test was interrupted, and the mean load was applied while holding the specimen at the temperature of testing. The increment in crack length measurement was 0.50 mm (0.020 in.), and the measurement error was ±0.025 mm (0.001 in.). The resulting a versus N data were reduced with a seven-point incremental polynomial technique [11] to produce da/dN versus ΔK data.

Results and Discussion

The crack retardation associated with a single periodic overload is generally reflected in a local purturbation in the a versus N crack growth curve. However, as ΔN_{OL} becomes small, the resolution in crack length measurement must be increased in order to perceive the transient variations in crack growth that occur between successive overloads. In the present experiment, ΔN_{OL} is exceedingly small relative to the increment in measurement of surface crack length, and no transient variations in crack growth are observed. Rather, the collection of all a versus N data represent a trend in crack propagation resulting from very frequent periodic overloads.

Reducing the a versus N data to the form of da/dN versus ΔK data and performing a least square regression produces analytical functions that represent the average crack growth rate for the specific combination of OLR and ΔN_{OL}. The regression equation (SINH) was based on the hyperbolic sine function and is given as [5-7]

$$\log (da/dN) = C_1 \text{ SINH } [C_2 (\log \Delta K + C_3)] + C_4 \qquad (1)$$

where

C_1 = 0.5, a material constant,
C_2 = horizontal shape coefficient,
C_3 = $-\log (\Delta K)$ at the point of inflection,
C_4 = $\log (da/dN)$ at the point of inflection, and
ΔK = baseline stress intensity factor range.

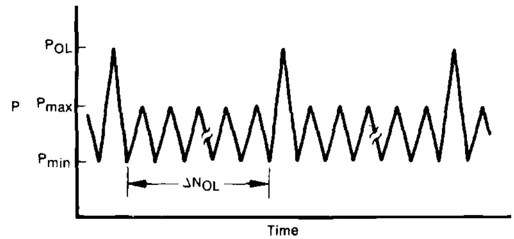

FIG. 4—*Periodic overload fatigue.*

The increased magnitude of the overload stress intensity range (ΔK_{OL}) is not reflected in the plotted value of ΔK. Rather, the overload is treated as an isolated variable influencing crack growth, and its impact is revealed in the dependent variable, *da/dN*. Thus, under the load sequencing of Fig. 4, ΔK is defined as $K_{max} - K_{min}$ for all cycles (including the overload), and *da/dN* is the calculated average crack growth per cycle (including the overload).

Defining fatigue with periodic overloading as a succession of repetitive overload-fatigue missions (elemental damage events) as in Fig. 4, one may plot a series of crack growth rate curves for the collection of test missions. Figure 5 presents such data, illustrating the effect of ΔN_{OL} on elevated temperature fatigue crack propagation in GATORIZED IN 100. For purposes of comparison, a single regression curve (without data) representing crack growth under constant amplitude loading has also been plotted. This baseline crack growth is observed to be essentially equivalent to propagation under periodic overloading with $\Delta N_{OL} = 5$ (6 cycles per overload-fatigue mission). The equivalence of crack growth rates results from a balance of overload accelerated crack growth and the subsequent crack retardation. As ΔN_{OL} increases to 20 and 40, the average effect of the overloading becomes more beneficial than damaging, and the resultant propagation rate is reduced significantly below that produced under constant ΔP fatigue.

The dependence of *da/dN* on ΔN_{OL} may be described by an interpolative model of the associated SINH curves. The coefficients of Eq 1 are defined as a function of ΔN_{OL}

$$C_i = a_i + b_i \log(\Delta N_{OL} + 1) \tag{2}$$

where $i = 2, 3, 4$.

Thus, over the range $5 \leq \Delta N_{OL} \leq 40$, *da/dN* is given by a continuous function (Eq 1) for which the three coefficients are uniquely defined (Eq 2). Interpolations on ΔN_{OL} define representative SINH curves giving average crack growth associated with periodic overload fatigue of ΔN_{OL} cycles be-

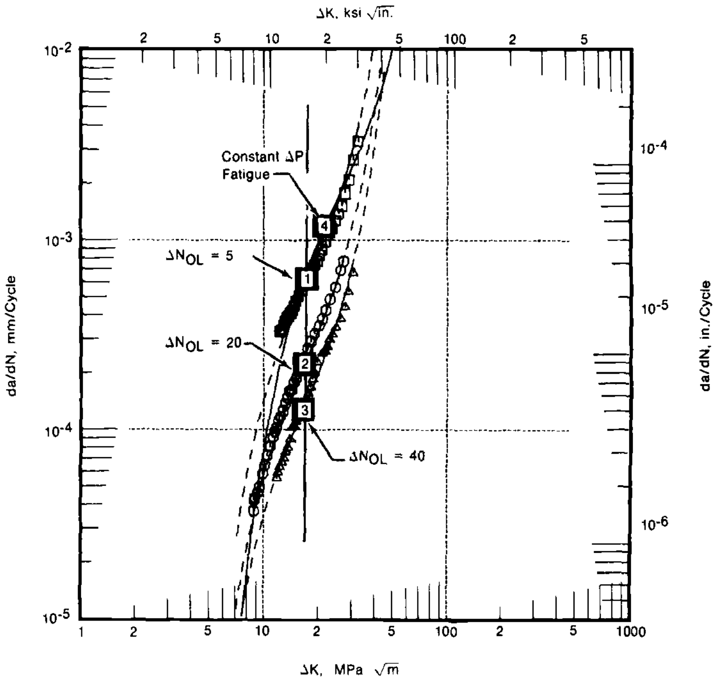

FIG. 5—*Effect cycles between overloads on fatigue of IN 100. OLR = 1.5. 0.167 Hz. 649°C.*

tween overloads. This permits prediction of crack growth where no actual data exist. The relationship of Eq 2 also provides the capability for limited extrapolation beyond the data base.

The effect of overload ratio on fatigue crack propagation may also be described by an interpolative model of the SINH coefficients. Figure 6 illustrates this effect for periodic overloading ($\Delta N_{OL} = 40$) with overload ratios of 1.0, 1.25, and 1.5. Data of overload ratio 1.0 is generated under constant ΔP fatigue, and any interpolative model of OLR must converge to this condition regardless of the value of ΔN_{OL}. The expression that defines the SINH coefficients as a function of overload ratio is

$$C_i = d_i + e_i(\text{OLR}) \tag{3}$$

where $i = 2, 3, 4$.

Thus, for periodic overload-fatigue with $\Delta N_{OL} = 40$, the combination of Eqs 1 and 3 uniquely define crack propagation for $1.0 \leq \text{OLR} \leq 1.5$.

Having established that the SINH coefficients are linear functions of overload ratio for the case of $\Delta N_{OL} = 40$, it assumed that a similar linear relationship describes the dependence of crack propagation for $\Delta N_{OL} < 40$. This allows combination of Eqs 2 and 3, permitting full interpolation over

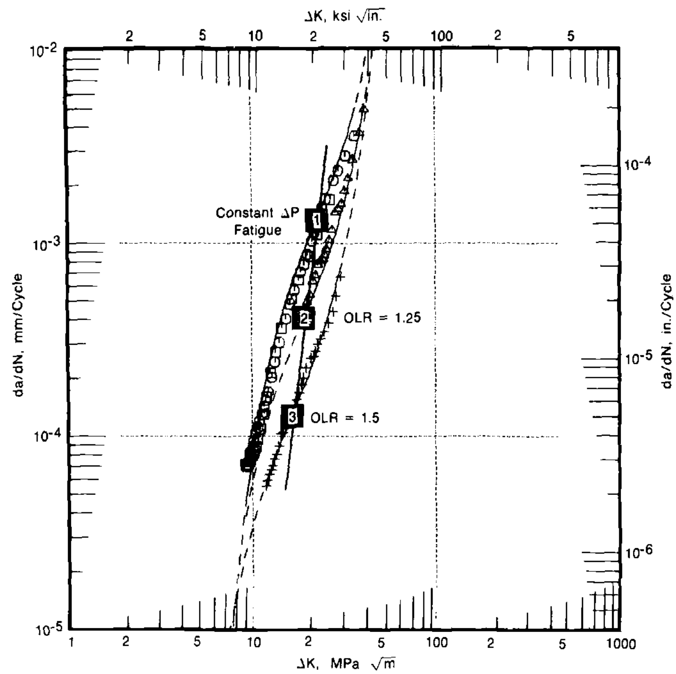

FIG. 6—*Effect of overload ratio on fatigue of IN 100,* ΔN_{OL} *= 40, 0.167 Hz, 649°C.*

the region defined by $1.0 \leq \text{OLR} \leq 1.5$ and $5 \leq \Delta N_{\text{OL}} \leq 40$. The coefficients of Eq 1 are given by

$$C_i = \alpha_i + \beta_i(\text{OLR}) + \gamma_i[\log(\Delta N_{\text{OL}} + 1)] + \delta_i(\text{OLR})[\log(\Delta N_{\text{OL}} + 1)] \quad (4)$$

where $i = 2, 3, 4$.

This interpolative SINH model provides capability for prediction of fatigue crack propagation in IN 100 as a function of overload ratio and the number of cycles between overloads. This interpolative model is limited to crack retardation effects under the frequently applied overloads that are characteristic of military gas turbine operation. The applicable range of OLR and ΔN_{OL} may be extended with additional testing.

Development of a similar interpolative model of crack propagation in Waspaloy has also been accomplished. As observed in Fig. 7, the beneficial influence of periodically applied overloads (OLR = 1.5) is much less pronounced in this material than in IN 100. Crack growth in Waspaloy with $\Delta N_{\text{OL}} = 5$ (6 cycles per overload-fatigue mission) is considerably more severe than propagation under constant ΔP fatigue, and the average effect of the overloading becomes beneficial for $\Delta N_{\text{OL}} = 20$ and 40. In spite of the significantly different retardation behavior between Waspaloy and IN

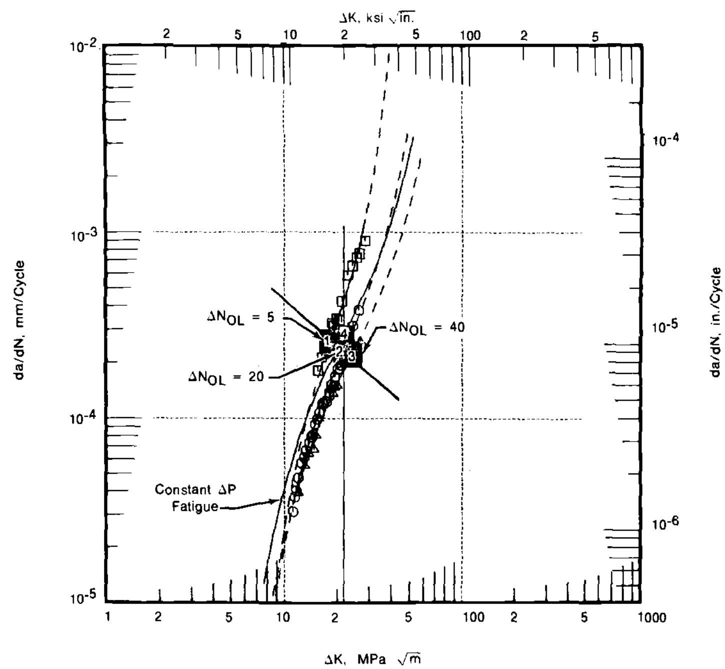

FIG. 7—*Effect of cycles between overloads on fatigue of Waspaloy, OLR = 1.5, 0.167 Hz, 649°C.*

100, an interpolative function of the form of Eq 2 is a satisfactory representation of the effect of ΔN_{OL} on crack growth in this alloy.

The model of the effect of overload ratio ($\Delta N_{OL} = 40$) on crack propagation in Waspaloy, Fig. 8, also demonstrates a much more limited effect than was observed in IN 100. A relationship of the form of Eq 3 describes SINH coefficients for Waspaloy crack propagation as a function of overload ratio. Combining the models of the effects of cycles between overloads and overload ratio provides interpolative capability for both variables simultaneously (Eq 4).

The coefficients of Eq 4 are given in Table 1 for crack propagation of IN 100 and Waspaloy at 649°C (1200°F), 0.167 Hz (10 cpm), and $R = 0.5$. Substitution into Eq 1 gives crack propagation rate as a function of OLR and ΔN_{OL}.

Post-Overload Crack Retardation

An interpolative SINH model representing crack growth under frequently applied periodic overloads is an effective method for prediction of crack growth resulting during a specific overload-fatigue sequence. However, the instantaneous response of a crack to the overload-fatigue block is not evi-

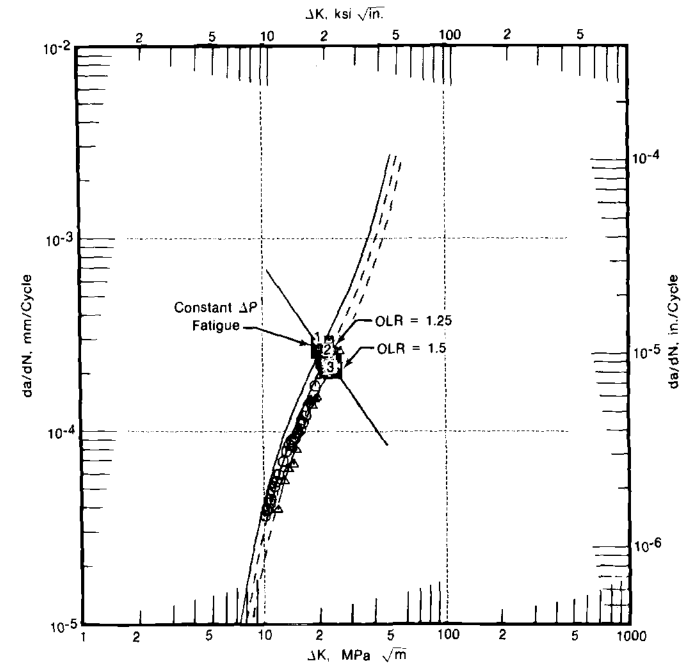

FIG. 8—*Effect of overload ratio on fatigue of Waspaloy,* ΔN_{OL} = *40, 0.167 Hz, 649°C.*

TABLE 1—*Coefficients of Eq 4*

	IN 100				Waspaloy			
	α	β	γ	δ	α	β	γ	δ
C_2	4.8410	−0.2140	0	0	−2.9984	6.8424	4.2414	−4.2414
C_3	−1.5448	0.1928	−0.0503	0.0503	−1.6853	0.3563	0.2780	−0.2780
C_4	−3.5196	0.6386	1.6534	−1.6534	−3.6536	0.0916	0.1845	−0.1845

dent. From knowledge of the process of crack retardation resulting from application of a single overload, a hypothesis concerning crack growth in response to frequent periodic overloading may be established.

The crack growth curve is expected to range between two general extremes depending upon the form of post-overload crack retardation. For a given value of ΔN_{OL}, these curves are illustrated in Fig. 9. Assuming delayed retardation does not occur, the minimum crack growth rate should immediately follow the overload. If delayed retardation is present, the minimum crack growth rate should be observed some number of cycles following the overload. If ΔN_{OL} is less than the period of delayed retardation, N_{DR},

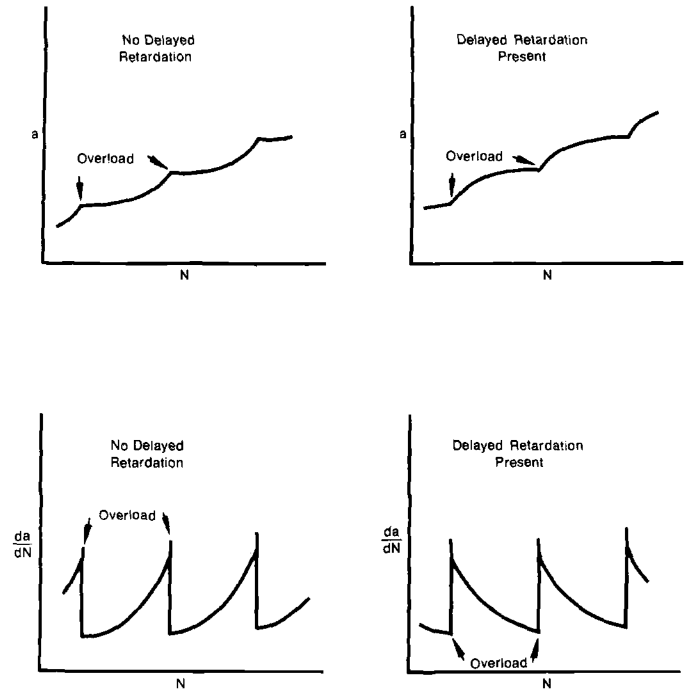

FIG. 9—*Fatigue crack propagation under periodic overload fatigue.*

a subsequent overload interrupts the delayed retardation process, and the minimum crack growth rate should immediately precede the overload.

Experimental determination of the nature of the instantaneous crack growth curve in response to periodic overloading is, however, a formidable task. As previously noted, it is extremely difficult to obtain accurate, meaningful measurement of crack advance between very frequent overloads using standard optical techniques. Additionally, measurement of crack length at the specimen surface is complicated by any discontinuities in crack advance due to microstructural variations. Such discontinuous fatigue crack growth is common in Waspaloy and to a lesser extent in IN 100. Even if precise measurement of the surface crack length were accomplished without microstructural interference, a question would remain concerning the shape of the crack front. That is, does the crack front geometry remain constant during periodic overloading, or do periodic changes in crack curvature accompany the overloads? The latter phenomenon is certain to complicate data interpretation. Measurement of incremental crack growth by determination of fatigue striation spacing was prevented by formation of a heavy oxide on the crack face during elevated temperature testing.

It is possible to determine the form of the instantaneous crack propagation curve indirectly. Unlike direct measurement, a SINH curve describing crack propagation under periodic overloading gives average behavior over the period of many overloads. The SINH representation also averages crack growth discontinuities due to variations in microstructure, crack front geometry, and judgement on the part of the technician. Thus, each curve represents a statistical mean of the microscopic crack growth rate as ΔK increases with crack length.

As noted earlier, increasing the number of fatigue cycles between successive overloads produces an increase in crack retardation and a corresponding reduction in average crack growth rate. Alternately, decreasing ΔN_{OL} reduces crack retardation, and, in the limit of zero cycles between overloads, the da/dN versus ΔK curve should approach the crack growth curve corresponding to constant overload fatigue. For the current example of constant ΔP fatigue ($R = 0.5$) interrupted by periodic overloads (OLR $= P_{OL}/P_{max} = 1.5$), the parameters defining constant overload fatigue are $R = P_{min}/P_{OL} = 0.333$ and

$$\Delta K_{OL} = \Delta K_{\text{baseline}} \, [(\text{OLR} - R)/(1 - R)] = 2\Delta K_{\text{baseline}}.$$

The propagation curve for $R = 0.333$ fatigue is obtained from an interpolative model of the effect of load ratio [1]. Maintaining the convention of assigning the value of $\Delta K_{\text{baseline}}$ to all overload cycles, the $R = 0.333$ constant ΔP curve is translated by $\Delta K_{\text{baseline}} = \Delta K_{OL}/2$ in order to represent the case of constant overload fatigue. For IN 100, this curve is presented in Fig. 10 and its relationship to the SINH curves representing periodic overload-fatigue is illustrated. A similar presentation of Waspaloy data appears in Fig. 11.

From the collection of curves for a single material, one may deduce an approximation to the instantaneous form of post-overload crack propagation due to periodic overloading. One assumption is required: the form of the post-overload crack propagation curve is similar for $\Delta N_{OL} = 5$, 20, and 40. Noting that the increase in crack length between successive overloads is very small, the associated increase in ΔK is determined to be correspondingly small and of little significance. Calculating crack growth rate at a specific value of ΔK from each of the overload curves gives the average advance per cycle under the indicated loading condition. The crack growth during each of the individual overload-fatigue missions is then calculated, and the difference in the crack growth for two different missions defines a point on the post-overload da/dN versus N curve. For example, by subtracting the crack advance due to a 21-cycle mission from the crack advance due to a 41-cycle mission, the Δa corresponding to Cycles 21 to 41 after the overload is obtained. The average value of da/dN for the cycle

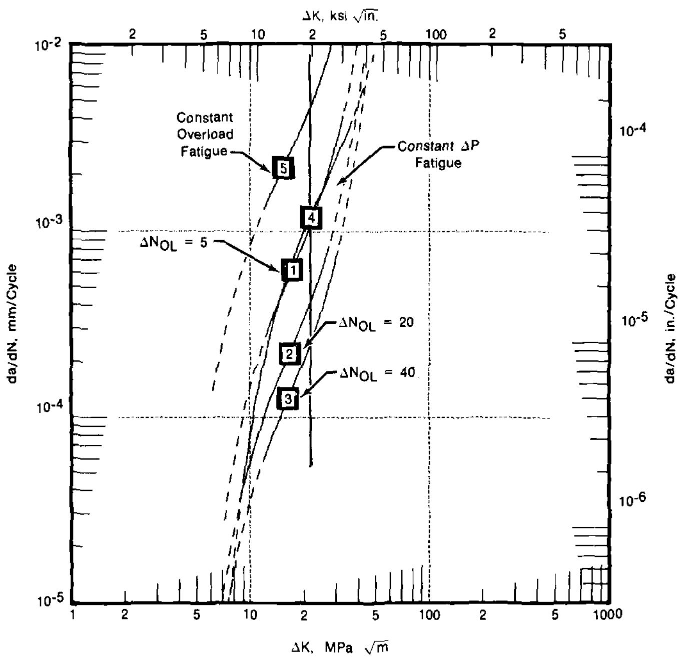

FIG. 10—*Effect of cycles between overloads on fatigue of IN 100. OLR = 1.5.*

interval of 21 to 41 cycles after the overload may now be obtained by dividing $\Delta a_{21\text{ to }41}$ by the corresponding $\Delta N_{21\text{ to }41}$. This procedure is given by

$$da/dN_{21\text{ to }41} = [41\,(da/dN)_{41} - 21\,(da/dN)_{21}]/(41 - 21). \qquad (5)$$

The value of $da/dN_{6\text{ to }21}$ may be obtained similarly, and $da/dN_{1\text{ to }6}$ may also be determined by subtracting the standard crack growth for one cycle of fatigue at the overload conditions from the six-cycle mission data.

Plotting the calculated values of da/dN at the midpoints of the cycle intervals (for example, $N = 31$ for the interval of 21 to 41 cycles) gives an approximation of the instantaneous crack propagation rate following an overload. For IN 100 and Waspaloy at $\Delta K = 22$ MPa$\sqrt{\text{m}}$ this data is presented in Fig. 12. While the exact path of the immediate post-overload crack propagation rate curve is unclear, as indicated by the broken line, the existence of delayed retardation is confirmed. In each alloy, the crack growth rate is maximized at the time of the overload and the average crack growth rate decreases in each of the subsequent cycle intervals, that is, 1 to 6, 6 to 21, and 21 to 41.

This finding is verification of the general crack behavior that was hypothesized earlier for mission crack growth subject to delayed retardation. That is, in IN 100 and Waspaloy a crack subjected to constant load ampli-

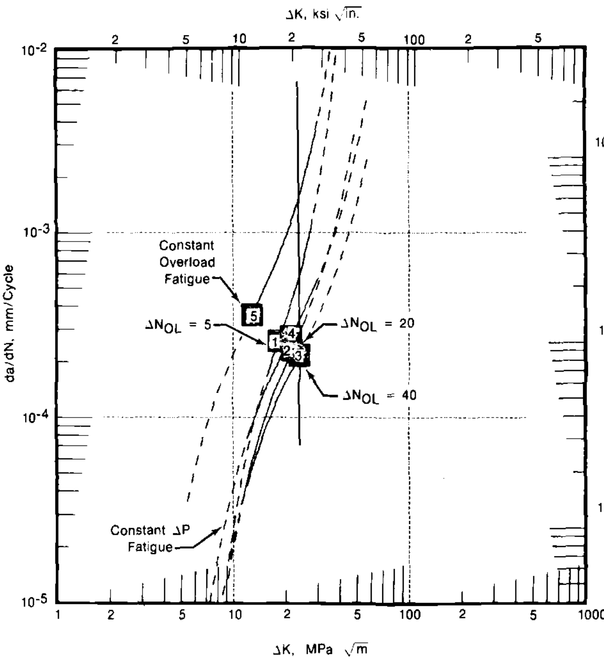

FIG. 11—*Effect of cycles between overloads on fatigue of Waspaloy, OLR = 1.5.*

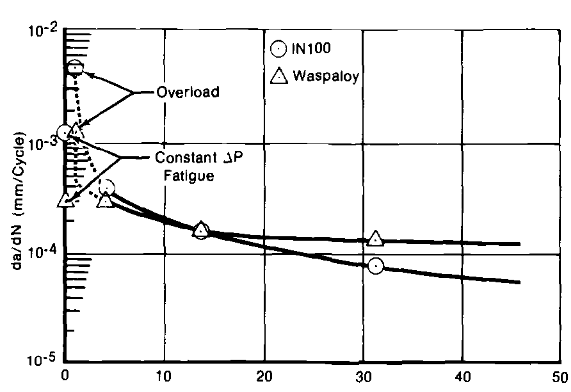

FIG. 12—*Post-overload crack growth exhibiting delayed retardation, OLR = 1.5, ΔK = 22 MPa√m.*

tude fatigue interrupted by periodic overloading will display a general decrease in the average macroscopic crack propagation rate, but, as illustrated in Fig. 13, the instantaneous response of a crack to such overloading is more complex. The full extent of crack retardation does not develop immediately following the application of an overload; rather, post-overload crack growth rate decelerates throughout the period of delayed retardation. Typically, this period is greater than the total number of baseline fatigue cycles applied between mission overloads, and delayed retardation is responsible for all beneficial effects of the overloading. Since crack growth rate decelerates during the entire period of delayed retardation, fatigue cycles immediately following an overload are considerably more damaging than later cycles.

This behavior deviates significantly from the general long-term effects of an overload on fatigue crack propagation; therefore, mission crack growth in IN 100 and Waspaloy is difficult to predict by any retardation model that is developed solely from experimental measurements of the total period of retardation N^*. Modeling of N^* addresses the ultimate effects of the crack retardation process, while retardation under mission loading is dominated by delayed retardation that is a transient response. Only a model that contains this transient capability is expected to effectively predict the synergistic effects of the frequent overloading that are common to engine operation.

Conclusions

The rate of elevated temperature fatigue crack propagation of IN 100 and Waspaloy, subjected to constant load amplitude fatigue interrupted by periodic overloads, decreases with increasing overload ratio and number of cycles between overload.

The combined effects of overload ratio ($1.0 \leq \text{OLR} \leq 1.5$) and number

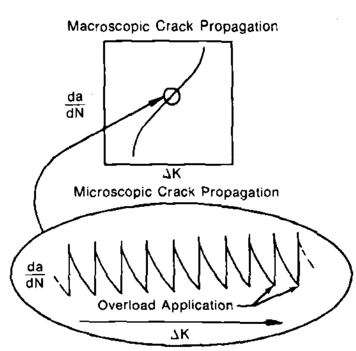

FIG. 13—*Fatigue crack propagation with frequent overloads.*

of cycles between overloads ($5 \leq \Delta N_{OL} \leq 40$) on crack propagation of IN 100 and Waspaloy are effectively described by an interpolative model based on the hyperbolic sine function.

Post-overload crack retardation resulting from frequently applied overloads (OLR = 1.5, $\Delta N_{OL} \leq 40$) exhibits delayed retardation in IN 100 and Waspaloy. The delayed retardation is not exhausted between the successive overloads and is entirely responsible for reduction in crack growth rate in these alloys.

Acknowledgment

The authors wish to acknowledge the support of the Air Force Materials Laboratory on Contract F33615-75-C-5197 [*5-7*] and Contract F33615-77-C-5153 [*1*].

References

[*1*] Larsen, J. L. and Annis, C. G., "Cumulative Damage Fracture Mechanics Under Engine Spectra," Technical Report AFML-TR-79-4159, Air Force Materials Laboratory, 1979.

[*2*] Wheeler, O. E., *Journal of Basic Engineering*, American Society for Mechanical Engineering, 1972, pp. 181-186.

[*3*] Willenborg, J., Engle, R. M., and Wood, H. A., "A Crack Growth Retardation Model Using an Effective Stress Concept," AFFDL-TM-71-1-FBR, Air Force Flight Dynamics Laboratory, 1971.

[*4*] Elber, Wolf in *Damage Tolerance in Aircraft Structures, ASTM STP 486*, American Society for Testing and Materials, 1971, pp. 230-242.

[*5*] Annis, C. G., Wallace, R. M., and Sims, D. L., "An Interpolative Model for Elevated Temperature Fatigue Crack Propagation," Technical Report AFML-TR-76-176, Part I, Air Force Materials Laboratory, Nov. 1976.

[*6*] Wallace, R. M., Annis, C. G., and Sims, D. L., "Application of Fracture Mechanics at Elevated Temperature," Technical Report AFML-TR-76-176, Part II, Air Force Materials Laboratory, Nov. 1976.

[*7*] Sims, D. L., Annis, C. G., and Wallace, R. M., "Cumulative Damage Fracture Mechanics at Elevated Temperature," Technical Report AFML-TR-76-176, Part III, Air Force Materials Laboratory, Nov. 1976.

[*8*] Corbly, D. M. and Packman, P. F., *Engineering Fracture Mechanics*, 1973, pp. 479-497.

[*9*] Rice, R. C. and Stephens, R. I. in *Progress in Flaw Growth and Fracture Toughness Testing, ASTM STP 536*, American Society for Testing and Materials, 1973, pp. 95-114.

[*10*] Gardner, F. H. and Stephens, R. I. in *Fracture Toughness and Slow-Stable Cracking, ASTM STP 559*, American Society for Testing and Materials, 1974, pp. 225-244.

[*11*] Hudak, S. J., Jr., Saxena, A., Bucci, R. J., and Malcolm, R. C., "Development of Standard Methods of Testing and Analyzing Fatigue Crack Growth Rate Data," Technical Report AFML-TR-78-40, Air Force Materials Laboratory, May 1978.

D. E. Macha,[1] *A. F. Grandt, Jr.,*[1] *and B. J. Wicks*[2]

Effects of Gas Turbine Engine Load Spectrum Variables on Crack Propagation

REFERENCE: Macha, D. E., Grandt, A. F., Jr., and Wicks, B. J., **"Effects of Gas Turbine Engine Load Spectrum Variables on Crack Propagation,"** *Effect of Load Spectrum Variables on Fatigue Crack Initiation and Propagation, ASTM STP 714,* D. F. Bryan and J. M. Potter, Eds., American Society for Testing and Materials, 1980, pp. 108-127.

ABSTRACT: This paper describes results of an elevated temperature fatigue crack growth study in IN-100, a nickel-base superalloy. The objective of this study was to determine if conventional fracture mechanics techniques can predict crack growth under conditions expected to occur in jet engine turbine disks. Results are reported for two types of experiments. The first group of tests examines isolated load events that may occur in a turbine disk load history. The influence of tensile overloads, compressive underloads, overload/underload sequences, and periods of sustained load on subsequent constant amplitude fatigue crack growth are discussed. The second group of specimens was subjected to a spectrum load history that combines many of the isolated load events. Cumulative damage crack growth predictions are performed by several procedures and shown to agree quite well with the experimental results. The influence of specimen thickness is considered for both the isolated event and the spectrum loading experiments.

KEY WORDS: fatigue crack growth, fatigue (materials), spectrum loading, elevated temperature, retardation, load interactions, sustained loading, nickel-base superalloy, life predictions, cumulative damage, crack propagation

Increased performance requirements for U.S. Air Force (USAF) gas turbine engines have resulted in components that see high operating stresses and severe service environments. It is not uncommon for cyclic stress levels to exceed the material yield strength or for operating temperatures to activate time-dependent processes such as creep or oxidation or both. Thus, advanced engine designs may result in finite life components, such as turbine

[1] Materials engineers, Air Force Materials Laboratory, Wright-Patterson Air Force Base, Ohio 45433.

[2] Visiting scientist, Air Force Materials Laboratory, Wright-Patterson Air Force Base, Ohio 45433; permanently attached to Aeronautical Research Laboratories, DSTO, Melbourne, Australia.

disks, that need to be periodically replaced during service in order to ensure structural integrity.

Traditionally, turbine disks have been designed and managed to a low cycle fatigue (LCF) "crack initiation" criterion. Because of the statistical nature of the fatigue behavior of most engineering alloys, significant scatter accompanies the number of loading cycles required to initiate a crack at a given stress level. For design purposes, this problem of material properties scatter is usually eliminated by degrading the failure curve to a conservative "design allowable" level where the probability of failure (that is, crack initiation) becomes very low. From a safety standpoint, this approach has generally been very successful, since a built-in safety factor is attained by assuming all components are manufactured from materials possessing minimum properties. However, lifetimes based on time to crack initiation for minimum properties are extremely conservative and may require the user to incur significant economic penalties. Use of advanced materials and manufacturing processes in modern turbine engines, for example, results in disks that are quite expensive. Premature retirement of structurally sound components may result in unnecessary economic penalties.

Retirement for Cause

In an attempt to reduce maintenance costs through longer component service lives, the USAF is investigating an alternate approach to optimize utilization of certain gas turbine engine members. This new concept, referred to as retirement for cause (RFC), differs from current practice in that each component would be removed from service only after its LCF crack initiation life is exhausted [*1*][3]. Thus, an individual turbine disk would be replaced only when a crack has initiated in the LCF critical location. Following a component inspection in which no cracks are detected, a disk would be returned to service for a specified period, after which it would be reinspected.

Determination of the safe operating time until the next inspection is the key for RFC to provide an effective life management tool, and requires that several technology areas are suitably developed. These include: an engine usage tracking capability that provides a definition of the flight spectrum experienced by the respective components, stress analysis methods capable of establishing localized stress-temperature-time histories at critical locations within the disks, reliable nondestructive inspection methods for detecting fatigue crack initiation, and finally, the capability to predict crack propagation in turbine disks that are subjected to service loading. The objective of this paper is to discuss this latter problem of predicting fatigue crack growth for turbine engine load histories.

[3]The italic numbers in brackets refer to the list of references appended to this paper.

Load Spectrum Variables

A variety of in-service variable amplitude load histories may be experienced by advanced turbine disks. These histories may consist of periodic overloads, overload/underload combinations, and periods of sustained load interspersed among relatively constant amplitude loading. The absolute importance of each loading event can depend on several factors. For example, it has been shown in a previous study [*2*] that in IN-100, a nickel-base superalloy disk material, the amount of retardation due to a tensile overload decreases as temperature increases. Further, the magnitude of retardation exhibited at the higher temperatures was found to be relatively small for overload values generally exhibited in a turbine disk load spectrum. Thus, retardation effects may not be as significant at higher temperatures as at intermediate temperatures where fatigue crack retardation may be more pronounced. Similarly, periods of sustained load may or may not contribute significantly to crack extension, depending on the load-temperature-time history.

The present paper describes results of an experimental study conducted to identify the importance of load spectrum variables on elevated temperature crack growth in IN-100. One set of experiments examined the isolated effects of peak tensile overloads, overload/underload sequences, and periods of sustained load on subsequent constant amplitude fatigue crack growth. A separate set of precracked specimens were subjected to a simplified turbine disk load history. Variables within this latter study included test temperature, specimen thickness, and length of sustained load period. Crack growth life predictions were performed for these spectrum loading experiments and compared with the experimental results.

Experimental Procedures

The experimental work reported here was conducted on Gatorized[4] IN-100, a fine-grained powder metallurgy nickel-base superalloy used for a turbine disk material. The material was manufactured to production specifications [*3*] in the form of a flat disk forging. All testing was conducted on servo-hydraulic closed-loop fatigue machines operated under load control. Gaertner traveling microscopes with digital displays of crack length were used to measure crack lengths on both specimen sides (front and back). Using this system, crack length measurements within ±0.025 mm (0.001 in.) were attainable. Although tunneling was often observed on the fracture surfaces (the crack front was slightly longer in the specimen interior), all crack length measurements reported here are averages of the front and back surface measurements.

[4]Trademark of United Technologies.

Isolated Events

Several experiments were conducted to isolate the effects of overloads, underloads (negative loads), overload/underload combinations, and periods of sustained load on subsequent steady-state (constant ΔK) fatigue crack growth. The isolated event tests employed two types of specimens. The effects of tensile overloads, tensile overload/compressive underload combinations, and compressive underloads were studied with through-the-thickness center-crack specimens [*4*] nominally 7.6 mm (0.3 in.) thick as shown in Fig. 1. Comparative tensile overload tests were also performed on 7.6 mm (0.3 in.) thick modified compact tension (MCT) specimens [5] as shown in Fig. 2.

These tests were conducted at a common temperature of 732°C (1350°F). A wire-wound resistance furnace was used for the MCT specimens. Quartz windows mounted in the furnace walls allowed crack length measurements to be made without disturbing the temperature distribution in the specimen. Temperature control was maintained by spotwelding four thermocouples (two on each side of the specimen) on the respective specimens above the anticipated crack growth plane. The maximum temperature variation with specimens tested in the wire wound resistance furnace was ± 2°C (± 3°F). Induction heating was employed for the center-cracked specimens (CCS).

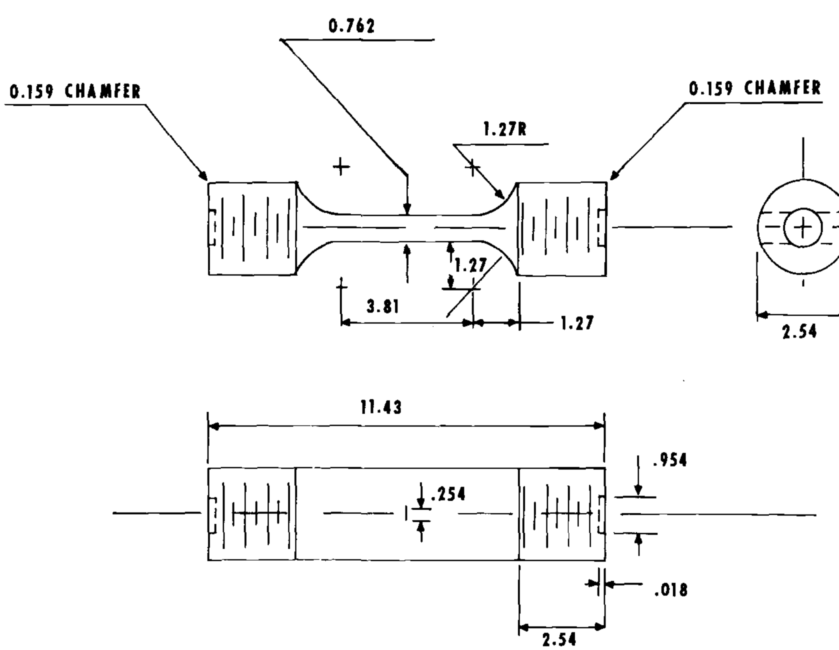

FIG. 1—*Through-the-thickness center-cracked specimen used for overload, underload, and combined overload/underload testing.*

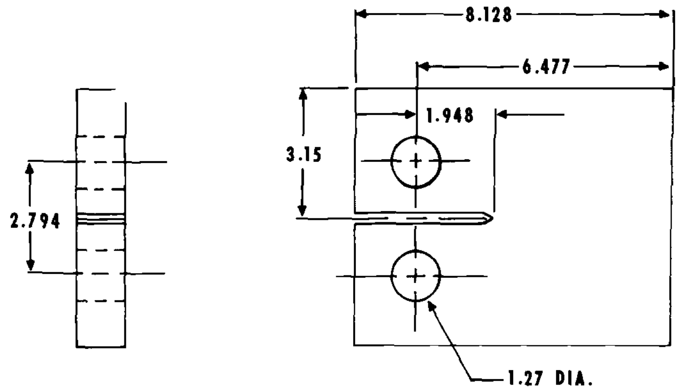

FIG. 2—*Modified compact tension (MCT) specimen used for overload testing and spectrum crack growth testing. (All dimensions in centimetres.)*

The induction windings were oriented parallel to the crack growth plane. The maximum temperature variation along this plane was maintained constant within ±15°C (±27°F) by spotwelding an array of thermocouples along the projected plane of crack growth and controlling the specimen temperature with the thermocouple nearest the crack tip. Both crack tips were measured on the CCS specimens (again front and back surfaces) and averaged to yield a single measure of crack growth. Load shedding was employed for both types of specimens to maintain the baseline cyclic K_{max} constant (within ±1 percent) at 25.3 MPa·$m^{1/2}$ (23.0 ksi·in.$^{1/2}$). The cyclic load frequency was fixed at 2.5 Hz, with a load ratio, R (R = minimum/maximum load), of 0.1.

A preliminary study of the effects of relatively short periods of sustained loading on constant amplitude cyclic crack growth was performed on a 12.7 mm (0.5 in.) thick MCT specimen. The fatigue crack was extended at 2.5 Hz with K_{max} fixed at 38.5 Mpa·$m^{1/2}$ (35 ksi·in.$^{1/2}$) and R = 0.1. Specimen temperature was maintained at 723°C (1350°F) by induction heating. After steady-state fatigue crack growth was established, a period of sustained K_{max} was imposed. Cyclic loading was then continued until steady-state conditions were resumed. Following this procedure, the effects of sustained load periods of 60, 100, and 201 min were examined.

Spectrum Crack Growth

All spectrum crack growth experiments were conducted on MCT specimens in laboratory air using the resistance furnaces. Three specimen thicknesses, nominally 3.3 mm (0.13 in.), 7.6 mm (0.3 in.), and 25.4 mm (1.0 in.) were tested at 649°C (1200°F). A single thickness of 7.6 mm (0.3 in.) was tested at 732°C (1350°F). Temperature control for these tests was the same as that described earlier for isolated event tests conducted in the resistance furnace.

The load spectrum used in this study is shown in Fig. 3. This spectrum was used in earlier programs [*6–8*] aimed at developing cumulative damage life prediction methods for gas turbine engine applications. The load history contains periods of both cyclic loading (Segments 1, 3, and 5) and sustained loading (Segments 2, 4, and 6). The total duration of the spectrum shown in Fig. 3 is 30 min. The periods of sustained load (Segments 2, 4, and 6) make up 62 percent of the flight time. The experimental details for the respective spectrum test variables are given in Table 1. It is noted here that Specimens 2, 4, 6, and 8 were tested to the complete load history, while the sustained load Segments 2, 4, and 6 were deleted from the load histories of Specimens 1, 3, 5, and 7.

Discussion of Isolated Events

As described earlier, several sets of experiments were conducted in an attempt to isolate the effects of certain load spectrum variables on elevated

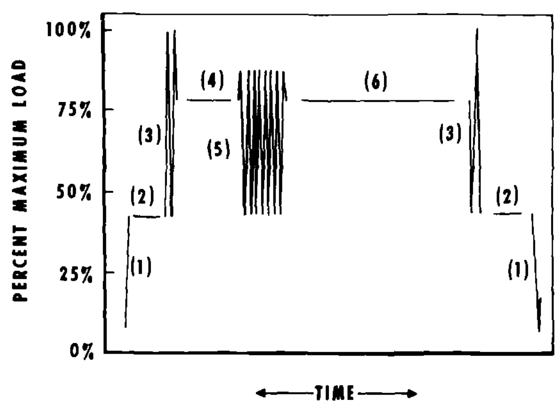

FLIGHT SEGMENT	FREQ.	PERIOD	STRESS RATIO
1	1CPM	-	0.20
2	-	120 SEC.	-
3	1CPM	-	0.46
4	-	306 SEC.	-
5	1CPM	-	0.52
6	-	578 SEC.	-

FLIGHT DURATION WITH HOLD TIMES-30 MINUTES
FLIGHT DURATION WITHOUT HOLD TIMES-11 MIN. 16 SEC.

FIG. 3—*Description of a simple load spectrum used to simulate in-service loads experienced by a turbine disk.*

TABLE 1—*Spectrum crack growth results.*

Specimen	Thickness, mm	Temperature	Spectrum[a]	Crack Lengths, mm: Initial	Crack Lengths, mm: Final	Actual Flights	Flights Between a = 20.68 mm and a = 43.92 mm
1	3.1	649°C	A	16.43	47.65	1828	1174
2	3.86	649°C	B	20.45	46.02	1237	1187
3	7.59	649°C	A	20.58	47.07	1088	1053
4	7.54	649°C	B	20.63	47.07	1007	984
5	25.25	649°C	A	20.47	46.33	953	921
6	25.20	649°C	B	20.68	46.23	1031	1013
7	7.54	732°C	A	20.34	44.68	208	196
8	7.59	732°C	B	20.64	43.92	178	174

[a] Spectrum A = no hold times, Spectrum B = with hold times.

temperature fatigue crack growth in IN-100. The general approach followed was to first establish steady-state fatigue crack growth behavior by application of a period of constant ΔK loading. This baseline loading was then perturbed by an isolated load event or sequence (for example, tensile overload, tensile overload followed by a negative load, period of sustained load), and the change in constant amplitude crack growth due to the isolated load occurrence was measured. The results of these fundamental studies are discussed in the following two subsections.

Overload/Underload Experiments

The parameters used here to characterize the effect of isolated overloads or underloads or both are defined in Fig. 4. The descriptive parameters employed in this discussion are the overload ratio ($U_{OL} = K_{OL}/K_{max}$) and the underload ratio ($U_{UL} = P_{UL}/P_{max}$). Here K and P are the relevant stress intensity factor and load applied by the test machine. The data shown in Fig. 4 provides a comparison of delay in crack growth (retardation) caused by a peak tensile overload ($U_{OL} = 2$) with the retardation caused by a tensile overload/compressive underload sequence ($U_{UL} = -1$). The delay in fatigue crack growth (N_D) is defined by extrapolating the re-established steady-state growth, following delay, to the crack length at which the overload or underload or both is applied. This definition of N_D represents the change in fatigue crack propagation life of the specimen caused by the overload or underload event or both. Since N_D is a quantity often subject to considerable scatter, the experiments described here were duplicated, and the average delay period reported in Figs. 5 and 6. Figure 5 summarizes the observed delay cycles as a function of overload ratio U_{OL} for the following conditions: (*a*) single peak tensile overloads applied to 7.6 mm (0.3 in.) thick CCS specimens (square symbols in Fig. 5); (*b*) single peak tensile overloads

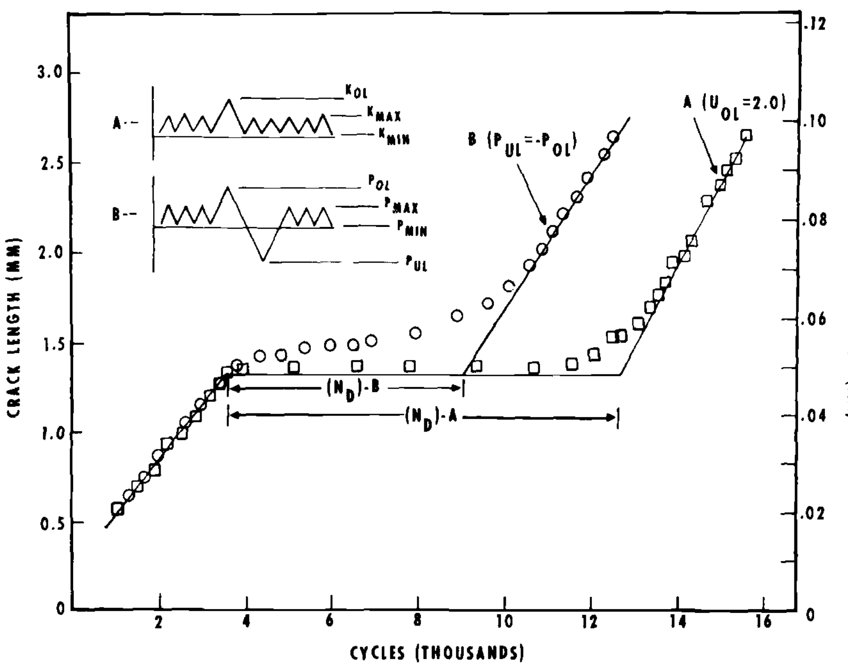

FIG. 4—*Typical fatigue crack growth curves and load history definition employed for overload/underload experiments.*

followed immediately by an equivalent compressive underload (that is, $U_{UL} = -U_{OL}$), using 7.6 mm (0.3 in.) thick CCS specimens (circles); (*c*) single peak tensile overloads applied to 7.6 mm (0.3 in.) thick MCT specimens (diamonds); and (*d*) single peak tensile overloads applied to 12.7 mm (0.5 in.) thick MCT specimens [*2*] (triangles).

Figure 5 indicates that for overload ratios between 1.2 and 2.0, the greatest cyclic delay is caused by single peak overloads imposed on a center-cracked specimen. Above overload ratios of 2.0, the number of delay cycles becomes increasingly sensitive to the level of overload. Apparent crack arrest (no crack growth in 250 000 cycles) was observed at an overload ratio of 2.3.

Underloads following an overload event have a relatively insignificant influence on retardation behavior. The large compressive underloads shown here ($P_{UL} = -P_{OL}$) are unrealistically high for normal turbine disk operations. Thus, since practical underload ratios at fracture critical locations are considerably smaller, they would be expected to have even less influence on the cyclic delay caused by prior overloads.

More significant differences in crack growth delay are found when comparing the results from the CCS and MCT specimens. As shown in Fig. 5, crack growth delays experienced in CCS tests were substantially greater than from MCT specimens of the same thickness. These differences are par-

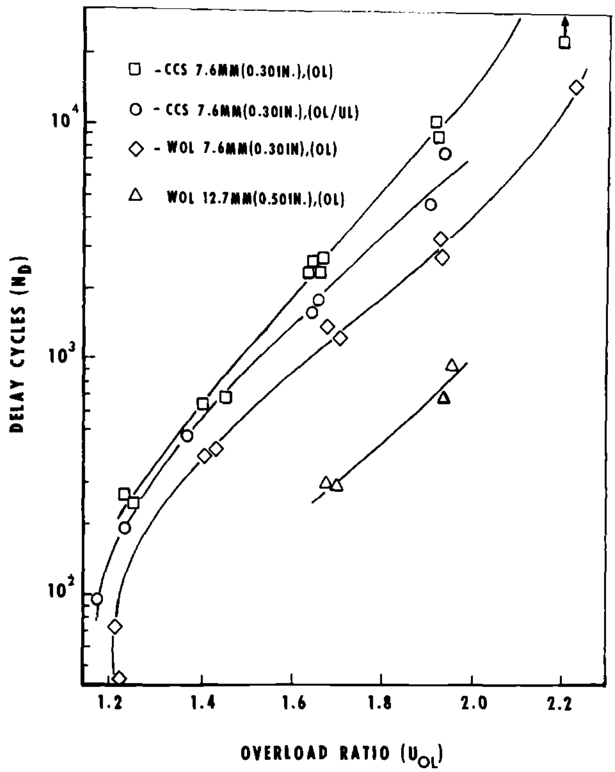

FIG. 5—*Summary of delay cycles versus overload ratio data,* K_{max} = *25.5 MPa·m$^{1/2}$*, T = *732°C.*

ticularly apparent at high and low overload ratios. This apparent dependence of fatigue crack retardation on specimen geometry suggests that, for elevated temperature applications in IN-100, caution should be exercised in using laboratory specimens to model cumulative damage effects in actual components.

Figure 5 also compares the effect of single-peak overload applications for MCT specimens of different thickness. Note that the number of delay cycles is substantially less in the thicker specimen. This dependence of fatigue crack retardation on specimen thickness is consistent with prior studies in other materials [*9*].

The effect of single-peak compressive underloads was also studied in the test matrix but is not included in Fig. 5 because of their relative insignificance. Fatigue crack growth delays of no more than 120 cycles were measured for all underload ratios between $-2.2 < U_{UL} < -1.2$. For all practical underloads, the effect on fatigue crack growth is within the experimental resolution.

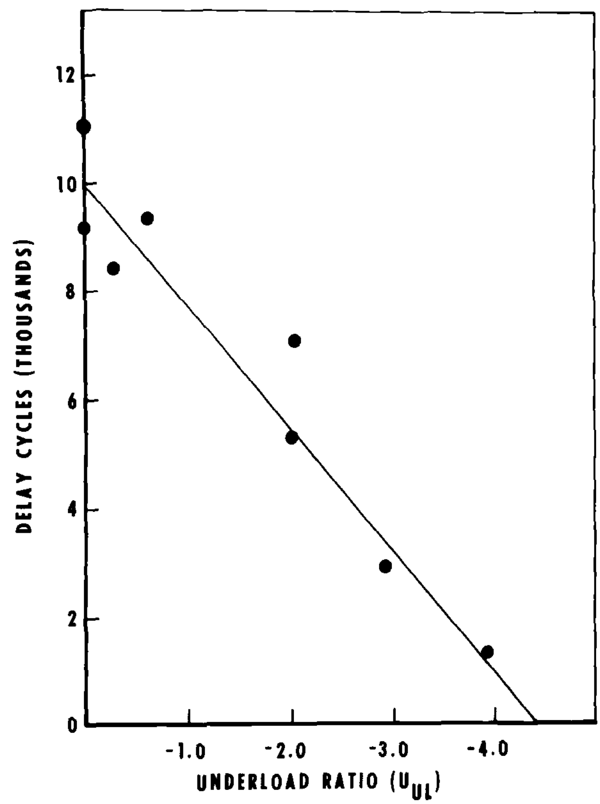

FIG. 6—*Summary of data showing effect of compressive underloads on fatigue crack retardation caused by an overload ratio of 2.0,* K_{max} = *25.5 MPa·m*$^{1/2}$, T = *732°C.*

Figure 6 presents the effect of various overload/underload sequences in which U_{OL} was fixed at 2.0, and the magnitude of the subsequent compressive underload was varied. For underload ratios between zero (no underload) and −4.0, the underload ratio appears to be linearly related to the cyclic delay, N_D. A maximum reduction in N_D of approximately 80 percent was observed at the highest compressive loading ($U_{UL} = -4$). However, since U_{UL} rarely exceeds −1 in service, the effect of underloads following peak tensile overload cycles may not be important.

Cyclic/Sustained Load Transition

This subsection describes the results of constant amplitude fatigue crack growth experiments that were interrupted by a sustained load period as shown in Fig. 7. The crack growth data shown in Fig. 7 were obtained for the 100-min hold time. In this figure, the average surface crack length is plotted

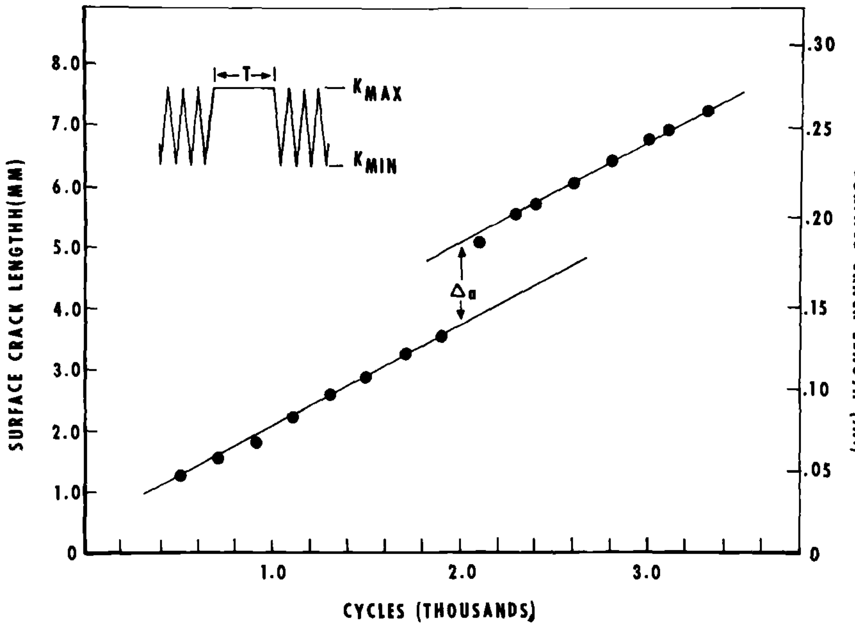

FIG. 7—*Typical crack growth curve for cyclic/sustained load interaction experiment, sustained load period = 100 min,* K_{max} *= 38.5 MPa·m*$^{1/2}$, T = *732°C.*

as a function of the number of applied fatigue cycles. After 1900 fatigue cycles, the 100-min period of sustained load at K_{max} was commenced. Upon completion of the sustained load period, cyclic loading was resumed. After 200 additional cycles (total cycle count of 2100 cycles), the crack length was measured. The linear steady-state relationship between crack length and cycles is indicative of the constant K_{max} fatigue loading applied to the specimen. Testing, and subsequent plotting of the data, in this manner provides a convenient method of establishing the crack growth increment (Δa in Fig. 7) associated with the various periods of sustained load. The results indicate 0.64 mm (0.025 in.), 1.35 mm (0.053 in.), and 3.43 mm (0.135 in.) of crack extension associated with the 60, 100, and 201 min hold times, respectively. In Fig. 8, the crack growth increment (Δa) is shown as a function of the period of sustained load. The solid line exhibits the relationship between crack growth increment (da) and period of sustained load predicted from steady-state sustained load crack growth test results for K_{max} = 38.5 MPa$-$m$^{1/2}$ (35 ksi$-$in.$^{1/2}$) at 732°C [*7,10*]. In Fig. 8, the numbers in parentheses indicate the difference between expected da and the measured Δa for each sustained load period tested.

Figure 8 indicates that for intermittent periods of sustained load exceeding 60 min, the rate of crack growth is equal to that associated with continuously applied sustained load testing. Although the rates are equivalent for the tests

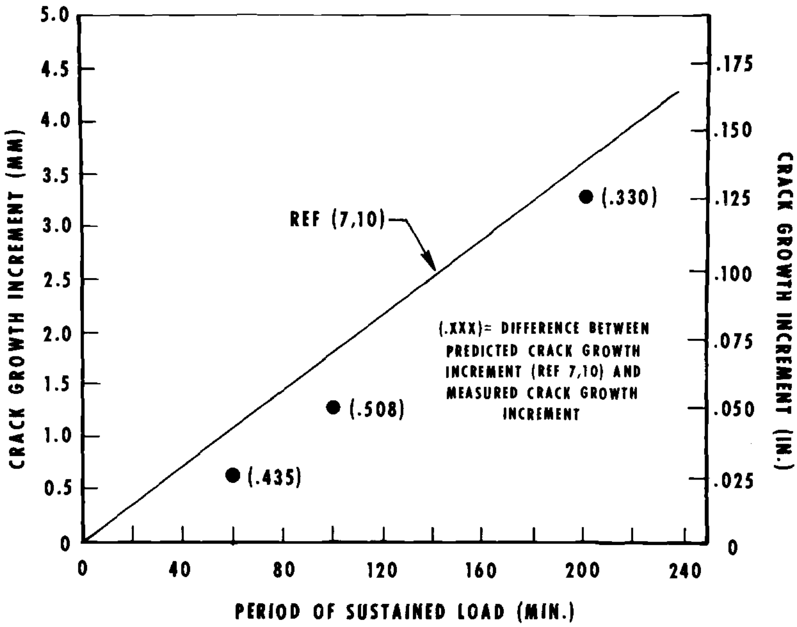

FIG. 8—*Comparison of sustained load crack growth increment resulting from cyclic/sustained load interaction experiments with pure sustained load data.*

reported (60 min $\leq t \leq$ 201 min), the absolute value of crack extension is less than measured under continuously applied sustained loading conditions. This observation ($\Delta a < da$) leads one to conclude that equilibrium sustained load crack growth does not commence immediately upon application of the sustained load but only after some period of time has elapsed (for example, incubation period). For the test parameters investigated here, the incubation period, although not well defined, appears to be in excess of 20 min. Additional testing at shorter sustained load periods is required for an accurate definition of this transition period.

The fracture surface of the specimen used for this study is shown in Fig. 9. The crack propagation direction is denoted by the arrow in the figure. The regions of fatigue crack growth are labeled Region A, while regions of sustained load growth are labeled Region B. Two important features of the fracture surface are readily observable. First, there is a distinct difference in crack surface morphology between regions of cyclic and sustained load crack growth. The fracture surface associated with fatigue crack growth is extremely smooth (Region A). This smooth crack surface morphology is characteristic of Gatorized IN-100 fatigue crack growth surfaces over a temperature range from 25°C (77°F) to 732°C (1350°F). Conversely, a very rough or ridged fracture surface is seen in the areas of sustained load crack

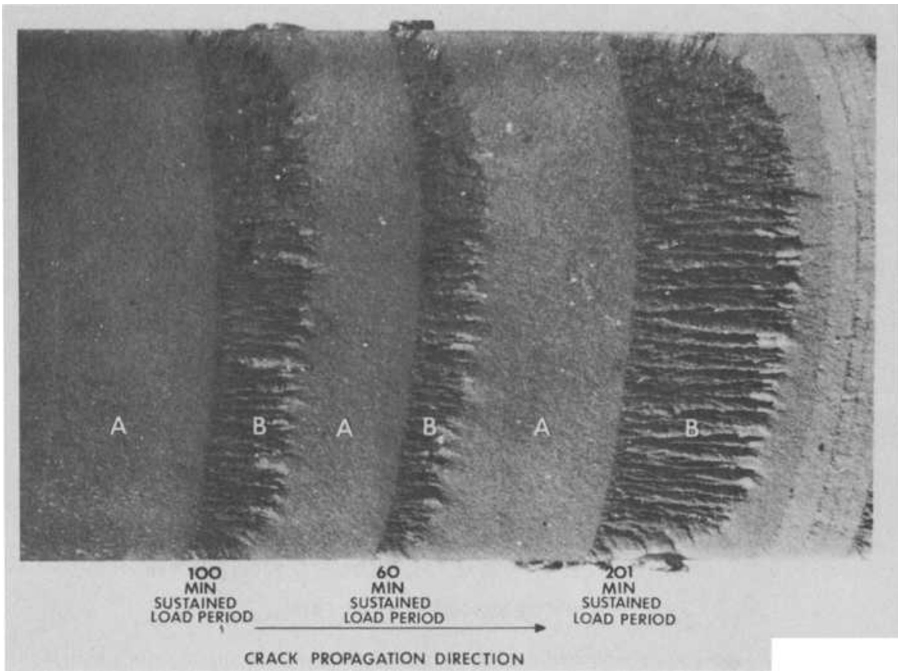

FIG. 9—*Fracture surface of specimen used to study cyclic/sustained load transition behavior in IN-100 at 732°C.*

growth (Region B). Again, this is characteristic of fracture surfaces associated with sustained load crack growth in Gatorized IN-100 [*11*].

The second important feature is the change in degree of crack front curvature when going from cyclic to sustained load crack growth. For the test parameters used here, there is limited crack front curvature associated with the fatigue crack growth process. The degree of curvature exhibited during sustained load crack growth is much larger, as readily evidenced in Fig. 9. Note that during each hold time, significant growth occurred in the interior of the specimen, while limited crack extension occurred at the specimen free surface. This behavior is especially evidenced in Fig. 9, for the 201-min hold time. Post-test measurements were made on the fracture surface to determine the maximum crack growth increment occurring in the specimen interior for each period of sustained load. The results indicated 1.6 mm (0.061 in.), 2.3 mm (0.089 in.), and 3.8 mm (0.151 in.) of growth at the maximum extension point for the 60, 100, and 201 min hold times, respectively. Recall that the crack growth increment calculated earlier from the a versus N data (Fig. 7) is a net or average crack extension increment associated with the respective periods of sustained load. As expected, the increment measured at the maximum interior point is larger than that calculated earlier. It is also worthwhile mentioning that the maximum crack growth increment measured at the specimen interior for each hold time is larger than the growth increment (*da*) calculated from continuous sustained load data (the solid line in Fig. 8).

In light of these observations (that is, change in crack surface morphology and crack front curvature), it is not surprising that the transition from equilibrium fatigue crack growth to equilibrium sustained load crack growth does not occur immediately. The importance of the transition behavior and its impact on life calculations for spectrum crack growth are discussed in the following section.

Discussion of Spectrum Loading

This section discusses the results of the MCT specimens subjected to the load history described in Fig. 3, and the corresponding fatigue crack growth predictions. The objective of these experiments was to determine the ability of conventional fracture mechanics methods to analyze elevated temperature crack growth in IN-100, as might be required for implementation of retirement-for-cause management of turbine disks. As described earlier, the test spectrum employed here has been used in previous studies [*6–8*] as a simplified example of a load history that may occur in turbine disks.

Experimental Results

Test parameters and the results of all spectrum crack growth testing are summarized in Table 1. In reviewing this data, one is able to evaluate the impact of two test variables. First, the importance of the sustained load segments within the spectrum, and, second, the effect of specimen thickness on crack growth behavior. The spectrum crack growth lives recorded in Table 1 represent the total flights associated with the various specimens. For the purpose of evaluating the effects of hold times and specimen thickness, comparative lives were determined over the crack length interval from $a =$ 20.68 mm (0.81 in.) to $a = 43.92$ mm (1.73 in.). These lives are also listed in Table 1. It is important to note here that the applied load was normalized by specimen cross section to yield identical stress intensity histories for each specimen.

A typical result from the evaluation of effects of hold times on spectrum crack growth is shown in Fig. 10 for the 7.6-mm (0.3-in.) thick specimens tested at 649°C (1200°F). Note that the specimen tested to the spectrum with no hold time exhibits only a 7 percent longer life than the companion hold time specimen. The thicker specimens (nominally 25.4 mm (1.0 in.) thick) exhibited the opposite result (see Table 1), where the hold time specimen had a longer life (1013 flights) than its companion tested without hold times (921 flights). The thinnest specimens (nominally 3.3 mm (0.13 in.) thick) exhibited nearly identical lives. At 732°C (1350°F), the hold time specimen had

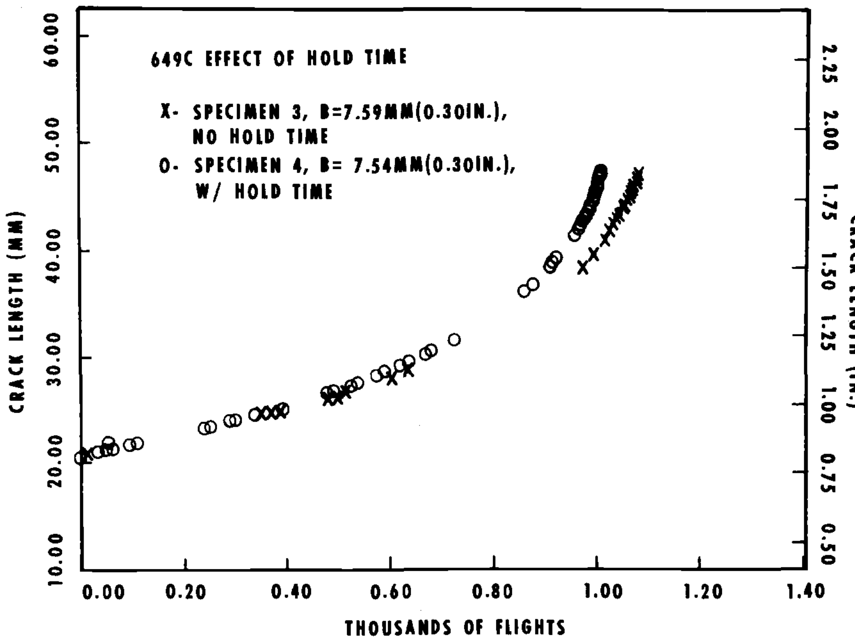

FIG. 10—*Typical crack growth data showing effect of hold time on spectrum crack growth behavior,* T = *649°C.*

an 11 percent decrease in life in comparison with the specimen tested to the spectrum without hold times.

From these results it is concluded that for the spectrum evaluated here at 649°C and 732°C, the periods of sustained load had only a minor contribution to the crack growth process. Recognizing that nearly 62 percent of the 30-min flight history consists of periods of sustained load, one might have anticipated a greater difference in life times between the spectrum with and without the hold times. But, remembering the earlier discussion concerning the cyclic/sustained load transition behavior in this material, the minor changes in life are not so surprising. It was noted earlier that at 732°C (1350°F), when the sustained load stress intensity was equal to the cyclic loading K_{max}, equilibrium-sustained load crack growth did not occur immediately during the dwell loading period, but only after some time in excess of 20 min.

In the spectrum tests conducted here, the sustained load portions of the spectrum (Segments 2, 4, and 6 in Fig. 3) occurred at stress intensity levels below the previous cyclic K_{max}, and, in addition, the longest dwell was less than 10 min. Thus, these factors would tend to minimize any contribution of the sustained load portions of the spectrum to the crack growth process, as observed here.

The effect of specimen thickness on spectrum crack growth at 649°C (1200°F) is shown in Fig. 11 for the spectrum tests without hold times. It is seen that as specimen thickness increases, the spectrum crack growth rate increases. The same behavior was exhibited in the tests conducted with hold times in the spectrum. This thickness dependence is consistent with the overload experiments described earlier in Fig. 5, and with prior studies [*6-8*] that indicate the crack growth rate behavior of Gatorized IN-100 is thickness dependent.

Crack Growth Predictions

Two procedures were used to predict crack growth lives for the spectrum loading experiments: a simple linear summation method, and a direct application of the cumulative damage analysis computer code CRACKS IV [*12*]. In the linear summation approach, constant amplitude fatigue crack growth was modeled by the hyperbolic sine equation (SINH) described in Ref *6*.

$$\log \frac{da}{dN} = C_1 \sinh [C_2 (\log (\Delta K) + C_3)] + C_4 \tag{1}$$

Here da/dN is the fatigue crack growth rate, ΔK is the cyclic range of the stress intensity factor, and C_1, C_2, C_3, and C_4 are empirical coefficients that

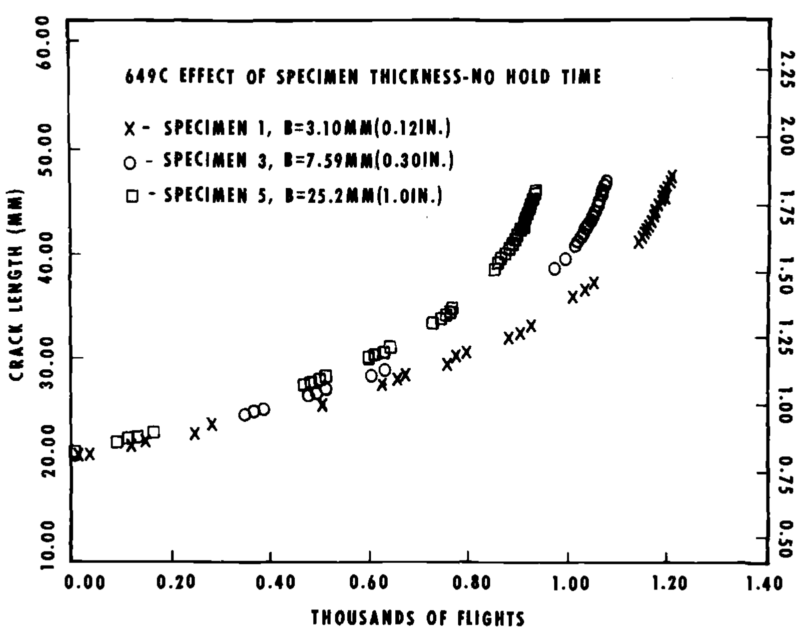

FIG. 11—*Typical crack growth data for spectrum loading (no hold times) showing effect of specimen thickness,* T = *649°C.*

may depend on the test frequency, stress ratio R, and temperature. Baseline testing sponsored by the Air Force Materials Laboratory [*6–8,13*] has established these coefficients for IN-100 for the 649°C (1200°F) test conditions employed here. Since complete baseline data were not available for 732°C (1350°F) crack growth, predictions were not made for those spectrum tests.

Computing da/dN on a cycle-by-cycle basis via Eq 1 gave the crack extension for the cyclic portion of the load histories. Simple estimates for the hold time effects on crack growth were performed in a similar manner by employing the sustained load crack growth rate da/dt versus stress intensity factor relationship established for the test temperature [*7,10*]. The cyclic and sustained load crack growth increments were then summed linearly to give the total crack growth per flight of loading. Repeating this process over the range of crack growth in each test gave the total number of flights to failure. Note that this procedure does not attempt to account for cyclic history effects (fatigue crack retardation) or potential interactions between the sustained and cyclic portions of the load history (incubation period).

The second life prediction method employed direct application of the CRACKS IV computer program developed at the Air Force Flight Dynamics Laboratory. This computer code is an updated version of the CRACKS program described in Ref *14*, and represents a state-of-the-art method for predicting variable amplitude fatigue crack growth. CRACKS IV provides several options for fatigue crack growth laws, retardation models, and specimen geometries. In the present work, the constant amplitude fatigue crack growth behavior was represented by the Forman equation [*15*], where

$$\frac{da}{dN} = \frac{C \Delta K^m}{(1 - R) K_c - \Delta K} \tag{2}$$

Here da/dN, ΔK, and R are as defined before, while C, m, and K_c are empirical constants. These constants were obtained by fitting Eq 2 directly to the fatigue crack growth data obtained from Ref *13*.

The CRACKS IV computations involve cycle-by-cycle integration of the fatigue crack growth law over the desired range of crack growth as before. In addition, it provides the option to estimate cyclic load interaction effects. The Willenborg [*16*] crack retardation scheme was selected from the library of CRACKS IV load interaction models to account for peak overloads. No provision is given in the current version of CRACKS IV to estimate crack growth during the periods of sustained load, so the holdtimes were ignored for these calculations.

A typical comparison between the predicted and experimental fatigue crack growth curves is given in Fig. 12 for one of the "no hold time" experiments. As indicated, CRACKS IV predictions are shown for two conditions: with and without the Willenborg retardation model. Note that the

Willenborg retardation model does not predict a significant retardation effect for this particular load spectrum. The other prediction, labeled "FLT-BY-FLT" in Fig. 12, was obtained by the simple linear damage summation procedure that employed the SINH model (Eq 1) for constant amplitude crack growth. As expected, this curve closely matches the linear damage CRACKS IV prediction.

The fatigue crack growth life estimates for all of the 649°C (1200°F) tests are recorded in Table 2. Note that the two linear summation procedures (employing the SINH and Forman crack growth models) give similar results that generally agree well (within 25 percent) with the experimental lives. The Willenborg retardation model predicts a slight increase in specimen life (about 7 percent), indicating that the load spectrum used here does not con-

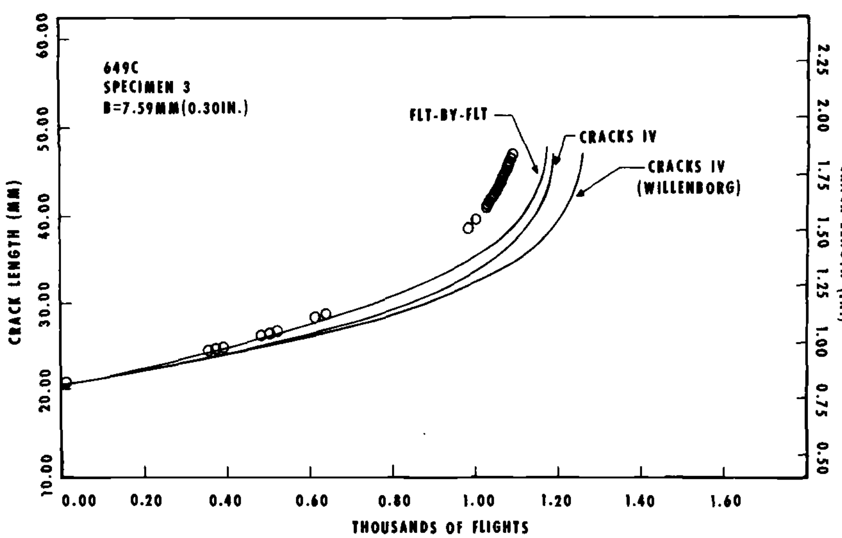

FIG. 12—*Comparison of fatigue crack growth predictions with test results for spectrum loading (no hold time),* T = *649°C.*

TABLE 2—*Results of spectrum crack growth predictions.*

Specimen	Crack Length, mm: Initial	Crack Length, mm: Final	Test Flights	Linear Summation Predictions: With Hold Time	Linear Summation Predictions: Without Hold Time	CRACKS IV Predictions	CRACKS IV Predictions with Retardation
1	16.43	47.65	1828	...	1708	1843	1963
2	20.45	46.02	1237	437	1159	1168	1249
3	20.58	47.07	1088	...	1173	1185	1266
4	20.63	47.07	1007	436	1140	1139	1218
5	20.47	46.33	953	...	1212	1234	1466
6	20.68	46.23	1031	403	1278	1194	1275

tain a significant load history effect. Linear summation predictions for the influence of holdtime (by addition of da/dt as computed from the da/dt versus K relation) greatly underestimate specimen life. As discussed earlier, an incubation period evidentally exists in IN-100 at 649°C (1200°F) that prevents the holdtimes from immediately contributing to crack growth in this particular load history.

Conclusions

1. The results of the overload/underload experiments suggest the following conclusions regarding crack growth behavior in IN-100 at 732°C (1350°F):

(*a*) The amount of fatigue crack retardation caused by single-peak tensile overloads depends on both specimen thickness and geometry. Greater delay was observed for the 7.6-mm (0.3-in.) thick specimens than for the 12.7 mm (0.5 in.) thickness, while the center-cracked specimens showed more delay than the MCT geometry.

(*b*) Isolated compressive underloads had little, if any, effect on subsequent constant amplitude fatigue crack growth.

(*c*) A compressive underload that followed a tensile overload did reduce the retardation period due to the overload, although this effect was small for underload ratios expected to occur in practical turbine disk load histories.

2. The effects of sustained load hold times on elevated temperature crack growth suggest there may be an incubation period required for sustained loads to contribute to crack growth in IN-100. This observation was consistent with both the simple dwell experiments, where sustained K_{max} periods did not immediately cause crack growth as predicted by a simple summation of fatigue and sustained load cracking mechanisms, and for the spectrum loading experiments where dwell periods did not significantly alter the fatigue crack growth life.

3. The relatively simple analysis methods of flight-by-flight linear summation using the hyperbolic SINH crack growth rate model and cycle-by-cycle linear summation using the Forman crack growth rate model (as incorporated in CRACKS IV) provided good crack growth life predictions, (that is,

$$0.93 < \frac{\text{predicted flights}}{\text{actual flights}} < 1.3$$

for the IN-100 specimens tested to the simple turbine disk load history at 649°C (1200°F).

Acknowledgments

The work reported here was conducted in-house at the Air Force Materials Laboratory. The authors gratefully acknowledge the technical assistance pro-

vided by N. Ashbaugh, R. Georgette, G. Mornhinweg, T. Richardson, and S. Wallace.

References

[1] Hill, R. J., Reimann, W. H., and Ogg, J. S., "A Retirement for Cause Study of an Engine Turbine Disk," presented at the 1978 Science and Engineering Symposium, 17–19 Oct. 1978, San Diego, Calif.

[2] Macha, D. E., "Fatigue Crack Growth Retardation Behavior of IN-100 at Elevated Temperature," to be published in *Engineering Fracture Mechanics.*

[3] Cowles, B. A., Sims, D. L., and Warren, J. R., "Evaluation of Cyclic Behavior of Aircraft Turbine Disk Alloys," NASA CR, 159409, NASA Lewis Research Center, Cleveland, Ohio, Oct. 1978.

[4] Larsen, J. M. and Annis, C. G., Jr., "Cumulative Damage Fracture Mechanics Under Engine Spectra," Interim Report 30 Sept. 1978, AFML Contract F33615-77-C-5153, Air Force Materials Laboratory, Wright-Patterson Air Force Base, Ohio.

[5] Imhoff, E. J. and Barsom, J. M. in *Progress in Flaw Growth and Fracture Toughness Testing, ASTM STP 536,* American Society for Testing and Materials, 1973, pp. 183–205.

[6] Annis, C. G., Wallace, R. M., and Sims, D. L., "An Interpolative Model for Elevated Temperature Fatigue Crack Propagation," AFML-TR-76-176; Air Force Materials Laboratory, Wright-Patterson Air Force Base, Ohio, Nov. 1976.

[7] Wallace, R. M., Annis, C. G., and Sims, D. L., "Cumulative Damage Fracture Mechanics at Elevated Temperature," AFML-TR-76-176, Part II, Air Force Materials Laboratory, Wright-Patterson Air Force Base, Ohio, April 1977.

[8] Sims, D. L., Annis, C. G., and Wallace, R. M., "Cumulative Damage Fracture Mechanics at Elevated Temperatures," AFML-TR-76-176, Part III, Air Force Materials Laboratory, Wright-Patterson Air Force Base, Ohio, April 1977.

[9] Shih, T. T. and Wei, R. P., "Effect of Specimen Thickness on Delay in Fatigue Crack Growth," *Journal of Testing and Evaluation,* 1974.

[10] Private communications, Dr. N. Ashbaugh, Systems Research Laboratories, Dayton, Ohio.

[11] Private communications, R. Donat, Air Force Materials Laboratory, Wright-Patterson Air Force Base, Ohio.

[12] Private communications, R. Engle, Air Force Flight Dynamics Laboratory, Wright-Patterson Air Force Base, Ohio.

[13] Private communications, C. G. Annis, Pratt and Whitney Aircraft Group, Government Products Division, West Palm Beach, Fla.

[14] Engle, R. M., Jr., "CRACKS, A Fortran IV Digital Computer Program for Crack Propagation Analysis," Technical Report AFFDL-TR-70-107, Air Force Flight Dynamics Laboratory, Oct. 1970.

[15] Forman, R. G., Kearney, V. E., and Engle, R. M., Jr., "Numerical Analysis of Crack Propagation in Cyclic-Loaded Structures," *Journal of Basic Engineering,* Series D, Vol. 89, No. 3, 1967, pp. 459–464.

[16] Willenborg, J. D., Jr., Engle, R. M., and Wood, H. A., "A Crack Growth Retardation Model Using an Effective Stress Concept," AFFDL-TM-71, FBR, Air Force Flight Dynamics Laboratory, Wright-Patterson Air Force Base, Ohio.

J. T. Wozumi,[1] *T. Spamer,*[1] *and G. E. Lambert*[2]

An Engineering Model for Assessing Load Sequencing Effects

REFERENCE: Wozumi, J. T., Spamer, T., and G. E. Lambert, **"An Engineering Model for Assessing Load Sequencing Effects,"** *Effect of Load Spectrum Variables on Fatigue Crack Initiation and Propagation, ASTM STP 714,* D. F. Bryan and J. M. Potter, Eds., American Society for Testing and Materials, 1980, pp. 128–142.

ABSTRACT: An engineering model has been developed to assess the impact of load spectrum variables on fatigue crack growth in metal structures. The model is based on the effective stress concept of Willenborg et al and Gallagher et al, and has been extended to accommodate retardation/acceleration phenomena peculiar to transport spectra. Development was accomplished by consideration of basic principles and previously reported results of simple overload/underload spectrum testing. The model does not rely on additional empirical parameters except material constant amplitude crack-growth rates. Formulation is such that flight-by-flight crack growth may be assessed without recourse to cycle-by-cycle integration.

Predictive accuracy of the model was compared with the results of crack propagation testing conducted on 28 center-cracked 7075 and 2024 aluminum specimens subjected to transport wing and fin load spectra. Mission parameter variables investigated in this testing were: altitude, gross weight, flight duration, speed, and touch-and-go landings. Use of the model produced improved accuracy over that exhibited by other models currently in use in the industry. The capability of the model to accurately predict acceleration effects is considered unique.

KEY WORDS: fatigue (materials), acceleration, crack propagation, cyclic loads, damage tolerance, residual stress, retardation

The increasing emphasis on damage tolerance analysis for certification of aircraft has expanded the requirement for reliable and cost effective crack-growth analytical schemes. Two aspects of conventional flight-by-flight crack-growth analysis were identified as contributory to the high cost and sometimes discouraging accuracy of the results: (1) requirement for cycle-by-cycle integration of crack growth, and (2) lack of a reliable model to predict acceleration/retardation effects. Procedures have been developed in an effort to rectify these problems and are reported herein.

[1]Senior specialist engineers, The Boeing Company, Seattle, Wash. 98124.
[2]Senior specialist engineer, The Boeing Company, Wichita, Kan. 67210.

Elimination of Requirement for Cycle-by-Cycle Integration

Current engineering techniques for prediction of crack propagation under spectrum loading are based on the cycle-by-cycle integration of constant amplitude material growth rate data. An additional level of complexity is introduced by the use of the techniques of Ref. *1*, *2*, and *3*[3] that require that the active plastic zone boundary and the instantaneous crack tip location be continuously monitored. This has the twin disadvantages of increasing computational/bookkeeping requirements and tends to obscure the analyst's appreciation of the salient spectrum features. It will be shown that this level of complexity is not required for most transport spectra and that a model based on the assumption that the crack tip does not advance significantly between overloads and underloads will produce a high degree of accuracy. While the derivation presented is for the case of applied overload, similar arguments may be advanced for treatment of underloads and result in similar conclusions.

In comparing calculated plastic zone sizes with retarded crack growth due to flight segment stresses (computed by use of the Willenborg model), it was observed that the segment growth is generally a small fraction of the plastic zone size. Using the assumptions listed below and the equations of Ref *1*, the following argument is advanced in support of this observation. It should be noted that use of equations from Refs *2* and *3* will produce similar conclusions.

The assumptions used in the derivation are based on characteristics observed to hold true generally for transport aircraft wing lower surfaces fabricated from aluminum alloy. They address the significant parameter of material yield stress, material crack growth rates, range of percent damage caused by the ground-air-ground cycle, and the limits of K_{max} at which the majority of crack growth life is expended.

Assumptions

1. Material yield stress, σ_y, ranges from 345 to 517 MN/m^2 (aluminum).
2. Where material fatigue crack growth rates may be expressed in the form, $da/dn = CK_{max}{}^n$, the limits of variability on C and n are

$$1.5 \times 10^{-10} \leq C \leq 4.9 \times 10^{-10}, n = 3.5$$

$$2.8 \times 10^{-11} \leq C \leq 1.1 \times 10^{-10}, n = 4.0$$

3. $$0.35\, da/dF \leq da/dGAG \leq 0.66\, da/dF$$

where

da/dF = total crack growth per flight,
$da/dGAG$ = total crack growth due to GAG, and

[3]The italic numbers in brackets refer to the list of references appended to this paper.

GAG = maximum stress excursion caused by ground-air-ground segments.

4. The majority of crack growth life is accumulated at $K_{max} \leq 16.5$ MN/m$^{3/2}$.

Derived Relations (Using Equations from Ref 1)

1. The plastic zone size, r_y, is given for plane strain by

$$r_y = \frac{1}{4\sqrt{2}}\left(\frac{K_{max}}{\sigma_y}\right)^2$$

The smallest plastic zone that may be anticipated is then

$$r_y = 2.1 \times 10^{-7} K_{max}^2$$

where $y = 517$ MN/m^2.

2. If $da/dGAG = 0.35\ da/dF$ and $da/dF = da/dGAG + da/dSEG$ where $da/dSEG$ = crack growth due to all flight segments

$$\frac{da}{dSEG} = 1.86\ da/dGAG = 1.86\ CK_{max}{}^n$$

3. If $C = 1.1 \times 10^{-10}$, $n = 4$, and $K_{max} = 16.5$ MN/m$^{3/2}$, then

$$\frac{da}{dSEG} = 5.57 \times 10^{-8} K^2$$

4. $da/dSEG/r_y = 5.57 \times 10^{-8} K^2/2.1 \times 10^{-7} K^2 = 0.26$

It is seen that the upper bound for the total crack growth due to all flight segments is a quarter of the plastic zone created by the *GAG* cycle. To evaluate the impact of the observation that the crack length does not change appreciably throughout the flight, consider the following.

The Willenborg model postulates that the effective stresses, $\sigma'_{c_{max}}$ and $\sigma'_{c_{min}}$, of the cyclic stress under consideration, $\sigma_{c_{max}}$ and $\sigma_{c_{min}}$, is given by the following relationship

$$\sigma'_{c_{max}} = \sigma_{c_{max}} - \sigma_{res} \tag{1}$$

$$\sigma'_{c_{min}} = \sigma_{c_{min}} - \sigma_{res} \tag{2}$$

where

$$\sigma_{res} = \sigma_{ap} - \sigma_{c_{max}} \tag{3}$$

where σ_{ap} = the stress required to produce a plastic zone, $r_{y_{ap}}$, sufficient to terminate retardation.

σ_{ap} may be represented by the following relationship, as can be seen in Fig. 1.

$$\sigma_{ap} = \sigma_{ol}\left[1 - \left(\frac{a_c - a_{ol}}{r_y}\right)\right]^{1/2}$$

where

σ_{ol} = overload stress,
a_c = crack length at any time following overload, and
a_{ol} = crack length at overload application.

If $a_c = a_{ol} + \delta a = a_{ol} + 0.26r_y$, then

$$\sigma_{ap} = \sigma_{ol}\,\{1 - 0.26\}^{1/2} = 0.86\,\sigma_{ol}$$

It can be seen that σ_{ap} is reasonably close to σ_{ol}. Recourse to the relationships presented in Eqs 1, 2, and 3 indicate that σ_{ap} operates on the crack growth relationship through a reduction in the effective stress ratio ($\sigma'_{c_{min}}/\sigma'_{c_{max}}$). Since most structural materials are relatively insensitive to changes in effective stress ratio, this places an upper bound on the potential error. Crack growth analysis conducted to date indicate that the error introduced by the assumption of a stationary crack tip is less than 8 percent. Results of several transport wing lower surface crack growth analyses where crack tip location is analytically accounted for are compared, in Fig. 2, with analysis incorporating the assumption of constraint σ_{ap}.

The conclusion that $\sigma_{ap} \approx \sigma_{ol}$ is significant inasmuch as the use of σ_{ap} as a

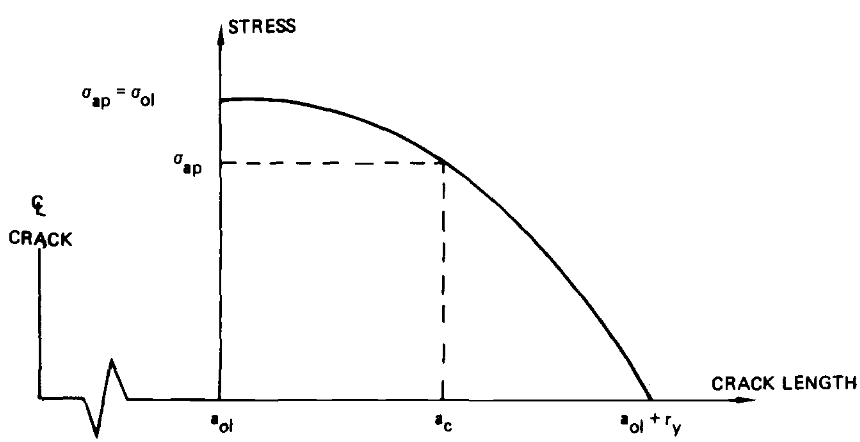

FIG. 1—*Schematic of* σ_{ap} *following overload.*

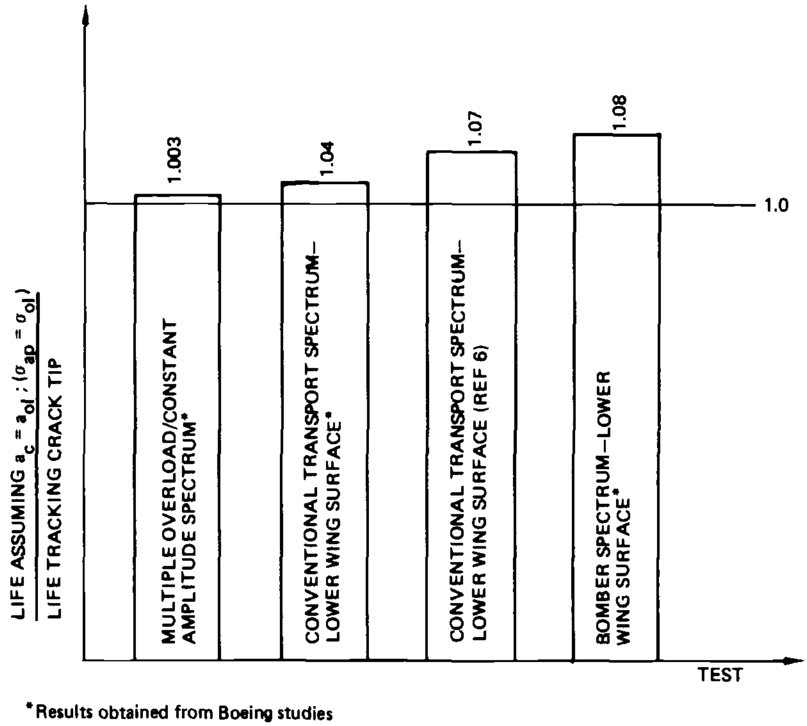

FIG. 2—*Comparison of life predictions—impact of assumption of stationary crack tip.*

constant value, equal to the overload stress, frees the analysis from necessity of tracking the crack tip location for each stress cycle. It may then be inferred that the sequence of loading following an application of overload is immaterial. Thus, for analytical purposes, flight segment stresses following application of an overload may be range-pair counted and calculated as block loadings.

The observation that cycle-by-cycle integration is not required for typical transport spectra damage calculations is valid only when the previously stated assumptions are satisfied. Thus, the following guidelines are presented for use of a stationary crack tip in analysis: (*a*) a check must be made to ensure that all conditions are conducive for its utilization (that is, $\sigma_{ap} \approx \sigma_{ol}$), or (*b*) an occasional analysis that tracks the crack tip through the plastic zone be made for comparison.

It is believed that a relationship exists between the validity of this postulation and the amount of crack growth accrued by the *GAG* cycle. Further investigation of this possible relationship is warranted.

Development of Acceleration/Retardation Model

The existence of retardation phenomena in spectrum loading is well documented, and some engineering models have been developed [1,4] that provide credible predictive accuracy for those spectra that exhibit net retardation. Spectrum crack growth testing reported in Refs 4, 5, and 6 provides clear evidence of acceleration for some spectra. It is postulated that the variables responsible for acceleration are present in most aircraft spectra; thus, use of a model insensitive to these variables may lead to gross inaccuracies.

Recent literature concerning load sequencing effects was reviewed to ascertain the predictive ability of existing analytical load interaction models [1-4] and to formulate, if possible, an improved engineering model. Correlation between test data and analysis using the referenced methods indicated that a revised model was required to better represent test results. The effective stress concept of Ref 1 and 2 was selected as the basis for formulation of an improved model due to its ability to produce predictions that adequately correlate with most test data. In addition, the concept lends itself to easy understanding and manipulation.

It was previously shown (Eqs 1, 2, and 3) that in the retardation process the reducing stress level, σ_{res}, is a function of the maximum cyclic and the preceding overload stress levels (σ_{ap}, σ_{ol}). Thus, Eq 3 may be rewritten in a general form as

$$\sigma_{res} = (\sigma_{ol} - \sigma_{c\max})^{\eta}$$

where η = overload effects parameter (note, $\eta = 1.0$ for Willenborg and Gallagher models).

Based on the results of numerous single-spike overload spectra tests [4,7,8], it was postulated that η may not be unity, but rather dependent upon the relative magnitude of the overload and maximum cyclic stress levels. Hence, the effective stress reduction would be a function of σ_{ol}, $\sigma_{c\max}$, and η as depicted in Fig. 3.

It was also observed that crack growth data obtained using single-spike underload test spectra is faster than that exhibited without underloads [4,5]. (An overload is defined as any stress level lower than the minimum of the cyclic stresses under consideration and may have a positive value.) The driving function of these acceleration effects appears to be dependent upon the relative magnitudes of the underload and minimum cyclic stress in a manner correspondent to the retardation phenomena. Hence, a similar effective stress concept was utilized to increase the cyclic stress levels to account for acceleration effects (Fig. 4). It was postulated that the amount of stress level increase is a function of the minimum cyclic and preceding underload stress levels.

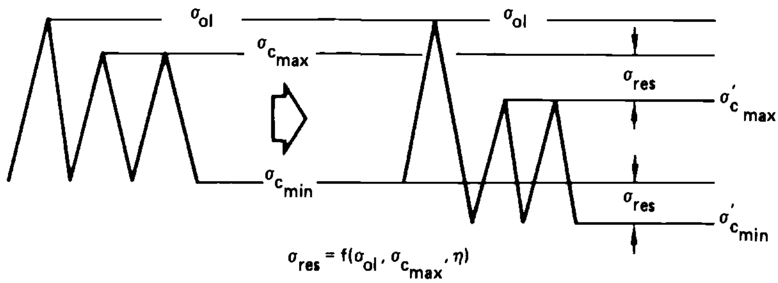

FIG. 3—*Effective stress concept (overload effects).*

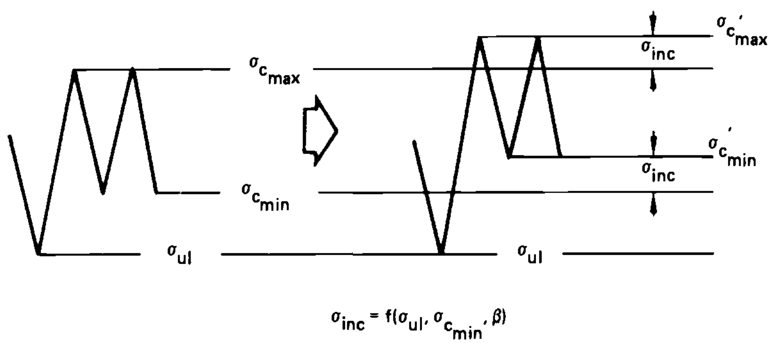

FIG. 4—*Effective stress concept (underload effects).*

$$\sigma_{\text{inc}} = |\sigma_{ul} - \sigma_{c_{\min}}|^{\beta}$$

where

σ_{inc} = the increase in effective stress to account for acceleration effects,
σ_{ul} = underload stress level, and
β = underload effects parameter.

The effective maximum and minimum cyclic stress levels due to acceleration effects would then be determined by

$$\sigma'_{c\max} = \sigma_{c\max} + \sigma_{\text{inc}}$$

$$\sigma'_{c\min} = \sigma_{c\min} + \sigma_{\text{inc}}$$

In order to utilize the preceding information relating to retardation and acceleration effects in a working mode, it was further postulated that both effects may be linearly superimposed (that is, no cross coupling exists). Hence, the effective stresses used for the revised load sequence model become

$$\sigma'_{c_{\max}} = \sigma_{c_{\max}} - \sigma_{res} + \sigma_{\text{inc}}$$

$$\sigma'_{c_{\min}} = \sigma_{c_{\min}} - \sigma_{res} + \sigma_{\text{inc}}$$

These effective stresses are then used to calculate the stress intensity factor for use with any appropriate material crack-growth rate relationship.

Determination of η

The overload effects parameter, η, was determined from the reduction of simple, constant amplitude/periodic single overload test data as reported in Refs *4, 7,* and *8.*

A wide scatter in the reduced data exists. A systematic variance capable of explaining this scatter is not evident. The functional relationship between η and $\sigma_{ol}'/\sigma_{c_{\max}}$ that provides the best correlation with test data is presented in Fig. 5. However, crack growth predictions are not found to be sensitive to cure fitting technique used to define η.

It should be noted that the model predicts complete retardation (shut-off) at $\sigma_{ol}/\sigma_{c_{\max}}$ ratios of 2.3 or greater. This corresponds quite well to crack growth shut-off ratios observed for aluminum alloys [*2,5*].

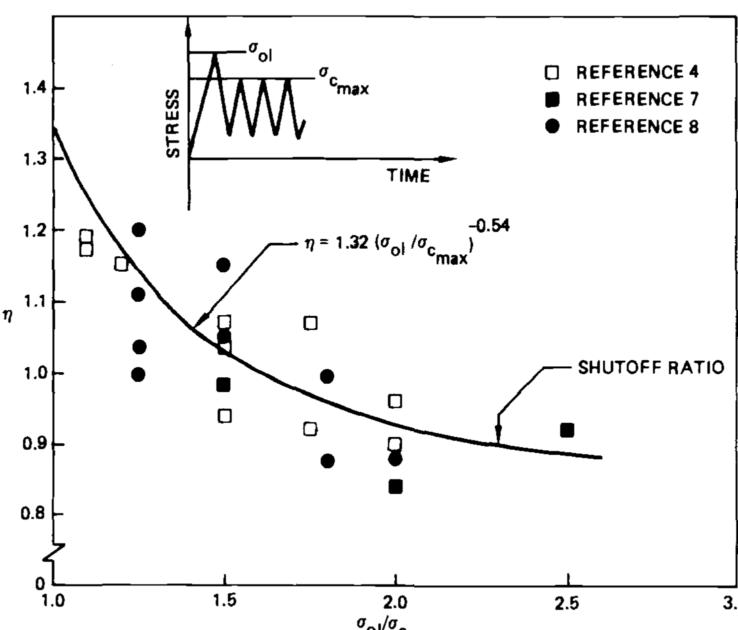

FIG. 5—*Overload effect parameters.*

Determination of β

The underload effects parameter, β, was determined from the reduction of constant amplitude/single-spike underload test data reported in Refs *4* and *5* and from Boeing test results. The functional relationship between and $|\sigma_{ul} - \sigma_{c\min}|$ shown in Fig. 6 appears to be well behaved. Only a limited amount of data was available for use in the development of β. For this reason, and because crack growth predictions are found to be sensitive to variations in β, additional verification of this parameter is warranted.

Transport Spectra Test Correlation

The developed model was applied to various transport aircraft test spectra to verify its accuracy and define any potential areas of concern. For this correlation, the results of crack propagation testing conducted on 28 center cracked 7075-T6 and 2024-T351 aluminum specimens subjected to transport wing and fin load spectra were used, (Ref *6* and Table 1). In these programs, effects of various transport aircraft usage parameters (that is, mission type, altitude, gross weight, flight duration, speed, etc.) were investigated. Mission profiles were based on U.S. Air Force bomber/transport utilization. Loads were derived from existing KC-135 response data. Mission types investigated include: (*a*) conventional transport (seven mission profiles), and (*b*) AMST (advanced medium STOL transport) low-level operation (five low-level profiles). In addition, three quasi-conventional transport mission types were synthesized from the low-level missions by elimination of the low-level cruise segment to permit assessments of contribution of those segments on crack growth.

Correlation between test results, using the developed model and the Willenborg, Wheeler, and Porter models [*1,3,4*], are shown in Fig. 7 for the following groups of mission types that are characterized as follows: conventional transport (wing, net retardation); benign (wing, net acceleration); low-level operation (wing net retardation); and low-level operation (fin net retardation). Additional correlation results for individual missions are presented in Tables 1 and 2.

The results show that all models except the Porter model [*4*] predict crack growth for conventional transport mission types about equally well. This is as expected, since acceleration effects are small in comparison to retardation effects for this mission group.

The developed model provides excellent correlation for benign mission types. All other analytical models, as well as linear analysis, significantly overpredict life for this case because of their total insensitivity to the acceleration phenomena.

Each of the load interaction models investigated, except the Porter model [*4*], predicted much faster crack growth than observed for low-level mission

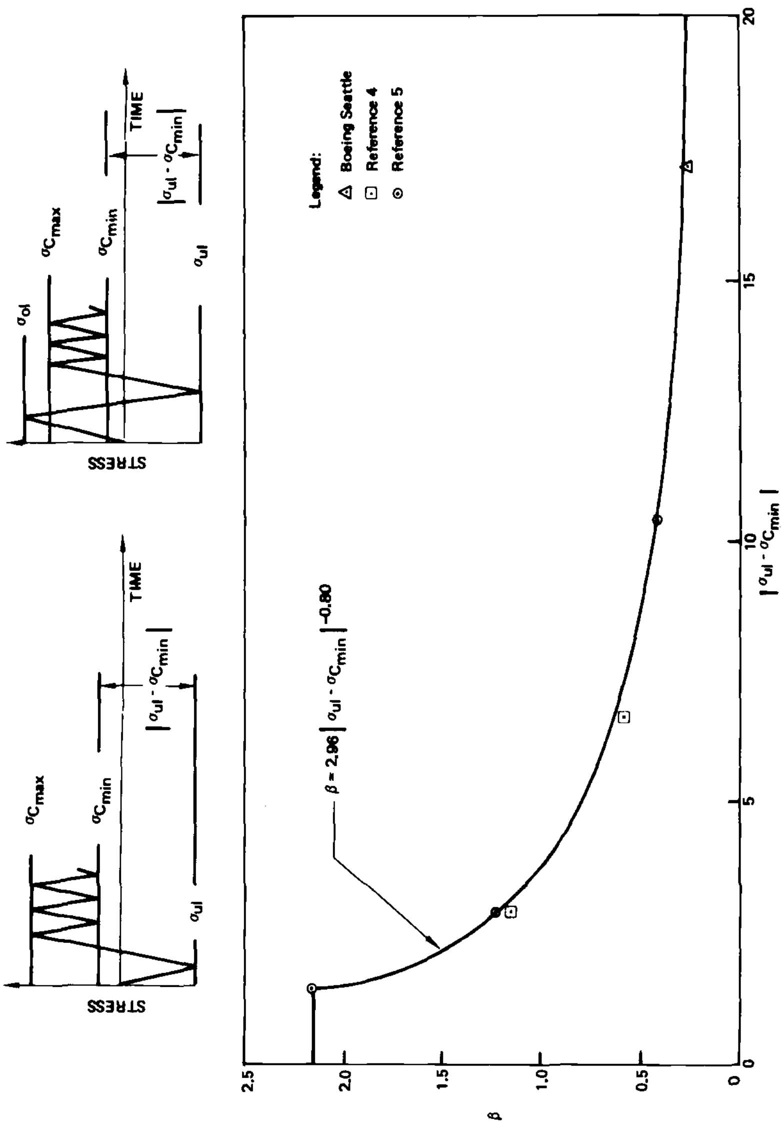

FIG. 6—*Underload effect parameters.*

TABLE 1—*Comparison of several analytical load-sequencing model predictions with Boeing Seattle test results (center-crack panels; lab air).*

		Predicted Flights/ Ratio of Predictions to Test					Crack Size, mm	
Mission Type	Test Flights, material	Modified Willenborg	Wheeler, m = 0.90	Porter	Developed Model	Linear	$2a_i$	$2a_f$
Cruise 1B[a]	3560 (2024)	4246/1.19	4016/1.13	5804/1.63	3599/1.01	3332/0.94	6.86	25.40
Benign No. 1[a]	1770 (2024)	1512/0.85	1390/0.79	2050/1.16	1265/0.71	1099/0.62	6.60	25.40
Benign No. 2[b]	3812 (7075)	6815/1.79	6690/1.75	6813/1.79	4483/1.18	6160/1.62	6.60	25.40
Benign No. 2[c]	2750 (7075)	5608/2.04	5608/2.04	5608/2.04	2737/0.99	5608/2.04	6.60	25.40
Low-level 3A[a]	503 (2024)	462/0.92	373/0.74	897/1.78	393/0.78	238/0.47	6.60	25.40
Low-level 3A without low-level segment[a]	1412 (2024)	1373/0.97	1305/0.92	1827/1.29	1266/0.90	1114/0.79	6.86	25.40
Low-level 3B (fin)[c]	320 (7075)	487/1.52	284/0.89	560/1.75	397/1.24	205/0.64	13.97	43.18
Low-level 3B (fin)[c]	192 (7075)	205/1.05	205/1.05	205/1.05	205/1.05	205/1.05	13.97	43.18

[a]Boeing Wichita test spectrum; material change.
[b]Replication of Boeing Wichita test.
[c]Modification of Boeing Wichita test spectrum.

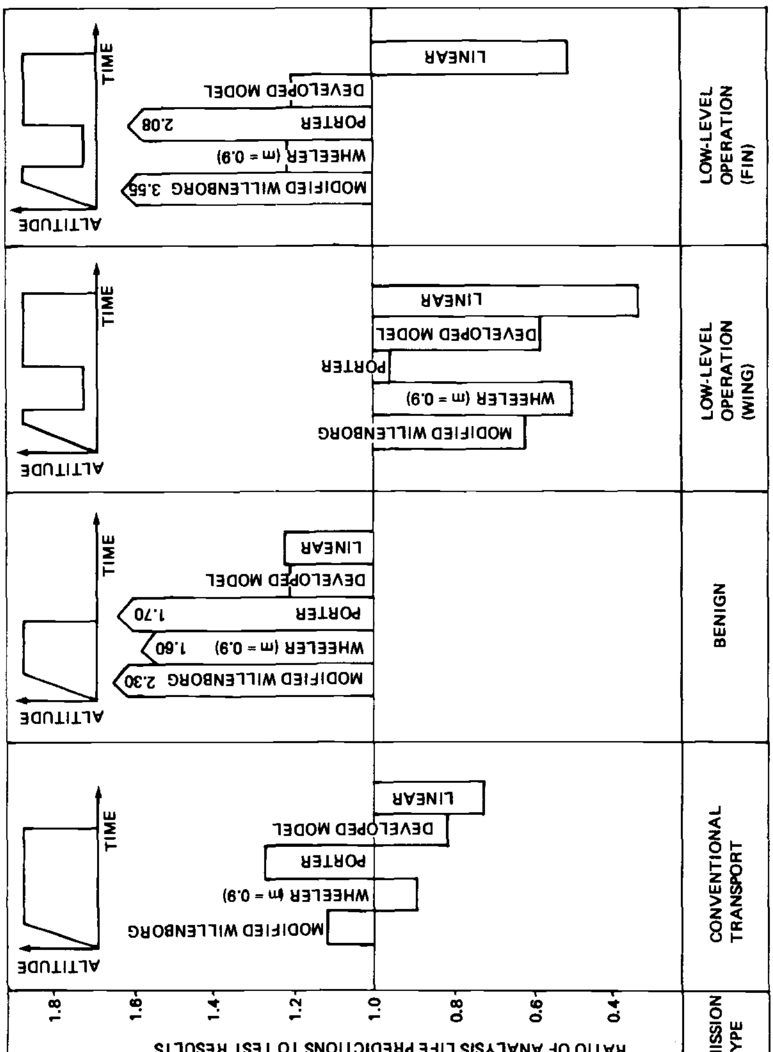

FIG. 7—*Correlation between test results and analytical predictions.*

TABLE 2—*Comparison of several analytical load-sequencing model predictions with Boeing Wichita test results (7075-T6 center-crack panels; lab air).*

		Predicted Flights/ Ratio of Prediction to Test					Crack size, mm	
Mission Type	Test Flights	Modified Willenborg	Wheeler m = 0.90	Porter	Developed Model	Linear	$2a_i$	$2a_f$
Low-level (2 tests)	425–520	260/0.55	185/0.39	426/0.90	261/0.55	104/0.22	6.35	25.40
Low level without low-level segment (2 tests)	540–600	775/1.36	630/1.11	957/1.68	635/1.10	426/0.75	6.35	25.40
Low-level 3A	327	160/0.49	116/0.35	208/0.64	161/0.49	97/0.30	6.35	25.40
Low-level 3A without low-level segment	780	826/1.06	785/1.01	1099/1.41	757/0.97	668/0.86	6.35	25.40
Low-level 3B	651	513/0.79	370/0.57	624/0.96	394/0.61	262/0.40	6.35	25.40
Low-level 3B without low-level segment	2150	2516/1.17	2450/1.14	3076/1.43	2226/1.04	2090/0.97	6.35	25.40
Benign No. 1	1002	1415/1.41	1080/1.08	1635/1.63	1034/1.03	816/0.81	6.35	25.40
Benign No. 2	4733	15 098/3.19	9990/2.11	8329/1.76	6664/1.41	7770/1.64	6.35	25.40
Cruise 1A	787	693/0.88	608/0.77	1000/1.27	581/0.74	468/0.59	6.35	25.40
Cruise 1B	1915	2676/1.40	1920/1.00	2472/1.29	1725/0.90	1604/0.84	6.35	25.40
Low-level 3A (fin)	526	2859/5.44	850/1.62	1087/2.07	618/1.17	322/0.61	6.35	12.70
Low-level 3B (fin)	540	895/1.66	450/0.83	1124/2.08	670/1.24	223/0.41	6.35	12.70
Refuel 2B	1445	1083/0.75	1020/0.71	2042/1.41	834/0.58	840/0.58	6.35	25.40
Touch and go 4B	846	1591/1.88	1040/1.23	1078/1.27	1015/1.20	767/0.91	6.35	25.40
Pattern + touch and go 5B	359	496/1.38	340/0.95	546/1.52	366/1.02	240/0.67	6.35	25.40

types (wing). No clear explanation for this deficiency is readily apparent. However, it is believed that stress intensity threshold effects that are not presently incorporated in the model may be a contributing factor.

Low-level mission (fin) analysis-test results show that the Wheeler model [3] provides the best correlation. However, it must be noted that these fin tests were used in part to determine the empirical shaping exponent required by that model. Predictions made using the developed model were acceptable, whereas those made using the Willenborg and Porter models [1,4] significantly overpredicted life.

Conclusions and Recommendations

The developed model is capable of making reasonable crack growth predictions for most transport aircraft type spectra while producing significant economics in computational resources. The predictive accuracy for spectra producing net retardation is judged at least as good as that obtained using alternate engineering methods, and its capability for predicting acceleration effects is unique.

A potential area of concern over the formulation of the model exists in its insensitivity to the effects of multiple overloads/underloads. Analysis of a number of transport aircraft wing loads spectra indicates that the existence of multiple overloads is infrequent and hence of minimal interest. While multiple underload conditions, due to ground operation, are frequent occurences, it has been reported by McGee and Hsu [5] that multiple underloads have a very small impact on subsequent crack growth. It is therefore believed that the effect of multiple overloads/underloads can be neglected in determining the retardation/acceleration phenomenon.

A major area of concern is the lack of acceptable predictive accuracy found for spectra containing low-level cruise segments. Although this mission type is not an operational requirement of conventional transport aircraft, it is a constituent of AMST utilization. Further development of the effective stress concept presented herein may well be required.

Acknowledgments

We wish to thank W. Bisler and W. Higby, The Boeing Company, for their contribution to the development of the crack growth model approach presented herein and permission to use the results of their studies.

References

[1] Willenborg, J., Engle, R., and Wood, H. A., "A Crack Retardation Model Using an Effective Stress Concept," Technical Memorandum 71-1FBR, Air Force Flight Dynamics Laboratory, Wright-Patterson Air Force Base, Ohio, Jan. 1971.

[2] Gallagher, J. P. and Hughes, T. F., "Influence of Yield Strength on Overload Affected Fatigue Crack Growth Behavior in 4340 Steel," AFFDL-TR-74-27, Air Force Flight Dynamics Laboratory, Wright-Patterson Air Force Base, Ohio, June 1974.
[3] Wheeler, O. E., "Crack Growth Under Spectrum Loading," Report No. FZM-5602, General Dynamics Corporation, Fort Worth Division, June 1970.
[4] Porter, T. R., *Engineering Fracture Mechanics*, Vol. 4, 1972, pp. 717–736.
[5] McGee, W. M. and Hsu, T. M., "Effects of Underloads on Fatigue Crack Growth," AFFDL-TR-77-2, Air Force Flight Dynamics Laboratory, Wright-Patterson Air Force Base, Ohio, March 1977.
[6] Lambert, G. E. and Bryan, D. F., "The Influence of Fleet Variability on Crack Growth Tracking Procedures for Transport/Bomber Aircraft," AFFDL-TR-78-158, Air Force Flight Dynamics Laboratory, Wright-Patterson Air Force Base, Ohio, Nov. 1978.
[7] Chanani, G. R., "Fundamental Investigation of Fatigue Crack Growth Retardation in Aluminum Alloys," AFML-TR-76-156, Air Force Flight Dynamics Laboratory, Wright-Patterson Air Force Base, Ohio, June 1976.
[8] Bell, P. D. and Creager, M., "Crack Growth Analysis for Arbitrary Spectrum Loading," Vol. I, AFFDL-TR-74-129, Air Force Dynamics Laboratory, Wright-Patterson Air Force Base, Ohio, Oct. 1974.

P. R. Abelkis[1]

Effect of Transport Aircraft Wing Loads Spectrum Variation on Crack Growth

REFERENCE: Abelkis, P. R., "**Effect of Transport Aircraft Wing Loads Spectrum Variation on Crack Growth,**" *Effect of Load Spectrum Variables on Fatigue Crack Initiation and Propagation, ASTM STP 714,* D. F. Bryan and J. M. Potter, Eds., American Society for Testing and Materials, 1980, pp. 143-169.

ABSTRACT: The effect of spectrum loading variations on crack growth were evaluated analytically and experimentally using C-15, KC-10A, and DC-10 transport aircraft wing loads spectra and 7475, 2024, and 7075 aluminum alloys. A total of 134 spectrum variations were generated in the following categories: (1) baseline spectra; (2) mission mix; (3) sequence of missions; (4) individual flight length; (5) flight segments; (6) exceedances spectra; (7) design stress level or usage severity; (8) valley/peak coupling; (9) low-load truncation; (10) high infrequent loads; (11) clipping of large loads; (12) miscellaneous variations, including the effect of flight loads alleviation system; and (13) combined variations. Spectra were generated as random cycle-by-cycle, flight-by-flight loading sequences. Crack growth tests, with cracks starting as through-thickness or corner cracks on one side of a hole, were performed on 47 of these spectra.

Analysis to test correlation shows 40 percent or better accuracy 78 percent of the time. However, different crack growth models had to be used to match the three aircraft baseline spectra: linear (C-15 and DC-10) and modified generalized Willenborg (KC-10A). Crack growth due to spectrum loading, with respect to loads interaction effects, appears to be a function of retardation and acceleration phenomena. An analysis model, incorporating both of these phenomena, is needed to properly predict spectrum variation effects.

Largest effect on crack growth life due to spectrum variations, as measured in flight hours, was due to mission mix, flight length, design stress level or usage severity, high infrequent loads, load alleviation system, and a change from a wing type to a vertical tail type spectrum. Using spectra variations that could be expected in service, fleet-wide crack growth variations by factors in the neighborhood of 100 and 10 could be experienced, depending on whether a short-term or a long-term spectrum variation is considered.

KEY WORDS: fatigue (material), spectrum loading, crack growth, aluminum alloys, transport aircraft, crack propagation

[1]Unit chief-Design, Douglas Aircraft Co., McDonnell Douglas Corp., Long Beach, Calif. 90846.

Crack growth in aircraft structures varies as a function of material, loading spectrum, and environment properties. Loading spectrum and environment properties vary as a function of aircraft type, aircraft usage, variability between the same type of aircraft within a fleet, and the type of structure. This paper presents the highlights of several studies [*1-3*][2] on the effect of transport aircraft wing lower surface loading spectrum variation on crack growth. The effects were evaluated experimentally and analytically.

The study described in Ref *1* involved the generation of 116 spectra variations representing the C-15 STOL transport wing lower surface loading; 33 of these spectra were tested on a 7475 aluminum alloy crack growth specimen. The KC-10A tanker/cargo aircraft wing lower surface loads spectra were developed in the Ref 2 study. Crack growth tests were performed on 12 different spectra using 2024 and 7075 aluminum alloy specimens. The effect of a DC-10 wing loads alleviation system on fatigue crack initiation and propagation was the objective of the study in Ref *3*. Tests were performed on 2024 and 7075 aluminum alloy specimens. In all of these studies, the spectra generated were of the random flight-by-flight type. The spectra variations ranged from realistic variations that might be expected among operational aircraft to variations to investigate spectrum development procedures. Tests represented crack growth out of an open hole.

Loads Spectra

The loads spectra were developed using commonly accepted procedures in the transport aircraft industry: definition of aircraft utilization-mission profiles, establishment of load factor exceedances spectra on segment-by-segment basis, calculation of the load factor-stress transfer function for the structural element being considered, and the generation and editing of the flight and cycle sequence. The generation and editing of the random sequence of flights and cycles was accomplished using the computer program described in Ref *4*. The random sequence is obtained through the use of a standard computer random number generation subroutine. Some of the basic terminology used in the generation of the spectra, and used throughout this paper, is illustrated in Fig. 1 and is defined as follows:

Peak—the point at which the first derivative of the load-time history changes from positive to negative sign.

Valley—the point at which the first derivative of the load-time history changes from negative to positive sign.

Range—the algebraic difference between successive valley and peak load.

R—loading ratio: the valley load divided by the following peak load.

Cycle—the portion of loading history from a valley to the next peak to the next valley.

[2]The italic numbers in brackets refer to the list of references appended to this paper.

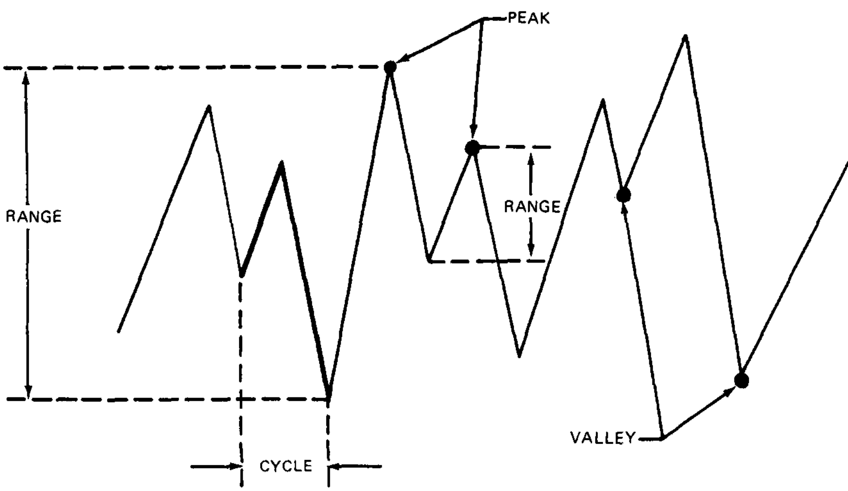

FIG. 1—*Fatigue loading terms.*

Flight—the portion of aircraft usage from engine-on to engine-off; normally involves one landing, except that a training flight may involve more than one in the form of touch-and-go landings. A mission may consist of one or more flights.

Baseline Spectra

The basic features of the aircraft usage, used in the three programs to generate the loads spectra, and the basic features of the baseline spectra are given in Table 1. Note that the C-15 has a high wing (landing gear in the fuselage), as opposed to the low wing on the KC-10A and DC-10 aircraft. As a result of this, the C-15 experiences higher compression stresses. Also, it should be noted that the KC-10 stresses in the baseline spectrum, as well as spectra variations, were increased by 20 percent above the nominal calculated values. The highest peak in the spectrum repeatable sequence (one-tenth of the projected service life) is the peak that occurs at least 0.5 times in that interval. The number of cycles per flight hour in the spectrum is influenced by the aircraft usage, stress level, and range truncation (RT). The large number of cycles in the C-15 spectrum is due to a very severe gust loads environment in the C-15 usage in the form of a low-level penetration mission. RT represents the cycle stress range that is used to eliminate all cycles with ranges below that value.

A portion of the C-15 baseline spectrum BS6 is shown by Fig. 2. The distributions of the peak, range, and R-values of this spectrum are given in Table 2. Note that most cycles have high positive R-values and relatively small stress ranges. The negative R-value cycles are the ground-to-air transi-

TABLE 1—*Basic features of aircraft usage and baseline spectra.*

	C-15	KC-10A	DC-10
Usage:			
Number of flights	8	6	1
Average flight hours/flight	0.97	6.61	2.77
Average flight hours/landing	0.65	1.25	2.77
Baseline Spectrum (wing lower surface):	Wing Root	Outboard of Landing Gear	
Flight hours	2 500	3 000	6 000
Landings	3 843	2 513	2 168
Range truncation, MN/m^2 (ksi)	27.6 (4.0)	20.7 × 1.2 (3.0 × 1.2)	17.2 (2.5)
Highest peak, MN/m^2 (ksi)	164.8 (23.9)	164.8 (23.9)	155.8 (22.6)
Lowest valley, MN/m^2 (ksi)	−167.5 (−24.3)	−61.4 (−8.9)	−51.0 (−7.4)
Total cycles	181 644	19 088	134 407
Average cycles/flight hour	72.7	6.3	22.4

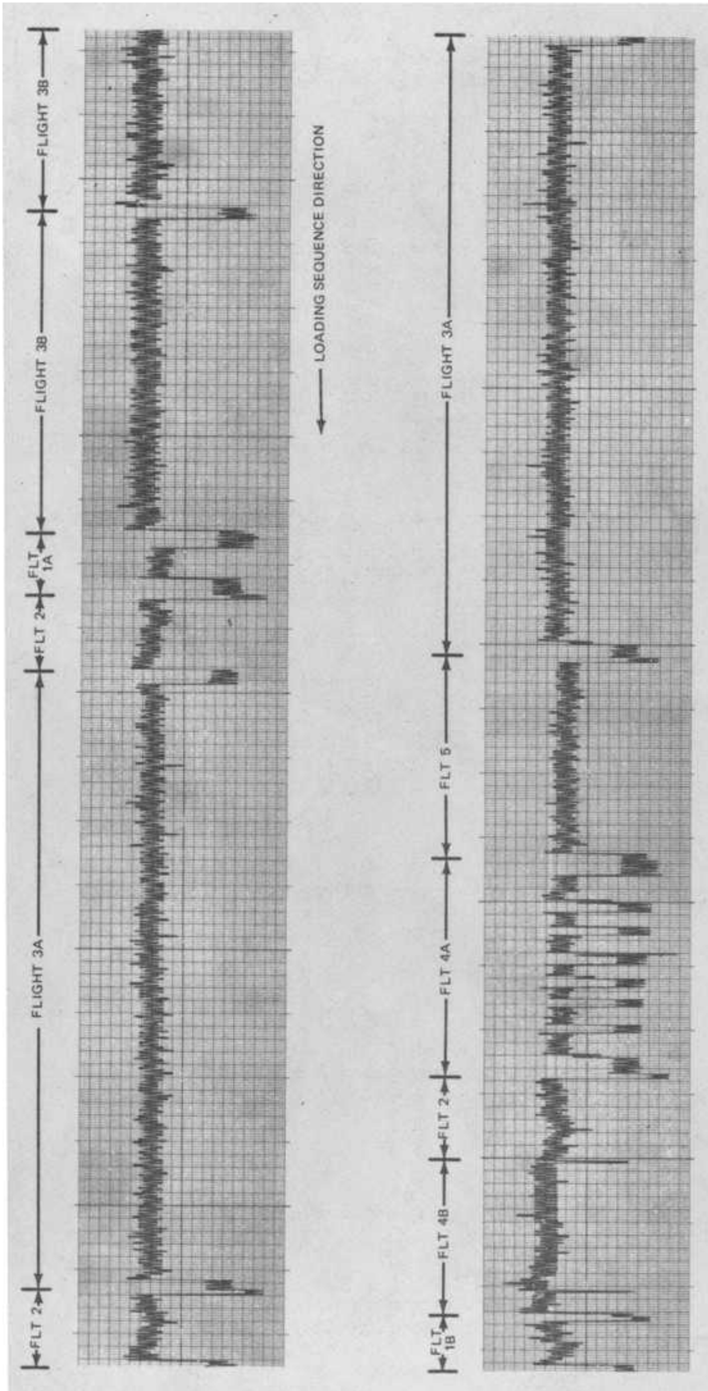

FIG. 2—*Portion of C15.BS6 spectrum.*

TABLE 2—*C-15 Baseline Spectrum BS6 Peak, Range, and* R *distributions (2 500 flight hours, 3 843 landings).*

Peak Distribution			Range Distribution			R Distribution	
Peak			Range				
MN/m^2	ksi	n cycles	MN/m^2	ksi	n cycles	R	n cycles
−82.7 to −68.9	−12 to −10	47	27.6 to 34.5	4 to 5	74 958	< −1.5	277
−68.9 to −55.2	−10 to − 8	9	34.5 to 41.4	5 to 6	66 142	−1.5 to −1.0	1 257
−55.2 to −41.4	− 8 to − 6	1 115	41.4 to 48.3	6 to 7	24 930	−1.0 to −0.8	1 359
−41.4 to −27.6	− 6 to − 4	4 457	48.3 to 55.2	7 to 8	7 864	−0.8 to −0.6	987
−27.6 to −13.8	− 4 to − 2	7 762	55.2 to 62.1	8 to 9	2 346	−0.6 to −0.4	289
−13.8 to 0	− 2 to 0	56	62.1 to 68.9	9 to 10	1 048	−0.4 to −0.2	107
0 to 27.6	0 to 4	0	68.9 to 82.7	10 to 12	365	−0.2 to 0	142
27.6 to 41.4	4 to 6	742	82.7 to 96.5	12 to 14	73	0 to 0.2	362
41.4 to 55.2	6 to 8	341	96.5 to 110.3	14 to 16	24	0.2 to 0.4	3 948
55.2 to 68.9	8 to 10	21 417	110.3 to 124.1	16 to 18	42	0.4 to 0.6	68 900
68.9 to 82.7	10 to 12	66 177	124.1 to 137.9	18 to 20	202	0.6 to 0.8	90 570
82.7 to 96.5	12 to 14	45 077	137.9 to 151.7	20 to 22	1 548	0.8 to 1.0	0
96.5 to 110.3	14 to 16	32 406	151.7 to 165.5	22 to 24	1 398	>1.0	13 446
110.3 to 124.1	16 to 18	1 751	165.5 to 179.3	24 to 26	484	...	...
124.1 to 137.9	18 to 20	260	179.3 to 193.1	26 to 28	189	...	...
137.9 to 151.7	20 to 22	20	193.1 to 206.8	28 to 30	30	...	...
151.7 to 165.5	22 to 24	7	206.8 to 213.7	30 to 31	1	...	...

tion cycles. The KC-10A and DC-10 baseline spectra are similar, to the C-15 spectrum except, due to smaller compression stresses, the ground-to-air transition cycle negative R-values are smaller.

Spectra Variation

The spectra variations studied and tested in the three programs are summarized in Table 3. The variations are grouped into the following fourteen categories.

Baseline Spectrum (BS)—A typical average spectrum used as a reference spectrum, based on projected usage, see Table 1.

Mission Mix (MM)—Different mission mixes from that in the baseline spectra, including spectra based entirely on one flight type.

Sequence of Missions (SM)—Different mission/flight sequences from that in the baseline spectra, including specific ordered sequences.

Flight Segments (FS)—Simplification of the flight profile by elimination or combining of segments.

Exceedances Spectra (ES)—The number of occurrences or the slope of the flight loads exceedances spectra increased or decreased by 15 percent.

Design Stress Level (DSL)—All stresses in a baseline spectrum increased or decreased by the same percent. Can be also viewed as representing a change in usage severity.

Valley-Peak Coupling (VPC)—Specific coupling of valleys and peaks as opposed to the random coupling in the baseline spectra.

Low-Load Truncation (LLT)—The range truncation (RT) level was in-

TABLE 3—*Spectra variations.*

	C-15		KC-10A		DC-10	
Variations	Analysis	Tested	Analysis	Tested	Analysis	Tested
Baseline spectrum (BS)	6	6	1	1	3	1
Mission mix (MM)	14	2	3	3	...	...
Sequence of missions (SM)	4	0	...	...	...	...
Individual flight length (FL)	6	1	...	...	...	...
Flight segments (FS)	5	0	...	...	...	...
Exceedance spectra (ES)	4	1	...	...	...	...
Design stress level (DSL)	10	3	1	1	...	...
Valley-peak coupling (VPC)	6	1	...	...	...	...
Low-load truncation (LLT)	16	5	4	4	...	...
High infrequent loads (HIL)	18	5	2	2	...	...
Clipping of large loads (CLP)	4	1	1	1	...	...
Load alleviation system effect	1	0	...	...	3	1
Miscellaneous (MISC)	9	3	...	...	...	...
Combined (COMB)	13	5	...	...	...	...
Total	116	33	12	12	6	2

creased or decreased relative to the values used in the baseline spectra (see Table 1): 20.7 to 34.5 MN/m^2 (3 to 5 ksi) in the C-15 spectra and 8.6 (1.2) to 24.1 (1.2) MN/m^2 (1.25(1.2) to 3.5(1.2) ksi) in the KC-10A spectra. All cycles with stress range below the RT level are eliminated from the spectrum.

High Infrequent Loads (*HIL*)—The frequency of occurrence or magnitude or both of the ten highest peaks in the baseline spectrum were increased.

Clipping of Large Loads (*CLP*)—All loads above or below a selected value set equal to that value.

Load Alleviation System Effect—The effect of wing load alleviation system on fatigue loads spectrum is to increase the 1.0 g stresses and to decrease the cycle stress ranges. These effects on the spectrum were arbitrarily assumed for the C-15 spectrum and calculated for a hypothetical system for the DC-10 spectrum.

Miscellaneous (*MISC*)—A number of miscellaneous parameters were investigated in this category: (1) the averaging interval of the maneuver and gust spectra—Δg = 0.05 and 0.20 versus 0.10 in the baseline spectrum; (2) spectrum length—shorter spectra than the baseline; (3) ignoring of the normal flight segment sequence to study the effect of cycle sequence within a flight; (4) removal of taxi, landing impact, and GAG cycles to show their combined effect; and (5) simplification of a baseline spectrum.

Combined (*COMB*)—Combinations of some of the preceding variations: VPC + LLT, LLT + DSL, HIL + LLT, HIL + DSL. Also, the baseline spectrum representing the wing was drastically changed to simulate a vertical tail loading.

Basic features of the spectra that were tested are given in Table 4.

Experimental Procedure

Crack growth tests were performed to evaluate the effect of loads spectra variations. A total of 47 spectra were tested using 63 wide-panel unstiffened specimens. Three aluminum alloys were used: 7475-T651, 2024-T351, and 7075-T651. The scope of the testing and a more detailed description of the test specimens are given in Table 5.

Specimens

The specimens are described in Table 5. In the C-15 and KC-10A programs, a precrack was generated from a mechanical notch in a 4.76 mm (0.1875 in.) diameter hole, using constant amplitude axial loading of S_{max} = 82.7 or 89.6 MN/m^2 (12 or 13 ksi), R = 0.01. Afterwards, the hole was reamed to a 6.35 mm (0.25 in.) diameter, leaving a pure fatigue crack at the edge of the hole. The DC-10 program specimen was not precracked.

Testing Equipment and Procedure

The specimens were tested in a Douglas-designed testing system consisting of a 1.5-million-pound test fixture with five individually controlled 150 000-pound capacity jacks using closed-loop electrohydraulic servosystems. The system allows for testing up to five specimens simultaneously under five different loading spectra. The loading spectra, in terms of valley and peak sequences, were input into the testing system from a magnetic tape through a computer.

The specimens were tested most of the time in groups of five. Antibuckling plates were used to prevent buckling under compression loads. The loads were applied at 4.0 Hz frequency. The loads accuracy was spot-checked through a strip chart recorder trace and monitored automatically through the computer with respect to a preset tolerance level.

In most tests, the crack was propagated at least to a length of 12.7 mm (0.5 in.). Surface crack lengths were measured approximately every 1.3 mm (0.05 in.) of crack growth. The measurements were made with a ×40 optical microscope within an accuracy of 0.025 mm (0.001 in.).

Test and Analysis Results and Correlation

Test and analysis results of the spectra that were tested are given in Tables 6 and 7. The results are in terms of life to propagate a crack on one side of the hole a specified length, in most cases 12.7 mm (0.5 in.). Some of the C-15 test data reflects also a small amount of cracking on the other side of the hole, but the effect on the reported data is negligible. Flight hours were chosen as the units for life, because it is the most commonly used parameter to measure service life of transport aircraft. Use of other parameters, such as "landings," "flights," or "cycles" can produce in some instances a different interpretation of the results when comparing lives due to different spectra.

Analysis

Crack growth analyses results shown in Tables 6 and 7 were performed using the linear model for KC-10 and a modified generalized Willenborg (MGW) model for the KC-10A and DC-10 spectra. The linear model does not account for any loading interaction effects, such as retardation or acceleration phenomena. The modification of the generalized Willenborg model (Refs *5* and *6*) consists of using different stress intensity factor threshold values for different R value da/dN curves. Stress intensity factors were calculated as

$$K = \sigma\sqrt{\pi a \sec\left(\frac{\pi a}{W}\right)}\cdot\beta$$

σ = gross area stress,
a = crack length (measured from edge of hole),

TABLE 4—*Basic features of test loads spectra.*

Identification	Description	Flight Hours	Number of Landings	Number of Cycles	Range Truncation, MN/m^2	(ksi)	Highest Peak, MN/m^2 (ksi)	Smallest Valley, MN/m^2 (ksi)
C15.BS1	Mission 1 (basic and alternate employment)	2500	2 528	45 807	27.6	(4.0)	152.4 (22.1)	−167.5 (−24.3)
C15.BS2	Mission 2 (long-range logistics)	2500	437	10 422	27.6	(4.0)	123.4 (17.9)	−123.4 (−17.9)
C15.BS3	Mission 3 (low altitude resupply)	2500	5 112	649 353	27.6	(4.0)	169.6 (24.6)	−108.2 (−15.7)
C15.BS4	Mission 4 (basic training)	2500	15 872	199 036	27.6	(4.0)	198.6 (28.8)	−193.1 (−28.0)
C15.BS5	Mission 5 (combat training)	2500	3 205	197 169	27.6	(4.0)	142.7 (20.7)	−102.7 (−14.9)
C15.BS6	Composite spectrum—Missions 1-5	2500	3 843	181 644	27.6	(4.0)	164.8 (23.9)	−167.5 (−24.3)
C15.BS4.MM8	Touch and go landings only from Mission 4	2500	25 000	248 187	27.6	(4.0)	191.7 (27.8)	−191.0 (−27.7)
C15.BS6.MM13	C15.BS6 spectrum without low altitude flying	2500	3 666	51 896	27.6	(4.0)	173.7 (25.2)	−167.5 (−24.3)
C15.BS1B.FL3	4.0-h long flight 1B	2500	625	18 245	27.6	(4.0)	168.9 (24.5)	−113.8 (−16.5)
C15.BS6.ES4	Slope of flight loads exceedance spectra decreased 15%	2500	3 843	117 516	27.6	(4.0)	156.5 (22.7)	−167.5 (−24.3)
C15.BS6.DSL1	Stresses increased 15%	2500	3 843	181 644	27.6 × 1.15	(4 × 1.5)	189.6 (27.5)	−192.4 (−27.9)
C15.BS6.DSL3	Stresses decreased 26%	2500	3 843	181 644	27.6 × .74	(4 × .74)	122.0 (17.7)	−124.1 (−18.0)
C15.BS6.DSL4	Stresses increased 35%	2500	3 843	181 644	27.6 × 1.35	(4 × 1.35)	222.7 (32.3)	−226.1 (−32.8)
C15.BS3.VPC1	Specific valley/peak coupling	2500	5 112	388 719	27.6	(4.0)	169.6 (24.6)	−108.2 (−15.7)
C15.BS3.LLT1	Range truncation level increased	2500	5 112	465 207	31.0	(4.5)	169.6 (24.6)	−108.2 (−15.7)
C15.BS3.LLT2	Range truncation level decreased	2500	5 112	1 169 011	24.1	(3.5)	169.6 (24.6)	−108.2 (−15.7)
C15.BS6.LLT2	Range truncation level decreased	2500	3 843	311 256	24.1	(3.5)	164.8 (23.9)	−167.5 (−24.3)
C15.BS6.LLT5	Number of taxi cycles increased from an average of 3.5 to 25.9 cycles per landing	2500	3 843	267 999	27.6	(4.0)	164.8 (23.9)	−167.5 (−24.3)
C15.BS6.LLT6	Range truncation level increased	2500	3 843	117 493	34.5	(5.0)	164.8 (23.9)	−167.5 (−24.3)
C15.BS6.HIL1	Number of ten highest peaks increased to 100	2500	3 843	181 747	27.6	(4.0)	164.8 (23.9)	−167.5 (−24.3)
C15.BS6.HIL2	Number of ten highest peaks increased to 200	2500	3 843	181 858	27.6	(4.0)	164.8 (23.9)	−167.5 (−24.3)
C15.BS6.HIL3	Magnitude of ten highest peaks increased	2500	3 843	181 641	27.6	(4.0)	228.2 (33.1)	−167.5 (−24.3)
C15.BS6.HIL4	Magnitude of ten highest peaks increased	2500	3 843	181 642	27.6	(4.0)	191.7 (27.8)	−167.5 (−24.3)
C15.BS6.HIL5	Combination of HIL2 and HIL3	2500	3 843	181 824	27.6	(4.0)	228.2 (33.1)	−167.5 (−24.3)

C15.BS6.CLP3	Stresses below zero set equal to zero	2500	3 843	168 198	27.6	(4.0)	164.8 (23.9)	0 (0)
C15.BS6.MISC2	Flight loads averaging interval $\Delta g = 0.20$, as opposed to $\Delta g = 0.10$ in C15.BS6	2500	3 843	375 893	27.6	(4.0)	171.0 (24.8)	−167.5 (−24.3)
C15.BS6.MISC6	Simplified C15.BS6 spectrum	2500	3 843	176 778	27.6	(4.0)	164.8 (23.9)	− 77.9 (−11.3)
C15.BS1.MISC9	Different sequence of cycles within flight	2500	3 843	56 697	27.6	(4.0)	152.4 (22.1)	−167.5 (−24.3)
C15.BS6.COMB3	Stresses increased 15% and range truncation decreased	2500	3 843	311 526	24.1 × 1.15	(3.5 × 1.15)	189.6 (27.5)	−192.4 (−27.9)
C15.BS6.COMB6	Stresses decreased 10% and range truncation decreased	2500	3 843	311 256	24.1 × 0.9	(3.5 × 0.9)	148.2 (21.5)	−151.0 (−21.9)
C15.BS6.COMB11	Vertical tail loads spectrum simulation	2500	3 843	161 813	27.6 × 2.0	(4.0 × 2.0)	161.3 (23.4)	−167.5 (−23.4)
C15.BS6.COMB12	Number of ten highest peaks increased to 100 and range truncation decreased	2500	3 843	311 357	24.1	(3.5)	160.6 (23.3)	−167.5 (−24.3)
C15.BS6.COMB13	Spectrum C15.BS6.COMB11 stresses increased 35%	2500	3 843	161 813	27.6 × 2.7	(4.0 × 2.7)	217.9 (31.6)	−217.9 (−31.6)
KC10.BS	Baseline composite spectrum (Missions 1-6)	3000	2 513	19 141	20.7 × 1.2	(3.0 × 1.2)	164.8 (23.9)	− 61.4 (− 8.9)
KC10.MM1	Mission 3	3000	258	65 158	20.7 × 1.2	(3.0 × 1.2)	191.7 (27.8)	− 55.8 (− 8.1)
KC10.MM2	Mission 5	3000	2 586	19 092	20.7 × 1.2	(30. × 1.2)	167.5 (24.3)	− 61.4 (− 8.9)
KC10.MM3	Different mission mix	3000	1 626	32 193	20.7 × 1.2	(3.0 × 1.2)	166.2 (24.1)	− 64.1 (− 9.3)
KC10.DSL1	Design stress level increased 15%	3000	2 513	30 924	20.7 × 1.2 × 1.15	(3.0 × 1.2 × 1.15)	189.6 (27.5)	− 70.3 (−10.2)
KC10.LLT1	Range truncation level increased	3000	2 513	11 675	24.1 × 1.2	(3.5 × 1.2)	164.8 (23.9)	− 61.4 (− 8.9)
KC10.LLT2	Range truncation level decreased	3000	2 513	35 144	17.2 × 1.2	(2.5 × 1.2)	164.8 (23.9)	− 61.4 (− 8.9)
KC10.LLT3	Range truncation level decreased	3000	2 513	73 103	12.9 × 1.2	(1.875 × 1.2)	164.8 (23.9)	− 61.4 (− 8.9)
KC10.LLT4	Range truncation level decreased	3000	2 513	109 881	8.6 × 1.2	(1.25 × 1.2)	164.8 (23.9)	− 61.4 (− 8.9)
KC10.HIL1	Number of ten highest peaks increased to 100	3000	2 513	19 141	20.7 × 1.2	(3.0 × 1.2)	164.8 (23.9)	− 61.4 (− 8.9)
KC10.HIL2	Magnitude of ten highest peaks increased	3000	2 513	18 973	20.7 × 1.2	(3.0 × 1.2)	206.2 (29.9)	− 64.1 (− 9.3)
KC10.CLP1	Magnitude of ten highest peaks reduced	3000	2 513	19 008	20.7 × 1.2	(3.0 × 1.2)	147.5 (21.4)	− 61.4 (− 8.9)
DC10.BS	Baseline spectrum (average flight)	6000	2 168	134 407	17.2	(2.5)	155.8 (22.6)	− 51.0 (− 7.4)
DC10.WLA	Wing with load alleviation system	6000	2 168	69 943	17.2	(2.5)	161.3 (23.4)	− 47.6 (− 6.9)

TABLE 5—*Test specimens and scope of testing.*

	Specimens[a]		Number of	
Program	Material[b]	Initial Notch	Spectra Tested	Specimens Tested
C-15	7475-T651	through-thickness 0.76 mm (0.03 in.) crack on one side of open hole; two holes in specimen	33	35
KC-10A	2024-T351	corner[c] crack on one side of open hole;	12	12
	7075-T651	one hole in specimen		12
DC-10	2024-T351	open hole (no precrack)		2
	7075-T651		2	2
Total			47	63

[a]Unstiffened 228.6 mm (9.0 in.) wide panel with a 6.35 mm (0.25 in.) diameter hole in center.
[b]Bare, 6.35 mm (0.25 in.) thick, aluminum alloy plate.
[c]

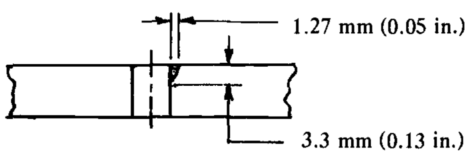

W = panel width,
β = correction factor for specimen and crack geometry,
= Bowie solution (Ref *7*) for the thru-thickness crack on one side of the hole, and
= Fujimoto solution (Ref *8*) for the corner crack on one side of the hole. Switch from Fujimoto corner crack to Bowie through-thickness solution was made after the corner crack grew through 80 percent of the specimen thickness.

The *da/dN* data used in the analysis were generated mainly with center-cracked panels from the same batch of material as used for the spectrum loading test specimens. The data covers all R- and K-values of the loads spectra.

Test and Analysis Correlation

Test results show substantial crack growth rate variations due to many of the loads spectra variations. The accuracy of predicting these effects with the state-of-the-art crack growth analysis methodology is indicated in Tables 6 and 7 in terms of the correlation factor

$$R_{\Delta N} = (\Delta N_{\mathrm{TEST}}/\Delta N_{\mathrm{ANAL}})$$

TABLE 6—*C-15 test and linear analysis results (7475-T651 aluminum alloy; see Table 5 for specimen description).*

Spectrum	ΔN^a Test	ΔN^a Analysis	$R_{\Delta N} = \frac{\Delta N_{\text{TEST}}}{\Delta N_{\text{ANAL}}}$
C15.BS1	15 365	16 255	0.95
C15.BS2	67 208	78 347	0.86
C15.BS3	1 368	1 124	1.22
C15.BS4	4 044	3 518	1.15
C15.BS5	6 992	8 124	0.86
C15.BS6	4 140	4 212	0.98
C15.BS4.MM8	3 957	3 011	1.31
C15.BS6.MM13	15 635	14 457	1.08
C15.BS1B.FL3	32 702	27 600	1.18
C15.BS6.ES4	7 992	7 006	1.14
C15.BS6.DSL1	3 475	2 460	1.41
C15.BS6.DSL3	13 310	15 415	0.86
C15.BS6.DSL4	1 740	1 373	1.27
C15.BS3.VPC1	1 247	1 024	1.22
C15.BS3.LLT1	1 510	1 199	1.26
C15.BS3.LLT2	816	864	0.94
C15.BS6.LLT2	4 334	3 559	1.22
C15.BS6.LLT5	3 499	4 213	0.83
C15.BS6.LLT6	5 310	4 589	1.16
C15.BS6.HIL1	5 929	4 190	1.42
C15.BS6.HIL2	7 136	4 160	1.48
C15.BS6.HIL3	6 772	4 206	1.61
C15.BS6.HIL4	4 920	4 210	1.17
C15.BS6.HIL5	9 819	4 001	2.45
C15.BS6.CLP3	5 679	4 451	1.28
C15.BS1.MISC9	10 265	12 721	0.81
C15.BS6.MISC2	2 937	2 179	1.35
C15.BS6.MISC6	4 298	5 029	0.85
C15.BS6.COMB3	2 438	1 900	1.28
C15.BS6.COMB6	5 290	5 261	1.01
C15.BS6.COMB11	12 922*	4 836*	2.67*
C15.BS6.COMB12	3 522	3 344	1.05
C15.BS6.COMB13	2 908**	873**	3.33**

[a] Flight hours to propagate the crack $a = 0.76 \rightarrow 13.46$ mm (0.03 → 0.53 in.), except as noted below:

*$a = 0.76 \rightarrow 4.78$ mm (0.03 → 0.188 in.)

**$a = 5.41 \rightarrow 9.45$ mm (0.213 → 0.372 in.)

TABLE 7—*KC-10A and DC-10 test and analysis results (see Table 5 for specimen description).*

	2024-T35					7075-T651				
	ΔN[a]			$R_{\Delta N} = \frac{\Delta N_{TEST}}{\Delta N_{ANAL}}$		ΔN[b]			$R_{\Delta N} = \frac{\Delta N_{TEST}}{\Delta N_{ANAL}}$	
		Analysis					Analysis			
Spectrum	Test	Linear	MGW[c]	Linear	MGW	Test	Linear	MGW	Linear	MGW
KC10.BS	53 500	18 500	53 000	2.89	1.01	41 500	16 300	32 000	2.55	1.30
KC10.MM1	17 400	14 100	16 700	1.23	1.04	14 200	8 400	9 390	1.69	1.51
KC10.MM2	65 000	17 800	46 800	3.65	1.39	44 900	17 700	32 700	2.54	1.37
KC10.MM3	34 000	17 300	31 200	1.97	1.09	27 500	13 400	18 700	2.05	1.47
KC10.DSL1	36 500	11 900	29 700	3.07	1.23	29 800	10 400	18 600	2.87	1.60
KC10.LLT1	67 500	19 600	60 000	3.44	1.13	56 200	19 500	40 800	2.88	1.38
KC10.LLT2	43 000	18 300	46 500	2.35	0.92	38 000	17 700	34 300	2.15	1.11
KC10.LLT3	34 500	17 200	38 200	2.0	0.90	27 000	15 900	29 000	1.70	0.93
KC10.LLT4	36 500	17 000	37 400	2.15	0.98	32 000	18 100	33 100	1.77	0.97
KC10.HIL1	57 800	≃18 500	61 900	3.12	0.93	59 700	≃16 300	42 100	3.66	1.42
KC10.HIL2	186 800	≃18 500	112 000	10.10	1.67	131 200	≃16 300	52 900	8.05	2.48
KC10.CLP1	46 800	≃18 500	48 300	2.53	0.97	37 200	≃16 300	29 800	1.16	1.25
DC10.BS*	23 800	25 700	36 400	0.93	0.66	13 500	12 800	16 600	1.05	0.81
DC10.WLA*	31 400	28 500	37 800	1.10	0.83	16 000	16 000	18 000	1.00	0.89

[a] Flight hours to propagate the crack $a = 1.27 \rightarrow 7.62$ mm ($0.05 \rightarrow 0.30$ in.) except as noted below.
[b] Flight hours to propagate the crack $a = 1.27 \rightarrow 14.0$ mm ($0.05 \rightarrow 0.55$ in.) except as noted below.
*$a = 1.17 \rightarrow 9.07$ mm ($0.046 \rightarrow 0.357$ in.)
[c] Modified generalized Willenborg model.

where ΔN is the life to propagate a crack over a specified crack length. First, let us look at the prediction accuracy for the baseline spectra in Table 8.

The scope of the C-15 spectrum program called for the use of the analysis model that correlated best with the baseline spectrum BS6 test result. The linear and the generalized Willenborg models were evaluated and the crack growth curves are shown in Fig. 3. The linear model produced excellent correlation and was used throughout that program. However, the KC-10A spectrum program produced just the opposite results. The modified generalized Willenborg (MGW) model gave good correlation, whereas the linear model predicted significantly shorter lives. Lastly, in the DC-10 spectrum program, the linear model produced excellent correlation, although the MGW model gave reasonable prediction for the 7075 material.

The obvious question is why the linear model predicts better in the two cases, but not fo the KC-10A spectrum. In general, it is believed that the linear model will give a good prediction if: (*a*) the retardation and acceler-

TABLE 8—*Prediction accuracy for the baseline spectra.*

		$R_{\Delta N} = (\Delta N_{TEST}/\Delta N_{ANAL})$		
Spectrum	Material	Linear	Generalized Willenborg	Modified Generalized Willenborg
C-15 (BS6)	7475	0.98	0.64	...
KC-10A	2024	2.89	...	1.01
	7075	2.55	...	1.30
DC-10	2024	0.93	...	0.66
	7075	1.05	...	0.81

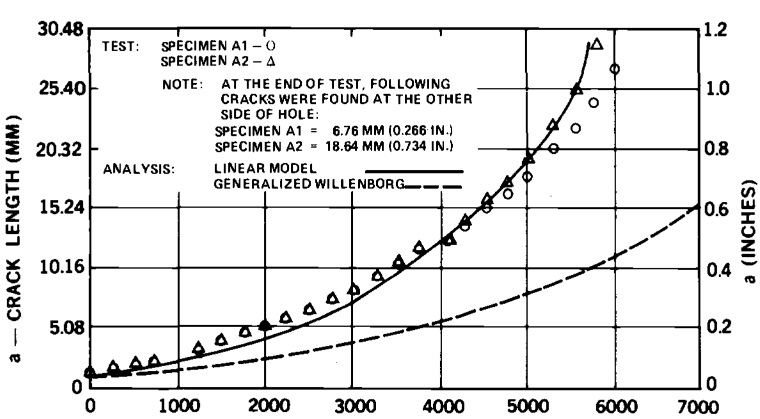

FIG. 3—*Test versus analysis crack growth comparison, Spectrum C15.BS6.*

ation features of the loading spectrum tend to offset each other, (*b*) the stress intensity factor solution accurately represents the test specimen and crack geometries and is compatible with the *da/dN* data, and (*c*) the *da/dN* data represents the actual material and thickness being considered. It is obvious that an appropriate combination of the three conditions produced a good prediction in the case of the C-15 and DC-10 spectra. Note, that in both cases, we are dealing with a through-thickness crack, same as *da/dN* data. The explanation in the case of the KC-10A spectrum might be some incompatibility of the *da/dN* data (through-thickness *da/dN* data versus corner crack), as well as some basic differences in the spectrum that produced an overwhelming net retardation that only the retardation oriented MGW model could match. For example, KC-10A compression stresses are significantly lower than C-15, although they are about the same as DC-10, see Table 1. Also, a distinct difference exists in the average number of flight (tension-tension) cycles for each ground-air (compression-tension) cycle: 43 and 61 in the C-15 and DC-10 spectra compared to 7 in the KC-10A spectrum. Also, the range truncation level of the three spectra are different.

From these results, it must be concluded that no single presently available linear or retardation oriented model can accurately predict crack growth under different spectrum loadings. This could be accomplished only by a model that properly accounts for the retardation and also acceleration features of the loading spectrum. As further evidence of this, let us look at the test to analysis correlation of all the spectra variations, using the analysis model that produced the best correlation for the baseline spectra. Figure 4 shows the distribution of the correlation factor $R_{\Delta N}$. In the majority of cases, 71 percent of the time, the predictions are conservative, $R_{\Delta N}>1.0$. It is also of interest to see which of the predictions deviate most from the test results. Looking at results that deviate more than 40 percent ($R_{\Delta N}>1.4$), it is not surprising to see, in the linear analysis results, spectra with variations on high infrequent loads (HIL) or design stress level (DSL). These changes produced more retardation, and the linear analysis can not account for that. More surprising is the large deviation of the BS6.COMB11 and COMB13 that represent drastically changed spectra from that of the baseline. These spectra, simulating vertical tail loading, have an overall mean load of zero, with the *R*-value of all cycles around -1.0. The largest deviation between test and the MGW model analysis results with the KC-10A spectra also occur with similar spectra variations: HIL and DSL changes, as well as mission mix (MM) variations. The MM spectra deviations can be attributed to a large increase in the $+R$ to $-R$ cycle ratio: from approximately 7 in the baseline spectra to 252 in MM1 and 20 in MM2. The reduction of the acceleration features of these spectra are not accounted for by the MGW model.

In all subsequent discussion of analysis results in this paper, unless otherwise noted, reference is made to linear analysis for the C-15 and DC-10 spectra and the MGW model for the KC-10A spectrum.

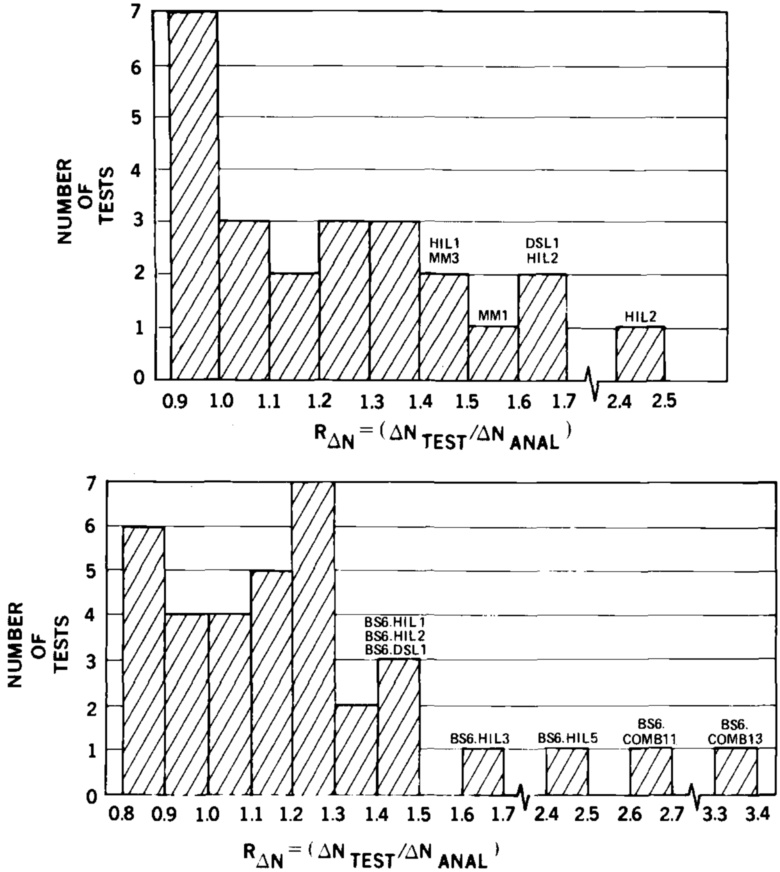

FIG. 4—*Test versus analysis crack growth comparison:* (top) *KC-10A, modified generalized Willenborg analysis, 24 tests;* (bottom) *C15 and DC-10, linear analysis, 35 tests.*

Discussion of Results

The level of significance of the loads spectra variation effects on crack growth are summarized in Table 9. The levels are classified as,

$$\text{not significant if } |(R'_{\Delta N} - 1)| < 0.2$$

$$\text{significant if } 0.2 \leq |(R'_{\Delta N} - 1)| \leq 1.0$$

$$\text{very significant if } |(R'_{\Delta N} - 1)| > 1.0$$

where

$R'_{\Delta N} = (\Delta N_{VAR}/\Delta N_{BS})$;

$\Delta N =$ life, in terms of flight hours, to propagate the crack a specified length;

TABLE 9—*Effect of spectra variations on crack growth—summary.*

Spectrum Variation	Number of spectra		$R'_{\Delta N}$ [a]		Effect on Crack Growth		
	Analyzed	Tested	Analysis	Test	Not Significant	Significant	Very Significant
Mission mix (MM)	22	10	0.26→18.60 [b]	0.33→16.19	...	...	X
Sequence of missions (SM)	4	0	0.96→ 1.01	...	X	...	...
Individual flight length (FL)	6	1	1.66→21.43	7.90	...	...	X
Flight segments	5	0	0.99→ 1.14	...	X	...	...
Exceedances spectra (ES)	4	1	0.66→ 1.66	1.93	...	X	...
Design stress level (DSL)	11	4	0.33→ 3.66	0.42→ 3.21	...	...	X
Valley-peak coupling (VPC)	6	1	0.78→ 0.95	0.91	...	X	...
Low-load truncation (LLT):							
Range truncation (RT) [c]	20	9	0.65→ 1.09	0.53→ 1.28	...	X	...
Taxi cycles	2	1	1.00 [b]	0.85	X	...	...
High infrequent loads (HIL)	20	7	0.81→ 2.11 [b]	1.08→ 3.49	...	...	X
Clipping large loads (CLP):							
Tension	3	1	0.91→ 1.00 [b]	0.87→ .90	X	...	...
Compression	2	1	1.02→ 1.06 [b]	1.37	...	X	...
Load alleviation system effect	4	1	0.95→ 2.30	1.19→ 1.32			X
Miscellaneous (MISC):							
Cycle sequence in flight	1	1	0.78	0.67	...	X	...
Spectrum length	4	0	1.0	...	X	...	X
Loads averaging interval	2	1	0.52→ 1.00	0.71	...	X	...
Simplified spectrum	1	1	1.19	1.04	X	...	...
No ground or GAG cycles	1	0	1.15	...	X (?)	...	...
Combined (COMB):							
VPC + RT	2	0	0.67→ 0.71	...	...	X	...
DSL + RT	4	2	0.43→ 1.63	0.59→ 1.28	...	X	...
HIL + RT	3	1	0.76→ 0.79 [b]	0.85 (?)	...	X (?)	...
DSL + HIL	2	0	0.57→ 3.23 [b]	...	...	...	X
Vertical tail spectrum	2	2	0.84→ 2.20 [b]	2.60→ 6.65	...	...	X

[a] $R'_{\Delta N} = (\Delta N_{VAR}/\Delta N_{BS})$
[b] Some of the analysis predicted trends are not verified by test results.
[c] With respect to RT = 27.6 MN/m^2 (4.0 ksi).

VAR = refers to spectrum variation being considered; and
BS = refers to the baseline spectrum or a reference spectrum to which the variation is being compared.

The classification is primarily based on test results. However, analysis results were also used (as long as they were considered to properly predict the trend) where no test data were available or when testing did not encompass the entire scope of variations considered in a given category. Following is a discussion of the individual spectrum variation categories, according to the significance level.

Not Significant

Sequence of Missions—Negligible effect of having different random or ordered sequences of individual flights.

Flight Segments—Reduction of the number of climb and descent gust segments, application of cruise segment load factor-stress transfer function to climb and descent segments, or elimination of landing impact cycles produced small effect.

Low-Load Truncation—Compression Loads—Increasing the number of compression-compression taxi cycles in the C-15 spectrum from 3.5 to 25.9 per landing decreased life 15 percent. This is a test result. Analysis shows no effect in varying the number of compression-compression cycles in the spectrum. For other data with respect to compression loads, see Fig. 5.

Spectrum Length—Negligible effect resulted from the variation in the C-15 repeatable spectrum length from 2500 to 293 flight hours, where 2500 flight hours are one-tenth of required service life.

Simplified Spectrum—Simplification of the C-15 random spectrum into an equivalent flight-by-flight spectrum, with a low-high-low block cycle arrangement within a flight, produced good correlation with the random spectrum, only a 4-percent increase in life (test result).

No Ground and GAG Cycles—Elimination of ground compression and GAG cycles produced only a 15-percent increase in life (analysis result). This appears to be a representative value as indicated by experimental data

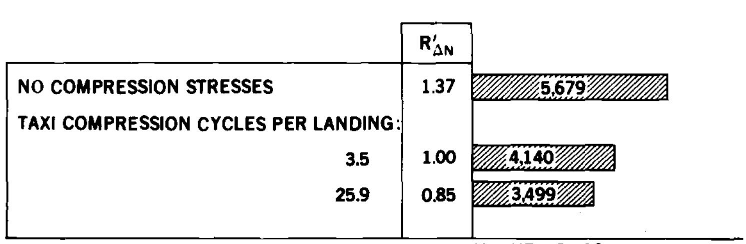

FIG. 5—*Effect of compression stresses, Spectrum C15.BS6, test results.*

in Ref *9*, where GAG cycles were shown to represent anywhere from 7 to 24 percent of the total crack growth.

Clipping Large Loads—Tension—Life decreased approximately 10 percent (test result) when the ten highest peaks in the spectrum were reduced to the level of the tenth highest peak. This is the result of reducing retardation features of the spectrum. More life reduction would be expected, up to a certain point, with further reduction of the clipping level.

Significant

Exceedance Spectra—Increasing or decreasing the number of cycles of flight loads by 15 percent produced approximately the same percentage decrease and increase in life. However, variation of the flight loads exceedance curve slopes by 15 percent produced life changes up to 66 percent.

Valley/Peak Coupling—The random valley/peak couplings in the C-15 six baseline spectra were changed to a restricted coupling. In five of the six spectra, the effect was small (a decrease in life up to 9 percent), but in one spectrum, the decrease was 22 percent.

Low-Load Truncation—Range Truncation—Elimination of cycles that do not contribute to crack growth (or crack initiation) is desirable in analysis and testing from cost and time viewpoints. The largest number of candidate cycles to be eliminated are those at the low-load end of the spectrum scale. The cycle stress range was used as the cycle elimination parameter. The C-15 and KC-10A baseline spectra range truncation levels were increased and decreased to study this effect. The effect is shown by Fig. 6. All data is normalized with respect to spectra truncated at 27.6 MN/m^2 (4 ksi) stress range. The optimum range truncation appears to be in the vicinity of 15.5 MN/m^2 (2.25 ksi). In a typical spectrum, the number of cycles is increased more than fivefold when the range truncation is decreased from 27.6 to 15.5 MN/m^2 (4 to 2.25 ksi). The corresponding life decrease approaches 50 percent. Analysis predicts the general trend and, in most cases, the magnitude, fairly well.

Clipping of Compression Loads—Clipping all the loads below zero (all compression loads excluded) produced a 37 percent increase in life (test result). This effect, together with the effect of compression-compression taxi cycles, is illustrated in Fig. 5.

Cycle Sequence in Flight—The cycles within a flight were chosen at random from any flight segments, without regard to the normal sequence of flight segments. The result (test) was a 33-percent decrease in life.

Loads Averaging Interval—The averaging interval of the incremental load factors in the exceedance spectra of the baseline spectra was $\Delta g = 0.10$. The variations were generated with $\Delta g = 0.05$ and 0.20. Use of $\Delta g = 0.05$ produced no effect. Use of $\Delta g = 0.20$ resulted in a 48 percent decrease in life. Use of $\Delta g \leq 0.10$ in transport spectra development is recommended.

SPECTRUM	MATERIAL	TEST	ANALYSIS
C15.BS3	7475	○	
C15.BS6		◇	
KC-10A	2024	△	
	7075	□	

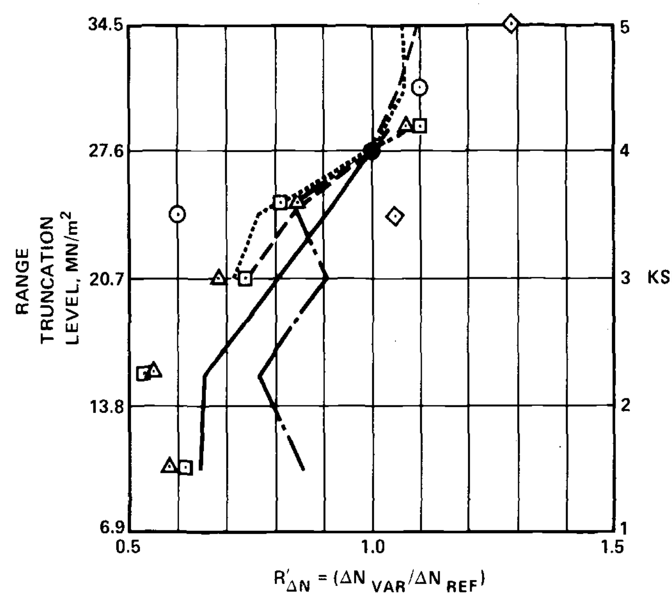

FIG. 6—*Effect of range truncation.*

Combined variations—Combined variations of valley/peak coupling, design stress level, and high infrequent loads with different range truncation level from that of the baseline spectra produced life variations with changes up to 63 percent. In some instances, the combined variation effect is approximately equal to the sum of individual variation effects.

Very Significant

Mission Mix—Different mission mixes, including individual flights, produced large life variations, ranging from a 74 percent decrease to an eightfold increase in life. The five C-15 individual mission spectra, identified as Spectra BS1 through BS5, are included here.

Individual Flight Length—Variation of C-15 Mission 1 flight lengths from approximately 0.5 to 4.0 h produced up to fivefold increase in life as measured in flight hours. However, if life is measured in terms of landings, see Fig. 7, this increase in flight length reduces life only up to 30 percent, indicating that the crack growth per flight is less sensitive to flight length when other factors are held constant or adjusted to reflect the flight length.

Design Stress Level—Changing the loads spectrum by multiplying all the stresses in the spectrum can be viewed as the effect of basic change in design stress level or change in usage severity. Decreasing the stresses by 26 percent or increasing by 35 percent produced a life increase of at least 266 percent and a decrease of at least 67 percent, see Fig. 8. Analysis to test correlation is good.

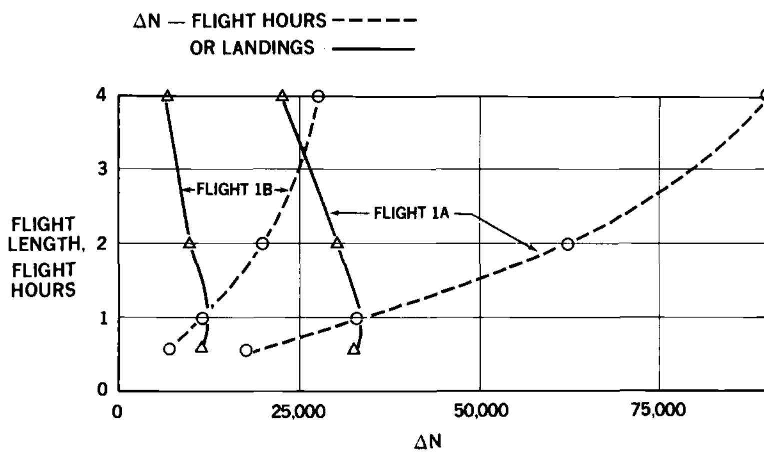

FIG. 7—*Effect of flight lengths. C-15 Mission 1 individual flights.*

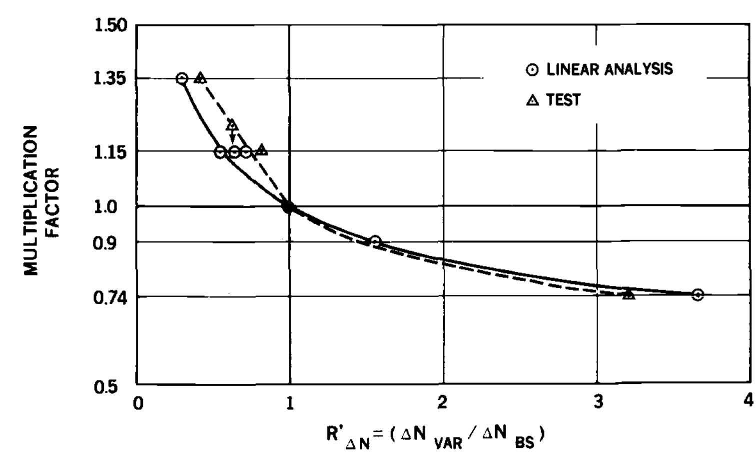

FIG. 8—*Effect of design stress level or usage severity. C15.BS6 and KC-10 spectra.*

High Infrequent Loads—Increase of the magnitude or frequency or both of the 10 highest peaks in the baseline spectra produced retardation effects that produced lives up to 3.5 times longer, see Fig. 9.

Load Alleviation System—Simulation of a load alleviation effect on flight loads in a C-15 spectrum (14-percent increase in 1.0 *g* stresses and 10 percent decrease in incremental stresses) produced only 5 percent decrease in life, as established by analysis. A more realistic development of the load alleviation system effect on the DC-10 wing spectrum at three different stations pro-

	SPECTRUM	MATERIAL
○ ◇	C-15	7475
△	KC-10	2024
□		7075

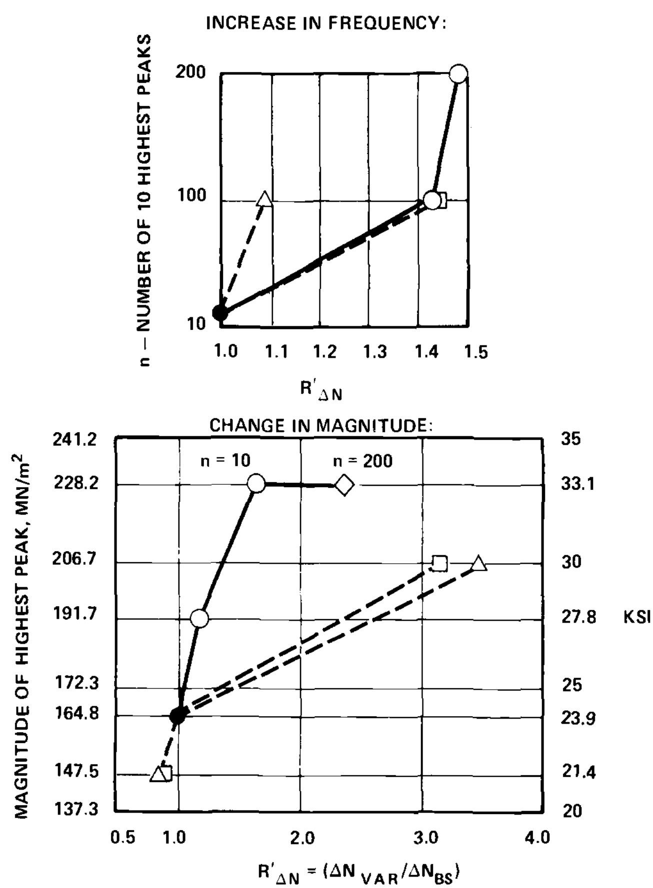

FIG. 9—*Effect of high infrequent loads, test results.*

duced the crack growth results in Table 10. These results indicate that a wing flight loads alleviation system will increase crack growth life along the whole span of the wing, with the largest increase in the outboard portion of the wing. At Station 433, the effect of the loads alleviation system was to reduce the flight 1.0 g stresses approximately 8 percent, while the incremental stresses were reduced anywhere from 25 to 65 percent depending on the segment and whether gust or maneuver loads were considered.

Combined Variation—Design Stress Level and High Infrequent Loads—The large effect on crack growth life, from 43-percent decrease to 223-percent increase, established by analysis, represents only a partial effect, since the linear analysis does not account for the HIL variation effect.

Combined Variation—Vertical Tail Spectrum—A drastic change from a C-15 wing lower surface spectrum to one typical of a vertical tail loading produced a very large increase in life (up to 655 percent). The linear analysis did not predict this effect.

Conclusions

Effect of spectrum loading variations on crack growth were studied using C-15, KC-10A, and DC-10 wing lower surface loads spectra and 7475, 2024, and 7075 aluminum alloys. The following conclusions were reached on the basis of the analytical and experimental results.

1. The effect of spectrum variations on crack growth were rated as not significant, significant, or very significant, on the basis of whether the effect on crack growth life in terms of flight hours was less than 20 percent between 20 and 100 percent, or more than 100 percent of the baseline or reference spectrum crack life:

   Not significant—sequence of missions, flight segments, low-load truncation—number of taxi cycles, clipping of tension loads, spectrum length, and simplified spectrum.

   Significant—variation of exceedances spectra, valley/peak coupling, low-load truncation—range truncation, clipping (elimination) of compression loads, cycle sequence in flight, and loads averaging interval.

   Very significant—mission mix, individual flight length, design stress

TABLE 10—*Load alleviation system effects.*

Wing Station	Material	$R'_{\Delta N} = (\Delta N_{WLA}/\Delta N_{BS})$ Analysis	Test
164	7075	1.07	...
433	2024	1.11	1.32
433	7075	1.25	1.19
827	7075	2.30	...

level or usage severity, high infrequent loads, load alleviation system, and change from wing to a vertical tail type spectrum.

2. Loads spectra variations that could be expected to occur in service among individual aircraft, or during different time intervals on the same aircraft, produce large crack growth rate variations, Table 11. Short-term variation is viewed as the variation between spectra over a short period of time, say one tenth of lifetime or less on the same or different aircraft in the fleet. Long term is viewed as the variations between spectra of different aircraft over a time period approaching the service life of the aircraft. Short-term variations pertain to crack growth in structures with frequent inspection requirements, while the long-term variations are considered to apply to slow crack growth structures that require very few or no inspections during the lifetime of the airplane.

3. No single analysis model was able to predict crack growth of all three baseline spectra. Linear model gave the best prediction for the C-15 and DC-10 spectra while a modified generalized Willenborg model was needed for the KC-10A spectrum. Spectrum variation effects were predicted by these models within 40 percent accuracy 78 percent of the time, mostly (71 percent of the time) on the conservative side. Crack growth due to spectrum loading, with respect to loads interaction effects, appears to be a function of retardation and acceleration phenomena. The only analysis model that will predict the crack growth trends properly is one that will incorporate both, the retardation and acceleration features. Retardation is normally associated with the effect of higher loads on the crack growth at lower loads, whereas acceleration is considered to be due to compression loads and, in some ways, due to higher loads following lower loads.

4. Comparison was made in Ref *1* between transport, bomber, and fighter aircraft wing lower surface loads spectra. Transport and bomber spectra were found to be sufficiently similar so as to consider the findings of the transport spectra variations to be applicable to the bomber spectra, but not to the fighter.

5. Generation of spectrum loading sequence should be as realistic as possible with respect to cycle and flight-mission sequence. The following guidelines are recommended for generating the loading sequence.

a. Make a length of the spectrum repeatable sequence approximately one tenth of the projected service lifetime requirement. This implies that

TABLE 11—*Loads spectra variations.*

Spectrum Variation	Crack Growth Rate: High	Baseline	Low	$\left(\frac{\text{High}}{\text{Low}}\right)$
Short-term	3.9	1.0	0.047	83
Long-term	3.0	1.0	0.27	11

the highest loads in the spectrum are those normally encountered in that time interval. Increasing the length would increase the highest load magnitude and produce more retardation. This would tend to produce a slower crack growth rate dependent on encountering the higher loads. This could be viewed as unconservative. On the other hand, decreasing the length would tend to produce conservative crack growth estimates, unless the less frequent loads are added in after a number of the spectrum repetitions.

b. Unless there is a specific requirement, sequence the missions in a random manner.

c. Unless there is a specific need to do otherwise, choose the sequence of cycles within a segment in a random manner. Use the actual sequence of segments.

d. Use the random valley/peak coupling.

e. Use of the preceding guidelines will produce random cycle-by-cycle, flight-by-flight spectrum. In any simplification of such spectrum, if desired for cost effectiveness in testing or analysis, retain the 25 highest peaks as they were, average other loading cycles into a fewer number of different loadings while retaining the same number of cycles, average transition cycles of large periodic mean load changes (such as GAG cycle) separately from other loading cycles, retain flight-by-flight format, and use a low-high-low sequence of cycles within a flight. Distribute the 25 highest peaks in the spectrum at equal intervals.

f. Use $\Delta g \leq 0.10$ as the averaging interval in the incremental load factor exceedance spectra usage. Use of $\Delta g = 0.05$ intervals is recommended for $\Delta g \leq 0.25$.

g. In order to eliminate cycles that do not contribute to crack growth, exclude tension-tension and tension-compression cycles with ranges less than approximately 15.5 MN/m^2 (2.25 ksi). The optimum truncation level is a function of spectrum type, material, structural detail, and crack length. The value quoted here is considered to be applicable to aluminum alloys of 2000 and 7000 series.

h. Compression loadings. Retain all compression valleys (do not clip) in compression-tension cycles. Compression-compression cycles appear to increase crack growth rate. Range truncation level was not established for these types of cycles.

6. With the availability of computers for analysis and testing, simplification of random cycle-by-cycle, flight-by-flight realistic sequence spectra should be kept to a minimum. Simplifications will always raise the question of equivalence.

Acknowledgments

This paper summarizes work performed at the Douglas Aircraft Company of McDonnell Douglas Corporation in the Structures Engineering Subdivision under the sponsorship of U.S. Air Force Contracts F33615-76-C-3116 and F33700-78-C-0001 and Independent Research and Development (IRAD) program of McDonnell Douglas Corporation.

The author acknowledges and expresses his appreciation to the following who contributed to the implementation and success of the programs on which this paper is based: J. M. Potter of Air Force Flight Dynamics Laboratory and D. Erskine of ASD, Wright-Patterson AFB, and E. G. Willoughby, A. Hoggard, and G. Coo of Douglas Aircraft Co.

References

[1] Abelkis, P. R., "Effect of Transport/Bomber Spectrum on Crack Growth," AFFDL-TR-78-134, Air Force Flight Dynamics Laboratory, Wright-Patterson Air Force Base, Ohio, Nov. 1978.
[2] Douglas Aircraft Co., "KC-10A Damage Tolerance and Durability Assessment Program", MDC-J8131, McDonnell Douglas Corp., 1979.
[3] Douglas Aircraft Co., "Effect of Wing Loads Alleviation System on Crack Initiation and Propagation in DC-10 Wing," unpublished data, 1979.
[4] Abelkis, P. R. et al, "A User's Manual for a Computer Program to Generate Fatigue Spectrum Loading Sequences," Air Force Flight Dynamics Laboratory, Wright-Patterson Air Force Base, Ohio, AFFDL-TR-78-136, 1979.
[5] Willenborg, J. et al, "A Crack Growth Prediction Model Using an Effective Stress Concept," AFFDL-TM-71-1-FBR, Air Force Flight Dynamics Laboratory, Wright-Patterson Air Force Base, Ohio, 1971.
[6] Gallagher, J. P. and Hughes, T. F., "Influence of Yield Strength on Overload Affected Fatigue Crack Behavior in 4340 Steel," AFFDL-TR-74-27, Air Force Flight Dynamics Laboratory, Wright-Patterson Air Force Base, Ohio, March 1974.
[7] Bowie, O. L., "Analysis of an Infinite Plate Containing Radial Cracks Originating from the Boundary of Internal Circular Hole," *Journal of Mathematics and Physics*, Vol. 35, 1956.
[8] Fujimoto, W. T., "Determination of Crack Growth and Fracture Toughness Parameters for Surface Flaws Emanating from Fastener Holes," McDonnell Aircraft Co. Paper MCAIR 76-005, 1976.
[9] Abelkis, P. R., "Use of Microfractography in the Study of Fatigue Crack Propagation Under Spectrum Loading," *Fractography in Failure Analysis, ASTM STP 645*, American Society for Testing and Materials, May 1978.

J. B. de Jonge[1] *and A. Nederveen*[1]

Effect of Gust Load Alleviation on Fatigue and Crack Growth in ALCLAD 2024-T3

REFERENCE: de Jonge, J. B. and Nederveen, A., "**Effect of Gust Load Alleviation on Fatigue and Crack Growth in ALCLAD 2024-T3,**" *Effect of Load Spectrum Variables on Fatigue Crack Initiation and Propagation, ASTM STP 714,* D. F. Bryan and J. M. Potter, Eds., American Society for Testing and Materials, 1980, pp. 170–184.

ABSTRACT: Active controls can be used to reduce gust induced loads on transport aircraft wings. Fatigue tests under flight simulation loading were done on simply notched sheet specimens made of ALCLAD 2024-T3 to assess the fatigue life increase that can be obtained by gust alleviation. Test results did show an important increase in crack initiation life. However, crack propagation life was hardly affected. The observed effect on fatigue life could be reasonably well predicted by Miner type life calculations. Miner type calculations, however, are bound to fail in predicting the effect of spectrum-variations such as deletion of ground-air-ground cycle or small gust cycles.

KEY WORDS: gust alleviation, fatigue tests, fatigue (materials), flight simulation, fatigue life prediction, crack propagation

Active control technology, which has developed very rapidly during the last few years, may be applied to reduce structural loads due to atmospheric turbulence [*1*].[2]

Gust load alleviation offers the possibility of either extending the service life of an existing structure or reducing the structural weight in the design stage of an aircraft. An important structural part that could be affected in this way is the lower wing skin of a transport aircraft. The loading history of this lower skin is illustrated in Fig. 1. On the ground, the lower skin is loaded in compression; during flight variable loads due to gust are superimposed on a mean tensile load associated with undisturbed flight. The transition from a mean compressive ground load to a tensile load in flight is an important load cycle in itself, usually indicated as ground-air-ground (GAG) cycle [*2,3*].

[1] Head, Loads Department, and research engineer, respectively, National Aerospace Laboratory, Nationaal Lucht en Ruimtevaart Laboratorium, Amsterdam, The Netherlands.

[2] The italic numbers in brackets refer to the list of references appended to this paper.

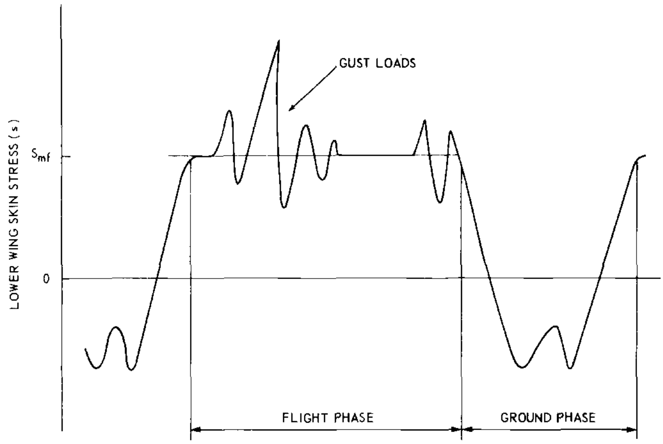

FIG. 1—*Stress history in the lower wing skin of a transport aircraft.*

This paper describes a series of fatigue tests under flight simulation loading on simply notched sheet specimens, intended to evaluate the effect of gust reduction, while leaving the GAG cycle essentially unchanged. To investigate the influence of various parameters, tests were also carried out in which the GAG cycle and small gust cycles were deleted, respectively.

In addition, fatigue life calculations on the basis of Miner's rule were made in order to assess the ability to predict the effect of spectrum changes by analytical means.

The results will be presented and discussed and the paper ends with a number of conclusions.

Gust Load Spectrum Twist

The standard load sequence TWIST (transport wing standard) has been developed by the Nationaal Lucht en Ruimtevaart Laboratorium (NLR) and the Laboratorium für Betriebsfestigkeit (LBF) [*4*]. It is considered as a representative load sequence for transport aircraft wing tension skins near the main landing gear attachment.

The sequence TWIST includes 4000 different flights. There are ten types of flight, ranging from "stormy" (A) to "tranquil" (J) conditions. Ten different gust load levels are considered. Table 1 gives the frequency of occurrence of each flight type and each load level within each flight.

The load spectrum pertaining to TWIST is shown in Fig. 2. It may be noted that the load scale is expressed as a relative stress S/S_{mf}, where S_{mf} is the mean stress pertaining to undisturbed flight at 1 g.

In the present investigation, TWIST was used as basic load sequence, referring to "nonalleviated" conditions. TWIST includes approximately 100

TABLE 1—*Definition of flight types and number of load cycles within each flight for TWIST and Mini-TWIST.*

Flight Type	Number of Flights in One Block of 4000 Flights	Number of Gust Loads (Full Cycles) at the 10 Amplitude Levels										Total Number of Cycles per Flight
		I	II	III	IV	V	VI	VII	VIII	IX	X	
A	1	1	1	1	4	8	18	64	112	391	900 (0)	1500 (600)
B	1	...	1	1	2	5	11	39	76	366 (385)	899 (0)	1400 (520)
C	3	...	...	1	1	2	7	22	61	277 (286)	879 (0)	1250 (380)
D	9	...	...	...	1	1	2	14	44	208	680 (0)	950 (270)
E	24	...	...	...	...	1	1	6	24	165 (168)	603 (0)	800 (200)
F	60	...	...	...	...	...	1	3	19	115 (107)	512 (0)	650 (130)
G	181	...	...	...	...	...	...	1	7	70 (72)	412 (0)	490 (80)
H	420	...	...	...	...	...	...	...	1	16	233 (23)	250 (40)
I	1090	...	...	...	...	...	...	...	...	1	69 (4)	70 (5)
J	2211	...	...	...	...	...	...	...	...	...	25 (2)	25 (2)
Total number of cycles per block of 4000 flights		1	2	5	18	52	152	800	4170	34 800	358 665 (18 422)	...
Cumulative number of load cycles per block of 4000 flights		1	3	8	26	78	230	1030	5200	40 000	398 665 (58 422)	...

Note: if different, figures between brackets refer to Mini-TWIST; otherwise Mini-TWIST equal to TWIST.

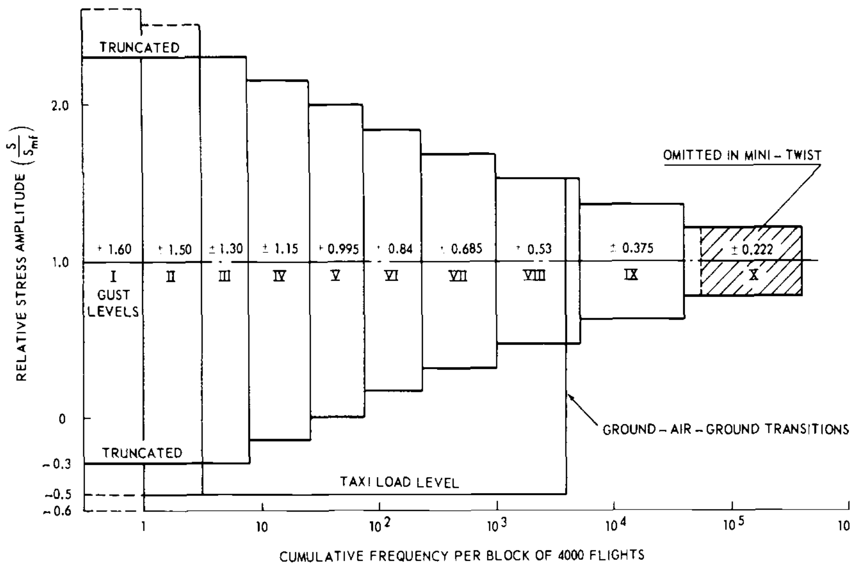

FIG. 2—*The load spectrum pertaining to TWIST and Mini-TWIST.*

load cycles per flight. This is a relatively high number, causing long testing times. For this reason the LBF and NLR recently established a shortened version of TWIST, indicated as Mini-TWIST.

As shown in Fig. 2 and Table 1, the main difference is that Mini-TWIST contains considerably less load cycles of the smallest amplitude, resulting in approximately 15 load cycles per flight. To assess the effect of deleting small load cycles, some tests with the Mini-TWIST load sequence were done.

Variations of the Basic Spectrum

Gust Alleviation

The response of an aircraft to continuous atmospheric turbulence is defined by the response parameter, $\bar{A}$, and the number of zero crossings N_0, where $\bar{A}$ is the ratio of root-mean-square incremental load to root-mean-square gust velocity, and N_0 is the total number of gust-induced loads per unit distance flown.

It may be assumed that the effect of a gust alleviation system on the aircraft response will predominantly be a reduction of the response parameter, $\bar{A}$, with little change in the number of zero crossings. In other words, the magnitude of gust-induced loads will be reduced, but their total number remains unchanged.

In accordance with this, in the present tests the effect of gust alleviation on load experience was simulated by reducing all stress amplitudes, S_{a_i}, by the same percentage, leaving their total number of occurrences unchanged. In the present tests, reductions of amplitudes to 80, 60, and 40 percent of the original values were considered.

Deleted GAG cycles

At the end of each flight contained in the TWIST sequence, the load is reduced from the in-flight stress level, S_{mf}, to the ground stress level $S_{\text{ground}} = -0.5\, S_{mf}$.

The GAG cycle is known to have a considerable influence on fatigue life and crack propagation. To quantify this influence, tests were done with the TWIST sequence in which the transitions from in-flight-to-ground stress level between two successive flights were deleted.

Test Specimens and Test Procedures

The specimen configuration is given in Fig. 3. The effective stress concentration, K_t, due to the holes is 2.66, based on net section stress.

The material was 2-mm ALCLAD 2024-T3 sheet. The specimens were clamped into a 250 kN frame fitted to a Material Testing Systems (MTS) servohydraulic testing machine. Buckling under compressive loads was prevented by felt-lined anti-buckling guides. The nominal test frequency was 15 Hz, the temperature was approximately 20°C, and the environment normal air was 40 to 60 percent relative humidity. Each specimen contains four potential crack initiation points, namely, the left and right side of either hole.

During testing, visual observation was used to determine the instant of crack initiation and to record subsequent crack propagation. Testing was continued until complete failure over a cross section through either one of the holes. In all cases, crack initiation had also occurred near the other hole.

To process the crack propagation data, observed half crack lengths, l, were plotted against number of flights, n. A smooth curve was drawn through all data points pertaining to specimens tested under the same spectrum. Values for dl/dn versus l were derived from this plot by measuring tangents to this curve. These data were reduced to dl/dn versus K_{mf} using the expression

$$K_{mf} = S_{mf} \sqrt{\pi l \sec \pi l / W}$$

Overview of Tests and Test Results

Table 2 gives an overview of the tests and main test results. It may be recalled that the stresses in TWIST are expressed on a relative basis; the actual stress level is defined by the magnitude of the mean stress, S_{mf}.

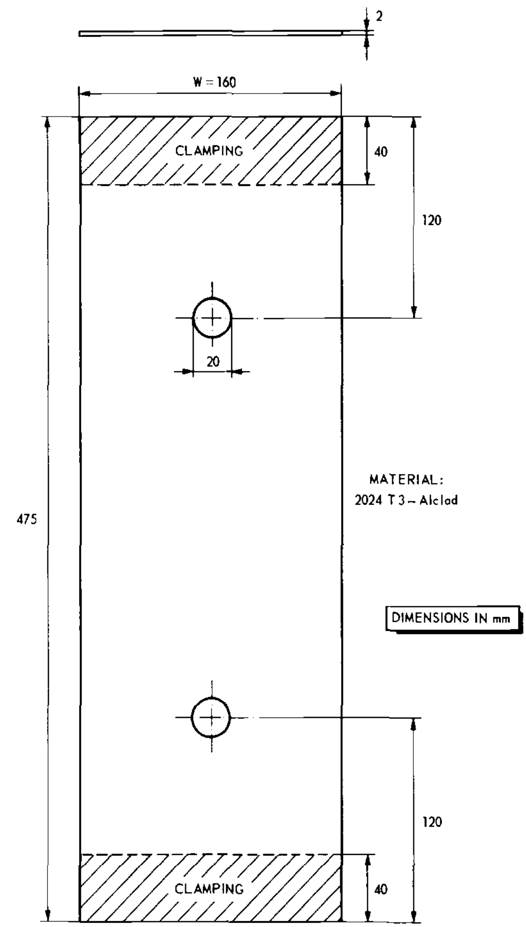

FIG. 3—*Spectrum configuration.*

The first group of tests presented in Table 2 was intended to evaluate the effect of gust alleviation; these tests were done at a mean stress, S_{mf}, (gross section stress) of 70 MPa.

Results are also depicted in Fig. 4. Gust alleviation turns out to have a considerable influence on crack initiation life. Reduction of the gust to 60 percent of the original value increased the crack initiation life by a factor of 3. As no cracks were found after 97 000 simulation flights, reduction to 40 percent appears to increase the crack initiation life by at least a factor of 9. Unexpectedly, however, gust alleviation did not result in a reduced crack propagation rate: the crack propagation life even tends to become shorter with decreasing gust severity.

In the second group of tests, the effect of stress level variation has been investigated. The results for the test with gust loads reduced to 60 percent are

TABLE 2—*Summary of tests and test results.*

Test Purpose	Program Description: Program	Program Description: Stress Level, S_{mf}, MPa	Program Description: Gust Reduction, %	Loading Code	Crack Initiation Life[a], flights	Crack Growth Life[b], flights $N_{l=30} - N_{l=12}$	Life Until Failure, flights	Remarks
Effect of gust alleviation	TWIST	70	100	7 T 1.0	11 600	8 600	23 897	
	TWIST	70	80	7 T 0.8	20 880	9 300	33 630	
	TWIST	70	60	7 T 0.6	32 492	6 458	42 259	
	TWIST	70	40	7 T 0.4	...	...	...	no cracks after 97 000 flights
Effect of stress level increase	TWIST	70	100	7 T 1.0	11 600	8 600	23 897	
	TWIST	80	100	8 T 1.0	10 250	5 100	16 485	
	TWIST	70	60	7 T 0.6	32 492	6 458	42 259	
	TWIST	80	60	8 T 0.6	23 675	5 445	29 519	
	TWIST	90	60	9 T 0.6	14 391	3 335	18 650	
	TWIST	100	60	10 T 0.6	9 384	2 660	12 907	
Determine damage GAG cycle	TWIST without GAG cycle	70	100	No GAG	40 678	29 000	77 618	
Determine damage small gust cycles	Mini-TWIST	70	100	Mini-TWIST	27 565	18 000	50 932	

[a] Crack initiation life defined as life until either a_l or a_r equals 2 mm; value presented is average initiation life for two holes.
[b] Crack growth life is defined as time to grow total crack length from $l = 12$ mm to $l = 30$ mm; value presented is lowest observed in either of the two holes.

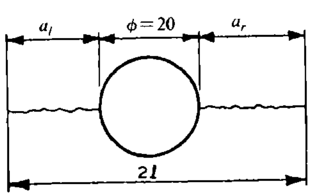

$$l = \frac{a_r + a_l + \phi}{2}$$

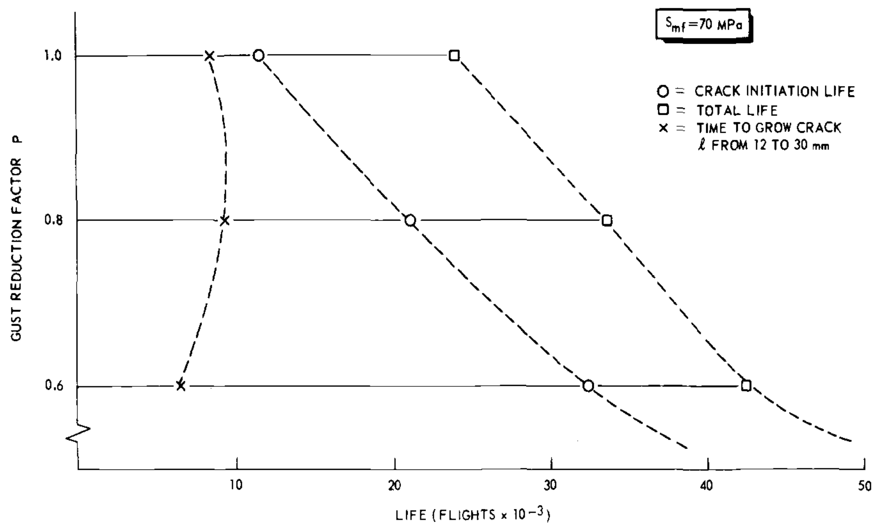

FIG. 4—*The influence of gust alleviation on crack initiation, crack propagation, and total life.*

plotted in Fig. 5. Increase of stress level leads to a decrease of crack initiation life and crack propagation life in approximately the same ratio. Deletion of the GAG transition turned out to cause an increase of both initiation and propagation life by a factor of 3.5.

Finally, the last test results shown in Table 2 indicate that the "damage per flight" for Mini-TWIST is approximately half as big as that for TWIST.

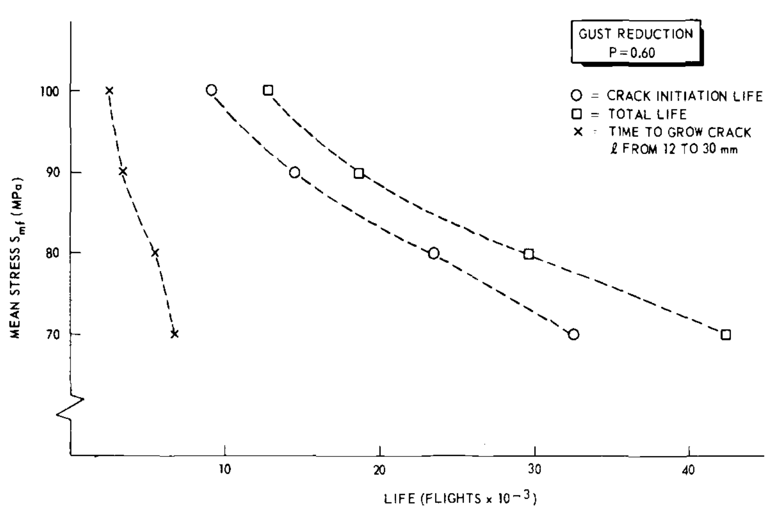

FIG. 5—*The influence of mean stress level on crack initiation, crack propagation, and total life.*

Fatigue Life Calculations

To assess the ability of simple analytical tools for predicting the effect of spectrum variations, life calculations on the basis of Miner's rule were made for all loading cases included in the experimental program.

NLR test results were used as basic S-N data obtained from open hole sheet specimens with a K_t-value of 2.43, made of the same 2024-T3 ALCLAD sheet of 2-mm thickness (see Fig. 6). This S-N curve was corrected for the proper K_t-value of 2.66 and approximated by two linear segments in a double-logarithmic grid, see Fig. 7. The endurance limit pertaining to a K_t-value of 2.66 is equal to $S_e = 22.1$ MPa.

A Miner calculation based on this S-N curve will attribute zero damage to all load cycles with amplitudes below the endurance limit. As experience has shown, such load cycles actually contribute to cumulative damage, and it is usual to modify the S-N curve for cumulative damage calculations by extending the sloping part below the endurance limit [*6, 7*].

In the present investigation, various extensions were evaluated; the one giving the best agreement with the obtained test results was the simple straight extension of the sloping part, indicated in Fig. 7. Calculations were carried out in the usual way. For each flight, a separate GAG cycle was included. The maximum stress taken for this GAG cycle is the maximum stress reached once per flight on the average or $S_{a_{VIII}}$ (see Table 1 and Fig. 2).

An example calculation is given in Table 3, and Table 4 presents a summary of the calculation results. Calculated lives are compared with total lives

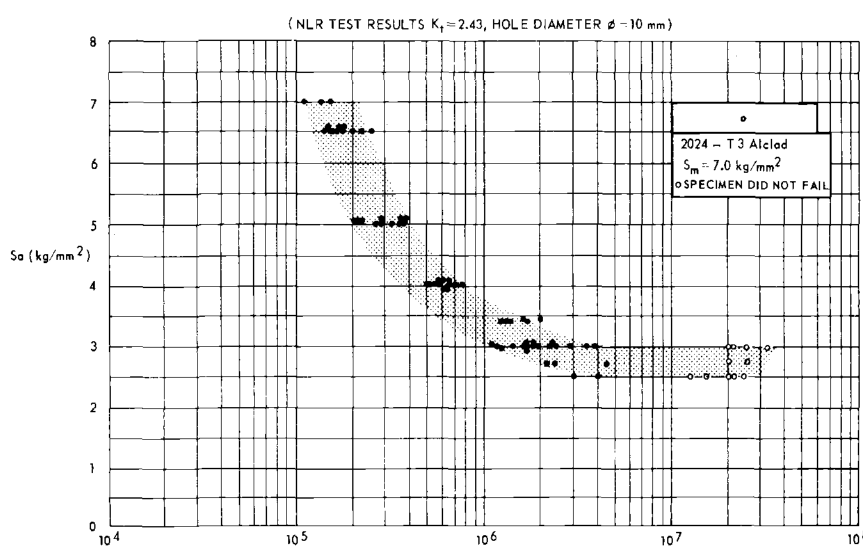

FIG. 6—*Reference S-N curve.*

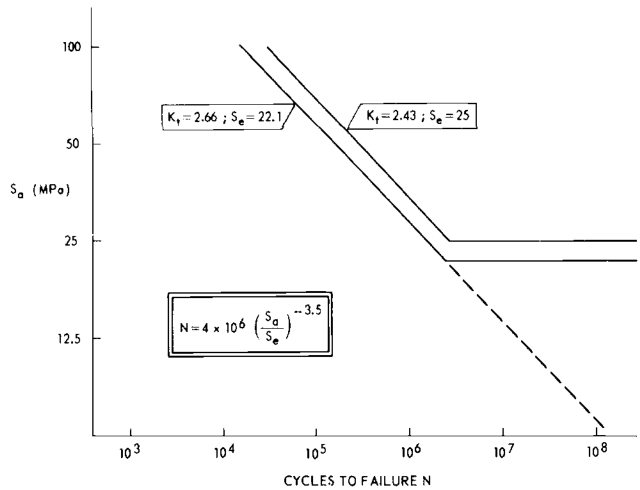

FIG. 7—*Approximated S-N curve used in fatigue life calculation.*

TABLE 3—*Example of fatigue life calculation.*[a]

Load Level	Column 1 Sa/S_{mf}	Column 2 S_a, MPa	Column 3 Cycles per 4000 Flights	Column 4 Damage per Cycle, l/N	Column 5 Damage per 4000 Flights, n/N
I	1.30	104	1	5.65 − 5	5.65 − 5
II	1.30	104	2	5.65 − 5	1.13 − 4
III	1.30	104	5	5.65 − 5	2.83 − 4
IV	1.15	92	18	3.68 − 5	6.62 − 4
V	0.995	80	52	2.26 − 5	1.17 − 3
VI	0.84	67	152	1.21 − 5	1.84 − 3
VII	0.685	55	800	6.08 − 6	4.86 − 3
VIII	0.53	42.5	4170	2.47 − 6	1.03 − 2
IX	0.375	30	34800	7.29 − 7	2.54 − 2
X	0.222	17.8	358665	1.17 − 7	4.20 − 2
			Sum damage gust cycles		8.67 − 2
GAG cycle	1.015	81.2	4000	2.38 − 5	9.51 − 2
		Total damage per 4000 flights $\Sigma\, n/N$ =			1.82 − 1
	Predicted life ($\Sigma\, n/N = l$) : 4000/0.182 = 21978 flights				

[a] Spectrum = TWIST; gust level = 100 percent; stress level = S_{mf} = 70 MPa (gross section stress); and S_{mf} (net section stress) = 160/(160 − 20) × 70 MPa = 80 MPa.

Legend
Columns 1 and 3 from Fig. 2 and Table 1.
Column 2 = Column 1 × 80.
Column 4 : $l/N = 2.5 \times 10^{-7} \times (S_a/22.1)^{3.5}$, see Fig. 7.
Column 5 = Column 3 × Column 4.
$S_{a\text{GAG}} = S_{mf} + S_{a\text{VIII}} - S_{\text{ground}}/2 = S_{mf}(1 + 0.53 + 0.50)/2.$

TABLE 4—*Results of fatigue life calculations.*

Column 1 Loading Code	Column 2 Test Life, flights	Column 3 Calculated Life, flights	Column 4 Test Life, Calculated Life, $\Sigma\, n/N$	Column 5[a] $\Sigma[n/N]_{rel}$	Column 6[b] $\Sigma[n/N]_{rel}$
7 T 1.0	23 897	21 978	1.09	1.00	...
7 T 0.8	33 630	34 057	0.99	0.91	...
7 T 0.6	42 259	50 844	0.83	0.76	1.00
8 T 0.6	29 519	31 931	0.92	0.85	1.11
9 T 0.6	18 615	21 064	0.88	0.81	1.06
10 T 0.6	12 907	14 659	0.88	0.81	1.06
8 T 1.0	16 485	13 848	1.19	1.09	...
NoGAG	77 618	46 678	1.66	1.52	...
Mini-TWIST	50 932	30 091	1.69	1.55	...

[a]Column 5 = $\Sigma\, n/N$ related to outcome for case 7 *T* 1.0.
[b]Column 6 = $\Sigma\, n/N$ related to outcome for case 7 *T* 0.6.

obtained in test rather than crack initiation lives, because S-N data also refer to total lives.

A first observation to be made is that the fatigue life predictions except for the NoGAG and Mini-TWIST case are reasonably accurate, the ratio of test life and calculated life ranging between 1.19 and 0.83 (Column 4).

The prediction of the stress level increase effect is remarkably good; the life decreased by a factor of 3.3 due to the rise in stress level from 70 to 100 MPa (gust levels 60 percent) was predicted within 6 percent (Column 6). The calculations overestimated the effect of gust alleviation, but the predictions are still reasonable. For example, the reduction in gust level to 60 percent, resulted in an actual life increase by a factor of 1.78 instead of the predicted factor of 2.31.

Finally, the results obtained with the NoGAG case and Mini-TWIST are interesting as they reveal some inherent weaknesses of the Miner hypothesis.

It may be recalled that Mini-TWIST differs from the normal TWIST in the deletion of the majority of the smallest load cycles. In the present case, these smallest cycles had an amplitude of 17.8 MPa that is markedly below the established endurance limit of 22.10 MPa. Still, their deletion resulted in a life increase by a factor of 2.13.

Although this observation is not new, the damage of small cycles is usually included in cumulative damage calculations by means of extending the sloping part of the S-N curve below the endurance limit [*6, 7*]. In the present calculations, the "straight" extension used still yielded an underestimation of the small cycle damage.

However, it will be clear that modification of the S-N curve is a rather artificial way "to obtain correct answers." Small cycles are damaging because they can cause cracks to grow, both on a micro- and a macro-scale, that were started by larger load cycles. In other words, their damage is interrelated with the occurrence of other larger load cycles. As Miners hypothesis is essentially based on the concept of a "damage per cycle" that is assumed to be independent of other cycles, it is by its very nature unsuited to reflect interaction effects.

Deletion of the GAG cycle, as in the NoGAG case, resulted in a test life increase by a factor 3.25. This was considerably more than predicted by the Miner calculation, namely, 2.12. In other words, the calculation underestimated the effect of the GAG cycle. The observed life increase of 3.25 would imply, according to Miner-type reasoning, that in the complete program 1/3.25 part of the total damage is caused by the gust cycles and 2.25/3.25 by the GAG cycle.

Hence, deletion of *all* gust cycles while maintaining the GAG cycle would result, according to the same reasoning, in a life increase by only a factor $3.25/2.25 \approx 1.44$.

However, returning to the result obtained with the Mini-TWIST program, it appears that deletion of only the *smallest* gust load cycles leads to a life increase by a factor of 2.13. These seemingly contradictory results show where and why Miner calculations are bound to fail.

The GAG cycle is a large load cycle and thus damaging in itself; this part can be taken into account in a Miner sum. However, the major effect of the GAG cycle is in its interaction with the damage caused by the gust load cycles. Due to the presence of the GAG cycle the damaging effect of the gust cycles is increased. This may be explained by the fact that favorable residual compressive stresses induced after high tensile loads and associated local plastic deformation are reduced or eliminated due to reversed plastic flow under the compressive loads associated with the ground condition [7].

Discussion

The alleviation of gust loads in the present test series resulted in a considerable increase in crack initiation life. However, no increase or even a decrease in crack propagation life due to gust load reduction occurred. For fail-safe type structures, this will mean that no gain in terms of inspection periods can be expected from gust alleviation, at least not for the type of material under consideration.

The same tendency is observed with regard to possible stress level increase. Indeed, if the gust loading is alleviated, the overall stress level might be increased and structural weight reduced while maintaining an acceptable fatigue crack initiation life. Taking the unalleviated condition with 70 MPa mean stress (Code 7 T 1.0) as reference, it may be noted that with a gust load reduction to 60 percent the same crack initiation life will be obtained at a mean stress level of 95 MPa. However, the crack propagation life would then be drastically reduced, from 8600 flights in the reference condition (7 T 1.0) to approximately 3000 flights in the alleviated condition.

According to our current design philosophy, which demands fail-safety or "damage tolerance" as it is also called, sufficiently slow crack propagation in relation to inspection periods and inspectability is the essential prerequisite for structural safety. Hence, the increase in stress level, allowable from the point of view of fatigue life, might well turn out to be unfeasible because of the resulting unacceptably high crack propagation rate.

Simple Miner type calculations gave reasonably accurate predictions of the fatigue life. The question may be raised whether our current analytical tools would have been able to predict the crack propagation behavior observed in the present tests. With regard to the results obtained with stress level increase, this is indeed the case.

Figure 8 shows that the observed crack propagation rates plotted versus K_{mf} reasonably fell on one straight line in a double-logarithmic grid. The line, dotted in Fig. 8, depicts the expression

$$dl/dN = -10^{-6}\,(K_{mf})^{2.76}$$

where dl/dN is given in mm/flight and K_{mf} in MPa $\sqrt{m}$.

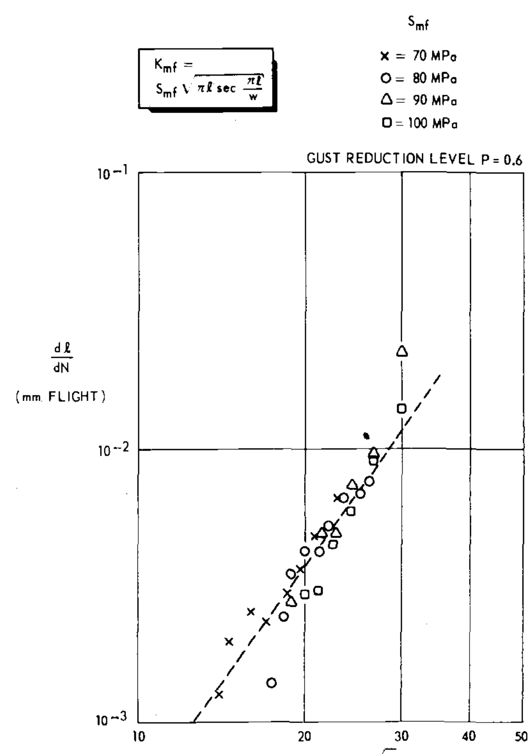

FIG. 8—*Crack propagation rate as a function of* K_{mf} *for different mean stress levels.*

This behavior is represented by a simple Paris-type crack propagation law, where the retardation effect associated with spectrum loading is covered by an "average" retardation factor, which is a function of the spectrum shape [8].

The large retardation effects of high loads on crack propagation in 2024-T3 ALCLAD under flight simulation loading is well known. For example in Ref 5, it was found that truncation of the applied load spectrum from $S_{a,\max} = 88$ MPa to $S_{a,\max} = 44$ MPa resulted in a decrease of crack propagation life by a factor of 3.9 compared to a decrease in crack initiation life (to 2 mm) by a factor of 1.5. The alleviation of gust loads considered in the present tests also implies a reduction of the magnitude of the retarding high loads. Obviously, the associated decrease of the retardation effect just compensated for the decrease in crack growth that resulted from the overall decrease in alternating stress level. It is clear that this behavior can only be predicted by crack growth models that account for retardation effects in a realistic manner.

In the author's opinion, crack closure plays a predominant role in crack growth retardation. Hence, accurate results can only be expected from models that include the crack closure phenomenon.

Conclusions

The effect of gust load alleviation on the fatigue properties of 2024-T3 aluminum alloy was investigated by means of flight simulation tests on simple notched sheet specimens.

1. Gust alleviation turned out to have a beneficial effect on fatigue life, but hardly influenced the crack propagation life.
2. If the favorable effect of gust alleviation on fatigue life is used to increase the mean stress level, S_{mf}, short crack propagation lives can be expected.
3. The change in fatigue life with gust alleviation and stress level variation or both were reasonably well predicted with analytical means.
4. The difference in damage per flight between the standard programs TWIST and Mini-TWIST was found to be large, both with regard to initiation life and crack propagation, and was considerably larger than predicted by analytical means.

References

[1] Grossner, W. F., Hollenbeck, W. W., and Eckholdt, D. C., "The C-5A Active Lift Distribution Control System," Symposium on Impact of Active Control Technology on Airplane Design, AGARD-CP-157, Advisory Group for Aerospace Research and Development, June 1975.

[2] Nauman, E. C., "Evaluation of the Influence of Load Randomization and of Ground-to-Air

Cycles on Fatigue Life," NASA TN-D-1584, National Aeronautics and Space Administration, Washington, D.C. 1964.
[3] Schijve, J., "Fatigue Tests with Random and Programmed Load Sequences with and without Ground-to-Air Cycles. A Comparative Study on Full-Scale Wing Center Sections," NLR Report S. 613, Nationaal Lucht en Ruimtevaart Laboratorium, 1965; also AFFDL-TR-66-143, Air Force Flight Dynamics Laboratory, 1966.
[4] De Jonge, J. B., Schutz, D., Lowak, H., and Schijve, J., "A Standardized Load Sequence for Flight Simulation Tests on Transport Aircraft Wing Structures," NLR TR 73029 U, Nationaal Lucht en Ruimtevaart Laboratorium. also: Bericht FB-73-106, Laboratorium für Betriebsfestigkeit.
[5] Schijve, J., Jacobs, F. A., Tromp, P. J., "Crack Propagation in Aluminum Alloy Sheet Materials Under Flight Simulation Loading," NLR TR 68117 U, Nationaal Lucht en Ruimtevaart Laboratorium, Dec. 1968.
[6] Haibach, E., contribution to discussion in *Proceedings*, Conference on Fatigue of Welded Structures, Brighton, 1970, The Welding Institute, Abbington, (Cambridge) U.K.
[7] Schijve, J., "The Accumulation of Fatigue Damage in Aircraft Materials and Structures," AGARDograph 157, Advisory Group for Aerospace Research and Development, 1972.
[8] De Jonge, J. B., Nederveen, A., and Tromp, P. J., "The Effect of Gust Alleviation on Fatigue in 2024-T3 ALCLAD," NLR Report TR 78064 U, Nationaal Lucht en Ruimtevaart Laboratorium, 1978.

R. W. Finger[1]

Prediction Model for Fatigue Crack Growth in Windmill Structures

REFERENCE: Finger, R. W., "**Prediction Model for Fatigue Crack Growth in Windmill Structures,**" *Effect of Load Spectrum Variables on Fatigue Crack Initiation and Propagation, ASTM STP 714,* D. F. Bryan and J. M. Potter, Eds., American Society for Testing and Materials, 1980, pp. 185-204.

ABSTRACT: The 30-year life requirement of the Boeing Mod II windmill results in a service life load spectrum having an excess of 200 million cycles. Determination of allowable stress levels for the type of steels being used in construction of the systems, requires a detailed knowledge of their crack growth behavior under representative spectrum. A spectrum load test program was conducted, using uniaxially loaded surface flaw specimens, to provide the data needed to ascertain the impact of differences in load spectra on crack growth behavior.

A total of four different load spectra were tested to provide enough diversity in test parameters to ensure that the actual load spectra for the system would be enveloped by those tested. The test results were analyzed using different crack growth models to determine which produced the best correlation between actual and predicted results. Excellent correlation between predicted and actual test results was obtained when a crack growth model containing both a threshold and retardation term was used. This model can be used to estimate the spectrum load crack growth behavior of steels covered by the ASTM Specification for General Requirements for Rolled Steel Plates, Shapes, Sheet Piling, and Bars for Structural Use (A 6-76a) and Specification for General Requirements for Steel Plates for Pressure Vessels (A 20-76b).

KEY WORDS: fatigue (materials), spectrum load, crack growth, steels, windmills

The rotor structure of a windmill is subjected to an extreme number of cycles during a lifetime. For example, to provide optimum service, the Boeing Mod II system must survive an excess of 200 million cycles during its 30-year service life. The loads on the blades are a combination of the centrifical dead weight and wind loadings. The dead weight and wind gust loads provide the oscillatory position of the loading. Determination of allowable operating stresses for this type of environment demands a detailed knowledge of the effects of load spectra variables on fatigue crack growth behavior. Spectrum load crack growth data were not available for this

[1] Specialist engineer, Boeing Engineering Company, Seattle, Wash. 98124.

specific problem. The existing data were for load spectra having significantly fewer cycles.

A test program was conducted to provide the data needed so that allowable operational stresses could be determined. The experimental program consisted of spectrum load tests on uniaxially loaded surface flaw specimens for up to 200 million cycles. A total of four different load spectra were tested to obtain data on the effects of variations in R ratio, low-load truncation, and the impact of negative R ratio cycles. Although four alloys were tested, the majority of the program was conducted using A533 steel with additional tests on A572, A633, and A588 steels. All tests except one were conducted on parent metal specimens with a test of a weld metal included to confirm the similarity in behavior between the two. The results of the tests were used to derive a crack growth model that accurately correlates the test results and can be applied to other load spectra.

This paper presents the load spectra, detailed test results, derivation of the crack growth model, and comparison between actual and predicted results. Primary emphasis is placed on the crack growth model development and verification. The significances of variations in load spectra are also examined.

Procedures

Tests were conducted on uniaxially loaded surface flaw specimens having either one or two flaws per specimen (see Fig. 1). The surface flaws were introduced by growing a fatigue precrack at the root of a starter notch produced by electric discharge machining (EDM). The two flaws were introduced separately. The flaw in the low-stress region was initiated first, followed by the flaw in the high-stress region. This was necessary because the load levels required to produce the fatigue precracks were different for each area. The load level for the low-stress region was approximately 10 percent greater than for the high-stress region. The flaw in the low-stress region was not affected by the procedure applied to the high-stress region.

After the fatigue operation, the specimens were subjected to a thermal treatment to relieve the plastic zone at the tip of the crack. This procedure has been developed at Boeing [*1*][2] and is used when specimens that are free of retardation effects associated with the precracking plastic zone are needed. The procedure consisted of heating the specimens to 1339 K and holding for 1.0 h and then air cooling to room temperature. The specimens were then free of any overload retardation effects that might have been imposed by the preparation of the fatigue crack. For their size, the

[2] The italic numbers in brackets refer to the list of references appended to this paper.

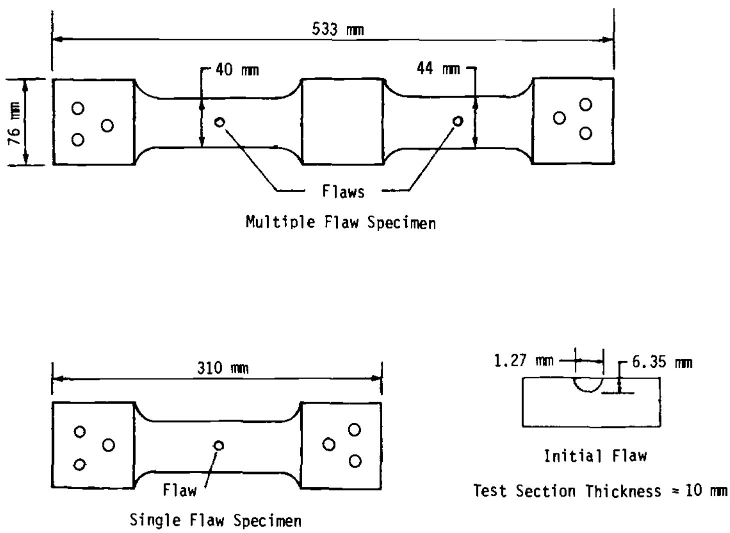

FIG. 1—*Test specimens.*

flaws were then representative of the worst possible defects that might be encountered during fabrication since they were cracks.

The selected size of defect for testing was based on the inspection procedures and capabilities to be used on the structure. Having selected a size, the intent here was to produce the worst possible defect of that size.

All tests were conducted using closed-loop, servo-actuated, hydraulic test machines programmed for one of four different load spectra. The machines were capable of applying individual load blocks at 30 Hz and averaging approximately 25 Hz for an entire load spectrum. These tests were conducted in laboratory air at these load frequencies.

The specimens were prepared using conventional machining procedures to the configurations presented in Fig. 1. When the flaw in the high-stress region of dual-flaw specimens had grown to the point where failure was imminent, the test was interrupted, the high-stress flaw was removed, and the specimen was remachined to the single-flaw configuration. The majority of the specimens were produced from A533 material. With the exception of one A533 weldment (Specimen W16) all of the tests were conducted on parent metal. All of the machining, pre-cracking thermal treatment, and testing procedures were identical for all of the materials including the weldment.

Experimental Work

Tables 1 through 4 present the four different load spectra used in the test program. Each load spectrum is presented in nondimensional terms.

TABLE 1—*Load Spectrum A.*

Load, % of maximum		
Maximum	Minimum	Cycles per Layer
43.4	6.2	9 076
49.7	−0.2	3 328
38.4	11.2	6 050
46.4	3.1	10 588
52.6	−3.0	908
55.0	−5.5	303
88.1	44.7	6 133
92.4	40.5	588
85.3	47.4	19 513
78.3	54.1	11 150
82.9	49.9	16 725
90.4	42.4	1 673
64.5	19.3	2 373
79.9	3.9	4 153
74.1	9.8	3 560
91.9	−8.1	356
96.9	−13.1	119
86.4	−2.5	1 305
83.9	−47.2	34
71.1	−34.4	370
44.8	−8.0	673
63.3	−26.5	1 178
56.2	−19.5	1 010
77.9	−41.2	101
89.0	52.1	13 050
97.7	43.4	1 305
84.2	56.9	8 700
91.9	49.2	15 225
100.0	41.1	435
95.0	46.1	4 785
52.8	20.7	9 267
70.3	3.2	1 390
62.7	10.9	16 217
58.9	14.6	13 900
73.3	0.2	463
66.7	6.8	5 097

The maximum and minimum load in each block is presented as a percentage of the maximum load in the entire spectrum. Load Spectrum B is a truncated version of Spectrum A. Spectrum D is a variation on Spectrum B. Spectrum G is unique and has not been derived from any prior spectrum.

The reduction of Spectrum A to produce Spectrum B was accomplished by eliminating the positive R ratio cycles that were furthest below the estimated threshold. Sixty-five percent of the load cycles in Spectrum A were discarded in producing Spectrum B. The life in terms of total spectra for specimens subjected to either Spectra A or B was expected to be very similar because the deleted cycles were below the threshold. Deletion of

TABLE 2—*Load Spectrum B.*

Load, % of maximum		Cycles per Layer
Maximum	Minimum	
49.7	0.2	3 328
52.6	−3.0	908
55.0	−5.5	303
88.1	44.7	6 133
92.4	40.5	558
90.4	42.4	1 673
79.9	3.9	4 153
74.1	9.8	3 560
91.9	−8.1	356
96.9	−13.1	119
86.4	−2.5	1 305
83.9	−47.2	34
71.1	−34.4	370
44.8	−8.0	673
63.3	−26.5	1 178
56.2	−19.5	1 010
77.9	−41.2	101
89.0	52.1	13 050
97.7	43.4	1 305
91.9	49.2	15 225
100.0	41.1	435
95.0	46.1	4 785
70.3	3.2	1 390
73.3	0.2	463
66.7	6.8	5 097

those cycles that are originally below the threshold and therefore not producing damage was not expected to impact the number of load spectra the specimens could endure because most of the life occurs during the initial crack growth.

Spectrum D is a variation of Spectrum B and was obtained by decreasing the delta loading and increasing the maximum loads. The delta loads of Spectrum D on a percent of maximum load basis, are 65 percent of the delta loads of Spectrum B. The maximum load in Spectrum D were also increased over the maximums in Spectrum B. The increase in maximum loads was not a fixed percentage as the change in delta loads were. Spectrum D was designed to provide data on all positive and generally fairly high R ratio spectrum.

Load Spectrum G was not derived from the other spectra. Spectrum G includes the shutdown load cycles that were not included in the other spectra. The two groups of the load spectra (A and B) are representative of operating and shutdown at low winds (A) and operating and shutdown at high winds (B). Although all the R ratios are positives, as in Spectrum D, the cycles are generally applied at lower R ratios than in Spectrum D.

TABLE 3—*Load Spectrum D.*

Load, % of maximum		
Maximum	Minimum	Cycles per Layer
67.2	34.5	3 328
69.0	32.7	908
70.6	31.1	303
92.2	63.9	6 133
95.0	61.1	558
93.7	62.4	1 673
86.9	37.2	4 153
83.0	41.0	3 560
94.7	29.4	356
98.0	26.1	119
91.1	33.0	1 305
89.5	3.8	34
81.1	12.1	370
63.9	29.4	673
76.0	17.3	1 178
71.4	21.9	1 010
85.6	7.7	101
92.8	68.7	13 050
98.5	63.0	1 305
94.7	66.8	15 225
100.0	61.5	435
96.7	64.8	4 785
80.6	36.8	1 390
82.6	34.8	463
78.3	39.1	5 097

The main consideration in the development of the load spectra was to have large variations in major parameters affecting crack growth behavior. An analysis procedure that accurately correlates with such a wide range of test results should be accurate when applied to other load spectra that are enveloped by those tested.

The targeted initial flaw size was 1.27 mm deep by 6.35 mm long. The flaw was monitored visually throughout the test. Most tests were terminated when the flaw had reached a length of 20 mm or the total cycles were equivalent to a life-time. The tests were terminated at a crack length of 20 mm to avoid damage to the second flaw in the multiple-flaw specimens and because at this point the crack growth rate had accelerated to the point where the remaining life was negligible. The low-stress portion of two of the multiple-flaw specimens were tested twice. This was done when there was no evidence of fatigue crack growth on the fracture face of the high-stress flaw. Specimens B3 and B1 were originally tested using Spectra A and B, respectively. Testing of the low-stress flaw of each was then continued using Spectrum D.

The post-cracking thermal treatment, used to eliminate overload effects, was developed at Boeing [*1*] and has been used successfully on other alloys

TABLE 4—*Load Spectrum G.*[a]

Load, % of maximum			
Maximum	Minimum	Cycles per Layer	Group
59.1	11.0	64	A
70.1	11.0	13	A
70.5	35.0	2	A
83.1	35.0	64	A
90.6	42.5	60	A
97.2	49.2	10	A
84.6	28.0	17	A
59.1	11.0	64	A
90.6	36.2	14	A
73.0	25.6	10	A
83.1	35.0	64	A
99.6	51.6	21	A
83.5	22.0	33	A
84.3	36.2	55	A
97.2	36.6	2	A
100.0	22.0	2	A
84.3	22.0	4	A
84.3	36.2	55	A
78.3	30.3	60	A
90.0	41.5	200	B
85.0	31.5	30	B
89.8	36.2	60	B
90.0	41.5	200	B
85.0	41.7	10	B
91.2	37.2	30	B
95.7	0	1	B

[a] Load Spectrum G is produced by:
1. Start from 0, go to 70.1, then cycle through Group A. Do this 9 times.
2. Start from 0, go to 70.1, then cycle through Group A and B.
3. Go to 1 and repeat.

including Inconel, aluminum, and PH steels. Elimination of the plastic zone associated with the precracking procedures makes it possible to conduct spectrum load or constant amplitude tests at low initial stress intensities without concern that the precracking procedure is biasing the results.

Table 5 presents the summary of the test results. The flaw sizes presented in this table were measured visually with the aid of a microscope from the fracture face of each specimen. The stress levels reported are the maximum (100 percent stress) for that test. The cyclic lives are presented both in terms of total cycles and equivalent lifetimes.

Discussion of Results

The objective of this program was to develop a crack growth model that accurately correlates the results of the spectrum load test and could

TABLE 5—*Spectrum load test results.*

Specimen Number	Load Spectrum	Maximum Stress, MPa	Initial Flaw Length, mm	Initial Flaw Depth, mm	Cycles in Millions	Equivalent Life Times, 1 lifetime = 30 years	Final Flaw Length, mm	Final Flaw Depth, mm
W1a	A	159.3	5.918	1.219	9.0	0.05	21.240	8.496
W1b[a]	A	159.3	5.817	1.295	9.0	0.05	23.645	9.458
B3a	A	131.7	5.588	1.118	174.8	0.91	5.588	1.118
B3b[b]	A	116.5	5.486	1.168	174.8	0.91	5.486	1.168
B8a	A	97.9	5.486	1.067	173.5	0.91	5.486	1.067
B9a	B	131.7	5.664	1.219	9.8	0.15	26.561	10.624
B4a	B	127.6	5.740	1.194	31.1	0.46	19.807	7.923
B4b	B	113.1	5.791	1.194	51.0	0.76	24.437	9.775
B9b	B	112.4	5.893	1.346	15.2	0.23	32.920	8.768
B1a	B	93.1	5.588	1.143	136.9	2.03	5.588	1.143
B1b[c]	B	82.7	5.740	1.245	136.9	2.03	5.740	1.245
B2a	D	151.7	5.766	1.219	22.1	0.33	20.660	8.264
B2b	D	139.2	5.867	1.219	25.0	0.37	20.429	8.172
B6b	D	124.1	5.842	1.270	24.2	0.36	20.475	8.190
B5b	D	117.2	6.299	1.270	37.5	0.56	23.078	9.231
B1b[c]	D	117.2	5.740	1.245	43.9	0.65	5.740	1.981
B3b[a]	D	117.2	5.486	1.168	67.5	1.00	5.486	1.168
B6b	D	109.6	5.842	1.219	67.5	1.00	5.842	1.219
W2	G	106.9	5.842	1.905	17.1	0.28	5.842	1.905
A572-1[d]	G	117.2	5.994	1.219	66.8	0.11	20.320	8.128
A588-1[e]	G	106.9	5.791	1.473	81.7	1.33	20.100	8.040
A633-1[f]	G	110.3	6.299	1.219	42.7	0.69	6.299	1.215

[a] W1b was a weldmetal specimen.
[b] B3b was originally tested under the load Spectrum A.
[c] B1b was originally tested under the load Spectrum B.
[d] A572-1 was produced from A572 material.
[e] A588-1 was produced from A588 material.
[f] A633-1 was produced from A633 material.

be used in the analysis of similar spectra. To accomplish this, an initial review of appropriate constant amplitude data [2-5] was conducted, and the following equation was derived for constant amplitude tests

$$da/dn = 5.74 \times 10^{-9} (1 - R)^{2.4} (K_{max})^{3.0}$$

where

da/dn = crack growth rate (mm/cycle),
R = minimum stress/maximum stress, and
K_{max} = maximum stress intensity (MPa$\sqrt{m}$).

The problem was then to translate this equation into a form that would accurately reflect the effects of spectrum loading. Two different procedures were originally considered. First, the inclusion of a retardation term to account for load interaction effects and, second, the inclusion of a threshold term. The first approach, inclusion of a retardation term alone, had been found to be adequate for predicting spectrum load test results of 17-4PH steel [1]. These tests, however, were conducted at higher initial stress intensities and, therefore, for significantly shorter times. Additionally, constant amplitude tests for the 17-4PH material had produced cyclic crack growth at maximum stress intensity levels as low as 2.75 MPa$\sqrt{m}$, which is significantly below the apparent threshold levels presented in Refs *2*, *3*, and *4* for Grade A steels. The adequacy of the retardation term alone could therefore be a consequence of a reduced threshold in the 17-4PH material as compared to that reported for the Grade A steels in the references as well as the high initial stress intensities.

The initial attempts at the data correlation were made using only a retardation term and excluding any potential threshold effects. This procedure results in a straight line relationship between log stress intensity and log cycles (or life). This procedure was discarded early, because it failed to adequately correlate with the long-term test results (see Fig. 2), although it did provide reasonable correlation with the short-term tests.

The second procedure investigated was the inclusion of a threshold term alone. The threshold stress intensity versus R ratio relationship was estimated in the following manner. First a plot of stress intensity versus R ratio was made for Specimen B1b using the initial flaw size. Since there was flaw growth in this specimen, at least one of the plotted points had to be above the threshold. Next, the stress intensity versus R ratio relationship for Specimen B3b was added to this plot. Since Specimen B3b did not experience any flaw growth, all of the points for the specimen had to be below the threshold. Using the plot and estimate of the threshold, stress intensity was made and then used to analyze all of the data. The originally estimated threshold did not provide satisfactory correlation between actual

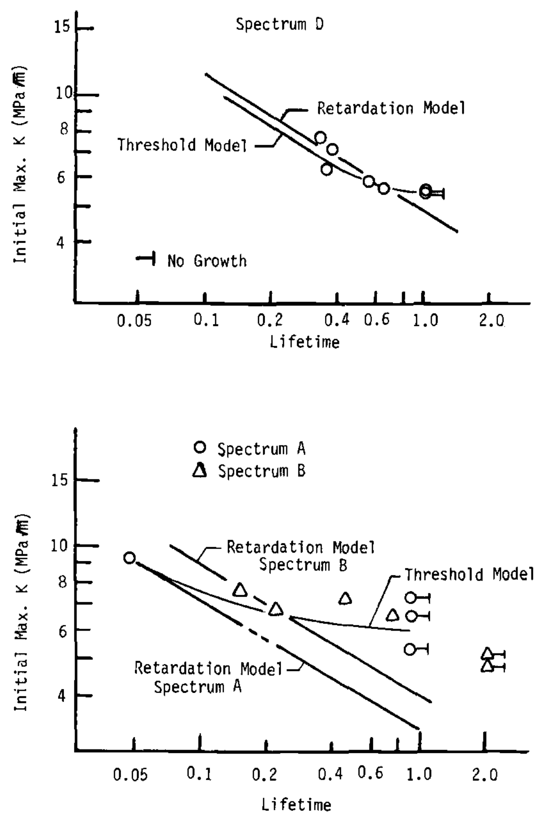

FIG. 2—*Initial maximum stress intensity versus lifetimes.*

and predicted results, therefore another estimate was made and the data was analyzed again. This procedure was repeated until a satisfactory correlation between actual and predicted results were obtained. Since most of the life would be accumulated during the early stages of crack growth, it was felt that elimination of the retardation term would not significantly impact the accuracy of this procedure. Although this threshold model produced good correlation with the long-term test results, it did not adequately correlate with the tests of shorter duration. These two attempts made it apparent that it was not possible to discard either the load interaction effects of the retardation model or the threshold effects of the threshold model if good correlation between predicted and actual results was to be obtained.

The third and final crack growth model investigated contained both a threshold and retardation term. The crack growth model has the following form:

for $K_{max} > K_{max}$ threshold (see Fig. 3). The threshold stress intensity is presented both in terms of maximum and delta stress intensity versus R ratio in Fig. 3.

$$da/dn = 5.74 \times 10^{-9}(1 - R)^{2.4}(K_{max})^{3.0}\left(\frac{K_{max}}{K_{0L}}\right)^{2.0}$$

For $K_{max} \leq K_{max}$ threshold and $da/dN = 0$
where

da/dn = crack growth rate, mm/cycles,
R = minimum stress/maximum stress,
K_{max} = maximum stress intensity for a layer of load cycles, and
K_{0L} = maximum stress intensity in the spectrum

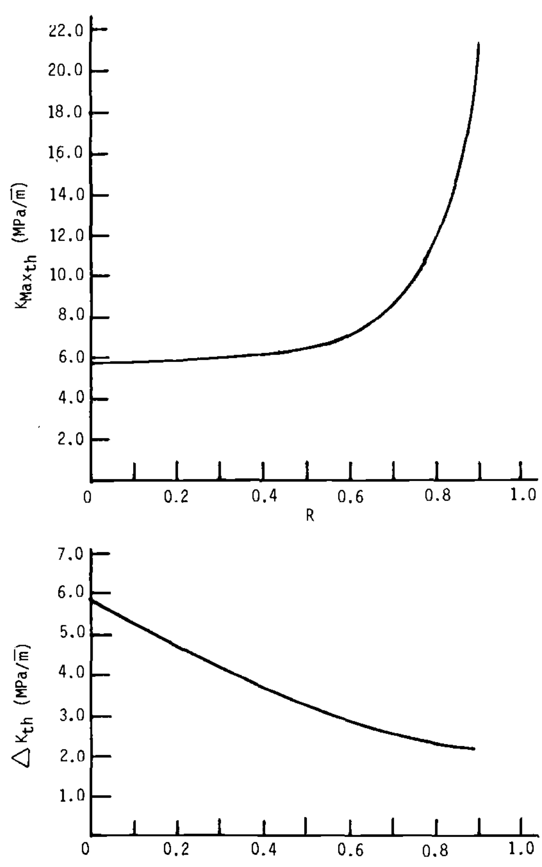

FIG. 3—*Threshold stress intensity versus* R *ratio for A572, A588, A633, and A533 steels.*

For negative R ratios let $(1 - R)^{2.4} = 1.0$, that is, there is no difference in crack growth behavior between $R = 0$ and negative R ratio cycles.

Using this model, the maximum variation between actual and predicted test results, when the comparison was made on the basis of actual stress to that stress that would predict the test life, was 12 percent, and the average variation for all the tests was 1 percent. The predicted stress was obtained by an interactive process. First, the actual test conditions (initial flaw size, stress level, and cycles) were used in the integration of the crack growth model to determine the predicted final flaw size. If the predicted final flaw size was larger than actual, a lower stress actual stress was selected and the integration repeated. If the predicted final flaw was larger than actual, a lower stress level was selected and the integration was repeated. This process was continued until the predicted final flaw size was the same as the actual. The stress level for which the predicted and actual final flaw size are the same is predicted stress level. The comparison was made in this manner rather than the typical comparison of cycles, actual and predicted, because of the threshold effect. If a comparison of actual to predicted cycles is made, a very slight variation in threshold can result in an actual finite test life while an infinite life was predicted. This procedure does not present a true picture of the correlation because seemingly large errors are a consequence of very slight variations in threshold between specimens. The objective of the test program was to develop and verify a procedure that could be used to determine allowable operating stresses for a 30-year life. Because the structure will have to operate near or below the threshold and also the objective is to be able to determine allowable stress levels, the data correlation was done on the basis of stress levels.

In Fig. 4, the ratio of actual stress to predicted stress for the tests are

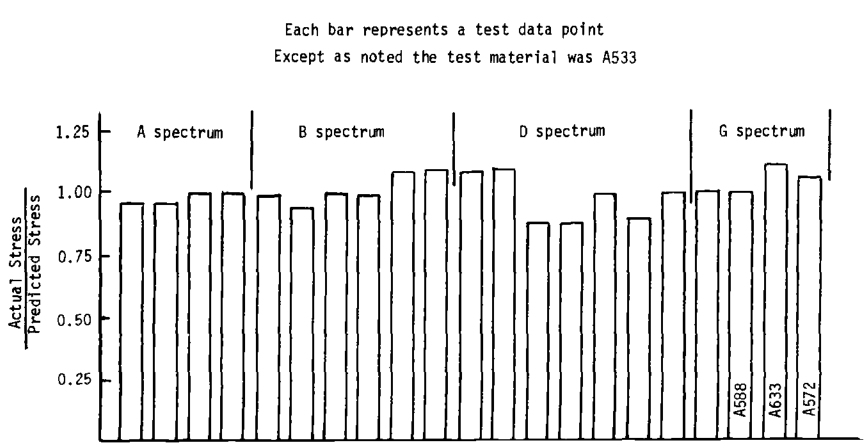

FIG. 4—*Comparison between actual and predicted results.*

evenly dispersed about the 1.0 line, where the actual and predicted stresses are identical. The threshold stress intensity versus R ratio relationship is the dominant factor in determining life. Since this relationship will experience a slight variation from specimen to specimen, similar to the variation in other fracture properties (fracture toughness, crack growth rates, etc.), the correlation (average error 1 percent with a 12 percent maximum error) presented in Fig. 4 is considered excellent.

The majority of the tests were conducted on the A533 material along with the tests on other materials to confirm the ability of the prediction procedure to handle the other steels. The analysis procedure was identical for all of the tests, regardless of the specimen material. Since all of the

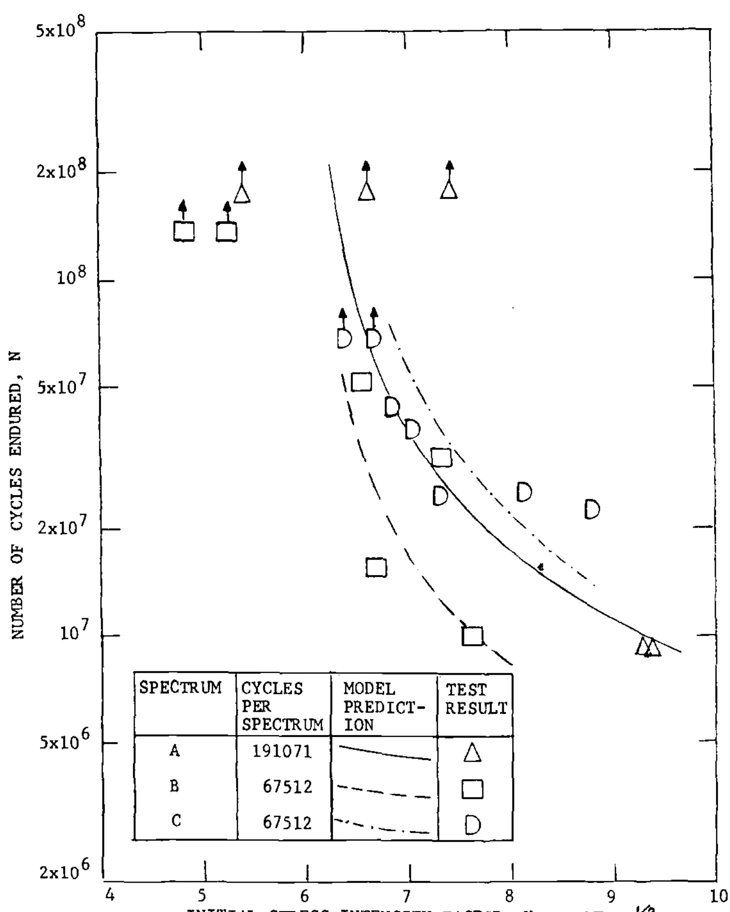

FIG. 5—*Results of application of Finger crack growth prediction model to Spectra A, B, and D compared with experimental fatigue test results. Material is A533 steel. Arrows attached to symbols indicate no observable crack growth during test.*

materials are similar in composition and strength level, it was anticipated that the accuracy of the procedure would not be influenced by material. The analysis procedure did work equally well for all of the materials tested. One specimen was also tested to provide data on weld metal. The behavior of this specimen was identical to a parent metal specimen.

Accurate correlation between predicted and actual test results for load spectra and life requirements similar to those presented here can only be obtained when a threshold and retardation crack growth model is considered. For shorter life, higher initial stress intensity problems, the threshold effects are inconsequential and can be ignored. The significant variables, therefore, become the stress ratio and maximum stress, since these are the control factors in the crack growth equation.

For long-term consideration, the threshold effect becomes dominant. Service life requirements, therefore, can only be obtained when, initially, the majority of the cycles are below the threshold stress intensity level. Here again, R ratio is a major parameter in determining when the stress intensity range is below the threshold stress intensity range. For as-welded structure, cracks initiate and grow in areas of high tensile residual stress. In these areas, the maximum stress is approximately yield and, therefore, the R ratio is primarily dependent upon the stress range applied, because the maximum is fixed near yield. Therefore, for as-welded structure, the stress range appears to be the dominant factor. For stress-relieved structure, both maximum stress and R ratio are important. This can only be accomplished by consideration of both the maximum stress and stress range, since the threshold stress intensity is a function of not only maximum but also delta stress intensity. Because the delta threshold stress intensity decreases with increasing maximum stress intensity, the allowable stress range for infinite life decreases as the maximum increases.

Conclusions

It has been shown that accurate correlation can be obtained between the predicted and actual results for a long-term test when a combined threshold and retardation crack growth model is employed. The model presented in this paper is applicable to Grade A steels, both parent and weld metal, for stress-relieved structure. Use of the model in predicting life behavior of as-welded structure for which the residual stress pattern is not known should be avoided. For stress-relieved structure, only the tensile load cases need be considered, because the model presented treated negative R ratios the same as R ratio of zero.

Acknowledgments

The author wishes to thank J. E. Lowe for permission to publish this account and J. N. Masters for his help and consultation during the study.

References

[1] Miller, D. D. and Finger, R. W. "Development of the Flaw-Growth Characteristics of 17-4 PH Steel Basemetal and Weldmetal," Boeing Document No. D312-80477-1, March 1977.

[2] Paris, P. C., Bucci, R. J., Wessel, E. T., Clark, W. G., and Mager, T. R. in *Stress Analysis and Growth of Cracks, Part I, ASTM STP 513,* American Society for Testing and Materials, 1972, pp. 141-176.

[3] Bucci, R. J., Clark, W. G., and Paris, P. C. in *Stress Analysis and Growth of Cracks, Part I, ASTM STP 513,* American Society for Testing and Materials, 1972, pp. 177-197.

[4] Schmidt, R. A. and Paris, P. C. in *Progress in Flaw Growth and Fracture Toughness Testing, ASTM STP 536,* American Society for Testing and Materials, 1973, pp. 79-94.

[5] Hudak, S. J., Safence, A., Bucci, R. J., and Malcolm, R. C., "Development of Standard Methods of Testing and Analyzing Fatigue Crack Growth Rate Data," AFTM-TR-78-40, May 1978.

DISCUSSION

W. F. Brown, Jr., B. Gross, and J. E. Srawley[1] *(written discussion)*—We offer the following comments on Mr. Finger's interesting paper. In assessing his proposed crack growth model, he neglects the ratio N_o/N_p of experimentally observed to predicted cyclic life at a given maximum stress, S_o, on the grounds that this ratio is highly sensitive to slight variations in the threshold K-value between specimens. Nevertheless, it seems to us that this ratio is of considerable interest in judging the adequacy of the available experimental data and of even more importance in assessing the usefulness of the model in predicting structural life. Thus, if the cycle life of specimens is highly sensitive to slight variations in their threshold K-value, the life of the structure should exhibit a similar sensitivity. Accordingly, we applied the model to each of the specimens in Table 5 that could be identified as failed by reference to Fig. 4. This entailed repeated layer-by-layer numerical integration of the model equation to obtain and accumulate the increments of crack growth for each layer until a crack length of 20 mm and depth of 9 mm was reached, as prescribed by Finger.[2] For each specimen, we ran the integration first at the experimental stress level, S_o, and then at a number of additional selected stress levels until we obtained a value of N_p within 1 percent of N_o; the predicted initial stress level, S_p, was then within a small fraction of 1 percent of the exact value corresponding to N_o. We were thus able to calculate N_o/N_p and S_o/S_p for each specimen, as given in Table 6.

There are some discrepancies between our stress ratios and those given

[1] Fracture Mechanics Section, Structures and Mechanical Technologies Division, National Aeronautics and Space Administration, Lewis Research Center, Cleveland, Ohio 44135.

[2] Certain information necessary for the numerical integration but not contained in his paper was furnished to us by Mr. Finger.

TABLE 6—*Results of application of Finger crack growth model to specimens.*

Spectrum	Specimen Number	Initial Stress Intensity Factor, MPa$\sqrt{m}$	Life in Spectra	Life Ratio, N_o/N_p	Stress Ratio, S_o/S_p
A	W1a	9.3113	47	0.90	0.97
A	W1b	9.4094	47	0.91	0.97
B	B9a	7.6143	145	0.97	0.99
B	B4a	7.3638	461	2.72	1.12
B	B4b	6.5412	756	1.58	1.03
B	B9b	6.7219	225	0.60	0.95
D	B2a	8.8104	328	1.60	1.11
D	B2b	8.1193	371	1.23	1.05
D	B6b	7.3046	359	0.63	0.93
D	B5b	7.0280	556	0.69	0.96
D	B1b	6.8342	650	0.60	0.95
G	W2	6.7491	1402	0.36	0.94
G	A572	6.9511	5475	3.22	1.07
G	A588	6.4810	6697	0.97	1.00
G	A633	6.5419	3500	1.03	1.00
			Mean	1.201	1.013
			Standard Deviation	0.803	0.061

by Fig. 4. We have no explanation for this other than a possible difference in precision of the respective numerical integration procedures. It is notable, however, that the means and standard deviations of the two sets of stress ratios are in good agreement if one considers only those specimens that failed. The standard deviation of 0.061 (Table 6), is, of course, a much more meaningful measure of the dispersion of the results than is Finger's "average error" (presumably the algebraic sum of the deviations divided by the total number of results). If one were to use the model to predict safe operation stresses, it would be prudent to reduce the predicted value by about 20 percent (approximately 3 standard deviations).

The mean of the life ratios N_o/N_p, 1.201, in Table 6 indicates that the model generally tends to underpredict the specimen life, and to that extent is on the safe side. On the other hand, the large value of the standard deviation, 0.803, reflects a degree of scatter in the experimental data that requires a large margin of safety to be applied to the model predictions in order to ensure an acceptable probability of survival at a high level of confidence. Indeed, it seems to us that it would be desirable to run many more actual tests than are reported by Finger in order to provide a better basis for statistical analysis. Under Spectrum A, only two specimens were tested to failure; under Spectra B and G, four each; and under Spectrum D, five. These sample sizes seem very inadequate for estimating allowable stresses in a very large structure that is expected to survive 200 million cycles of loading. Further, we believe that it is unrealistic to assume that weld behavior will be equivalent to that of the parent metal on the basis of results from only one welded specimen. It should be noted that a large amount of welding is involved in steel spar windmill blade construction and that welds will be likely sources of failure origins.

For Spectra A, B, and D, we obtained enough model prediction results to be able to plot the curves in Fig. 6 of the number of cycles endured, N_p, versus the initial stress intensity factor, K_{OLO}. All the experimental data points are also shown for comparison. It is clear from this figure that the model predicts that the life in terms of cycles for Spectrum A will be two to three times as great as for Spectrum B. Since the number of cycles

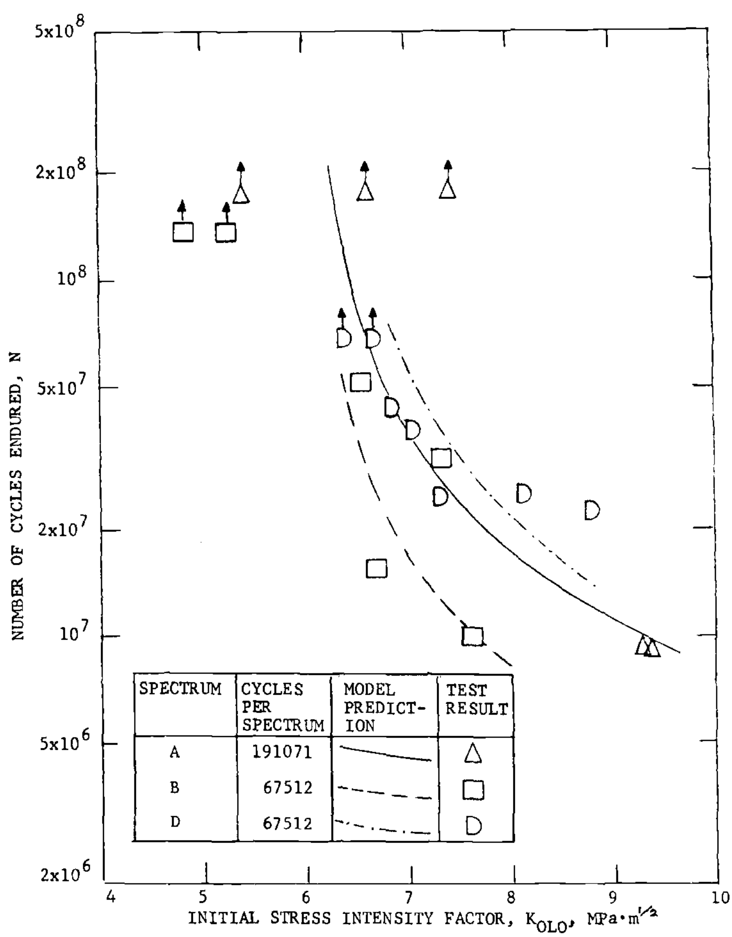

FIG. 6—*Results of application of Finger crack growth prediction model to Spectra A, B, and D compared with experimental fatigue test results. Material is ASTM/ANSI A533 steel. Arrows attached to symbols indicate no observable crack growth occurred during test.*

per spectrum is 2.8 times as large for Spectrum A as for Spectrum B, this means that the predicted life in terms of spectra should be about the same for Spectrum A as for Spectrum B. This is clearly due to the manner of truncation of Spectrum A to obtain Spectrum B, as suggested by Mr. Finger. The experimental data, however, is quite inadequate to confirm or deny the prediction.

It can be deduced from a detailed comparison of Spectra B and D that the model equation should predict a rate of crack growth under Spectrum D of about one-third of that under Spectrum B at any given crack size. This is consistent with the relative positions of the curves for Spectra B and D in Fig. 6. In this comparison, the experimental results do tend to support the prediction.

We note that Mr. Finger's model treats negative R ratio load cycles as equivalent to load cycles with $R = 0$. The experimental data presented cannot be used to test this assumption. However, we wish to point up that constant amplitude data presented by Hudak et al[3] for 2219 T851 aluminum alloy show crack growth rates at very low ΔK values to be higher at $R = -1$ than for R ratios greater than zero, and at high ΔK values the reverse is true.

We are somewhat concerned about the heat treatment applied to the precracked specimens to relieve the crack front plastic zones. This is stated to consist of heating to 1339 K (1950°F), holding for 1.0 h, and cooling to room temperature (rate unspecified). By comparison, ASTM/ANSI Specification for Pressure Vessel Plates, Alloy Steel, Quenched and Tempered, Manganese-Molybdenum and Manganese-Molybdenum-Nickel (A 533-78) calls for austenitizing at 1550 to 1800°F, water quenching, and subsequent tempering at not less than 1100°F. It seems that these two heat treatments should produce quite different structures, and we therefore wonder whether the present results are representative of A533 Type B steel when supplied according to the ASTM/ANSI specification, or as used in windmill construction.

Finally, we wish to point up that the steels tested by Mr. Finger are subject to accelerated crack growth in the presence of moisture. For example, the results by Atkinson and Lindley[4] for A533-B steel tested in the presence of distilled water show a two-fold increase in the crack growth rate when the frequency of loading is decreased from about 25 Hz to about 0.3 Hz, which is characteristic of the rotating speed of large windmills. These results relate to constant amplitude tests carried out at $R = 0.05$ and apply to a ΔK of 45 ksi-in$^{1/2}$. Because it is doubtful that large

[3] Hudak, S. J., Saxena, A., Bucci, R. J., and Malcom, R. C., "Development of Standard Methods of Testing and Analyzing Fatigue Crack Growth Rate Data," AFML-TR-78-40, Air Force Materials Laboratory, May 1978.

[4] Atkinson, J. D. and Lindley, in *The Influence of Environment on Fatigue*, Mechanical Engineering Publications Limited, New York, 1977, p. 65.

windmill blades can be effectively protected from moisture over many years, it is important to know to what extent the moisture effects reported by Atkinson and Lindley will occur at lower ΔK values and to what extent moisture will affect the threshold K values.

R. W. Finger (*author's closure*)—In response to the discussion, the author wishes to offer the following comments. The purpose of the test program and model development was to define a methodology that could be used to determine allowable operating stresses for windmill structures. The first step was to develop a model that reliably predicted test specimen behavior. Having accomplished this, the model could then be used to predict the typical behavior of the structure for an assumed set of conditions (operating stresses, initial flaw size, etc.). Appropriate factors could then be applied to make sure that the actual conditions in the structure were sufficiently different from the assumed so that the service life requirements would be assured. Time and budgetary considerations limited the size of the test program, and these limitations are reflected in the factors being used for the actual design. A larger test program, as suggested by the reviewers, would probably allow some relaxation in the conservatism used in the selection of these factors. The purpose of this paper was to present a crack growth model and spectrum load crack growth data that are applicable to windmill type load environments, not to supply allowable operational stresses. The generation of allowable operational stresses requires a knowledge of the inspection techniques, fabrication procedures, and acceptance criteria being used for the actual structure.

The assumption that negative R ratio crack growth rates are the same as $R = 0$ rates is consistent with the data presented by Hudak et al for 10Ni steel in reference cited by the reviewers. It is also consistent with my experience on numerous tests of surface flaw specimen under both uniform and spectrum load conditions. The reviewers comments were based on a single test of an aluminum specimen, either a center-crack or a compact-tension type. The test was conducted using a decreasing K procedure, therefore, the low ΔK region had the longest crack length. In light of the wide precrack starter notch in both configurations, compression loading on either specimen type can result in tension at the crack tip for long fatigue cracks. This problem will be especially acute for the compact tension specimens, because the specimen halves will tend to rotate about the initial portion of the fatigue crack. The application of compression loads would thereby induce an additional tension load cycle (of some unknown magnitude) that is not accounted for in the calculation of crack growth rate. The validity of data generated in this manner is questionable at best.

The thermal treatment procedure used to relieve the effect of the crack front plastic zone was developed at Boeing and has been used on other steels, aluminums, and nickel alloys. Comparisons have been made of the crack growth rates for specimens that have and have not received this type treatment. These comparisons have not revealed any difference in the crack growth rates. Although changes in heat treatment can have a significant effect on conventional fatigue behavior, the author has not seen this effect on crack growth behavior.

H. D. Dill,[1] *C. R. Saff,*[1] *and J. M. Potter*[2]

Effects of Fighter Attack Spectrum on Crack Growth

REFERENCE: Dill, H. D., Saff, C. R., and Potter, J. M., "**Effects of Fighter Attack Spectrum on Crack Growth,**" *Effect of Load Spectrum Variables on Fatigue Crack Initiation and Propagation, ASTM STP 714,* D. F. Bryan and J. M. Potter, Eds., American Society for Testing and Materials, 1980, pp. 205–217.

ABSTRACT: The purpose of this program was to systematically evaluate the effect of variations in flight stress spectra on crack propagation using analysis in conjunction with experimental correlations. Over 100 spectrum variations were generated, derived from four baseline load factor spectra. Three constant amplitude and 30 spectrum tests were performed to verify predictions of the effects of spectrum variations and to provide data useful in defining guidelines for structural verification of future aircraft. Spectrum variations shown to have the greatest impact on crack growth life are those affecting the maximum peak stresses.

KEY WORDS: crack propagation, fatigue (materials), stress analysis, predictions, loads (forces)

Variations in applied load spectra have been shown to significantly affect crack propagation behavior. It is important, therefore, to quantify and evaluate load spectra effects to improve crack propagation prediction capability and aid in the formulation of design, analysis, and test spectra. The range of load history variations that needs to be considered is limited because each aircraft in a fleet has similar weight and performance limits. A load history sensitivity study is realistically constrained to a basic spectrum with parameter variations on the order of 10 to 20 percent. As an example, within a fleet of aircraft with a design limit load factor of 8 *g*'s, it would be normal for the majority of aircraft to experience that level of load factor a relatively few times in its life. Out of the remainder of the fleet, it may be possible to find a few aircraft that had experienced no more than 6.5 *g*'s

[1] Section chief-Technology and senior engineer-Technology, respectively, McDonnell Aircraft Co., St. Louis, Mo. 63166.
[2] Aerospace engineer, Air Force Flight Dynamics Laboratory, Wright-Patterson Air Force Base, Ohio 45433.

or more than 9.5 *g*'s (this range of usage could result in factor of three on life).

Thus, study of spectrum effects is limited to determining the sensitivity of crack growth life to small representative variations from a baseline history. The primary purpose of this study was determination of this sensitivity. Identification of load history variables that have a large effect on crack growth can significantly influence development of load histories used for design verification testing and requirements for recorder systems to track structural damage.

During the design phase of an aircraft, reliance is placed on analytical approaches to determine crack growth life, with limited supportive testing. Knowledge is required of both the sensitivity of crack growth life to spectra variations and the accuracy of crack growth prediction methodology. A secondary purpose of this investigation was to determine the capability of existing crack growth analysis methods to predict growth behavior under realistic loading conditions.

The investigation is reported in detail in Ref *1*.[3] Over 100 spectrum variations were generated, derived from four baseline load factor spectra for F-15 aircraft lower wing skins. These baseline spectra are air-to-air, air-to-ground, instrumentation-and-navigation, and a combination, the design mix. Stress exceedance curves for the lower wing skin of the F-15 aircraft were used to develop the baseline stress spectra. Cycle-by-cycle stress histories were generated using techniques based on random noise theory to obtain realistic coupling of peaks and valleys. Computer programs used to create each of the load histories were documented in Refs *2* and *3*. Using these computer programs, it is possible to exactly duplicate each of the over 100 load histories used in this study.

Crack growth was predicted prior to test for each spectrum using the Willenborg model [*4*] as the primary analysis method. The contact stress model [*5*], which accounts for crack closure effects, was used as a secondary method. It was improved to account for residual stress effects at the hole and large scale yielding to correlate with trends observed in test. Hence, in general, the predictions of the contact stress model were more accurate than those of the Willenborg model. Three constant amplitude and 30 spectrum tests were performed to verify the predictions, to evaluate the effects of spectrum variations, and to provide data useful for defining guidelines for structural verification of future aircraft.

Baseline Exceedance Curves

Design missions of the F-15 aircraft were used as the basis for generating fatigue stress spectra. The design mix spectrum was based on a mission

[3]The italic numbers in brackets refer to the list of references appended to this paper.

analysis of expected usage and included 365 air-to-air missions, 355 air-to-ground missions, and 96 instrumentation-and-navigation training missions per 1000 h. External wing loading distributions were defined for each flight condition by speed, altitude, gross weight, and airplane configuration. The baseline stress spectra and their variations were defined at fatigue and fracture critical locations of the F-15 lower wing skin outboard of the manufacturing splice at butt line 155. Baseline stress exceedance curves are shown in Fig. 1. The spectrum also contains compression loading representing ground loads. The baseline limit stress used in the program was 207 MPa (30 ksi), gross.

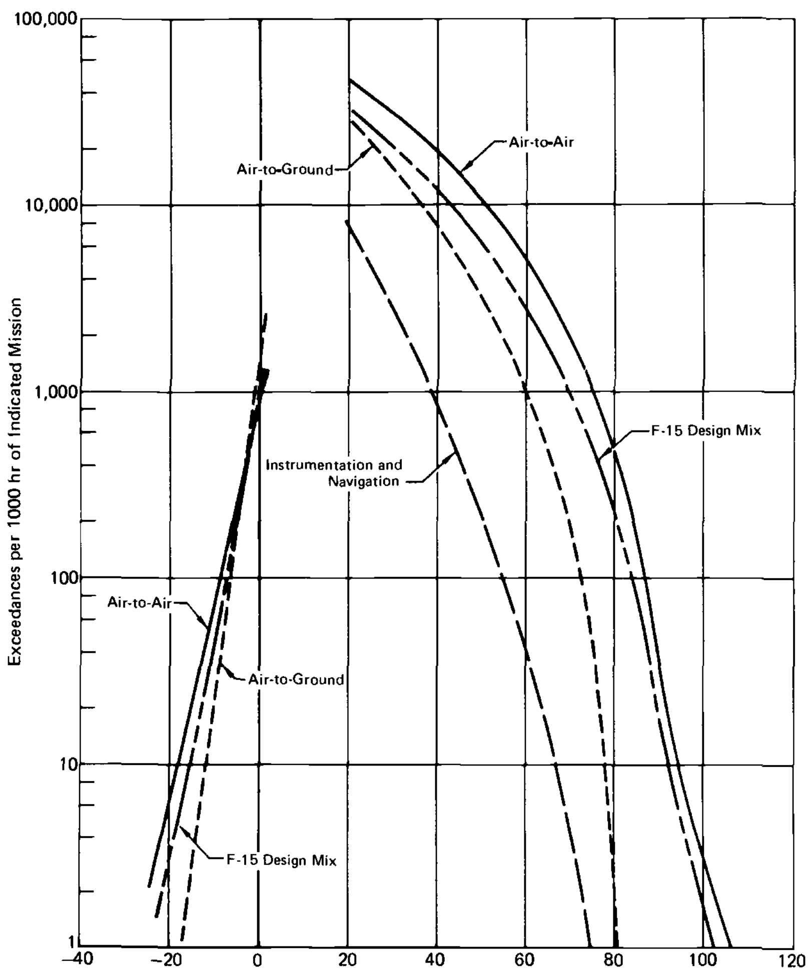

FIG. 1—*Baseline stress spectra.*

Test Program

Aluminum alloy 7075-T7351 was the test material. Specimens (Fig. 2) containing through-thickness cracks emanating from open holes were used for the spectrum tests. Electrical discharge machined (EDM) starter notches were created at pilot holes located as shown in Fig. 2. Specimens were pre-cracked until the visible length of the longest crack was 0.13 cm. Subsequently, the pilot holes were reamed to a diameter of 0.635 cm. This procedure left a fatigue pre-crack of approximately 0.05 cm emanating from one of the holes in the specimen. During the testing, surface crack lengths were optically monitored and recorded at intervals of 500 spectrum flight hours. In addition, during one 1000-h block of simulated flight hours on each specimen, the crack length was measured every 50 spectrum hours.

Impact of Spectrum Variations

The impact of spectrum variations on crack growth life and the accuracy of the Willenborg and contact stress crack growth models in assessing this

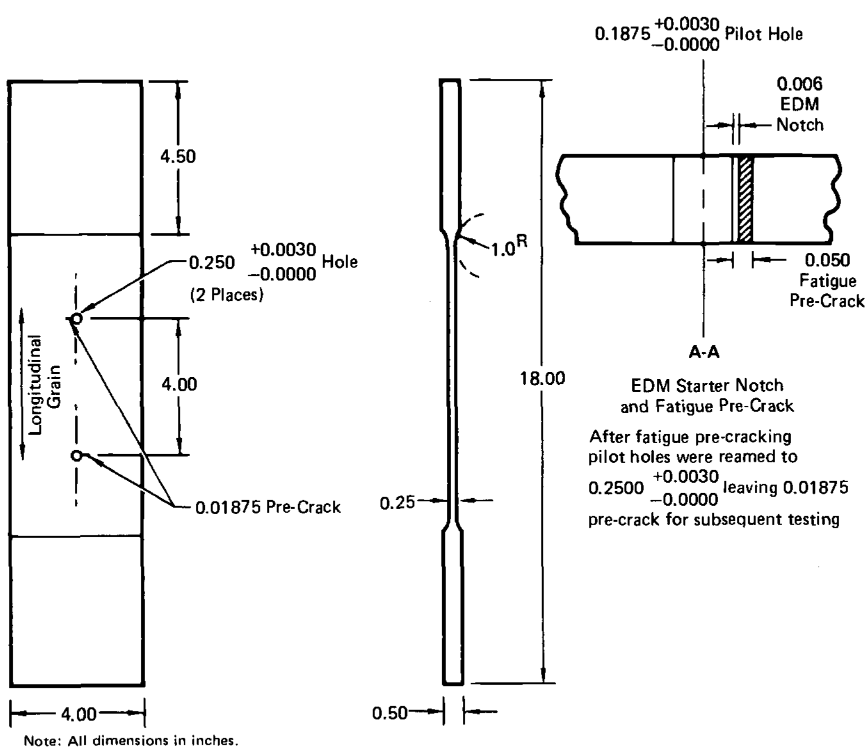

FIG. 2—*Open hole specimen.*

impact is summarized in Table 1. For purposes of comparison, the crack growth life in each case was determined to be the amount of flight hours necessary for the crack to grow from 0.13 to 1.27 cm measured from the edge of the hole. Variations shown to have the greatest impact are those affecting the maximum peak loads. These variations include mission mix, high- and low-load truncation, exceedance curve variations, and limit stress variations. Variations shown to produce lessor impact include those that affect all but the highest peak loads throughout the spectrum, such as sequence of missions, compression loads, and peak and valley coupling. Spectrum variations shown to produce little effect are reordering of loads within a mission and flight length variations.

Spectrum variations generated in this program apply to the lower wing skin of a fighter aircraft, therefore the assessment of these variations may not apply to other structural areas.

Some of the more significant spectrum variations are described in the following paragraphs.

Sequence of Missions

The effect of this variation is shown in Fig. 3 where the missions were sequenced based on the highest load in each mission, either in increasing order of loads (Lo-Hi), or decreasing order of loads (Hi-Lo). Both models predict reductions in crack growth life with either Lo-Hi or Hi-Lo sequencing. Tests were performed using Hi-Lo sequencing and results were in agreement with predictions of the models.

Mission Mix

The ratio of air-to-air missions to total missions in the 1000-h design mix spectrum was varied. The analysis and test data presented in Fig. 4 indicate that the effect of this variation is to reduce life as the number of air-to-air missions increases.

High- and Low-Load Truncation

These variations had the greatest impact on crack growth life of all the variations. One variation is that of truncation of cycles having small peaks from the design mix spectrum. As shown in Fig. 5, life with the design mix is sensitive to the truncation level imposed. When cycles with peaks below 45 percent design limit stress (DLS) were removed from the spectrum (51 percent of the cycles) very little effect on life was predicted. However, when cycles with peaks less than 50 percent DLS were removed (65 percent of the cycles), crack growth life was predicted to increase markedly. Life

TABLE 1—*Effect of spectra variations on crack growth and prediction accuracy.*

Spectrum Variation Type	Range of Crack Growth Life			Maximum Error within 25% of Life	
	Less than 10% Variation	Less than 50% Variation	Greater than 50% Variation	Willenborg Model	Contact Stress Model II
Reordering of loads within a mission	✓	...	...	No tests performed	
Sequence of missions	...	✓	...	✓	✓
Mission mix	...	...	✓	✓	✓
Individual flight length	✓	...	...	✓	✓
High- and low-load truncation	...	...	✓	✓	...
Compression loads	...	✓	...	...	✓
Exceedance curve variations	...	...	✓	...	✓
Coupling of peaks and valleys	...	✓	...	...	...
Test limit stress level	...	...	✓	...	✓

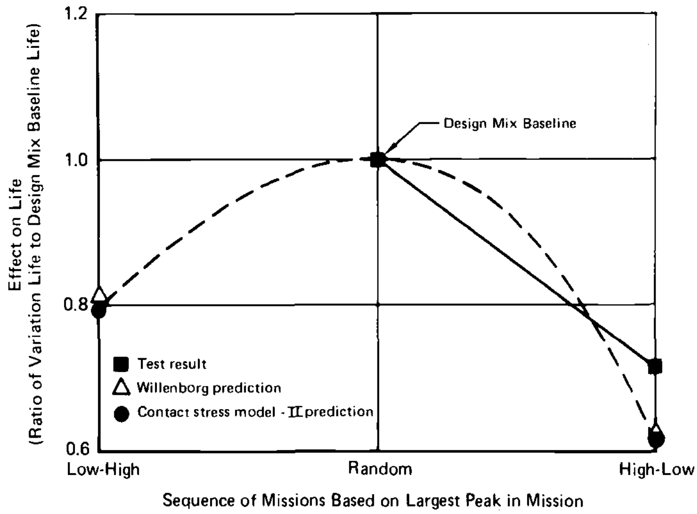

FIG. 3—*Effect of mission sequence on crack growth life.*

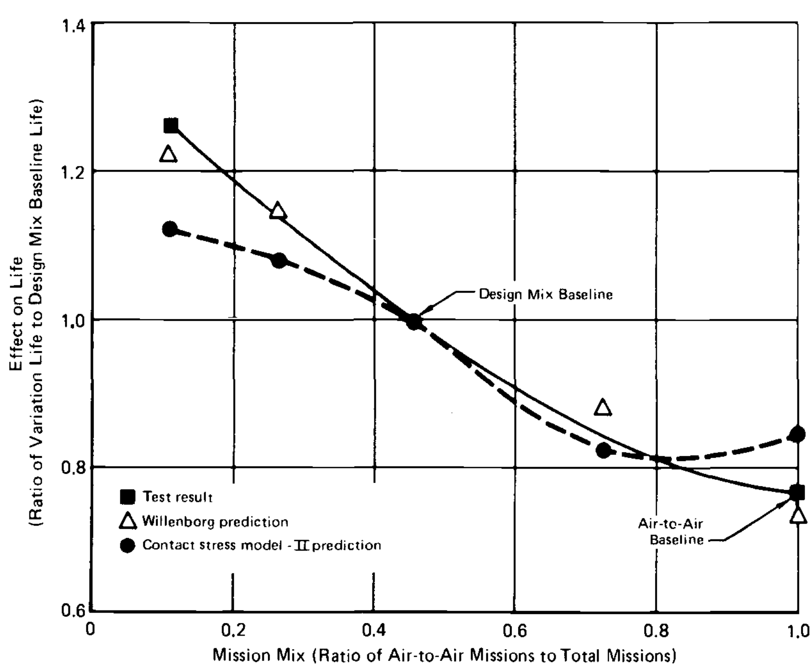

FIG. 4—*Effect of mission mix on crack growth life.*

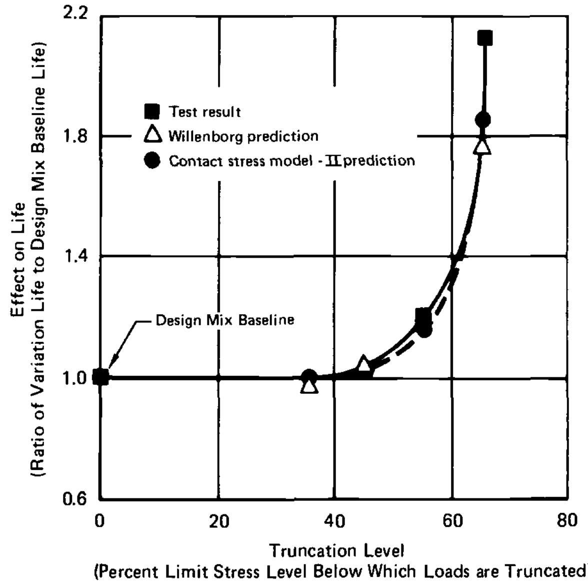

FIG. 5—*Effect of low-load truncation on crack growth life.*

increased a factor of two over the baseline when cycles with peaks less than 65 percent DLS were removed from the spectrum (91 percent of the cycles). Test results agreed well with predictions of these variations.

Another truncation variation affected the highest loads in the design mix spectrum. Variations involving addition of a single overload cycle to the 1000 flight hour block had the most significant impact on the crack growth life of all variations tested. As shown in Fig. 6, a single cycle with a peak stress level of 135 percent DLS applied once every 1000 h increased the crack growth life by more than a factor of six. In contrast, clipping the highest load in the spectrum to some lower level decreased the crack growth life; for example, when loads were clipped to 85 percent DLS, the life was 75 percent of the baseline value.

The crack growth models predicted the trends of high- and low-load truncation results.

Compression Loads

Compression loads were found to have moderate effects on crack growth life. Data in Fig. 7 indicates the effect of ground load variations on life as compared to the design mix spectrum life. The design mix spectrum includes ground loads of −5 percent DLS and −10 percent DLS and negative maneuver loads up to −27 percent DLS. Increasing these loads to −30 percent DLS reduced life by 20 percent, while setting all compression

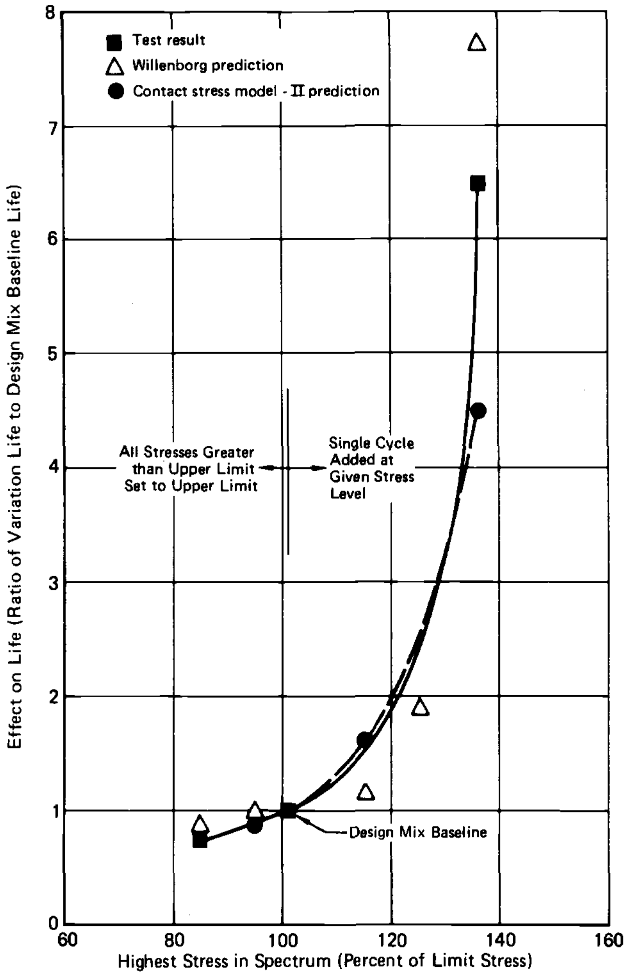

FIG. 6—*High- and low-load truncation. Effect of modifying highest load level in spectrum on crack growth life.*

loads (including ground loads) to zero increased life by less than 10 percent. The Willenborg model as used in this study could not account for compression load variations. However, the contact stress model predictions were in reasonable agreement with the test results.

Exceedance Curve Variations

Exceedance curve variations are among the most common variations encountered during aircraft design and analysis. Variations included three exceedance curves of lesser maximum stress and three curves of greater

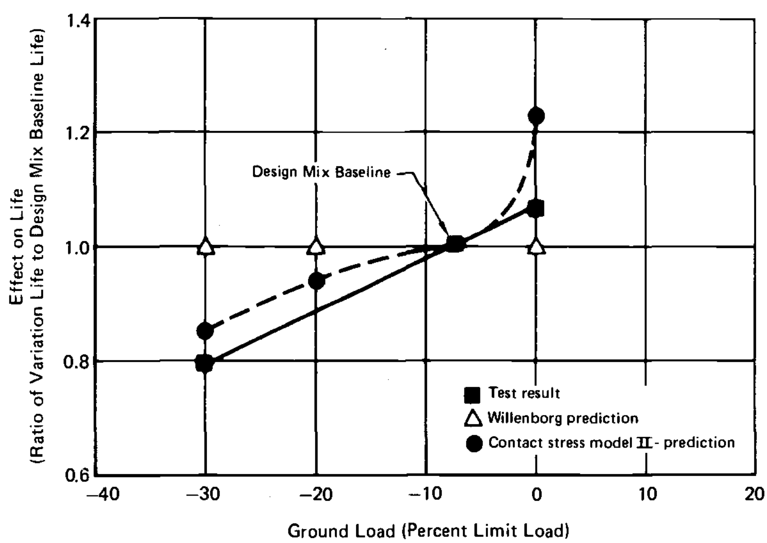

FIG. 7—*Compression loads. Effect of ground load variation on crack growth life.*

maximum stress (Fig. 8). Figure 9 depicts the effect of these variations on crack growth life of the air-to-air baseline spectrum. The results indicate that crack growth life decreases monotonically with increasing maximum stress. The agreement between analysis and test is close.

Limit Stress

The effects of limit stress became apparent during the performance of the test program when it was found that the prediction errors of the Willenborg model could be correlated with the maximum stress level in each spectrum as shown in Fig. 10. In order to assess these effects, two specimens were tested to the design mix spectrum, one at 137 MPa (19.8 ksi) and one at 277 MPa (40.2 ksi) limit stress, with all the spectrum stresses decreased and increased accordingly. Results of these tests and analyses are also shown in Fig. 10. The Willenborg model does not correlate well with these limit stress test results.

Summary

In conclusion, spectrum variations involving mission mix, high- and low-load truncation, exceedance curves, and stress level appear to have the greatest impact on crack growth life. These factors probably encompass the main ingredients of spectrum development and could be expected to have the greatest impact on fatigue and fracture analyses. The Willenborg

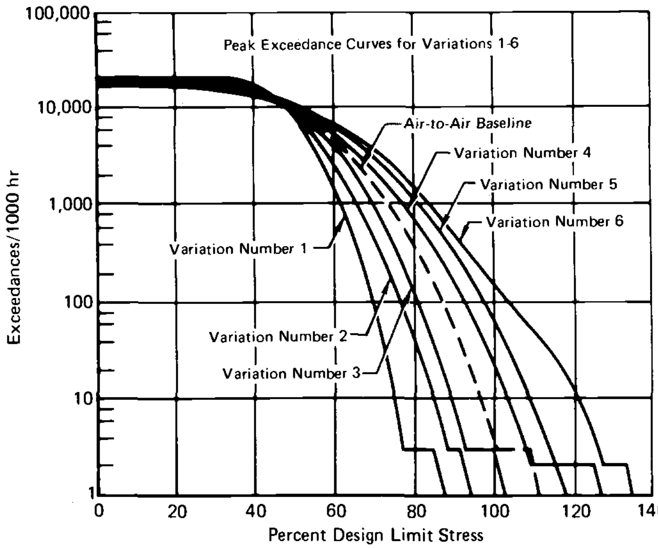

FIG. 8—*Exceedance curve variations.*

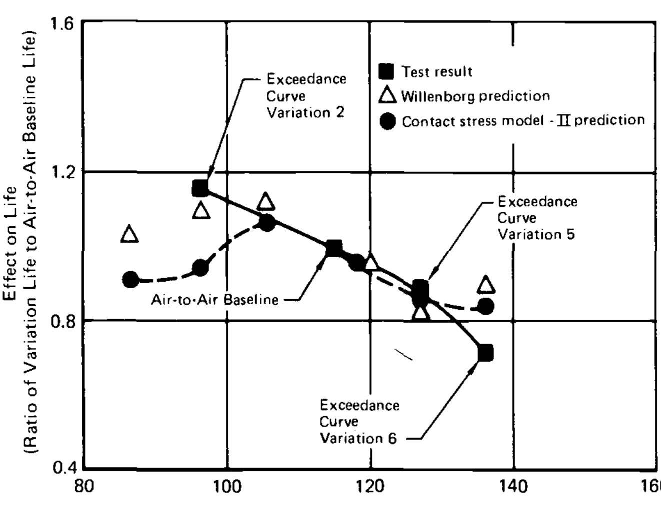

FIG. 9—*Effect of exceedance curve variations of air-to-air baseline spectrum on crack growth life.*

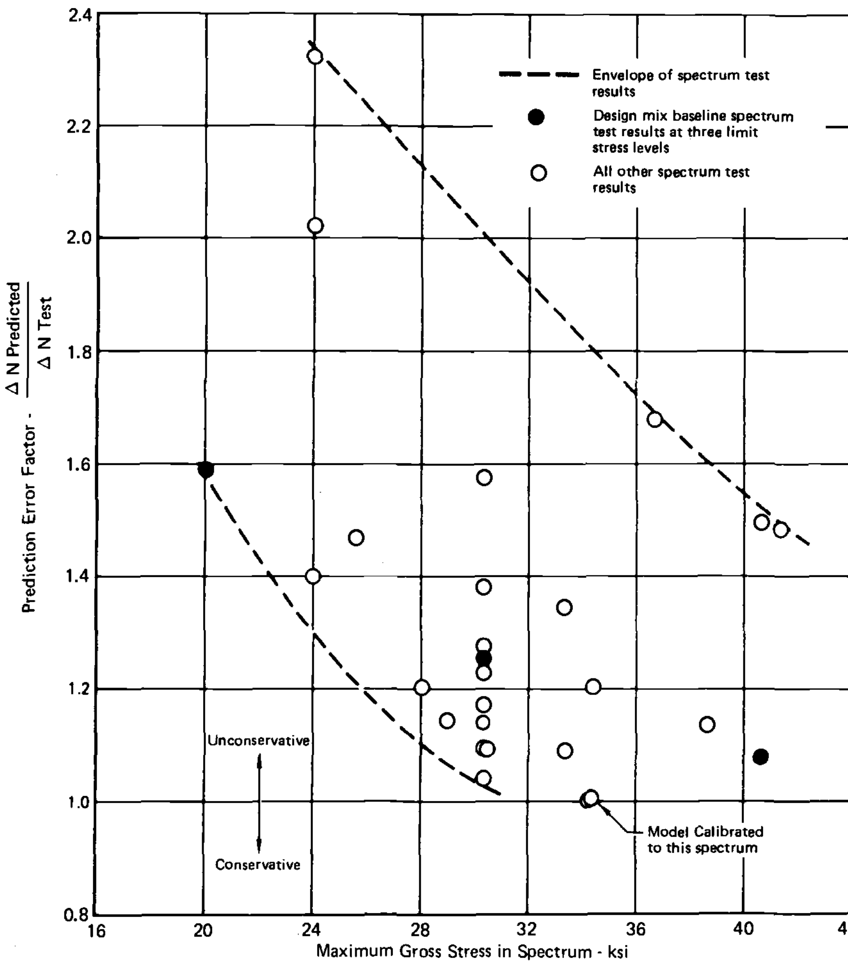

FIG. 10—*Effect of stress level on crack growth prediction with Willenborg model.*

model appeared to be reasonably accurate in accounting for spectrum variations. With the exception of the case of the 135 percent overload, the contact stress model was as accurate as, or more accurate than, the Willenborg model.

Acknowledgment

This work was accomplished under the sponsorship of the Air Force Flight Dynamics Laboratory, Wright-Patterson Air Force Base, Contract F33615-75-C-3112.

References

[1] Dill, H. D. and Saff, C. R., "Effects of Fighter Attack Spectrum on Crack Growth," AFFDL-TR-76-112, Air Force Flight Dynamics Laboratory, Wright-Patterson Air Force Base, Ohio, March 1977.

[2] Dill, H. D. and Young, H. T., "Stress History Simulation, Vol. I—A User's Manual for a Computer Program to Generate Stress History Simulations," AFFDL-TR-76-113, Vol. I, Air Force Flight Dynamics Laboratory, Wright-Patterson Air Force Base, Ohio, Nov. 1976.

[3] Young, H. T., Foster, F. R., and Dill, H. D., "Stress History Simulation, Vol. II—A User's Manual for a Computer Program to Modify Stress History Simulations," AFFDL-TR-76-113, Vol. II, Air Force Flight Dynamics Laboratory, Wright-Patterson Air Force Base, Ohio, Nov. 1976.

[4] Willenborg, J., Engle, R. M., and Wood, H. A., "A Crack Growth Prediction Model Using an Effective Stress Concept," AFFDL-TM-71-1-FBR, Air Force Flight Dynamics Laboratory, Wright-Patterson Air Force Base, Ohio, 1971.

[5] Dill, H. D. and Saff, C. R. in *Fatigue Crack Growth Under Spectrum Loads, ASTM STP 595,* American Society for Testing and Materials, 1976, pp. 306–319.

C. E. Larson,[1] *D. J. White,*[1] *and T. D. Gray*[1]

Evaluating Spectrum Effects in U.S. Air Force Attack/Fighter/Trainer Individual Aircraft Tracking

REFERENCE: Larson, C. E., White, D. J., and Gray, T. D., **"Evaluating Spectrum Effects in U.S. Air Force Attack/Fighter/Trainer Individual Aircraft Tracking,"** *Effect of Load Spectrum Variables on Fatigue Crack Initiation and Propagation, ASTM STP 714,* D. F. Bryan and J. M. Potter, Eds., American Society for Testing and Materials, 1980, pp. 218-227.

ABSTRACT: The results of an analysis performed to evaluate damage rates at several locations in an airplane structure subjected to usage variations are presented. The results reveal not only the response of several locations to spectra variations, but also the correlation of damage rates at remote locations with the damage rate of a reference location.

KEY WORDS: fracture mechanics, damage index, spectrum variables, damage tolerance, fatigue (materials), crack propagation

In an attempt to maximize the structural useful life of its airplane weapon systems, the U.S. Air Force has introduced a concept called force management. The objective of this concept is to provide the methods and procedures for defining all force maintenance actions. These actions include structural inspections, structural rework if required, component replacement as required, and retirement. The mission of force management is to program these actions to optimize economic and safety considerations. The specifics of force management are delineated in MIL-STD-1530A.[2]

This standard provides for a fracture mechanics approach to the airframe durability/fatigue life evaluation problem. That is, it is assumed that the structure has initial production flaws or cracks that require monitoring or tracking throughout the airframe's usage to preclude crack growth to critical proportions. Attendant requirements are also defined in MIL-STD-1530A

[1] Senior engineering specialist, senior engineering manager, and senior engineering specialist, respectively, Vought Corporation, Dallas, Tex. 75265.

[2] "Aircraft Structural Integrity Program, Airplane Requirements," MIL-STD-1530A, U.S. Air Force Aeronautical System Division, Dec. 1975.

and supporting specifications concerning the design of new airframes for inspectability, fail safety, and materials selection (for slow crack growth).

The basic elements of force management include an individual aircraft tracking program (IAT), a loads and environment spectra survey (L/ESS), and a force structural maintenance plan. The investigation described in this paper applies to, and was done in support of, the IAT functions of force management.

A primary objective of an IAT program under MIL-STD-1530A is to predict the potential growth of flaws in critical areas of each airframe. The flaw growth data are then used to derive maintenance intervals for individual aircraft. Before fracture mechanics techniques were available, this task was accomplished by methods based on accumulated fatigue damage. This has resulted in two categories of IAT programs, one based upon fatigue damage and one upon crack growth damage calculations, depending upon when the aircraft was designed. Only one fighter/attack aircraft (the F-16) has been developed under the MIL-STD-1530A requirements, although several have been evaluated using the methods of fracture mechanics.

The individual aircraft usage data for U.S. Air Force aircraft is acquired by use of an "activity indicator." There are presently two recording devices in use: the counting accelerometer (CA) and the mechanical strain recorder (MSR).

A counting accelerometer is a device consisting of a transducer that senses aircraft center of gravity vertical acceleration and a digital indicator that displays the cumulative occurrences of specific acceleration levels. An MSR is a self-contained mechanical device that senses and records total deformation over the effective gage length of the structure to which it is attached. A tensile deformation of the structure causes a stylus to scratch a metal foil tape contained in a cartridge. The excursion of the stylus is proportional to the deformation. The tape advances as successive recordings are made.

The basic objective of IAT is to use the data acquired from the airplane activity indicator in a fashion that allows periodic calculation of a damage index. This capability is the heart of the force management concept and is receiving considerable attention in an attempt to produce reliable and accurate results. The problem is basically one of having a very small amount of information in a case where a large amount is needed. Generally, an airplane will have only one indicator and a large number of structural locations that require tracking. The implementation of IAT then requires a transfer function that relates indicator data to damage at a reference location and methods for predicting damage at remote locations.

A fundamental difference between the CA and the MSR is that the CA requires one additional transfer function relating acceleration to stress at the reference location. That is, the stress that is calculated from a given load factor for the purpose of damage prediction assumes some average value for important flight parameters such as weight. An MSR records the stress (obtained from strain) directly without knowledge of the maneuver or flight condition that causes the load.

The study reported here was directed at two questions inherent to the IAT process using CA and MSR. (1) How much error is introduced by use of the CA relative to the MSR in damage index calculations or life expended? (2) Can the damage rate at remote locations be correlated with the calculated damage rate at the reference location?

Analysis

The approach to investigating the questions at hand consisted of choosing several structural locations in an airplane and analyzing the response of each location to usage spectra variations. This analysis was guided by the MIL-STD-1530A assumptions of initial flaws in safe crack growth structure. Failure was assumed when the applied stress intensity factor reached the critical stress intensity factor for the part thickness.

The airplane selected for this study is the U.S. Air Force A-7D. The structural locations chosen are the eight described by Figs. 1 and 2. The baseline usage spectrum chosen was derived during the A-7D U.S. Air Force Aircraft Structural Integrity Program. Stresses were calculated by a finite element analysis of the structure.[3] The structural locations were selected not because of their criticality, but to give a reasonable distribution of points in the airplane. In fact, to produce failure at the points selected, the theoretical stresses were increased to produce the final spectra.

Table 1 itemizes the nine spectra variations used in the study. These varia-

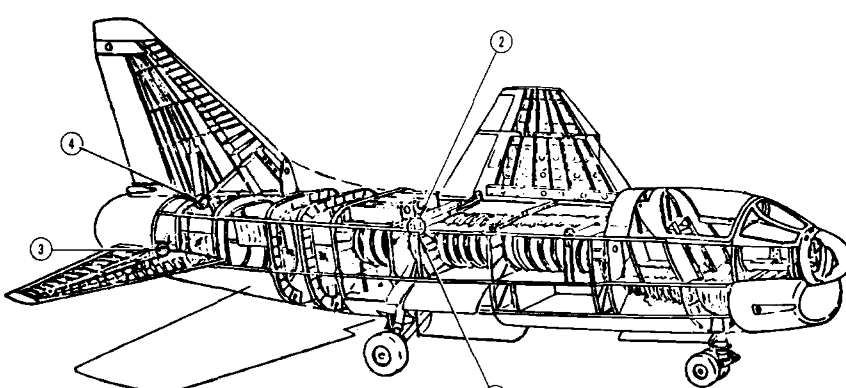

FIG. 1—*Location of fuselage analysis points. Force management analytical points: (1) longeron at FS 480, (2) wing attach lugs, (3) horizontal tail, and (4) vertical tail.*

[3]White, D. J. et al, "Flight Spectra Development for Fighter Aircraft," Technical Report NADC-76132-30, July 1977.

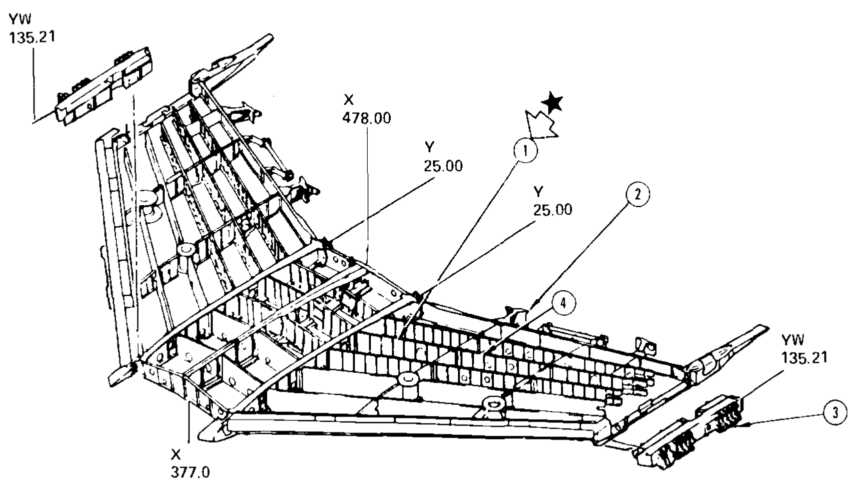

FIG. 2—*Location of wing analysis points. Force management analytical points: (1) WS 32, (2) WS 53, (3) OWP lugs, and (4) stub hole.*

TABLE 1—*Spectra variations used in analysis.*

1. W = 1.075 W (one standard deviation of A-7D weight)
2. W = 1.15 W
3. MN = 1.15 MN (one standard deviation of A-7D Mach number)
4. ALT = 1.15 ALT (one third of a standard deviation of A-7D altitudes)
5. $N_Z = 1.15\, N_Z$
6. $N_Z \leq 6.5\, g$
7. 30-30-40 mix (the baseline spectrum was a 30% general, 50% air-to-ground, and 20% air-to-air mix)
8. 10-50-40 mix
9. 50-50-0 mix

tions represent reasonable variations in airplane mission parameters. For example, reprogramming of fuel usage can cause weight variations of the magnitude shown.

The vertical and horizontal tail locations are made of 4340 steel while the remaining six locations are 7075-T6 aluminum. The initial flaw lengths are seen to be 0.01 in. for the steel and 0.05 in. for the aluminum. The EFFGRO fracture model[4] with the Vroman retardation option was used for the crack growth analysis.

A unique stress spectrum for each of the eight structural locations was generated for each of the ten mission variations. A total of 80 EFFGRO crack growth analyses were then accomplished. Figures 3 and 4 are included to characterize the results of these crack growth histories. The end point of

[4]"Crack Propagation Analysis by G. Vroman's Model," North American Rockwell Report NA-72-92, prepared by M. Szamossi, 1 Feb. 1972.

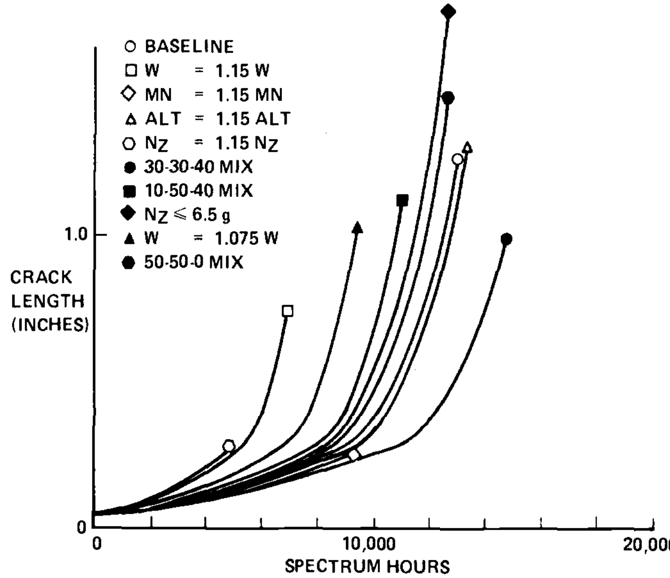

FIG. 3—*Crack growth at WS 32.*

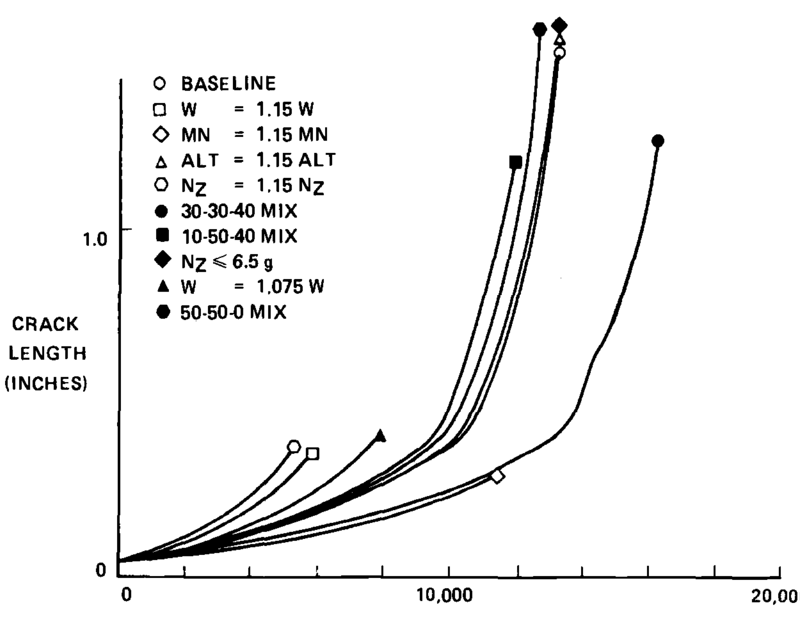

FIG. 4—*Crack growth at WS 53.*

each curve notes fracture. It is seen that the content of the different spectra impact the crack growth rates as well as the critical crack lengths.

Dividing the (spectrum) time to failure for each of the spectra by the time to failure under the baseline spectrum results in the normalized crack growth life data of Table 2. The variations in life range from a −88 percent in the case of the horizontal tail under Spectrum 4 to +800 percent for the same location under Spectrum 3. Variations of this magnitude are difficult to explain physically and likely point out that the analysis is method limited in the case of the horizontal tail. That is, the method of predicting the horizontal tail stresses possibly fails for variations of this magnitude in the spectrum parameters. It is judged that trends in the results are preserved, however.

The significance of the data of Table 2 is that large changes in life are apparent under the influence of relatively small changes in Mach number and weight. The counting accelerometer is blind to both these variables. The counting accelerometer is at least partially blind to the mission variations represented by Spectra 8, 9, and 10. The Mach number and weight experience effective variations by shifting the time spent in the subject missions. The MSR has an obvious advantage in these cases, since it reflects the actual load experienced at the location.

Figures 5 through 8 address the remaining question with respect to IAT—that of being able to track the damage state at locations remote to the reference location. In these figures, the crack growth curve data is normalized to give an indication of the rate of damage at the stations remote to wing station (WS) 32, the reference for the A-7D. The data is normalized as follows. For a given location, the minimum failure crack length was read for each spectrum. Each of the spectrum times corresponding to these lengths were divided by the time it took to reach the minimum length for the baseline spectrum. The normalized values of each of the locations are plotted against the values of the reference station, WS 32. Note that the 45-deg line on the graphs represents perfect correlation of the damage at the various locations with the damage at the reference. Note also that the lower half of the divided quadrant represents conservative comparisons while the upper half is nonconservative.

An examination of the data in Fig. 5 through 8 reveals that the error in the damage rates of WS 53, pylon stub hole, and the outer wing panel, relative to the reference is especially good. The average of the variations in damage rate for these locations is 5 percent. For the wing attach lug, the variation from perfect correlation is about 10 percent and for the longeron, about 18 percent. These variations are considered moderate when taken as an average, but the maximum variations for particular spectra are 27 and 48 percent, respectively. These large variations make the usefulness of such damage transfer somewhat tenuous for these stations. The variations in the damage rate correlations for the two tail stations are considered completely out of order.

TABLE 2—*Spectrum variation effects.*

Location	Baseline	1.075 W	1.15 W	1.15 MN	1.15 ALT	1.15 N_Z	$N_Z \leq 6.5$	30-30-40	10-50-50	50-50-0
WS 32	1.0	0.72	0.53	0.72	1.02	0.38	0.97	1.13	0.92	0.96
WS 53	1.0	0.59	0.44	0.85	1.00	0.40	1.00	1.23	0.88	0.95
Vertical tail	1.0	0.27	0.08	1.00	1.00	1.00	1.00	1.30	0.80	0.32
OWP fold lug	1.0	0.76	0.52	1.19	1.00	0.47	1.00	1.20	0.84	0.94
Stub hole	1.0	0.54	0.36	0.54	0.99	0.30	0.96	0.77	0.54	0.95
Horizontal tail	1.0	1.33	1.47	0.12	1.00	0.45	1.07	0.55	0.57	9.00
Wing attach lug	1.0	0.77	0.61	1.13	1.00	0.47	0.97	1.07	0.77	0.89
Longeron	1.0	0.80	0.61	0.35	1.00	0.55	1.16	0.51	0.49	0.78

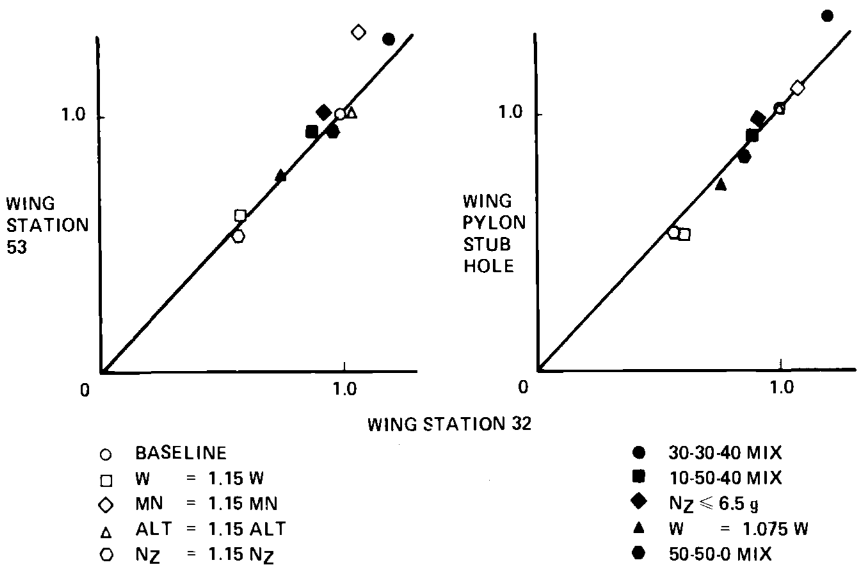

FIG. 5—*Normalized rate of crack growth at WS 53 and pylon stub hole.*

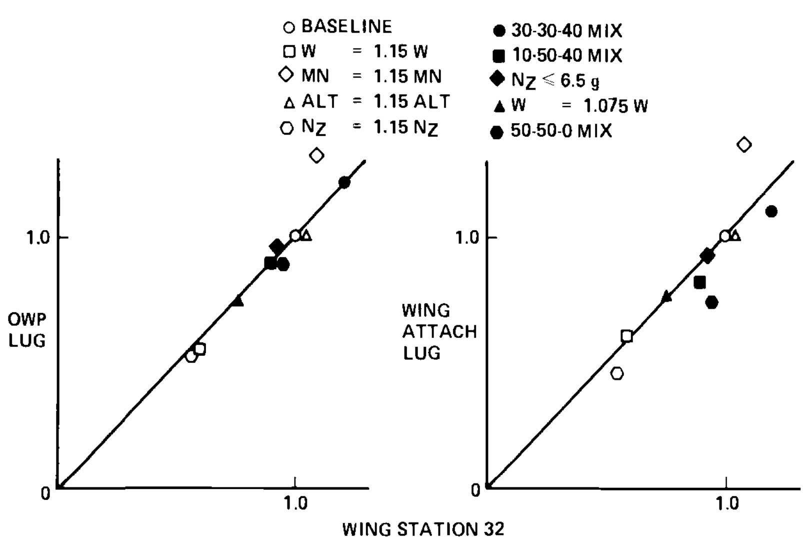

FIG. 6—*Normalized rate of crack growth at OWP and WA lugs.*

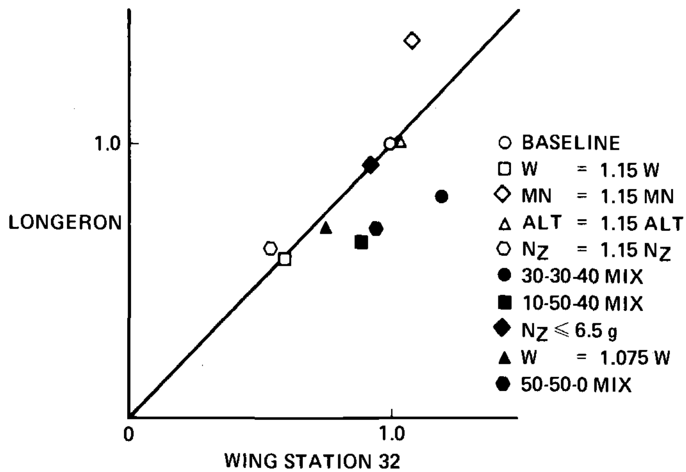

FIG. 7—*Normalized rate of crack growth at longeron.*

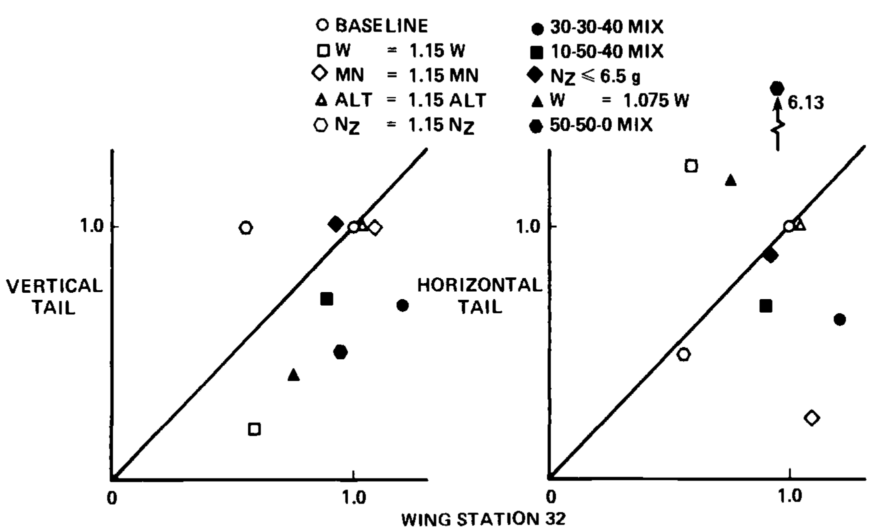

FIG. 8—*Normalized rate of crack growth at vertical and horizontal tails.*

Conclusions

The conclusion concerning the relative superiority of the CA versus the MSR for IAT is that the MSR is considerably more efficient and accurate in terms of providing a damage index *per se*. A thorough cost analysis and comparison of the two methods could mitigate this ranking to some extent. For example, it could be that the supposed higher cost of the data retrieval and processing for the MSR could outweigh the accuracy liabilities of the CA.

Also, the CA accuracy can always be improved by frequently updating the stress to acceleration relationship. This process is a cost item, however. For purposes of this investigation, the MSR is chosen as the superior method.

A conclusion with respect to the second IAT question is much more differential. It is seen that some remote locations can be damage tracked through a reference station while others cannot. Gross indications here are that locations associated with the wing track well, the fuselage not so well, and the tails not at all. For airplanes having critical structure only in the wing, it follows the successful IAT is highly likely with a single activity indicator. For airplanes with a wide distribution of critical locations, multiple indicators may be required. In any event, careful analysis is required.

Acknowledgments

The authors would like to acknowledge the support and permission to publish this account of Dr. Alan Berens of the University of Dayton Research Institute (the prime contractor) and Ms. Marge Artley and Captain Donald Halloway, U.S. Air Force, both of the Air Force Flight Dynamics Laboratory. The work was performed under a Flight Dynamics Laboratory contract entitled "Force Management Methods," awarded in September 1976.

Summary

Virtually every life analysis method that exists is based on assumptions of the analyst as to the significance of one of the spectrum variables over another. Over the recent past, ASTM Committees E-9 and E-24 have published state-of-the-art documents on the effect of overloads, truncation, block loading, and other specific fatigue considerations, but there has been no systematic documentation of the effects of representative variations in the loads spectra on fatigue life. The majority of those past publications that have addressed spectrum fatigue have been documentations of the fatigue performance of structures under specific loads spectra with very little variation in any of the loads parameters.

The purpose of this symposium was to document the significance of load spectra variation on structural life as measured by crack initiation and crack growth. The papers presented herein represent the efforts of individuals to determine the specifics of these effects within their structures' usage environment.

This special technical publication presents an excellent state-of-the-art of the service spectrum fatigue technology. This field encompasses the technologies of loads environment characterization, knowledge of typical variations in structural usage, materials characterization, and initiation and crack propagation prediction analysis under other than non-constant amplitude conditions.

Socie and Artwohl describe a method of drastically truncating service load histories analytically while retaining the original fatigue damage. The authors use simple notched coupons for their test elements. Truncation of this sort is normally done to reduce the number of cycles necessary to simulate the structural life in a laboratory test. As a result of this study, these authors conclude that the method to be used in low-load truncation should be different for the crack initiation and the crack propagation phases of the structures life.

Carroll reports an interesting study of apparent time-at-load dependency in fatigue behavior under simple periodic overload, underload, sustained load, and also flight-by-flight loading conditions. In this study, direct measurements indicated time dependent changes in notch strain with sustained compression loading. These notch strain changes were related to changes in the local notch stress (or residual stress) levels. Subsequent testing determined that the sustained load levels could change the fatigue life by a factor of ten if periodically applied. Carroll found no major sustained load effect in flight-by-flight loading, though.

Bucci, Thakker, Sanders, Sawtell, and Stanley discuss the difference found in attempting to rank experimental heats of aluminum alloy materials under constant and non-constant amplitude loading. Inconsistency in variable amplitude fatigue crack growth rate indicated to the authors that there were competing damage growth mechanisms with controlled changes in basic microstructure and temper.

The paper by Hsu and McGee describes an extensive study of the effects of compressive load cycling on spectrum fatigue crack growth. Their study indicated that multiple compressive cycling gave approximately the same crack growth rate as a single compressive cycle in flight simulation tests of center cracked panels. This paper adds significantly to the knowledge of crack growth under the typical condition of primarily tensile fatigue loading with periodic compression cycling.

Larsen and Annis present the results of a series of tests incorporating military turbine engine mission type loading. Their studies indicate that this type of usage produces a high load relatively often (more than once per mission) giving crack growth behavior that is heavily affected by the delayed retardation phenomena.

Macha, Grandt, and Wicks studied crack growth for military turbine engine load spectra using an approach of isolating the loading events. Using this approach, Macha et al monitored the effects of overloads, underloads, and sustained load on crack growth at elevated temperature. They found that retardation was produced that was proportional to the level of the overload. Underload level within the range found in actual structures were found to have a relatively insignificant effect on the crack growth behavior. Crack growth for a sustained period within an applied load history was at the same rate as during a continuous sustained load test following an incubation period of slower growth.

Wozumi, Spamer, and Lambert compared crack growth predictions, using several methods, to spectrum test results for the purpose of evaluating and improving their analytical capability. Improvements were made to the most promising analytical method based on their evaluation of its performance in these spectrum conditions.

Abelkis describes an exhaustive study of spectrum loading effects for transport airframes. The effort covered 134 variations in usage, high- and low-load truncation, compression loads, flight loads alleviation, and sustained loading under realistic flight-by-flight loading. The most important features for transport airframes, as measured by crack growth rate, were found to be mission mix, flight length, usage severity, and high load levels. The least important effects were mission sequence and ground or compression cycles.

deJonge and Nederveen compared fatigue behavior for a basic transport history and variations simulating a feedback controlled system for reducing the amplitude of gust induced loads. They also studied the effect of deleting the ground-air-ground load cycle from the load history. The authors discovered that the gust alleviation system resulted in an increase in crack initiation life but no change in crack propagation life (flights from 24 to 60 mm total crack length out of 20 mm hole). The elimination of the ground-air-ground cycle resulted in a 3.5 times increase in both initiation and crack growth life.

Finger discusses the effect of windmill load spectra variation on crack growth. He created four different load spectra based on the extremes of wind condition and conducted crack growth tests to develop their prediction capability. The tests indicated that a crack growth prediction methodology required both stress intensity threshold terms and retardation behavior modifications to produce excellent correlations with results.

Dill, Saff, and Potter describe a combined analytical and experimental study of crack growth with multi-mission fighter aircraft load histories. In this study, the authors created over 100 load spectra based on typical and extreme usage of an advanced capability aircraft. Variations were made in load sequence, design stress level, high- and low-load truncation, mission mix, and other usage variables. The load spectrum variables that were found to be most significant were those that affected the basic usage and the highest stress level; for example, design stress level, high-load truncation, and mission mix. Least significant were sequence of loads and compression loads.

Larsen, White, and Gray describe a primarily analytical study of the effect of spectrum variables on crack growth. In this study, the authors developed basic loads spectra for specific locations on a fighter aircraft and variations to those spectra based on their knowledge of the statistics of fleet usage differences. Thus, they have produced a set of analytical predictions of crack growth changes as a function of specific fleet "standard deviations" of usage. This unusual approach results in the ability to better define the crack growth potential of the extreme usage aircraft in a large fleet under changing conditions.

D. F. Bryan

The Boeing Wichita Company Wichita, Kans. 67210; symposium cochairman and coeditor.

J. M. Potter

AFFDL/FBE, Wright-Patterson AFB, Ohio 45433; symposium cochairman and coeditor.

Index

T

U

V

W